UAB
Universitat Autònoma de Barcelona

Neuronal Regeneration and Degeneration in Postnatal Mice: Mechanisms and Subtype-Specific Responses

Beatriu Molina Esteve

UAB
Universitat Autònoma de Barcelona

Neuronal Regeneration and Degeneration in Postnatal Mice: Mechanisms and Subtype-Specific Responses

Presented by

Beatriu Molina Esteve

ACADEMIC DISSERTATION

To obtain the degree of PhD in Neuroscience by the Universitat Autònoma de Barcelona

January 2026

Thesis supervisors

Dr. Esther Udina Bonet

Dr. Natalia Lago Perez

Thesis tutor

Dr. Esther Udina Bonet

Group of Neuroplasticity and Regeneration,

Institut de Neurociències

NeuroPlasticity & Regeneration

INc Institut de Neurociències

This study was supported by:

- The project PID2021-127626OB-I00 “Rejuvenating peripheral neurons to improve specific regeneration after nerve injuries in experimental models” from Ministerio de Asuntos económicos y Transformación Digital of Spain to Esther Udina i Bonet
- The Universitat Autònoma de Barcelona by means of Personal Investigador en Formació (PIF) grant to Beatriu Molina Esteve

Cover designed by Anna Agudo (@atena_arts)

A l'Alèxia i el Bruno

Index

I. Summary

Peripheral nerve injuries during early postnatal stages result in mechanisms of neuronal regeneration and degeneration that are fundamentally different from those observed in adults. This doctoral thesis investigates the regenerative capacity of motor and sensory neurons following peripheral nerve injury in mice at distinct postnatal developmental stages (P4, P10, and P30), hypothesising that motor and sensory neurons exhibit greater regenerative capacity and selective reinnervation of target organs during early juvenile stages compared with later stages, owing to the activation of distinct genetic growth programmes.

The investigation comprises three coordinated experimental studies. Chapter 1 evaluated neuronal survival and axonal regenerative capacity in motoneurons following sciatic nerve crush injury in ChAT-Cre/Ai9(RCL-tdT) mice, complemented by subtype-specific neuronal translatome analysis via ChAT-Cre/RiboTag and assessment of Wallerian degeneration at distinct postnatal stages. Chapter 2 employed PV-Cre/Ai9(RCL-tdT) and TrpV1-Cre/Ai9(RCL-tdT) mice to separately study proprioceptive and nociceptive sensory neurons, including transcriptomic analysis of dorsal root ganglia and *in vitro* conditioning lesion assays. Chapter 3 evaluated branch-specific regeneration (muscular versus cutaneous) following femoral nerve injury and repair using retrograde tracers.

Results demonstrated that nerve injury at P4 induced substantial motoneuron death (~50%), whilst P10 and P30 showed minimal neuronal loss; however, when corrected for neuronal survival, P4 mice demonstrated the greatest axonal regenerative capacity, with surviving neurons achieving 100% regeneration. Translatome analysis revealed that P30 animals activated a robust programme of regeneration-associated genes (RAGs), including classical markers such as Atf3, Gap43, and Ngfr, whereas P4 neurons showed minimal RAG activation, suggesting they retain an intrinsic growth state facilitating regeneration without transcriptional reprogramming. P10 exhibited a transitional phenotype with altered RAG activation and reduced regenerative capacity. Regarding sensory neurons, proprioceptive axons in P30 achieved complete regeneration, whilst P4 and P10 demonstrated lower regeneration percentages; nociceptive neurons achieved 100% regeneration at 14 days post-injury across all ages. Transcriptomic analysis of dorsal root ganglia via GSEA revealed that only P30 animals

presented significant RAG activation, whilst injured P4 and P10 animals showed no upregulated RAGs compared with same-age controls. Branch-specific regeneration analysis demonstrated that motoneurons at P10 showed significantly greater regeneration towards the motor branch than in adults, whilst non-proprioceptive sensory neurons exhibited no clear age-related differences.

This study provides fundamental evidence that neuronal regenerative capacity at early postnatal stages is primarily determined by the intrinsic growth state of neurons rather than by extrinsic factors of the Wallerian degeneration microenvironment. The absence of robust RAG activation in P4 despite efficient regeneration suggests that immature neurons maintain a constitutive growth capacity that is progressively repressed with maturation.

I. Abbreviations

ACTB – β-actin

ADCYAP1 – Adenylyl cyclase activating polypeptide 1

AMPA - α-amino-3-hydroxy-5-methyl-4-isoxazolepropionic acid

ANOVA – Analysis of Variance

AP-1 – Activator protein 1

AQP4 – Aquaporin 4

ARG1 – Arginase 1

ARTN – Artemin

ATF2/3 – Activating transcription factor 2/3

BAX – BCL2 associated X protein

BDNF – Brain-derived neurotrophic factor

bFGF – Basic fibroblast growth factor

BSA – Bovine Serum Albumin

Calb1 – Calbindin

CCL2 – C-C motif chemokine ligand 2

CD68 – cluster of differentiation 68

cDNA – Complementary DNA

ChAT – Choline acetyltransferase

CL – Conditioning Lesion

c-Jun – Jun proto-oncogene

CNS – Central Nervous System

CNTF – Ciliary neurotrophic factor

CREB – cAMP response element-binding protein

CR3 – Complement receptor 3

DAPI – 4',6-diamidino-2-phenylindole

DMEM – Dulbecco's Modified Eagle Medium

DNA – Deoxyribonucleic acid

dpi – Days Post-Injury

DLK – Dual leucine zipper kinase

DPX – Dibutyl phthalate xylene

DRG – Dorsal Root Ganglion

ECM – Extracellular matrix

Epon – Epoxy resin embedding medium

ER – Endoplasmic Reticulum

ErbB – Receptor tyrosine-protein kinase

Erg2 (Krox-20) – Early growth response 2

ERK – Extracellular signal-regulated kinase

FABP7 – Fatty acid binding protein 7

FASTQ – Format for storing biological sequences

FDR – False Discovery Rate

FGF – Fibroblast growth factor

FOXO1 – Forkhead box O1

GAP43 – Growth associated protein 43

GDNF – Glial cell line-derived neurotrophic factor

GO – Gene Ontology

GSEA – Gene Set Enrichment Analysis

HA – Hemagglutinin

HGF – Hepatocyte Growth Factor

hiFBS – High Foetal Bovine Serum

HSB – High salt buffer

I – Input

IGF-1 – Insulin-like Growth Factor 1

IL – Interleukin

IP – Immunoprecipitate

JAK – Janus kinase

JNK – c-Jun N-terminal kinase

JIPs – JNK-interacting scaffold proteins

JUN – JunB proto-oncogene

JunD: JunD proto-oncogene

KEGG – Kyoto Encyclopedia of Genes and Genomes

LFB – Luxol fast blue

LGALS3 – Galectin 3

LiCO3 – Lithium carbonate

LIF – Leukaemia inhibitory factor

MAG – Myelin-associated glycoprotein

MAL – Myelin and lymphocyte protein

MAPK – Mitogen-activated protein kinase

MARCO – Macrophage receptor with collagenous structure

MBP – Myelin basic protein

MCP-1 (CCL2): Monocyte chemoattractant protein-1

MERTK – MER proto-oncogene

tyrosine kinase

MKK4 – Mitogen-activated protein kinase 4

MN: Motoneuron

MNX1 – Motor neuron and pancreas homeobox 1

MOBP – Myelin-associated oligodendrocyte basic protein

MPZ – Myelin protein zero

mRNA – Messenger RNA

MS4A4C – Membrane spanning 4 domains A4C

mTOR – Mechanistic target of rapamycin

NC – Neural crest

NCAM1 – Neural cell adhesion molecule 1

NDS – Normal Donkey Serum

NEFH – Neurofilament heavy chain

NES – Normalized Enrichment Score

NF-κB – Nuclear factor kappa B

NGF – Nerve growth factor

NGFR – Nerve growth factor receptor

NGS – Next-generation sequencing

NK – Natural killer

NLS: Nuclear localisation signal

NMDA – N-methyl-D-aspartate

NOD – Nucleotide-binding oligomerization domain

NO: Nitric oxide

NT-3 – Neurotrophin-3

NTRK1-3 – Neurotrophic receptor tyrosine kinase 1-3

Oct-6 (POU3F1) - POU domain, class 3, transcription factor 1

OLIG1/2 – Oligodendrocyte transcription factor 1

ORO – Oil Red O

P311 (NREP) – P311 protein/neuronal regeneration-related protein

P – Postnatal Day

P53 – Tumour protein p53

P75^{NTR} – p75 neurotrophin receptor

Pax3 – Paired box 3

PBS – Phosphate buffered saline

PBST – PBS with Triton X-100

PCA – Principal Component Analysis

PCR – Polymerase chain reaction

PDGF – Platelet-derived growth factor

PDL – Poly-D-Lysine

PEP1-2 – Peptidergic (1-2)

PFA – Paraformaldehyde

PI3K – Phosphatidylinositol 3-kinase

PI3K-AKT – Phosphatidylinositol 3-kinase/protein kinase B

PLP1 – Proteolipid protein 1

PMP22 – Peripheral myelin protein 22

PMR – Preferential Motor Reinnervation

PNI – Peripheral nerve injury

PNS: Peripheral nervous system

PRX – Periaxin

PSA – Polysialic acid

PTN – Pleiotrophin

PV – Parvalbumin (proprioceptive neurons)

qPCR – Quantitative polymerase chain reaction

RAC1 – Ras-related C3 botulinum toxin substrate 1

RAGs – Regeneration-Associated Genes

RAP1 – Ras-proximate-1

RIG – Retinoic acid-inducible gene

RNA – Ribonucleic acid

ROS: Reactive oxygen species

RQN – RNA quality number

RT-qPCR – Reverse Transcription quantitative Polymerase Chain Reaction

SEM – Standard Error of the Mean

SHH – Sonic hedgehog

SLC18A3 – Solute carrier family 18 member A3

SOX2 – SRY-box transcription factor 2

Runx1-3 – Runt-Related Transcription Factor 1-3

SEMA3A – Semaphorin 3α

Sox2/11 – SRY-box transcription factor 2/11

Sprr1a – Small proline-rich repeat protein 1a

STAT3 – Signal transducer and activator of transcription 3

TGF – Transforming growth factor

TLR – Toll-like receptor

TMEM119 – Transmembrane protein 119

TNF – tumour necrosis factor

TNS1 – Tensin 1

TPM – Transcripts Per Million

TREM2 – Triggering receptor expressed on myeloid cells 2

TrkC – Tropomyosin receptor kinase C

TRPA1: Transient Receptor Potential Ankyrin 1

TrpV1 – Transient Receptor Potential Cation Channel, subfamily V, member 1 (nociceptive neurons)

TUBB2B – Tubulin beta 2B class IIb

UMAP – Uniform Manifold Approximation and Projection

VEGF – Vascular endothelial growth factor

VGLUT3: Vesicular glutamate transporter 3

wpi – Weeks post injury

WT – Wild Type

ZPK – Zipper-like protein kinase

II. Introduction

1. Peripheral Nervous System

The Peripheral Nervous System (PNS) represents a highly heterogeneous network that performs an extensive range of essential functions, from mediating communication between the brain and the body to regulating development, stem cell niches, and regenerative processes. According to its structure and function, the PNS can be subdivided into four major domains: sensory, motor, autonomic, and enteric (Murtazina & Adameyko, 2023).

The PNS ensures the continuous bidirectional flow of information between the central nervous system (CNS) and peripheral tissues. Sensory fibres convey information from peripheral sense structures to the CNS, while motor fibres transmit commands from the CNS to peripheral effectors. This integration of afferent and efferent components allows the PNS to maintain homeostasis and coordinate responses to external and internal stimuli. (Figure 1)

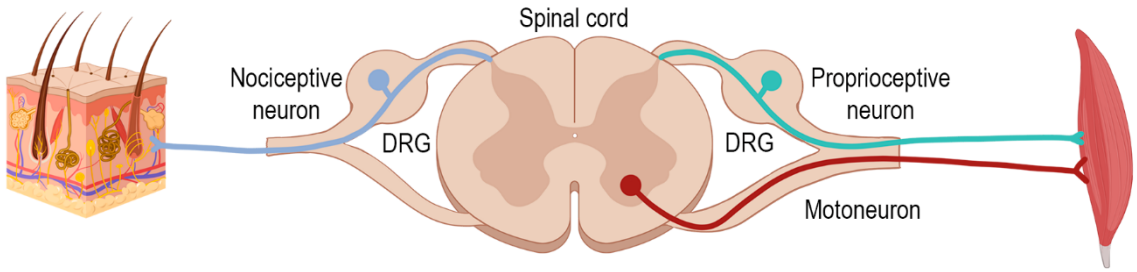

Figure 1. Schematic representation of the interface between the central and peripheral nervous systems, showing the spinal cord with dorsal root ganglia, and illustrating a proprioceptive neuron, a nociceptive sensory neuron and a spinal motoneuron connecting the skin and skeletal muscle.

Peripheral nerves, which extend from the spinal cord and brainstem, may contain both motor and sensory components. Cranial nerves emerge from the brainstem, whereas the spinal nerves that will form the rest of the somatic nerves emerge from the spinal cord. The cell bodies of sensory neurons are located in the dorsal root ganglia (DRG), whereas those of somatic motoneurons are situated in the ventral horn of the spinal cord. The sensory neurons of the DRG are pseudounipolar, giving rise to one branch that projects towards peripheral targets and another that

enters the spinal cord via the dorsal rootlets. These central projections terminate in specific laminae of the dorsal horn, where they synapse with defined interneuron populations according to their sensory modality (Topp and Boyd 2012; Murtazina and Adameyko 2023). The somatic motoneurons, in turn, send their axons through the ventral horn and into ventral rootlets, which subsequently join with sensory fibres to form mixed spinal nerves containing both motor and sensory components (Topp & Boyd, 2012).

1.1 Peripheral Sensory Nervous System

The sensory domain of the PNS comprises several categories of neurons that allow organisms to perceive and respond to environmental stimuli. Most peripheral nerves contain the projections of somatosensory neurons, which continuously survey the body environment by detecting and relaying information about touch, pain (nociception), temperature (thermoception), and body position (proprioception).

Somatosensory neurons relay information from the skin, muscles, tendons, and internal organs regarding mechanical, thermal, and chemical stimuli, allowing the brain to construct an integrated representation of the body's state. These neurons are predominantly located in the DRG along the spinal cord. Their peripheral branches innervate distinct target tissues, whereas their central branches project into specific spinal laminae, where they form synapses with interneurons that process modality-specific inputs (Murtazina & Adameyko, 2023).

During embryogenesis, sensory neurons arise from two distinct sources: neurogenic placodes and the neural crest (NC). Placode-derived neuroblasts delaminate from the preplacodal ectoderm and migrate into the mesenchyme to form cranial sensory ganglia such as olfactory, cochlear, vestibular, geniculate, trigeminal, nodose and petrosal ganglia. Neural crest cells delaminate from the dorsal neural tube, migrate extensively and, together with boundary cap stem cells, populate the trigeminal, jugular and dorsal root ganglia, where distinct DRG subtypes emerge through RUNX1/3-mediated fate specification and NTRK1–3 signalling, while SEMA3A contributes to correct central targeting. All peripheral glial cells, including Schwann

and satellite cells, are neural crest-derived, and some specialised nociceptive Schwann cells in the skin are now recognised as primary pain sensors (Murtazina & Adameyko, 2023).

Single-cell transcriptomic studies have refined DRG sensory neuron classification, identifying at least eleven major transcriptionally distinct types that correlate with specific modalities and conduction properties (Usoskin et al., 2015). Myelinated, low-threshold mechanoreceptors (NF1–NF3) expressing Ntrk2, Ret, Calb1 and Ntrk3 encode discriminative touch, whereas NF4 and NF5 neurons, characterised by TrkC and parvalbumin expression, correspond to proprioceptors that signal body position and movement. Unmyelinated or thinly myelinated C-fibre populations include NP1–NP3 nociceptors, which express receptors such as TRPV1, TRPA1 and various G-protein-coupled receptors and mediate heat, chemical and pruritic stimuli, and peptidergic PEP1–PEP2 neurons that participate in inflammatory and thermal pain, while tyrosine hydroxylase-positive (TH) neurons expressing VGLUT3 are implicated in pleasant touch and certain nociceptive pathways. Each subtype exhibits a specific combination of ion channels, receptors and transcription factors, providing a molecular basis for selective encoding of modalities such as pain, itch, temperature and proprioception within the peripheral sensory nervous system (Usoskin et al., 2015).

1.2 Peripheral Motor Nervous System

The motor division of the PNS comprises projections from motoneurons (MNs) located within the CNS that innervate skeletal muscles, as well as synaptic connections with autonomic neurons and neuroendocrine cells that control visceral organs. (Murtazina & Adameyko, 2023).

During development, somatic MNs arise from radial glial progenitors located within the ventral neural tube. These progenitors occupy the pMN domain, defined by the expression of the transcription factor *Olig2*. Along the rostrocaudal axis, graded expression of Hox family transcription factors confers positional identity, resulting in the specification of distinct motor columns and the diversification of MN subtypes corresponding to particular muscle targets (Murtazina & Adameyko, 2023).

Motor fibres can be classified according to their targets and function. Somatic motor axons innervate skeletal muscles of somatic origin, branchial (also called pharyngeal arch–derived) motor axons supply muscles derived from pharyngeal arches, and visceral motor axons project to smooth and cardiac muscle and glands. Somatic motoneurons can be further divided into α-motoneurons, which are thickly myelinated (12–20 μm in diameter) and innervate extrafusal skeletal muscle fibres, and γ-motoneurons, which are smaller (2–8 μm) and innervate intrafusal muscle spindle fibres, maintaining spindle sensitivity during muscle contraction (Topp & Boyd, 2012).

1.3 Histological Organisation of Peripheral Nerves

At the microscopic level, the fundamental functional unit of a nerve is the nerve fibre, which is composed of an axon and its associated Schwann cells. Myelinated nerve fibres contain serially arranged Schwann cells, each of which wraps an individual segment of axon in multiple compact layers of plasma membrane, forming a myelin sheath. During development, only axons with a diameter of approximately 0.7 μm or larger become myelinated. In contrast, unmyelinated nerve fibres are formed by axons that remain in close association with Schwann cell processes, yet without the compacted membrane structure characteristic of myelinated fibres (Topp & Boyd, 2012).

Nerve fibres are grouped in fascicles, and fascicles in trunks, that forms the nerves. These different structures are encased within three concentric layers of connective tissue: the endoneurium, perineurium, and epineurium (Figure 2).

The **endoneurium** is the innermost compartment, enveloping individual nerve fibres. It consists of endoneurial fluid, longitudinally oriented type I and II collagen fibres, and a fine network of collagen fibrils intimately associated with the continuous basal lamina surrounding each axon–Schwann cell unit. The basal lamina is composed primarily of type IV collagen, laminin, fibronectin, and heparan sulphate. The endoneurial space also contains fibroblasts, macrophages, and mast cells.

The **perineurium** forms the intermediate connective tissue layer, encapsulating bundles of nerve fibres (fascicles). It consists of concentric layers of perineurial cells connected by tight junctions and interspersed with collagen and elastic fibres arranged in circumferential, oblique, and longitudinal orientations. These layers provide both tensile strength and a diffusion barrier, thereby protecting nerve fascicles from mechanical stress and maintaining the internal microenvironment.

The outermost layer, the **epineurium**, is composed of dense irregular connective and adipose tissue. It holds multiple fascicles together within a nerve trunk and contains bundles of type I and III collagen fibrils and elastic fibres oriented longitudinally along the nerve. The interfascicular epineurium allows gliding between nerve fascicles and supports blood vessels and nerve branches entering from extraneural regions. (Topp & Boyd, 2012)

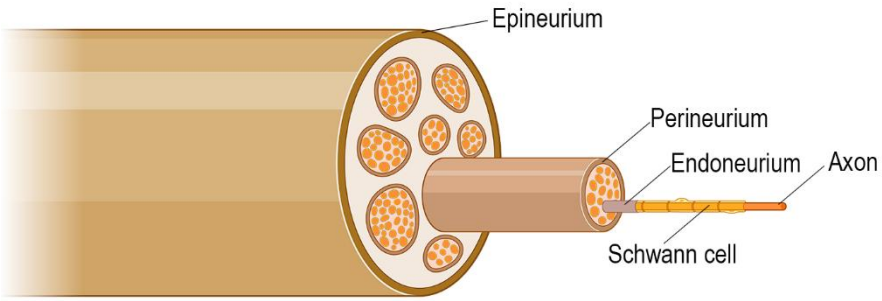

Figure 2. Schematic representation of the connective tissue coverings of a peripheral nerve, illustrating individual myelinated axons ensheathed by Schwann cells and surrounded successively by endoneurium, perineurium forming a nerve fascicle, and the outer epineurium enclosing the entire nerve trunk. Created with Biorender

2. Peripheral nerve injury

Peripheral nerve injuries (PNIs) cause significant disability worldwide, as they lead to the loss of motor, sensory, and autonomic functions in the body regions innervated by the affected nerve or nerve trunk. PNIs most commonly result from motor vehicle accidents, and less frequently from penetrating trauma (Robinson, 2004). In newborn infants, these injuries typically involve the brachial plexus, lumbosacral plexus, or facial nerve, with an estimated incidence of 2–7.5 cases per

1,000 live births. The functional outcome following major nerve injury is often unsatisfactory in adults; however, children tend to experience better recovery and faster functional restoration after nerve repair. This improved outcome is likely due to their greater neural plasticity and biological advantages compared with adults, including shorter regeneration distances, accelerated axonal growth, and enhanced cortical adaptability (Costales et al., 2019). However, neonatal injuries can lead to devasting and irreversible functional loss due to the massive death of injured neurons. Despite advances in surgical techniques, many affected children remain permanently disabled, often requiring long-term pain management and rehabilitative care (Kemp et al. 2015; Devi et al. 2018).

2.1 Classification of nerve injuries

In 1942, Seddon proposed a classification of nerve injuries dividing them in three main types (Figure 3):

I. *Neurapraxia*: it represents the mildest form of PNI, characterized by a temporary interruption of nerve conduction without structural damage of the axon. It commonly results from transient compression, ischaemia, or mild mechanical trauma – such as in tourniquet paralysis, Saturday-night palsy, or crutch palsy – In these cases, the force applied to the nerve is insufficient to disrupt axonal continuity or trigger degeneration but affect the myelin sheath. Clinically, is distinguished by motor weakness or paralysis with minimal muscle wasting and preserved electrical excitability, indicating that these axons remain intact. Sensory symptoms such as numbness, tingling or burning sensations are common. Proprioceptive functions, including vibration and postural sense, are often more affected, whereas sweating and autonomic functions are generally preserved. Recovery occurs rapidly and completely within six to eight weeks. The process does not involve axonal regeneration but rather the restoration of physiological conduction through remyelination or the resolution of focal myelin compression.

II. *Axonotmesis*: it refers to a severe form of PNI in which the axons and myelin sheaths are completely disrupted, but the connective tissue framework of the nerve — particularly the endoneurium, perineurium and epineurium — remains at least partially intact. Such injuries typically occur because of crushing, compression, or severe contusion, where the force is sufficient to interrupt axons but not the connective tissue. At the site of the injury, the nerve may initially appear narrowed or swollen, sometimes with mild thickening of the epineurium or perineural adhesions. Despite the complete degeneration of the distal stump, spontaneous regeneration almost always follows, as the preserved connective tissue scaffolding provides a pathway for regrowing axons. Over the course of several weeks to months, new nerve fibres extend through the lesion site and continue distally in an anatomically organized manner, guided by the remaining connective tissue structures.

III. *Neurotmesis*: it represents the most severe form of peripheral nerve injury, characterized by complete disruption of the nerve's axons, myelin sheath and connective tissue framework. At the injury site, a proximal neuroma can be formed if regenerating axons proliferate into scar tissue, while smaller gliomatous swelling may appear at the distal stump, composed mainly of Schwann cells and fibrous tissue. Clinically, neurotmesis results in total loss of sensory and motor function within the affected nerve's territory, accompanied by muscle atrophy and degeneration. Without surgical intervention, recovery does not occur, as the continuity of the nerve pathway is lost. Even after microsurgical repair, functional restoration is often incomplete due to irreversible changes in denervated end-organs and misdirected axonal regeneration.

However, in 1951, Sunderland proposed a new classification for PNI. He defined five degrees based on changes induced in the normal structure of the nerve. In ascending order of severity: (I) affecting the conduction of the axon; (II) affecting the continuity of the axon; (III) affecting the endoneurial tube and its contents; (IV)

affecting the funiculus and its contents and (V) affecting the entire trunk. First and fifth degree corresponds to neurapraxia and neurotmesis of Seddon's classification respectively. Additionally, Sunderland subdivided the axonotmesis into three degrees to solve the variability that patients with axonotmesis had on their prognosis, depending on factors such as intraneural haemorrhage and the discontinuity of endoneurial tubules and perineural layers (Figure 3).

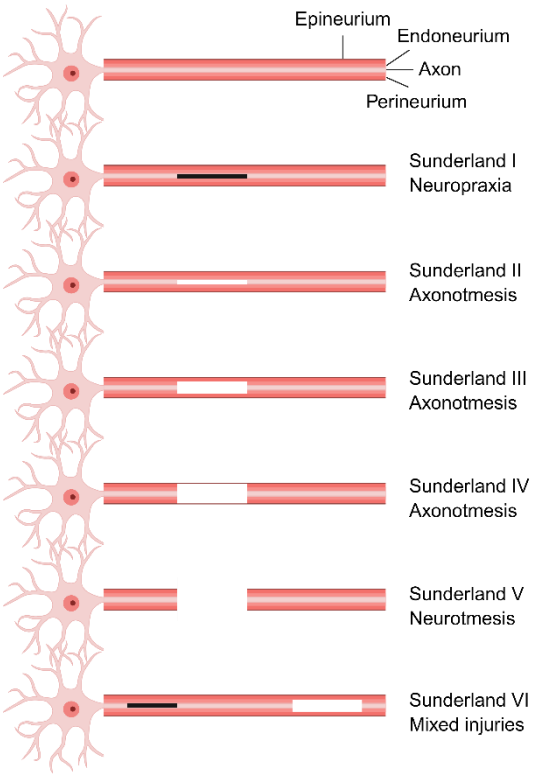

Figure 3. Schematic representation of the different injury grading systems for PNI (adapted from (Lopes et al., 2022), created with Biorender)

2.2 Neuronal death following PNI

Neuronal death after peripheral nerve injury depends on a combination of injury-related factors (severity and location of the lesion) and neuron-related factors (age and cell type), which together determine whether an axotomized neuron can switch to a regenerative state or instead undergoes apoptosis (Kemp et al., 2015; Lowrie & Vrbová, 1992).

Influence of age: the susceptibility of neurons to die after axotomy is markedly higher in the early postnatal period and decreases with maturation (Lowrie & Vrbová, 1992; Schmalbruch, 1984). In rodents, nerve injuries performed within the first 4–5

postnatal days induce massive motoneuron loss, a vulnerability that declines substantially over subsequent weeks and is largely absent by adulthood (Navarrete & Vrbová, 1984; Schmalbruch, 1984; Lowrie & Vrbova, 1984; Kemp et al., 2015).

Type and severity of the lesion: The type of peripheral lesion also critically influences neuronal survival (Costales et al., 2019). Neurotmesis (Sunderland V) is associated with the highest rates of motoneuron and sensory neuron death in neonatal animals (Schmalbruch, 1984). In contrast, axonotmesis, although severe, preserve the basal lamina tubes and allow faster reinnervation; nevertheless, when performed in very young animals (e.g. P3–P5), even crush can still trigger substantial motoneuron and sensory neuron loss (Lawson & Lowrie, 1998; Costales et al., 2019). In adult rodents, the same injuries usually do not induce significant death of DRG neurons and cause only limited motoneuron loss, indicating that mature neurons tolerate disconnection better and rely more on functional deficits than on cell loss to express injury consequences (Lewis et al., 1999).

Distance from the lesion to the soma: the proximity of the lesion to the cell body is another major determinant of neuronal survival. Axotomies performed close to the spinal cord or DRGs are more likely to induce neuronal death than distal nerve injuries, because they produce a stronger interruption of retrograde trophic support and more intense injury signalling at the soma (Lowrie & Vrbová, 1992).

Neuronal subtype and trophic dependence: neuronal subtype strongly influences vulnerability to post-injury death (Costales et al., 2019). Spinal motoneurons are particularly sensitive to axotomy during early postnatal stages, due to their high dependence on target-derived trophic factors and the immaturity of Schwann cells (Schmalbruch, 1984; Lawson & Lowrie, 1998; Iwasaki et al., 1997). In contrast, DRG sensory neurons show greater heterogeneity in their survival responses, with variable susceptibility to post-injury death depending on their developmental stage and intrinsic neuroprotective mechanisms (Kemp et al., 2015)

2.3 Postnatal neuronal death following PNI

Profound biological differences exist between the immature and mature nervous systems. Peripheral nerve section in neonatal rodents results in substantially greater neuronal death in both the dorsal root ganglia and the ventral horn compared with adults (Birch & Achan, 2000). Neonatal spinal motoneurons and primary sensory neurons are particularly vulnerable to degeneration following peripheral axotomy. In rats, sciatic nerve transection at birth induces degeneration in 53–89% of sensory neurons (Schmalbruch, 1984) and up to 80% of spinal motoneurons (Lawson & Lowrie, 1998).

Extensive apoptotic cell death has been demonstrated in spinal motoneurons after neonatal sciatic nerve transection, with apoptotic cells also found among interneurons, sensory neurons, and glial cells (Chiarotto et al., 2014). The heightened vulnerability of neonatal motoneurons is thought to stem from their strong dependence on trophic support from target muscles and terminal Schwann cells, which are essential for neuronal maintenance and survival during early postnatal development.

Loss of trophic input following proximal nerve injury, combined with direct injury-induced stress, triggers intracellular signalling cascades that promote apoptosis in both motoneurons and sensory neurons (Lowrie & Vrbová, 1992). Neuronal death typically occurs within the first few days post-injury, defining a short but critical therapeutic window.

2.3.1 Mechanisms of Neuronal Death

Apoptosis

Apoptosis is the predominant form of neuronal death following neonatal peripheral nerve injury. Morphologically, it is characterised by nuclear condensation and fragmentation, and molecularly by DNA cleavage. The number of apoptotic motoneurons observed matches the total neuronal loss in the early post-injury stages,

indicating that apoptosis fully accounts for the degeneration seen in this context (Lawson & Lowrie, 1998).

Apoptosis also affects spinal interneurons, sometimes in a delayed manner and even contralaterally to the lesion site, implying a broader circuit-level response to injury.

At the molecular level, apoptosis involves the activation of pro-apoptotic proteins such as Bax and caspase pathways and is strongly influenced by oxidative stress. Neonatal neurons show heightened vulnerability to oxidative damage compared with mature neurons, exacerbating injury-induced apoptosis. Treatment with the antioxidant N-acetylcysteine reduces Bax expression and neuronal death, highlighting oxidative stress as a major mediator of injury-induced apoptosis (Catapano et al., 2017).

Excitotoxicity mediated by Glutamate

The phenomenon of glutamate-mediated excitotoxicity is a major contributor to motoneuron death during early postnatal stages (Petsanis et al. 2012; Cabaj and Slawinska 2012).

Glutamate, the principal excitatory neurotransmitter, acts on ionotropic receptors—mainly NMDA and AMPA/kainate—on the neuronal membrane. Peripheral nerve injury can lead to excessive activation of these receptors, resulting in massive calcium (Ca^{2+}) influx. This abnormal calcium entry activates degradative enzymes such as proteases, lipases, and nucleases, damaging the cytoskeleton, membranes, and genetic material (Petsanis et al., 2012).

The consequence is either necrotic or apoptotic cell death, depending on the intensity and duration of receptor activation. Motoneurons in early postnatal stages are particularly susceptible due to their high density of NMDA receptors (Petsanis et al. 2012; Cabaj and Slawinska 2012). Following axotomy, this receptor density may further increase, heightening vulnerability to excitotoxicity.

Excessive excitability is also linked to persistent inward currents (PICs) of sodium and calcium, which amplify depolarisation and calcium influx, exacerbating cell death cascades (Cabaj & Slawinska, 2012).

Pharmacological interventions targeting excitotoxicity provide strong evidence for this mechanism: blocking NMDA receptors with antagonists such as MK-801 or DAP5 can reduce apoptosis by up to 60% during the critical post-injury period (Lawson and Lowrie 1998; Petsanis et al., 2012).

Importantly, excitotoxic damage is developmentally regulated—it is most pronounced during the first five postnatal days, coinciding with the peak expression of glutamate receptors (Petsanis et al., 2012). This explains why neonatal motoneurons are far more susceptible than adult neurons. Additionally, the absence of muscle reinnervation establishes a bidirectional degenerative interaction between nerve and muscle, where both structures negatively influence each other's survival (Petsanis et al., 2012).

c-Jun Activation and the JNK pathway

A key signalling event in the apoptotic cascade is the activation of c-Jun, a transcription factor that functions as an early and potentially reversible regulator of neuronal fate (Q. Yuan et al., 2014). Depending on its dimerization partners — such as ATF-2 or ATF-3 — c-Jun can promote either apoptosis or regeneration (*for its role in regeneration, see section below: 2.4.2 Neuronal changes*).

Phosphorylation of c-Jun through the JNK (c-Jun N-terminal kinase) pathway acts as a molecular switch: in pro-apoptotic contexts, it induces the expression of death-promoting genes. This mechanism has been observed in multiple injury models, including optic nerve lesions, where inhibition of c-Jun provides neuroprotection (Q. Yuan et al., 2014).

Further insights into this signalling cascade were provided by Itoh et al. (2014), who demonstrated that ZPK/DLK (dual leucine zipper kinase) and its downstream effector MKK4/MAP2K4 form the critical upstream gate that triggers JNK activation.

Following axotomy, excitotoxic calcium influx activates DLK, which phosphorylates MKK4, subsequently activating JNK and leading to c-Jun phosphorylation. Conditional deletion of MKK4 in neurons protects up to 70% of motoneurons from post-axotomy death, confirming the pathway's central role (Itoh et al., 2014).

This mechanism suggests that the DLK–MKK4–JNK–c-Jun axis links excitotoxic stress to apoptosis, integrating calcium-dependent and transcriptional signals in the execution of neuronal death.

Neurotrophic deprivation and Survival mechanisms

Neonatal neuron death after axotomy also arises from the loss of retrogradely transported neurotrophic factors from targets and distal nerve pathways (Iwasaki et al., 1997).

Exogenous application of neurotrophic factors such as CNTF (ciliary neurotrophic factor), BDNF (brain-derived neurotrophic factor), and LIF (leukaemia inhibitory factor) has been shown to provide partial protection when applied locally after nerve injury. Moreover, bFGF (basic fibroblast growth factor) and PDGF (platelet-derived growth factor) exert similar neuroprotective effects by promoting neuron survival and preventing post-axotomy degeneration (Iwasaki et al., 1997).

Both bFGF and PDGF, along with their receptors, are present in the developing nervous system, suggesting endogenous neurotrophic roles in vivo. These factors likely act not only directly on neurons but also in coordination with glial-derived cytokines and growth factors released after injury. The glial response is therefore considered a key element in the local rescue of neurons, facilitating both survival and potential regeneration (Iwasaki et al., 1997).

Extracellular and Environmental Factors

The extracellular environment itself contributes to neuronal vulnerability. The distal nerve stump in neonatal animals displays reduced expression of β1-integrins,

molecules essential for axon–extracellular matrix interactions and regenerative signalling (Liang Low et al., 2003). This deficit leads to an unfavourable milieu for both axon regeneration and neuronal survival, amplifying the effects of intrinsic apoptotic and excitotoxic mechanisms.

2.4 Peripheral Nerve Regeneration

2.4.1 Wallerian Degeneration

Wallerian degeneration is an active process of anterograde degeneration that occurs in the distal nerve stump following axotomy or crush injury (Waller, 1851; Stoll & Müller, 1999). First described by Augustus Waller in 1850 through experiments on severed glossopharyngeal and hypoglossal nerves in frogs, this process represents a highly orchestrated programme of axonal and myelin breakdown essential for creating a permissive microenvironment that allows successful regrowth of nerve fibres from the proximal nerve segment (Stoll & Müller, 1999; Rotshenker, 2011).

In the peripheral nervous system, Wallerian degeneration unfolds as a coordinated sequence of cellular and molecular events involving degenerating axons, Schwann cells, resident and recruited macrophages, and fibroblasts, all working in concert to clear axonal and myelin debris and to establish the conditions necessary for axonal regeneration (Stoll & Müller, 1999; Gaudet et al., 2011).

Initial injury response: membrane sealing and early signals

Immediately following nerve transection or crush, the severed axon undergoes rapid sealing of the cut membrane within minutes, a process mediated by massive influx of Ca^{2+} ions that activates Ca^{2+}dependent enzymes including calpain and phospholipase A_2, facilitating membrane fusion and preventing catastrophic loss of axoplasm (Stoll & Müller, 1999; Rotshenker, 2011). During the ensuing latency phase, the distal axonal segment remains morphologically relatively intact and retains the capacity to conduct action potentials, despite being irreversibly committed to degeneration (Stoll and Müller, 1999).

In parallel with axonal sealing, a rapid innate immune response is initiated in the distal nerve. Resident macrophages become activated and begin to release pro-inflammatory cytokines, whilst denervated Schwann cells release early signals such as tumour necrosis factor alpha (TNF-α) and interleukin-1 beta (IL-1β), initiating recruitment of circulating monocytes into the nerve (Stoll & Müller, 1999; Gaudet et al., 2011).

Axonal and myelin degeneration: molecular cascades

Fragmentation of axons becomes morphologically evident by light microscopy at 36–44 hours post-lesion in mice and rats, although this timing varies across species and depends on axon diameter and the length of the distal segment, with larger axons and longer distal stumps fragmenting more slowly (Stoll & Müller, 1999; Rotshenker, 2011). Axonal breakdown proceeds in an anterograde direction at velocities of approximately 10–24 mm per hour and is driven by Ca^{2+}-dependent activation of calpain and ubiquitin-proteasome pathways that disassemble the axonal cytoskeleton, leading to granular disintegration of neurofilaments, microtubules and other internal organelles (Stoll & Müller, 1999).

Concurrent with axonal fragmentation, the myelin sheath undergoes progressive disintegration (Stoll & Müller, 1999). Schwann cells respond to axonal degeneration by shedding and extruding their myelin sheaths, initially forming characteristic myelin ovoids—spherical or ellipsoidal myelin fragments enclosing axonal debris—within the endoneurial tubes (Stoll & Müller, 1999; Jung et al., 2011). This process is facilitated by actin polymerisation-dependent mechanisms that drive the physical fragmentation of myelin lamellae and the dissolution of Schwann cell–axon junctional complexes including Schmidt-Lanterman incisures and paranodal loops (Jung et al., 2011; Gomez-Sanchez et al., 2015).

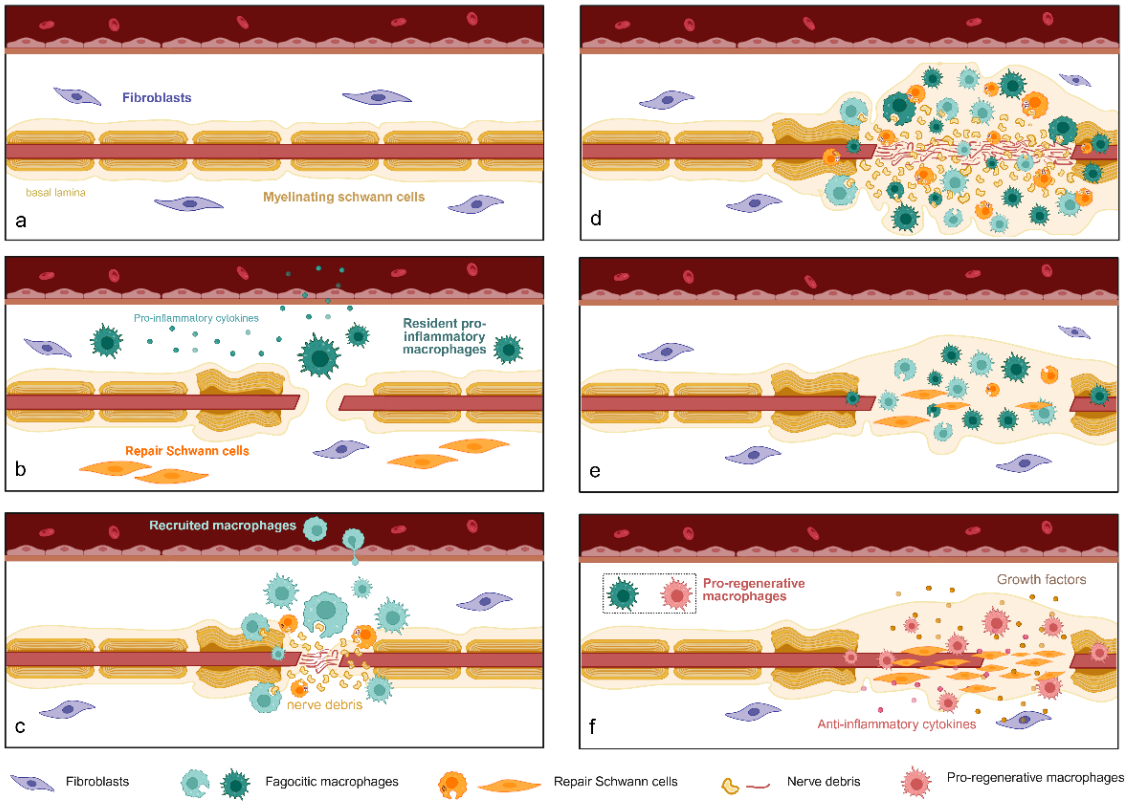

Figure 4. Schematic representation of the Wallerian degeneration in a peripheral nerve following axonal injury. (a) A single intact axon is shown under homeostatic conditions, surrounded by myelinating Schwann cells, interspersed fibroblasts, endothelial cells and an intact basal lamina. (b) Within the first 24 hours after injury, resident macrophages initiate a local pro-inflammatory response by releasing inflammatory cytokines, which both drive the phenotypic switch of myelinating Schwann cells into repair Schwann cells that begin to dedifferentiate and dismantle their myelin sheaths, and promote the recruitment of circulating macrophages. (c) Between 24 and 48 hours post-injury, blood-derived macrophages massively infiltrate the damaged nerve and, together with Schwann cells, phagocytose myelin and axonal debris, making the disintegration of the axon and myelin increasingly evident. (d) During the peak degenerative phase (48–72 hours), debris clearance continues with intense phagocytic activity by macrophages and Schwann cells. (e, f) At later stages, as debris are removed and tissue homeostasis begins to be restored, Schwann cells that previously adopted a phagocytic role realign along the basal lamina to form Bands of Bügner, which provide guidance for regrowing axons while releasing growth factors that support regeneration; in parallel, macrophages progressively acquire a pro-regenerative phenotype and secrete anti-inflammatory cytokines to consolidate a regenerative milieu. (Created in Biorender by Marina Pujol-Masip)

Schwann cell transcriptional reprogramming

In parallel with axonal and myelin breakdown, Schwann cells initiate a profound transcriptional reprogramming that converts them from myelinating cells into repair-supportive cells (Jessen & Mirsky, 2016). Schwann cells downregulate myelin-associated genes such as myelin protein zero (MPZ), peripheral myelin protein 22 (PMP22) and myelin basic protein (MBP) and undergo dedifferentiation and proliferation to increase their numbers within the denervated nerve stump (Stoll & Müller, 1999; Jessen & Mirsky, 2016).

This transcriptional reprogramming is orchestrated primarily by the rapid and sustained upregulation of the transcription factor c-Jun, which is detected within hours of nerve injury and remains elevated in denervated Schwann cells throughout the regenerative period (Arthur-Farraj et al., 2012). c-Jun acts as a master regulator that both suppresses the myelin programme by directly repressing myelination-promoting transcription factors including Krox-20 (Egr2) and Oct-6 (Pou3f1) and activates a comprehensive repair-associated gene expression programme (Arthur-Farraj et al., 2012; Fontana et al., 2012).

c-Jun directly activates the transcription of neurotrophic factors (GDNF, BDNF, artemin, LIF), cytokines and chemokines, trophic receptors ($p75^{NTR}$, GDNF family receptor alpha 1), and molecules involved in Schwann cell proliferation, migration and guidance of regenerating axons (Arthur-Farraj et al., 2012; Fontana et al., 2012; (Jessen & Mirsky, 2016). Genetic ablation of c-Jun specifically in Schwann cells results in severely impaired nerve regeneration, increased neuronal death, reduced Schwann cell proliferation and failed activation of repair-associated genes, demonstrating the indispensable role of c-Jun in orchestrating the Schwann cell response to injury (Arthur-Farraj et al., 2012). c-Jun-mediated transcriptional changes are sustained through autocrine signalling loops involving neuregulin-1, endothelin and other factors that maintain the repair phenotype during chronic denervation (Jessen & Mirsky, 2022). Additional transcription factors including Sox2, Notch pathway components, Pax3 and Runx2 also contribute to the establishment and maintenance of the repair Schwann cell state, and recent studies have revealed extensive epigenetic remodelling,

including changes in histone modifications and chromatin accessibility at injury-induced enhancers, that underpin the stable activation of the repair programme (Jessen & Mirsky, 2016; Ramesh et al., 2022; He et al., 2025).

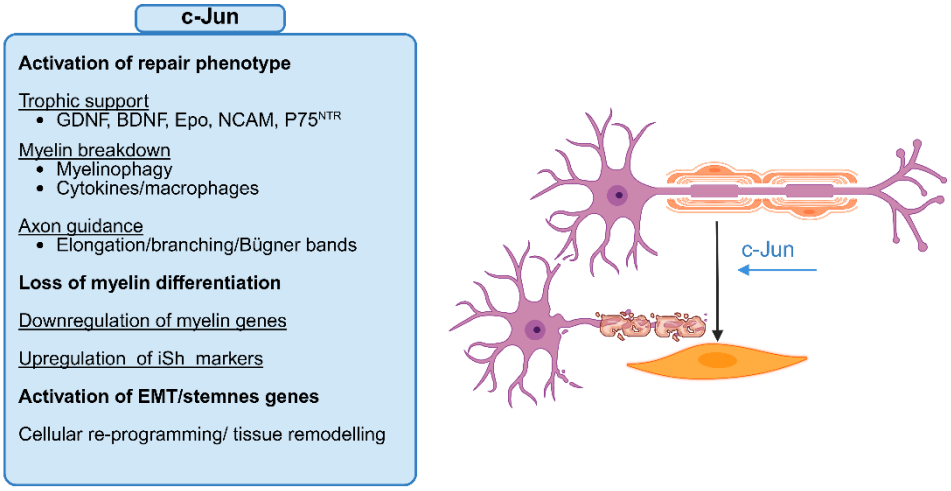

Figure 5. Role of c-Jun in the reprogramming of Schwann cells to a repair phenotype after nerve injury. c-Jun upregulation in Schwann cells promotes trophic support (for example via GDNF, BDNF, Epo, NCAM and $p75^{NTR}$), drives myelin breakdown through myelinophagy and macrophage recruitment, and contributes to axon guidance by supporting elongation, branching and the formation of Bügner bands. In parallel, c-Jun induces loss of myelin differentiation by downregulating myelin genes, upregulating immature Schwann cell markers, and activating EMT- and stemness-associated genes, leading to cellular reprogramming and tissue remodelling that favours axonal regeneration. (Adapted from (Jessen & Mirsky, 2022), created with Biorender)

By approximately 48–72 hours post-injury, proliferating Schwann cells reorganise longitudinally to form *Bügner bands*, aligned tubes of basal lamina and Schwann cells that provide structural guidance channels for regenerating axons (Stoll & Müller, 1999).

Innate immune response: recruitment and polarisation of macrophages

IL-1β, produced by Schwann cells and macrophages, promotes Schwann cell de-differentiation through activation of c-Jun and the activator protein-1 (AP-1) complex, upregulating the repair phenotype marker p75 neurotrophin receptor ($p75^{NTR}$) and downregulating myelin-associated genes (G. Chen et al., 2019). IL-6, expressed in a biphasic pattern with early Schwann cell-derived and later macrophage-derived peaks,

functions both as a pro-inflammatory mediator and as a modulator of the transition to anti-inflammatory states (Gaudet et al., 2011). Schwann cells and macrophages express toll-like receptors (TLRs), particularly TLR2 and TLR4, which recognise damage-associated molecular patterns released from degenerating axons and myelin, activating intracellular signalling cascades involving nuclear factor-kappa B (NF-κB) and mitogen-activated protein kinases (MAPKs) that drive the expression of pro-inflammatory cytokines and chemokines such as monocyte chemoattractant protein-1 (MCP-1 or CCL2) (Gaudet et al., 2011; Boivin et al., 2007).

Macrophages infiltrate the distal nerve stump from the circulation over the first one to two weeks following injury, reaching peak numbers by 7–14 days post-injury (Stoll & Müller, 1999; Gaudet et al., 2011). During the early post-injury period, macrophages predominantly adopt a pro-inflammatory phenotype, secreting pro-inflammatory mediators including nitric oxide (NO), reactive oxygen species (ROS) and matrix metalloproteinases, and actively phagocytosing myelin debris through receptor-mediated pathways involving complement receptors (CR3), scavenger receptors and galectin-3 (Stoll & Müller, 1999; P. Chen et al., 2015). Galectin-3 (MAC-2), a β-galactoside-binding lectin, is strongly upregulated in activated macrophages and Schwann cells during Wallerian degeneration and plays a critical role in promoting myelin phagocytosis by activating intracellular signalling pathways including Ras/PI3K and by modulating actin cytoskeleton dynamics (Rotshenker et al., 2008; Reichert & Rotshenker, 2019). The clearance of axonal and myelin debris is essential for removing inhibitory myelin-associated molecules such as myelin-associated glycoprotein (MAG) and Nogo, which would otherwise impede regenerating axon growth (Stoll & Müller, 1999).

Temporal resolution: from pro-inflammatory to anti-inflammatory states

Between 7 and 14 days post-injury, the inflammatory milieu in the distal nerve stump shifts from a predominantly pro-inflammatory to an anti-inflammatory and tissue-reparative phenotype (Gaudet et al., 2011; Rotshenker, 2011). This transition is characterised by macrophage polarisation from pro-inflammatory to alternatively resolutive/anti-inflammatory phenotypes, which secrete anti-inflammatory cytokines

including interleukin-10 (IL-10) and transforming growth factor beta (TGF-β), and express surface markers such as arginase-1 and CD206 (P. Chen et al., 2015; Mokarram et al., 2012). IL-10, which is produced at low levels by resident fibroblasts early after injury but at much higher levels by recruited macrophages beginning around day 7, acts to downregulate the production of pro-inflammatory cytokines including TNF-α and IL-1β, thereby resolving the inflammatory response (Rotshenker, 2011). By 14–21 days post-injury, most myelin debris has been cleared from the distal stump, macrophage numbers begin to decline, and the cytokine network returns towards baseline (Stoll & Müller, 1999; Rotshenker, 2011).

Resolutive macrophages support nerve regeneration by releasing neurotrophic factors such as nerve growth factor (NGF), brain-derived neurotrophic factor (BDNF) and vascular endothelial growth factor (VEGF), promoting Schwann cell proliferation and migration, and facilitating angiogenesis and extracellular matrix remodelling (Chen et al., 2015; Gaudet et al., 2011). Schwann cells themselves secrete a broad repertoire of neurotrophic and neurotropic factors including glial cell-derived neurotrophic factor (GDNF), artemin and leukaemia inhibitory factor (LIF), establishing a trophic environment that supports axonal elongation and guidance (Stoll & Müller, 1999; Jessen & Mirsky, 2016).

2.4.2 Neuronal Changes

One of the most prominent morphological changes observed in the soma of axotomized neurons is chromatolysis, characterised by dispersal of Nissl bodies due to disintegration of the rough endoplasmic reticulum, together with elevated RNA and protein levels (Hanz and Fainzilber 2006; Abe and Cavalli 2008; Allodi et al., 2012). Neurons also undergo intense genetic changes after injury.

During embryonic development, neurons display a strong intrinsic growth capacity that is progressively repressed towards adulthood to allow stable synaptic maturation. After a peripheral nerve lesion, however, injured neurons switch from a “transmitting” to a “growing” state, undergoing a genetic reprogramming that promotes the expression of growth-associated factors (Allodi et al., 2012).

The signals that initiate and sustain the switch of neurons to a pro-regenerative program arise through a series of partially overlapping mechanisms that unfold in a temporally ordered manner (Figure 6) (Allodi et al., 2012). A burst of action potentials at the lesion site and the disruption of axonal transport are key elements in triggering the growth programme (Hanz and Fainzilber 2006; Patodia and Raivich 2012; Allodi et al., 2012). Immediately after axotomy, membrane disruption combined with the opening of voltage-dependent Na^+ channels and inversion of the Na^+/Ca^{2+} pump promotes an intense Ca^{2+} influx at the lesion site. A Ca^{2+} wave then propagates towards the soma, further amplified by Ca^{2+} release from the endoplasmic reticulum. This Ca^{2+} signal plays a crucial role in the earliest stages of regeneration by activating downstream signalling cascades (Abe & Cavalli, 2008).

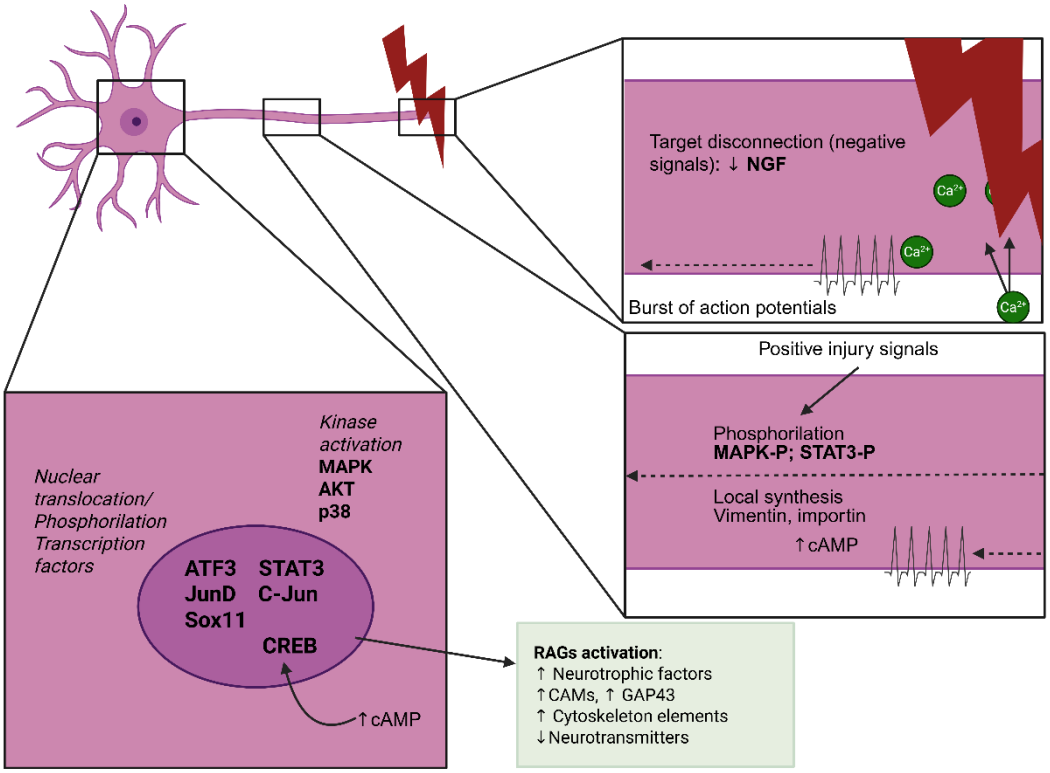

Figure 6. In response to axonal injury, signals generated at the lesion site reach the soma and shift the neuron into a pro-regenerative state, characterised by activation of multiple transcription factors. Three main signalling mechanisms are involved: a burst of action potentials produced by the lesion, the loss of normal retrograde transport of trophic molecules from the target (negative signals, such as reduced NGF), and the retrograde transport of phosphorylated proteins, including MAPK and STAT3, which act as positive injury signals. Together with locally induced changes such as increased cAMP and local synthesis of proteins like vimentin and importin, these pathways drive nuclear translocation and activation of transcription factors (ATF3, JunD, Sox11, STAT3, c-Jun, CREB), leading to the expression of

regeneration-associated genes (RAGs) that enhance the production of GAP43, BDNF, other neurotrophic factors, cell-adhesion molecules, cytoskeletal components, and neurotransmitters. (Adapted from (Allodi et al., 2012), created with Biorender)

Retrograde Injury Signalling

Retrograde injury signalling comprises a rapid electrophysiological response at the lesion site, followed by the generation and retrograde transport of specific signalling complexes that convey information about the presence and severity of axonal damage to the neuronal soma (Hanz and Fainzilber 2006; Abe and Cavalli 2008; Patodia and Raivich 2012).

Initial lesion signals and importins

Axonal injury induces a rapid ionic influx that triggers electrophysiological changes propagating retrogradely, providing the earliest indication of damage to the cell body. Subsequently, there is a marked reduction in retrogradely transported trophic factors, such as the approximately ten-fold decrease in nerve growth factor (NGF) after sciatic nerve axotomy, suggesting that trophic factor deprivation itself acts as an injury signal. In parallel, a second phase is characterised by the *de novo* appearance of activated or modified proteins generated at the lesion site, many of which gain access to retrograde transport via nuclear localisation signal (NLS)-binding importin complexes (Hanz & Fainzilber, 2006).

Classical NLS-dependent nuclear import relies on importin α, which binds NLS-containing cargo, and importin β, which associates with importin α and mediates translocation of the complex through the nuclear pore (Hanz & Fainzilber, 2006). In peripheral axons, several isoforms of importin α are constitutively present and associated with dynein, whereas importin β protein is largely absent under basal conditions but its mRNA is locally translated after injury, enabling assembly of importin α/β heterodimers on the retrograde motor (Hanz and Fainzilber 2006; Ben-Yaakov et al., 2012). Local activation of NLS-bearing signalling proteins within injured axons generates high-affinity cargo that binds the importin α/β complex and enters the retrograde transport pathway towards the soma (Hanz & Fainzilber, 2006). Notably, the

importin β1 isoform is the critical form locally synthesised in response to injury, and its function is indispensable for retrograde transport of key signalling molecules such as the transcription factor STAT3 (Ben-Yaakov et al., 2012).

Vimentin–Erk complex and importin-dependent transport

Proteomic analyses identified type III intermediate filaments as prominent components of retrogradely transported injury signals. In injured sciatic nerve, vimentin fragments arise in the axoplasm through local translation and calpain-mediated cleavage. Concurrent phosphorylation of Erk1/2 produces a signalling complex in which phosphorylated Erk binds directly to vimentin, which in turn interacts with importin β, thereby linking activated Erks to importin-dependent retrograde transport. This calcium-dependent interaction encodes both the occurrence and extent of injury in relation to sustained calcium elevation at the lesion site. (Hanz & Fainzilber, 2006).

Transcription factors as retrograde signals

Several transcription factors have been detected in peripheral axons and are proposed to contribute to retrograde injury signalling. Following peripheral nerve axotomy, levels of the cytokines leukaemia inhibitory factor (LIF) and interleukin-6 (IL-6) and the neurotrophic factor CNTF increase, activating the JAK–STAT3 pathway and making axonal phosphorylated STAT3 a strong candidate retrograde injury signal (Hanz & Fainzilber, 2006). Recent work has established that axonal STAT3 is locally translated in sensory axons and, upon injury, becomes phosphorylated and activated (Ben-Yaakov et al., 2012). Phosphorylated STAT3 associates with dynein in the axoplasm and is transported retrogradely to the neuronal cell body, where it accumulates in the nucleus and modulates neuronal survival responses. Importantly, retrograde transport of STAT3 is mediated by its interaction with importin α5, linking activated STAT3 directly to the importin-dependent transport pathway (Ben-Yaakov et al., 2012). Additional data indicate that activating transcription factors ATF2 and ATF3 are also transported retrogradely after sciatic nerve lesion, although it remains

unresolved whether their retrograde transport is mediated by axonal importins (Hanz & Fainzilber, 2006).

Kinase-based retrograde signalling and alternative linkages

Multiple kinases have been implicated as components of retrograde injury signalling complexes, including Erk1/2, p38 MAPK and JNK, which become activated in lesioned sciatic nerve. Phosphorylated Erk is retrogradely transported via the vimentin–importin pathway, whereas phosphorylated JNK travels retrogradely in association with JNK-interacting scaffold proteins (JIPs) and upstream kinases. Most of these kinases lack a classical NLS and are therefore unlikely to bind importin α directly, implying the existence of alternative mechanisms for their linkage to retrograde transport, as exemplified by the vimentin-dependent mechanism for phospho-Erk (Hanz & Fainzilber, 2006).

Recent work has revealed a complementary pathway for JNK signalling in which JIP scaffold proteins, previously shown to interact with kinesins, also participate in forming vesicular complexes containing activated JNK and the scaffold protein Sunday driver (Syd) in injured axons. These vesicles undergo retrograde transport through the association of Syd with the dynactin complex, suggesting that JNK–Syd and Erk–vimentin–importin assemblies may use distinct interfaces on dynein, thereby providing multiple, non-exclusive docking sites for injury-related signals on the retrograde motor machinery (Figure 7). This molecular diversity within retrograde injury signalling complexes likely underpins the capacity of different neuronal populations and injury paradigms to encode and convey rich, context-specific information about axonal damage to the neuronal soma (Hanz & Fainzilber, 2006).

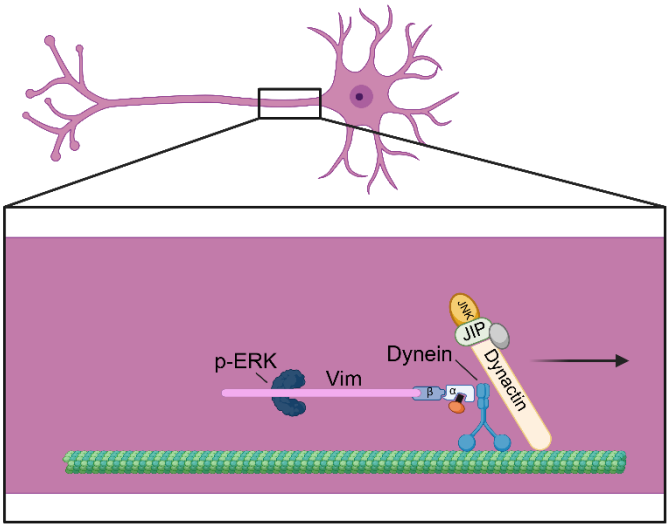

Figure 7. Multiple mechanisms allow retrograde injury signals to couple to the dynein motor complex. Importin α binds directly to dynein and, upon association with importin β, generates a high-affinity docking site for cargo proteins that contain a nuclear localisation signal (NLS). Phosphorylated Erk (pErk1/2) can associate with this complex indirectly by binding to vimentin, which in turn interacts with importin β, whereas Jnk and its associated proteins attach to a separate site in a dynactin-dependent manner. Abbreviations: Vim, vimentin; pERK, phosphorylated Erk1 or Erk2; β, importin β; α, importin α; NLS, cargo protein containing a nuclear localisation signal; D, dynein; Jnk, c-Jun N-terminal kinase; JIP, Jnk-interacting protein. (Adapted from (Hanz & Fainzilber, 2006), created with Biorender)

Neuronal cell body responses and RAG expression

The retrograde signalling response to axonal injury triggers profound alterations in cellular signalling, gene transcription, protein synthesis and post-translational modifications within the neuronal soma (Hanz & Fainzilber, 2006). Several kinases become activated in the cell body, including Erk1/2 and JNK, and there is a marked increase in Janus kinase (JAK) activity together with a regeneration-enhancing elevation of intracellular cyclic adenosine monophosphate (cAMP) (Hanz and Fainzilber 2006; Abe and Cavalli 2008). These kinase-mediated events activate downstream transcription factors such as c-Jun, JunD, Fos, ATF3, STAT3, P311, Sox11 and C/EBPβ, which together drive a broad RAG programme (Hanz and Fainzilber 2006; Ben-Yaakov et al. 2012).

As a result, growth-associated proteins including GAP-43, CAP-43 and small proline-rich repeat protein 1a (Sprr1a), as well as structural proteins like actin and tubulin, neuropeptides and neurotrophic growth factors, are upregulated. In contrast, developmental proteins such as neurofilament subunits and neurotransmitter-synthesising enzymes are typically downregulated. Axotomized neurons thus

downregulate mRNAs encoding proteins required for neurotransmission and upregulate those necessary to rebuild peripheral processes. Actin, tubulin and the growth-associated protein GAP-43 are rapidly overexpressed following lesion (Figure 8). Collectively, these changes reprogramme the neuronal soma from a state specialised for synaptic transmission and maintenance to one optimised for vigorous axonal outgrowth and regenerative capacity (Hanz & Fainzilber, 2006). This upregulation of RAGs, however, is not maintained permanently in either neurons or Schwann cells (Figure 8 b, c) (Sulaiman & Gordon, 2013).

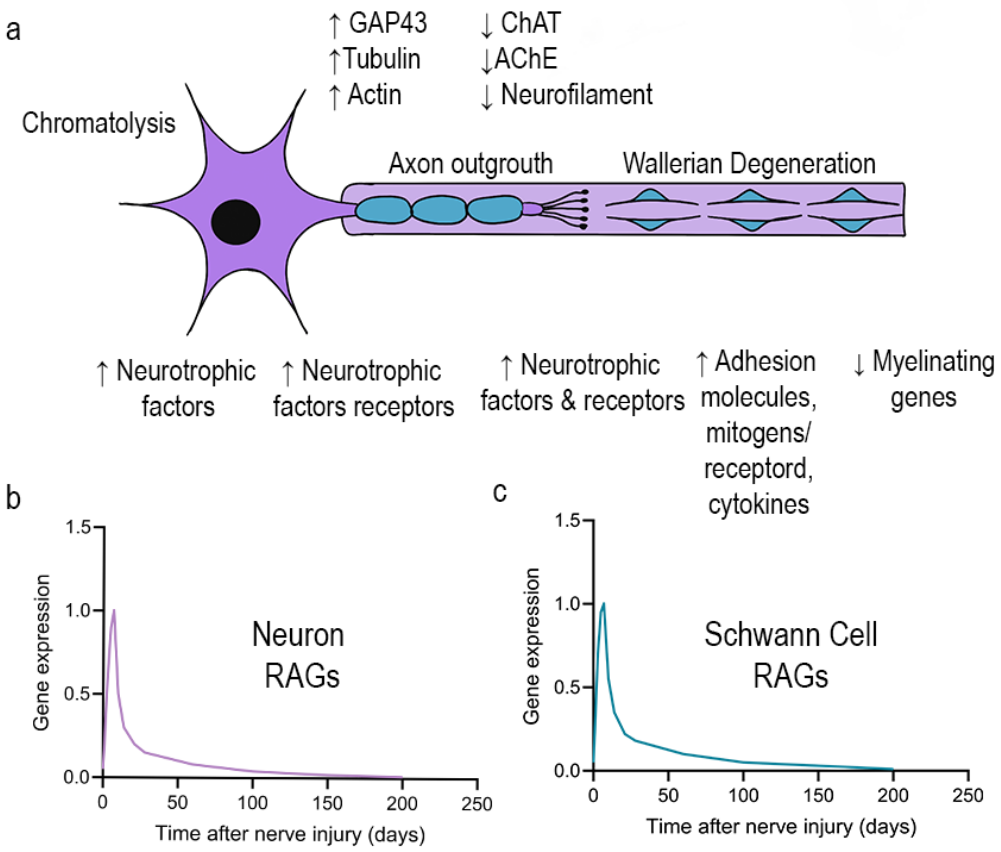

Figure 8. After a nerve injury, regeneration associated genes (RAGs) are upregulated transiently in the neurons while genes associated with normal synaptic transmission are downregulated (a and b). c. Schwann cells in the denervated nerve stump undergo proliferation during Wallerian Degeneration and express many RAGs while myelin-associated genes are downregulated. (Adapted from Sulaiman and Gordon 2013)

Key Transcription Factor Networks Regulating Regeneration

c-Jun and AP-1 signalling. The activator protein 1 (AP-1) transcription complex, consisting of homo- or hetero-dimeric complexes between members of the Jun, c-Fos and activating transcription factor (ATF)/cAMP response element binding protein (CREB) families, is a well-characterised regulator of neural development. c-Jun is produced as an immediate early gene following nerve injury and persists at high levels in injured neurons throughout the peripheral regenerative process. In mature neurons, c-Jun promotes axonal regeneration and outgrowth, accelerates regeneration velocity and functional recovery, and supports neuronal survival. Therefore, it plays a similar role than in denervated Schwann cells, favouring the creation of a permissive distal environment for axonal growth (*section 2.4.1 Wallerian degeneration*) but contrast with the pro-apoptotic role of c-Jun in postnatal injured neurons (*section 2.3.1 Mechanisms of Neuronal Death*)

c-Jun operates within an interconnected regulatory network: it interacts with NF-κB and JAK-STAT pathways to phosphorylate STAT3, whilst STAT3 reciprocally enhances AP-1 transcriptional activity. Furthermore, c-Jun cooperates with C/EBPβ and C/EBPδ to coordinately regulate regeneration-associated genes including GAP-43 (Patodia & Raivich, 2012 Allodi et al., 2012; Mahar and Cavalli 2018).

ATF3. ATF3 is a member of the ATF/CREB family of basic leucine zipper domain transcription factors. Normally expressed at low levels, ATF3 is rapidly activated in sensory, sympathetic and motor neurons following peripheral nerve injury, as well as in disconnected Schwann cells and endoneurial fibroblasts distal to the injury site. ATF3 enhances both the number of neurons extending neurites and the length of individual neurites and exerts important survival functions by preventing JNK-mediated neuronal death. Critically, ATF3 forms functional hetero-dimers with c-Jun, an interaction that leads to enhanced transcriptional activation of regeneration-associated genes and substantially increased neurite outgrowth (Patodia and Raivich 2012; Allodi et al., 2012; Mahar and Cavalli 2018).

STAT3. The functional significance of retrograde STAT3 transport has been demonstrated through multiple experimental approaches. Reduction of STAT3 expression in DRG neurons results in marked increases in neuronal apoptosis following peripheral nerve injury, an effect that can be rescued by re-expression of constitutively active STAT3. Interference with STAT3 retrograde transport significantly increases the fraction of dying neurons in the DRG, highlighting the critical anti-apoptotic role of axonally synthesised and retrogradely transported STAT3. STAT3 may contribute to the survival of motoneurons through the activation of motoneuron survival factors such as Reg-2 and B-cell lymphoma extra-large (Bcl-xl) (Abe and Cavalli 2008; Patodia and Raivich 2012; Mahar and Cavalli 2018).

Sox11 and other factors. Sox11 is expressed at high levels during development and in regenerating sensory neurons, where it regulates neurite outgrowth and cell survival. Additional transcription factors such as CREB, which mediates cAMP signalling through homo- or hetero-dimerisation with other basic leucine zipper factors, contribute to the regenerative response (Abe and Cavalli 2008; Patodia and Raivich 2012; Mahar and Cavalli 2018).

Activation of these transcription factors will lead to changes in gene expression of the injured and regenerating neurons, with an increase of actin, growth associated tubulin isotypes and growth associated protein GAP-43, and a decrease of neurofilament proteins, ion channels and proteins involved in the neurotransmission machinery (Allodi et al., 2012).

mTor: Activation of the mTOR pathway is essential for the growth capacity of peripheral neurons. It increases the levels of GAP-43 after injury (Allodi et al., 2012). mTOR is also another possible regulator of the JAK/STAT pathway, that promotes axon regeneration.

2.4.3 The growth cone

Following peripheral nerve injury, regenerating axons extend new growth cones at their tips, which act as specialised sensory–motile structures that explore the

environment and convert extracellular cues into directed axonal elongation. The growth cone comprises three distinct structural domains defined by their cytoskeletal composition and dynamic properties (Dent and Gertler 2003; Lowery and Vactor 2009). The peripheral (P) domain forms a flattened, veil-like expansion at the leading edge of the growth cone, termed the lamellipodium, from which numerous thin, finger-like protrusions called filopodia extend several micrometres beyond the growth cone margin (Dent, Gupton, and Gertler 2011; Vitriol and Zheng 2012). The P-domain is enriched in highly dynamic actin filaments (F-actin) organised into both branched networks within lamellipodia and parallel bundles within filopodia (Fan et al. 1993; Schaefer et al. 2008). The central (C) domain occupies the core region of the growth cone and contains stable bundled microtubules extending from the axon shaft, numerous organelles including mitochondria and vesicles, and central actin bundles (Lowery and Vactor 2009; Vitriol and Zheng 2012). The transition (T) zone lies at the interface between the P- and C-domains and is characterised by actomyosin contractile structures termed actin arcs, which form a hemicircumferential ring perpendicular to F-actin bundles (Schaefer et al. 2008; Vitriol and Zheng 2012). (Figure 9)

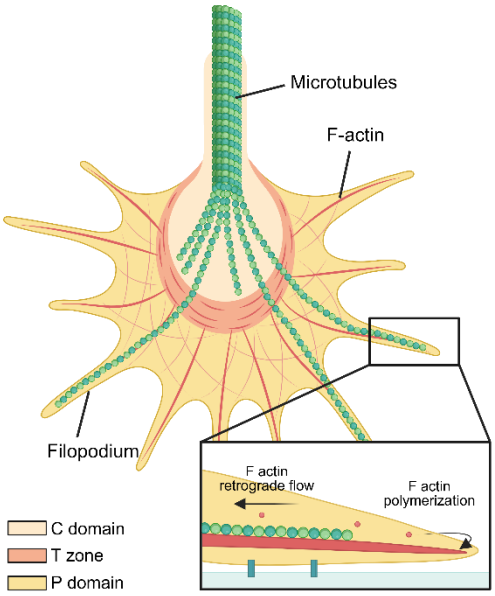

Figure 9: The growth cone can be divided into three regions: the central domain (C), the transition zone (T), and the peripheral domain (P). Actin filaments (F-actin) are concentrated in the T and P domains, where they extend to form filopodia, while microtubules are mainly located in the C domain but project into the P domain along F-actin bundles. During axonal elongation, the growth cone forms adhesive contacts with the substrate that steer and support axonal regeneration. (Adapted from (Bolívar Martín, 2023) Created with Biorender)

Growth Cone Formation After Injury

After axotomy, a rapid Ca^{2+} influx at the lesion site, combined with transient local activation of calpain and other Ca^{2+} dependent enzymes, drives membrane

resealing and the transformation of the distal axon stump into a new growth cone (Gitler and Spira 1998; Bradke, Fawcett, and Spira 2012). The phosphorylation state of axonal proteins critically influences growth cone formation, as inhibition of protein kinase C and tyrosine kinases markedly impairs this process (Geddis & Rehder, 2003).

Cytoskeletal Dynamics and Axon Extension

Axon elongation is driven by coordinated actin and microtubule dynamics that proceed through three overlapping stages: protrusion, engorgement and consolidation (Dent and Gertler 2003; Schaefer et al. 2008). During protrusion, polymerisation of F-actin at the leading edge extends lamellipodia and filopodia, whilst retrograde flow generated by membrane tension and myosin II–dependent contractility is partially resisted at adhesion sites, permitting net forward advance through a "molecular clutch" mechanism (Suter and Forscher 2000; Gomez and Letourneau 2014). In the engorgement phase, dynamic microtubules invade protrusive regions and stabilise selected protrusions; subsequent bundling and alignment of these microtubules underlie consolidation into new axon segments (Schaefer et al. 2008; Cammarata, Bearce, and Lowery 2016).

Growth Cone Guidance and Turning

Growth cone guidance depends on the integration of attractive and repulsive extracellular cues such as netrins, semaphorins, ephrins and slits, which signal through distinct receptor complexes to bias cytoskeletal dynamics (Tessier-Lavigne and S. Goodman 1996; Kolodkin and Tessier-Lavigne 2011). Netrin-1 elicits attraction via DCC-containing receptors or repulsion via UNC5-containing complexes, whereas class 3 semaphorins such as Sema3A generally induce growth cone collapse and retraction through neuropilin/plexin receptors (G Culotti and C Merz 1998; Kolodkin and Tessier-Lavigne 2011). Intracellularly, members of the Rho family of small GTPases, Rac1 and Cdc42 promoting protrusion, and RhoA driving contractility and collapse, serve as central molecular switches coupling extracellular signals to local cytoskeletal remodelling (J Dickson, 2001).

Growth-Associated Protein 43 in Growth Cone Function

The membrane–associated growth–associated protein 43 (GAP-43) is highly enriched in growth cone membranes and serves as a widely recognised marker of active axonal growth (Skene et al., 1986). GAP-43 participates in growth cone motility by organising $PI(4,5)P_2$-rich membrane domains, interacting with neural cell adhesion molecules and modulating Ca^{2+}-dependent signalling (Chung et al., 2020). Phosphoproteomic studies demonstrate that JNK-dependent phosphorylation of GAP-43 at serine 96 is strongly associated with both developmental axon elongation and peripheral nerve regeneration, providing a molecular readout of active growth cone–mediated regrowth (Kawasaki et al., 2018). During peripheral nerve regeneration, Schwann cells secrete neurotrophic factors that support axonal regrowth and guidance, and regenerating growth cones respond to these signals by resuming outgrowth towards their targets (Abe & Cavalli, 2008).

2.5 Preferential regeneration

Peripheral neurons are capable of structural regeneration after injury, but functional recovery critically depends on the precision with which regenerating axons reconnect with their original targets (Robinson & Madison, 2005; Brushart, 1993). When target reinnervation is inaccurate, even robust axonal regrowth can result in poor motor control, sensory dysfunction and maladaptive plasticity, underscoring that *specificity* is as important as growth per se (Irintchev, 2011; Bolívar & Udina, 2022).

2.5.1 Preferential Motor Reinnervation

Preferential motor reinnervation (PMR) describes the propensity of regenerating motor axons to re-enter motor pathways and reinnervate muscle, rather than inappropriate cutaneous branches, when given equal access to both options (Brushart, 1988; 1990; 1993). The rat and mouse femoral nerve provide an especially powerful model to study this process, as proximally motor and sensory fibres run together, whereas distally they segregate into a pure motor branch to quadriceps and a purely cutaneous saphenous branch (Figure 10), offering an unbiased choice between

muscle and skin pathways after repair (Brushart, 1988; G. A. Robinson & Madison, 2005; Madison et al., 1996). In this model, early after repair motor axons collateralise into both branches, but over time collaterals in cutaneous pathways are selectively pruned while those in the quadriceps branch are stabilised, yielding a majority of motoneurons correctly projecting to muscle (Brushart, 1990; Madison et al., 1996; Irintchev, 2011).

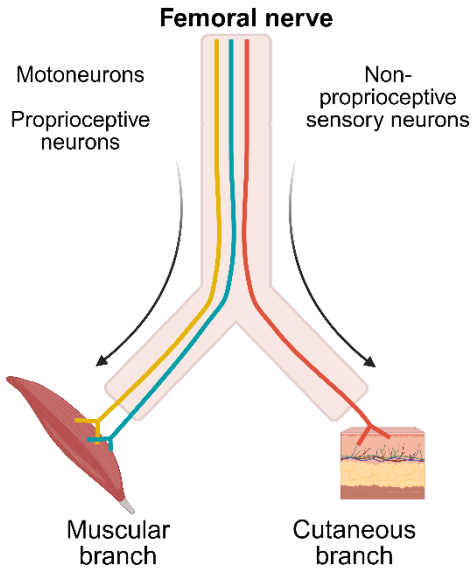

Figure 10: Schematic representation of the femoral nerve and its main branches. Motor and proprioceptive axons project through the muscular branch to innervate the quadriceps muscle, whereas non-proprioceptive sensory axons course through the cutaneous branch to innervate the skin.

Quantitative studies in rodents have shown that, within the first weeks after femoral nerve repair, similar numbers of motor axons can be detected in both muscle and cutaneous branches, whereas by 8–10 weeks approximately 60–70% of motoneurons project to the quadriceps branch and only 20–30% persist in the saphenous branch, with a minority maintaining collaterals in both (Irintchev, 2011). PMR is robust enough to be observed even when proximal and distal stumps are misaligned or separated by a short gap, indicating that it cannot be explained solely by mechanical alignment and likely reflects selective trophic, tropic and contact-dependent interactions within motor pathways (Brushart, 1988; Madison et al., 1996; Brushart, 1993). Nonetheless, this phenomenon is not absolute: under some experimental conditions motor axons can preferentially reinnervate skin, and the strength of PMR is modulated by species, age, lesion level and repair strategy (Robinson, 2004; Robinson & Madison, 2006; Robinson & Madison, 2003).

2.5.2 Sensory Specificity and Heterogeneity

In contrast to the relative clarity of "correct" versus "incorrect" targets for motoneurons, sensory neurons represent a highly heterogeneous population, including proprioceptors, low-threshold mechanoreceptors and nociceptors, which are normally distributed across both muscle and cutaneous branches (Bolívar & Udina, 2022). As a result, there is no single anatomically defined "appropriate" distal pathway for most dorsal root ganglion (DRG) neurons, making it more challenging to define and quantify preferential sensory regeneration compared with PMR (Madison et al., 1996; Bolívar & Udina, 2022). Proprioceptive afferents, which innervate muscle spindles and Golgi tendon organs and are characterised by large, heavily myelinated cell bodies often expressing parvalbumin in rodents, provide one of the few sensory subpopulations for which muscle-directed regeneration can be specifically tracked (Madden et al., 2020; Bolívar & Udina, 2022).

Anatomical studies using the femoral nerve model have demonstrated that, like motoneurons, muscle afferents projecting to quadriceps show a significant tendency to reinnervate their original muscle branch over the cutaneous branch after transection, providing evidence for target-specific sensory regeneration (Madison et al., 1996). Moreover, the accuracy of sensory reinnervation was highly correlated with that of motor fibres in the same animals, suggesting that both populations respond in parallel to shared guidance cues within motor pathways (Madison et al., 1996; Bolívar & Udina, 2022). However, other models and nerve territories often reveal substantial sensory misrouting and non-specific reinnervation, indicating that sensory specificity is more fragile and context-dependent than PMR and may vary markedly between sensory subtypes (Robinson & Madison, 2005; Khan et al., 2023).

2.5.3 Developmental Influences on Regenerative Specificity

Developmental stage exerts a profound influence on the accuracy of peripheral nerve regeneration. In neonatal mammals, several models have shown remarkably precise muscle reinnervation after facial or limb nerve transection, with near-restoration of original motor unit patterns despite substantial neuronal loss, implying

that immature motor axons are guided with high fidelity by developmental patterning cues and target-derived signals (Aldskogius & Thomander, 1986; Robinson & Madison, 2006). This high degree of target-specific regeneration is thought to reflect a permissive environment rich in diffusible and contact-mediated cues, as well as a more plastic and growth-competent intrinsic state of motoneurons and muscle afferents in early life (Aldskogius & Thomander, 1986; Irintchev, 2011).

With maturation, regenerative accuracy declines: adult animals show increased axonal misrouting, reduced PMR strength under some conditions, and greater dependence on surgical alignment and pathway integrity to achieve specific reinnervation (Robinson, 2004; Robinson & Madison, 2006; Brushart, 1993). These age-dependent changes highlight that specificity emerges from an interaction between intrinsic neuronal growth programmes, the molecular identity of Schwann cell pathways, and the trophic landscape of target tissues, all of which shift across development (Bolívar & Udina, 2022; Madison et al., 1996). Understanding how these factors cooperate to promote PMR and sensory specificity in neonatal and juvenile stages, and why they lose efficacy with age, is therefore crucial for designing strategies that enhance accurate reinnervation and functional recovery after peripheral nerve injury.

3. The paradigm of the postnatal stage

The postnatal period represents a unique paradigm for peripheral nerve regeneration, in which high intrinsic growth potential coexists with extreme vulnerability to neuronal death and developmental remodelling. During early life, lower motoneurons and sensory neurons retain a robust capacity to elongate axons and to reform functional connections, provided they survive the initial insult and encounter a permissive environment in the distal nerve stump (Allodi et al., 2012; Christie & Zochodne, 2013). At the same time, the peripheral nerve milieu is undergoing profound maturation, involving the transition of Schwann cells from an immature, proliferative phenotype to myelinating and repair-specialised states, and progressive refinement of synaptic and circuit connectivity (Jessen & Mirsky, 2016; Stoll & Müller, 1999). These converging processes make the postnatal stage a particularly informative window for

dissecting how intrinsic growth programmes, Wallerian degeneration, survival pathways and target specificity are coordinated in vivo.

Classical studies demonstrated that axotomy during the first postnatal days is followed by massive loss of spinal motoneurons, with susceptibility sharply declining as animals mature (Romanes, 1946; Schmalbruch, 1984; Li et al., 1998). Lesions close to the cell body or performed within the first week of life can result in the degeneration of more than half of the affected motoneuron pool, and more recent work has shown that early nerve injuries also induce substantial death of sensory neurons in dorsal root ganglia (Kemp, Chiang, et al., 2015; Kemp, Szynkaruk, et al., 2015). Proposed mechanisms include glutamate-mediated excitotoxicity, immaturity of postnatal Schwann cells and insufficient trophic support from denervated targets, all of which can tip the balance from regeneration towards apoptosis (Iwasaki et al., 1995; Komiyama & Suzuki, 1992). This high rate of neuronal loss has historically overshadowed the regenerative capacity of surviving postnatal neurons, despite evidence that, once they endure the acute post-lesion period, they can extend axons vigorously and contribute to meaningful functional recovery (Donnerer, 2003; Christie & Zochodne, 2013).

At the transcriptional level, mature peripheral neurons respond to axotomy by downregulating genes associated with synaptic transmission and upregulating a broad set of regeneration-associated genes (RAGs), including cytoskeletal, signalling and transcription factor modules that define a pro-regenerative state (He & Jin, 2016. However, this canonical RAG response might differ across ages or neuronal subtypes.

The postnatal stage is also critical for understanding how regenerative specificity emerges. Peripheral neurons regenerate structurally across the lifespan, but the accuracy with which regenerating axons reconnect with appropriate targets declines with age (Aldskogius & Thomander, 1986; Irintchev, 2011). In neonatal rats, facial nerve transection is followed by remarkably precise reinnervation of original muscle targets despite significant motoneuron loss, implying that immature motor axons are guided by strong intrinsic and extrinsic patterning cues (Aldskogius &

Thomander, 1986). PMR is also more marked in juvenile than adult rats (Brushart, 1988).

Taken together, these data position the postnatal period as a powerful paradigm to interrogate how survival, intrinsic growth state, Wallerian degeneration and target specificity are coordinated in motoneurons and defined sensory subpopulations. By systematically comparing injuries at P4, P10 and P30, and by analysing both motor and sensory neurons in models such as the sciatic and femoral nerves, this thesis aims to clarify whether early postnatal neurons rely on a fundamentally different regenerative programme, how this interacts with the maturation of Schwann cells and distal stumps, and to what extent developmental stage shapes the precision of reinnervation in both motor and sensory systems.

IV. Hypothesis and objectives

The general objective of this thesis is to determine the regenerative capacity of motor neurons and sensory neurons, as well as their ability to survive following peripheral injury at different postnatal stages (Postnatal Day 4, Postnatal Day 10, and Postnatal Day 30).

This work is based on the hypothesis:

1. Peripheral motor and sensory neurons exhibit greater regenerative capacity and more accurate target-specific reinnervation at postnatal stages compared to later stages, due to the activation of distinct genetic growth programmes following nerve injury.

To address this hypothesis, the thesis is structured into three chapters with the following specific objectives:

Chapter 1. Assessment of Motoneuronal Regeneration and Wallerian Degeneration Following Axotomy in Postnatal mice.

- To evaluate the survival capacity and axonal regenerative capacity of motoneurons after peripheral nerve injury at different postnatal stages (P4, P10 and P30) taking advantage of Chat-Cre/Ai9(RCL-tdT) mice.
- To analyse the translatome of motoneurons from mice injured at different postnatal stages (P4, P10 and P30) taking advantage of Chat-Cre/Ribotag mice.
- To characterize the histological dynamics of the Wallerian degeneration and the ultrastructural changes in the injured sciatic nerve of mice injured at P4, P10 and P30.
- To analyse the transcriptomic changes occurring at the distal portion of the sciatic nerve in mice injured at P4, P10 and P30.

Chapter 2. Outgrowth of Mouse Sensory Neurons is not Mediated by Regeneration Associated Genes in Early Postnatal Stages.

- To evaluate the survival capacity and axonal regenerative capacity of proprioceptive and nociceptive sensory neurons after peripheral nerve

injury at different postnatal stages (P4, P10 and P30) taking advantage of Pv-Cre/Ai9(RCL-tdT) and TrpU1-Cre/Ai9(RCL-tdT) mice.

- To analyse the transcriptomic changes of sensory neurons from mice injured at different postnatal stages (P4, P10 and P30).
- To assess whether a conditioning lesion applied at P4, P10 and P30 enhances neurite outgrowth in cultured sensory neurons.

Chapter 3. Age matters: Neuronal Subtype-specific Regeneration After Femoral Nerve Injury.

- To quantify and compare the regenerative capacity of motoneurons, proprioceptive and non-proprioceptive sensory neurons following femoral nerve injury and repair at P10 versus adulthood.
- To assess the specificity of target reinnervation of these neuronal populations, determining their preference for muscle versus cutaneous branches at P10 and adult stages.

V. Experimental design

Chapter 1. Assessment of motoneuronal regeneration and Wallerian Degeneration following axotomy in postnatal mice.

To evaluate how postnatal motoneurons react after a peripheral nerve injury we performed two sets of experiments. To evaluate the motoneuron survival and the axonal regeneration, we have performed a sciatic nerve crush to P4, P10 and P30 ChAT-Cre/Ai9 mice. 4-, 7- and 14-days post injury we have extracted the injured and contralateral sciatic nerves and the L3-L5 portion of the spinal cord. To calculate the % of surviving motoneurons, we have counted the number of motoneurons present in the ventral horn of the spinal cord. We have compared the ipsilateral side versus the contralateral one. To calculate the percentage of axons that have regenerated after the injury, 5 millimetres form the crush site we have counted the total number of axons regenerated and normalized versus the contralateral nerve. To analyse the translatome of the injured motoneurons, we have performed a crush injury in the sciatic nerve to P4, P10 and P30 ChAT-Cre/Ribotag mice. 7 days after the injury we have isolated the mRNA of the injured motoneurons and performed a RNAseq. We compared our results with age-matched animals.

To evaluate the dynamics of the Wallerian degeneration in the different postnatal stages, we have performed a sciatic nerve cut without repair to P4, P10 and P30 mice. Histological and ultrastructural analyses were performed 2, 4, 7 and 14 dpi in the injured and contralateral nerves. 4 dpi RNA was extracted from the injured and control sciatic nerves for further RNAseq analyses.

<table>
<tr><th colspan="2">Evaluation of motoneurons</th></tr>
<tr><td colspan="2">In vivo</td></tr>
<tr><td>Animals</td><td> 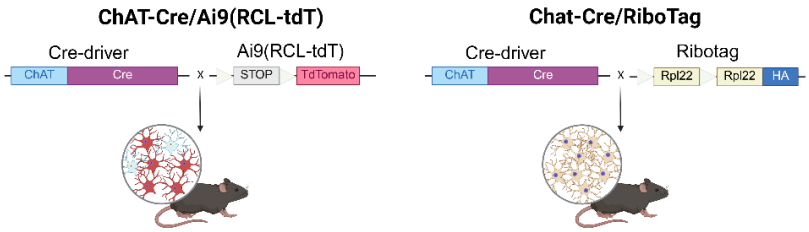
</td></tr>
<tr><td>Age</td><td>Postnatal 4, Postnatal 10, Postnatal 30</td></tr>
<tr><td>Experimental design</td><td> 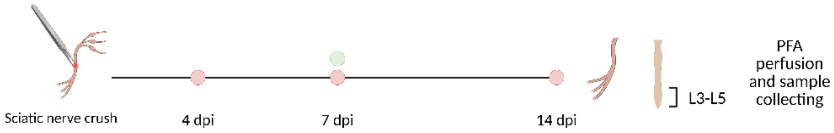
</td></tr>
<tr><td>Histological approach</td><td> 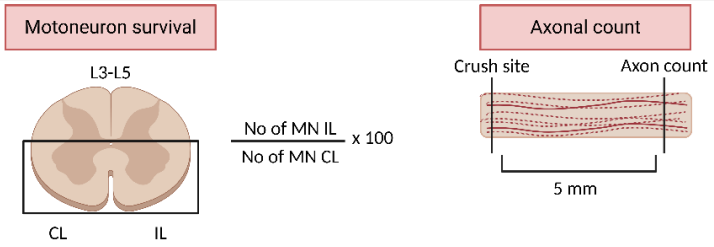
</td></tr>
</table>

Chapter 2. Outgrowth of Mouse Sensory Neurons is not Mediated by Regeneration Associated Genes in Early Postnatal Stages.

To evaluate how postnatal proprioceptive and nociceptive sensory neurons react after a peripheral nerve injury we performed two sets of experiments. To evaluate the neuronal survival and the axonal regeneration we have performed a sciatic nerve crush to P4, P10 and P30 PV-Cre/ Ai9 and TrpU1-Cre/Ai9 mice. 4-, 7- and 14-days post injury we have extracted the injured and control sciatic nerves and the L3-L5 DRGs. To calculate the percentage of neurons that have survived we counted the total number of tomato-positive cells present in the ipsilateral DRGs and compared it with the contralateral side for both proprioceptive and nociceptive neurons. To evaluate the percentage of axons that have regenerated, we counted the number of axons fully regenerated 5 millimetres from the crush site. To evaluate the transcriptome of the sensory DRGs, we have extracted the RNA 7 days after the injury from the ipsilateral and contralateral L3-L5 DRGs in the different postnatal stages. To evaluate if postnatal neurons do not need to activate a pro-regenerative program since they are already in an outgrowth state remanent from embryonic stages, we have evaluated the effects of a conditioning lesion *in vitro*. We have performed a sciatic nerve crush in P4, P10 and P30 WT mice. 7 dpi we have extracted the ipsilateral and contralateral L3-L5 DRGs, isolated the neurons and cultivated them for 24 hours. We have quantified the number and length of the neurites present to assess if injured neurons, being “conditioned”, grow better than uninjured ones.

Evaluation of sensory neurons	
In vivo	
Animals	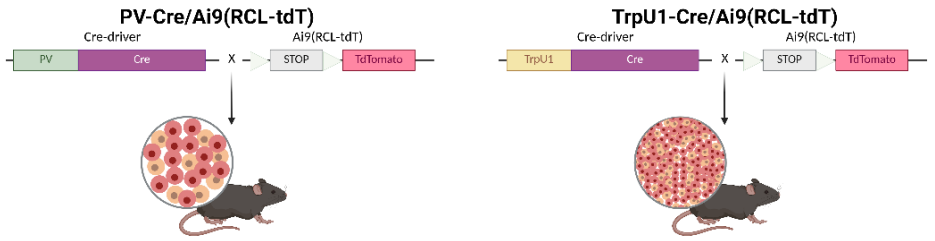
Age	Postnatal 4, Postnatal 10, Postnatal 30
Experimental design	
Histological approach	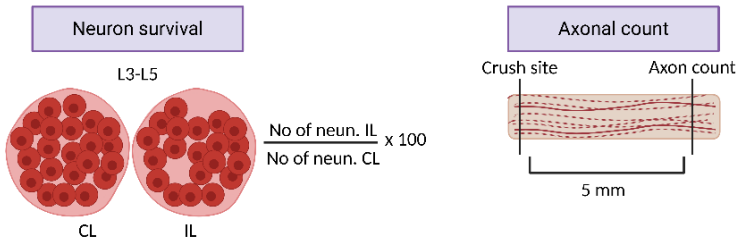
Transcriptomic analysis	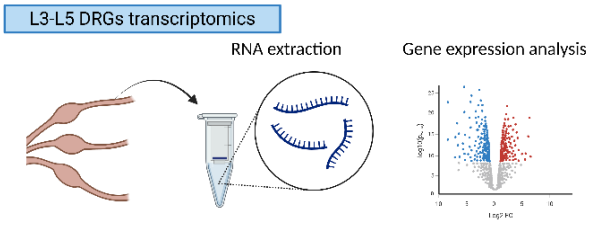

In vitro	
Animals	C57BL6/J mice
Age	Postnatal 4, Postnatal 10, Postnatal 30
Experimental design	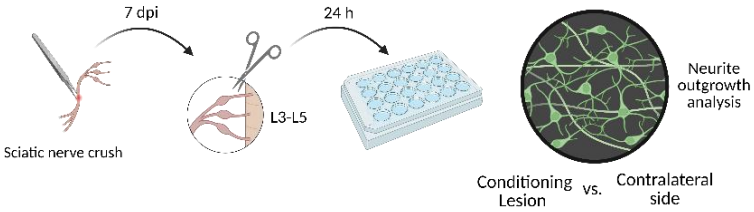

Chapter 3. Age matters: neuronal subtype-specific regeneration after femoral nerve injury.

To evaluate the preferential regeneration of motoneurons, proprioceptive neurons and non-proprioceptive sensory neurons, we have performed a femoral nerve cut with repair with fibrin glue at Pv-Cre/Ai9 P10 mice. 8 weeks after the injury we have applied retrograde tracers (Fluorogold and True Blue) in the muscular and cutaneous branch to evaluate the specific regeneration of these neuronal groups. 1 week after the retrograde tracers application we have extracted the Lumbar portion of the spinal cord and the L3-L5 DRGs, both ipsilateral and contralateral to evaluate the regeneration. We have compared our results with results previously obtained in our laboratory of adult animals (Bolívar & Udina, 2022).

<table>
<tr><th colspan="2">Evaluation of preferential reinnervation</th></tr>
<tr><td colspan="2">In vivo</td></tr>
<tr><td>Animals</td><td> 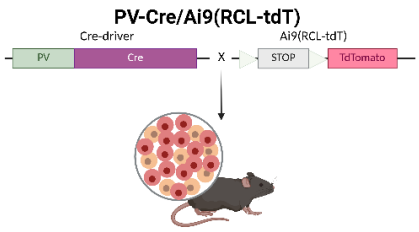
</td></tr>
<tr><td>Age</td><td>Postnatal 10, Adults (3m)</td></tr>
<tr><td>Experimental design</td><td> 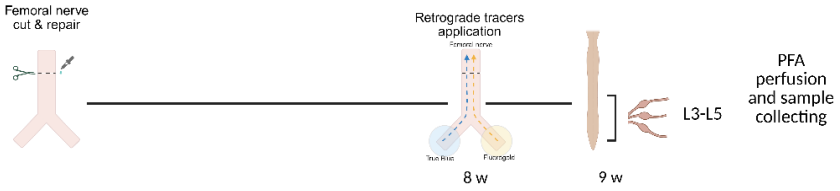
</td></tr>
<tr><td>Histological approach</td><td> 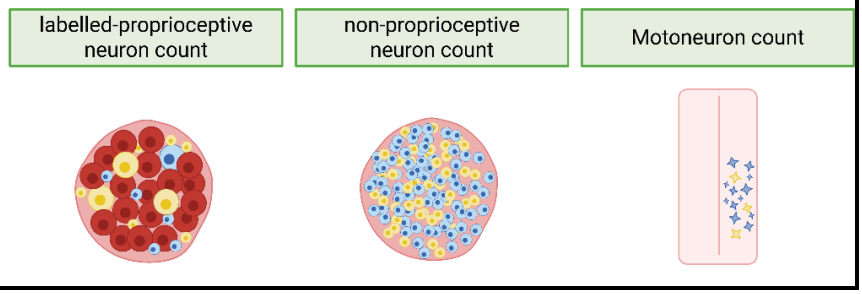
</td></tr>
</table>

VI. Results

Chapter 1

Assessment of motoneuronal regeneration and Wallerian Degeneration following axotomy in postnatal mice

Assessment of Motoneuronal Regeneration and Wallerian Degeneration Following Axotomy in Postnatal Mice

Beatriu Molina-Esteve[1,2], Marina Pujol-Masip[1], David Ovelleiro[3], Jose Antonio Gomez-Sanchez[4], Natalia Lago[1,2*], Esther Udina[1,2*]

Affiliations

[1] Universitat Autònoma de Barcelona, Cell Biology, Physiology and Immunology, Bellaterra, Spain

[2] Centro de Investigación Biomédica en Red sobre Enfermedades Neurodegenerativas (CIBERNED), Bellaterra, Spain

[3] Peripheral Nervous System, Vall d'Hebron Institut de Recerca (VHIR), Vall d'Hebron Hospital Universitari, Vall d'Hebron Barcelona Hospital Campus, Barcelona, Spain

[4] Instituto de Investigación Sanitaria y Biomédica de Alicante (ISABIAL), Alicante, Spain

** These authors share senior coauthorship*

Abstract

Nerve injuries during early postnatal stages results in markedly different outcomes compared to adult injury, with significant motoneuronal death masking potential regenerative capacity. This study systematically evaluated motoneuronal survival, axonal regeneration, and Wallerian degeneration following peripheral nerve injury at distinct postnatal stages (P4, P10, and P30) in mice. Using ChAT-Cre/Ai9(RCL-tdT) and ChAT-Cre/RiboTag transgenic models, we assessed both histological and transcriptomic responses after sciatic nerve lesions. Injury at P4 induced substantial motoneuron death (~50%), whilst P10 and P30 animals showed minimal neuronal loss. However, when correcting for neuronal survival, P4 mice demonstrated the highest regenerative capacity, with surviving neurons achieving 100% axonal regeneration. Motoneuron-specific translatome analysis revealed that P30 animals activated a robust regeneration-associated gene (RAG) programme, including classical markers such as Atf3, Gap43, and Ngfr. In contrast, P4 neurons showed minimal RAG upregulation, suggesting they retain an intrinsic growth state that facilitates regeneration without requiring transcriptional reprogramming. P10 animals exhibited a transitional phenotype with impaired RAG activation and reduced regenerative capacity. Wallerian degeneration proceeded efficiently across all developmental stages, with age-specific differences in myelin clearance kinetics and macrophage recruitment. Transcriptomic analysis confirmed consistent downregulation of myelination programmes and upregulation of pro-regenerative markers following injury, regardless of age. These findings indicate that regenerative capacity is primarily determined by the intrinsic growth state of motoneurons rather than extrinsic factors.

Graphical abstract

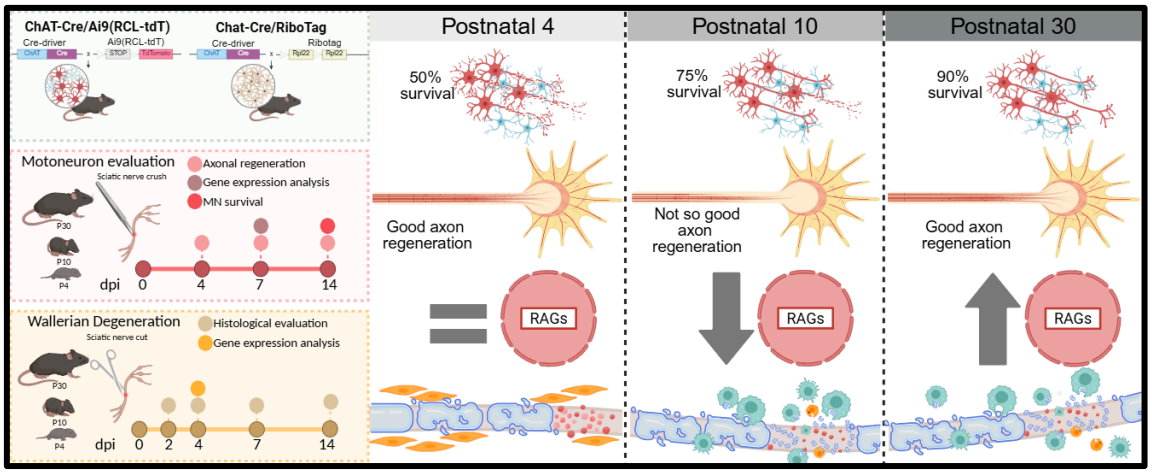

Keywords: Neonatal nerve injury, Neuronal death, Nerve regeneration, Wallerian degeneration, Transcriptomic analysis

Introduction

Lower motor neurons serve as the final effectors of the somatic motor system. Originating in the spinal cord or brainstem, their axons extend through nerves to innervate skeletal muscles. Consequently, any damage to these neurons results in muscle weakness or paralysis in the affected regions. Although the cell bodies of lower motor neurons reside within the central nervous system (CNS), they share the capacity for axonal regeneration following nerve injury with peripheral neurons. Successful peripheral nerve regeneration is attributed to two critical processes: (1) the intrinsic ability of injured neurons to switch from a neurotransmitter to a pro-regenerative state to facilitate axonal elongation and (2) the degeneration of the distal nerve stump, the so-called Wallerian degeneration, where the myelin and axonal debris at the distal stump are cleaned, and the creation of a pro-regenerative milieu provides guidance for axons to re-establish connections with their target organs (Allodi et al., 2012). Activation of a genetic repair program by denervated Schwann cells (Jessen and Mirsky, 2016) and resident macrophages and recruitment of hematogenous ones are key elements for successful Wallerian degeneration (Stoll & Müller, 1999).

The activation of an intrinsic growth program in axotomized peripheral neurons involves the downregulation of genes related to neural activity and neurotransmission and the upregulation of several transcription factors related to growth and cytoskeleton elements (He & Jin, 2016). These upregulated genes are usually known as regeneration-associated genes (RAGs). However, it is evident that neurons must survive injury to be able to switch to a pro-regenerative state. A greater susceptibility to death is observed when lesions are close to the cell body or occur at a young age. Classical works have described the marked death of motoneurons when axotomized within the first days after birth. In 1946, Romanes concluded that motoneurons are likely to die even if they are only temporarily separated from their target muscle, and this susceptibility to target deprivation diminishes with maturation, with the first six days of life being crucial for neuronal survival (Romanes, 1946). Other classical studies have confirmed this massive death (Schmalbruch 1984; Li et al., 1998). A more recent paper has shown that nerve injuries in neonatal rodents induce massive loss of

motoneurons but also sensory neurons (Kemp et al., 2015). Overactivation of glutamate has been implicated as a possible mechanism for motoneuron death (Iwasaki et al., 1995). The immaturity of postnatal Schwann cells has also been pointed as a contributor to this death (Komiyama & Suzuki, 1992).

This massive death of neurons at postnatal stages is probably the reason why the regenerative potential of young motoneurons has been neglected in the literature. Although young neurons might have greater regenerative potential than adult neurons, this capacity can be overwhelmed by the massive neuronal loss observed at early postnatal stages.

Therefore, the aim of this study was to evaluate the regenerative capability of motoneurons after nerve injury at different postnatal stages, considering the rate of neuronal death and the genetic program activated. The degree of Wallerian degeneration of the distal stump during these different periods will also be analysed to explore the efficacy of this response at the immature stage and its impact on the regenerative process. Postnatal ages 4, 10 and 30 were selected to represent a highly vulnerable age to axotomy (P4) a transient intermediate stage between development and maturity, both for the neuron and the Schwann cells (P10) and a juvenile age which reflects onset of maturity (P30)

Material and methods

Mice

Postnatal 4 (P4), postnatal 10 or 11 (P10) and postnatal 30 to 35 (P30) day-old mice were used for all studies. Males and females were used in approximately equal numbers for all the groups in all the experiments. The mice were housed in a controlled environment (12-h light–dark cycle, 22 ± 2°C) in open cages with water and food ad libitum. P4 and P10 mice were housed with their mothers. The strains used in this study were acquired from Jackson Laboratory (Bar Harbor, ME, USA) and maintained in our animal facility. C57BL/6J mice were used as wild type (WT) animals. Mice expressing the fluorescent protein TdTomato in the motoneurons ChAT-Cre/Ai9 were generated by breeding homozygous Ai9 (RCL-tdT) mice (JAX stock #007909) (Madisen et al., 2010) with ChAT-IRES-Cre (choline acetyltransferase, JAX stock #006410) (Rossi et al., 2011). The same Cre-driver lines were bred to homozygous Ribotag mice (Sanz et al., 2019), resulting in mice that express hemagglutinin (HA)-tagged ribosomes in motoneurons: ChAT-Cre/Ribotag.

Experimental design

For the evaluation of axonal regeneration and assessment of neuronal death, a sciatic nerve crush injury was applied to ChAT-Cre/Ai9(RCL-tdT) mice at P4, P10, and P30, followed by histological analysis (Figure 11a). To characterize the translatome of motoneurons after sciatic nerve crush injury at these developmental stages, RNA was isolated from injured and uninjured Chat-Cre/RiboTag mice (Figure 11b). To investigate Wallerian degeneration histology and the Schwann cell transcriptome, a sciatic nerve transection without repair was performed in WT mice at P4, P10, and P30 (Figure 11c).

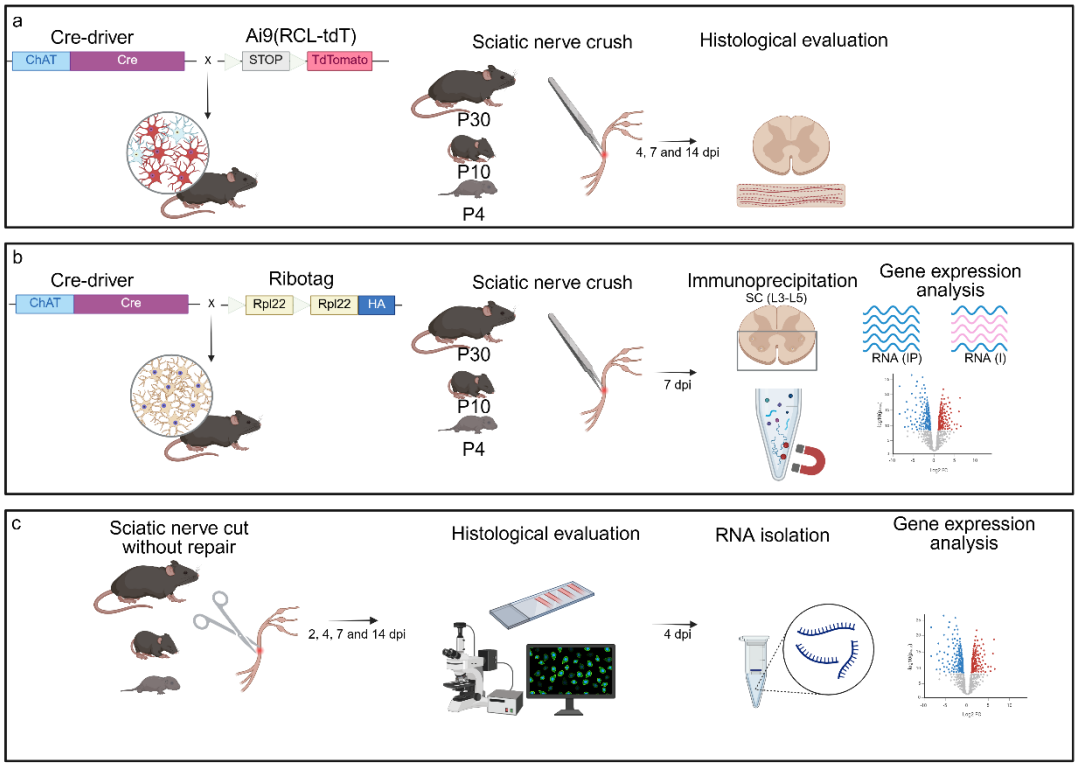

Figure 11. Experimental design (a) Schematic representation of the ChAT-Cre/Ai9(RCL-tdT) transgenic mice and experimental design used for the evaluation of motoneuronal survival and axonal regeneration. (b) Schematic representation of the Chat-Cre/Ribotag transgenic mice and the experimental design used for motoneuron translatome analysis. (c) Schematic representation of the experimental design used for Wallerian degeneration dynamics evaluation and sciatic nerve transcriptomics.

Surgeries

All experimental procedures were approved by the Animal Experimentation Ethical Committee of the Universitat Autònoma de Barcelona and followed the European Communities Council Directive 2010/63/EU and Spanish National law (RD 53/2013). All surgical procedures were carried out aseptically under an operating microscope. All surgical interventions were carried out via the use of ketamine (90 mg/kg or 18 mg/kg) and xylazine (10 mg/kg or 2 mg/kg) intraperitoneally in P30 and P10 mice respectively. In P4 animals, short-term hypothermia was used to anaesthetize the pups, taking advantage of the short period needed to perform the surgery (Flecknell et al., 2015) . Sciatic nerve crush was performed as follows: a mid-thigh incision was made, and the right sciatic nerve was exposed and crushed. Standard N°. Five Jeweller forceps were used for 30 seconds, resulting in axonotmesis or Sunderland grade 2

injury (Bridge et al., 1994). A 10–0 polypropylene suture was fitted into the epineurium to landmark where the crush site was at the tissue harvest. For the cut injury, the right sciatic nerve was exposed and cut proximally, resulting in complete neurotmesis or Sunderland grade 5 injury (Bridge et al., 1994). A 10–0 polypropylene suture was used to suture the proximal stump of the nerve with the muscle to prevent coaptation of the proximal and distal stumps and to avoid axonal regeneration. The skin incision was sutured with a 6–0 silk suture and disinfected with povidone iodine. All the mice were kept in a warm environment until recovery. Following surgery, all the mice were returned to their home cages and allowed to recover. During the follow-up, assessment of general health and mobility was performed daily for the first week. All the animals were sacrificed at the time of study termination under deep anaesthesia, with Dolethal (0.03 ml/30 g) administered intraperitoneally, and death was confirmed by decapitation.

Motor axon regeneration and motoneuron death

To evaluate the number of motor axons per nerve and the number of motoneuron cell bodies 4, 7 and 14 days post injury (dpi), the ipsilateral and contralateral sciatic nerves and the lumbar spinal cord were removed, the samples were postfixed in 4% Paraformaldehyde (PFA) in phosphate buffer saline (PBS) for at least 2 hours and stored in PBS with 30% sucrose at 4°C, being post-fixed before storage. The sciatic nerves were placed on a glass slide and mounted with Fluoromount-G medium (Southern Biotech). Pressure was applied to the coverslips to flatten the nerves, and images 5 millimetres (mm) distal from the lesion point were taken via a confocal microscope (Leica SP5, 20x, z-step size of 1 µm). All intact axons were counted in stacks of 5 µm every 10 µm to avoid double counting and compared to the contralateral side. The spinal cord was serially cut (20 µm) on a cryostat (Leica), collected on glass slides, mounted with Fluoromount-G medium (Southern Biotech) and imaged with an epifluorescence microscope (Nikon Eclipse Ni, Japan) at 20x. Ipsilateral and contralateral intact motoneurons containing a clear nucleole were counted every 100 µm.

Ribotag assay

To analyse the translatome of the injured motoneurons in the different postnatal stages, 7 days after sciatic nerve crush injury, the ventral portion of the lumbar spinal cord (L3-L5) was dissected and placed on cold Gey's solution enriched with glucose (6 mg/mL) and homogenized in 1 mL of buffer. Age-matched uninjured animals were used as control groups (P4+7, P10+7, P30+7). After the homogenate was centrifuged, 50 µL of the supernatant was stored as an input (I) sample, whereas 5 µL of anti-HA antibody (Covance, #MMS-101R) was added to the remaining lysate and incubated for 4 hours at 4°C with rotation. Then, 200 µL of protein A/G magnetic beads (Thermo Fisher, #88803) were washed and added to the lysate overnight at 4°C with rotation. The samples were washed with high-salt buffer (HSB) to remove nonspecific binding from the immunoprecipitate (IP), and the beads were removed via a magnet. RNA was isolated from the samples via an RNeasy Micro Kit (QIAGEN, #74004) and quantified via a Quant-it RiboGreen RNA Assay Kit (Thermo Fisher, #R11490). The integrity of the RNA was assessed by using the RNA quality number (RQN), an objective metric of total RNA quality ranging from 10 (highly intact RNA) to 1 (completely degraded RNA). RQN was obtained via Lexogen CORALL library preparation - RiboCop - DA Services Bundle (Isogen Life Science B.V.). All the samples had RQN >6.

qRT-PCR analysis

One µL of RNA was assayed via a TaqMan RNA-to-Ct 1-step Kit (Thermo Fisher, #4392938). Specific transcripts were detected via TaqMan assays: Actb (Mm02619580_g1), Fabp7 (Mm00445225_m1), and Chat (Mm01221882_m1). Relative expression was obtained by normalizing to Actb RNA levels with a standard curve method.

Motoneuron specific RNA sequencing

Library preparation and RNA sequencing. Lexogen next-generation sequencing (NGS) services (Vienna, Austria) were used to perform RNA quality control and RNA sequencing. Libraries were prepared via the CORALL mRNA-Seq V2 preparation kit. All

the samples were sequenced via the Illumina NextSeq 500 platform in runs of 2×150 bp, yielding at least 15 million reads per sample. FASTQ files were evaluated for quality via FastQC (v0.11.9). The reads were aligned to the coding DNA reference database of the mouse genome (Ensembl, GRCm39, release 103) via Salmon (v1.4.0). The quantified transcript reads were mapped to genes and imported into the R environment (v4.4.0). Genes with fewer than 100 counts across all samples were excluded from further analysis. Differential expression analysis was performed via the DESeq2 library (v1.44.0). Principal component analysis (PCA) plots were generated via the plotPCA function from DESeq2. Hierarchical clustering was performed via the pheatmap (v1.0.12) package, which focuses on the most variable genes across samples. Gene set enrichment analysis was conducted via STRINGdb and multiple databases provided by the STRING platform, including GO, KEGG, Pfam, and InterPro. Only genes with a P value<0.05 were included. Pathway analysis was performed via the Bioconductor libraries KEGGREST and pathview. The KEGG database was accessed via a RESTful web service. Pathways were analysed on the basis of genes P values via the Wilcoxon test, and graphical representations of pathways were generated, highlighting proteins by expression level.

Histological analysis of Wallerian degeneration

To evaluate the dynamics of Wallerian degeneration in the different postnatal stages 2, 4, 7 or 14 dpi, the ipsilateral and contralateral sciatic nerves were removed, fixed in 4% PFA in PBS for at least 2 hours and stored in PBS supplemented with 30% sucrose at 4°C. Longitudinal sciatic nerve sections of 8-µm thickness obtained with a cryostat (Leica, Wetzlar, Hermany) were subjected to Luxol fast blue staining (LFB, Sigma; St. Louis, MO, USA) for myelin clearance quantification. Following gradual dehydration, the sections were immersed in a 1 mg/mL LFB solution in 95% ethanol and 10% acetic acid overnight at 37°C. The sections were subsequently rinsed in distilled water, destained in a solution of 0.05% $LiCO_3$ in distilled water for 10 seconds and finally rinsed in 70% ethanol. The sections were then dehydrated and mounted with DPX mounting medium (Sigma; St. Louis, MO, USA). Images were acquired at 20x via an epifluorescence microscope under bright light (Nikon Eclipse Ni, Japan). For lipid

accumulation quantification, the sections were incubated in Oil Red O (ORO) solution for 10 minutes at room temperature and then placed under running tap water for 30 minutes. The sections were then mounted with Fluoromount-G medium (Southern Biotech). Images were acquired at 20x via an epifluorescence microscope under bright light (Nikon Eclipse Ni, Japan). For phagocyting macrophage density quantification, samples were permeabilized with PBS and 0.3% Triton X-100 (PBST) and blocked with 1.5% normal donkey serum (NDS) (Vector Laboratories). The sciatic nerve slices were incubated overnight at 4°C with a rat anti-CD68 antibody (1:500, Bio-Rad). The slices were washed and incubated with secondary anti-rat antibody (Alexa Fluor 488, Invitrogen) for 2 h at room temperature. After washing, the slides were mounted with Fluoromount-G medium (Southern Biotech). Images were acquired at 20x via an epifluorescence microscope (Nikon Eclipse Ni, Japan). To analyse the percentage of degenerating fibres in the distal nerve after a sciatic nerve cut without repair, semithin sections of the distal nerves were obtained at 2, 4 and 7 dpi and postfixed in glutaraldehyde–paraformaldehyde (3%/3%) in cacodylate buffer solution (0.1 M, pH 7.4). The samples were postfixed in 2% Osmium Tetroxide, dehydrated through ethanol series, and embedded in epoxy resin embedding medium (Epon) resin. Transverse semithin sections (0.5 μm) were stained with toluidine blue and examined via light microscopy.

To quantify myelin loss over time in the different postnatal stages postinjury, the percentage of the area stained with LFB, ORO and anti-CD68 immunostaining was measured via Fiji/ImageJ software.

Sciatic nerve RNA analyses

To analyse the transcriptomics of the injured sciatic nerves in the different postnatal stages 4 days after cut injury, the ipsilateral and contralateral sciatic nerves were extracted and snap frozen until RNA extraction. RNA from the sciatic nerve was isolated via the RNeasy Micro Kit (QIAGEN, #74004). The contralateral nerves served as the control group.

Library preparation and RNA sequencing

BGI Genomics Co., Ltd. (Shenzhen, China) performed the RNA quality control and RNA sequencing. Libraries were prepared via the DNBSEQ Eukaryotic Strand-Specific mRNA Library Kit. All samples were sequenced via the DNBSEQ (DNBSEQ Technology) platform in runs of 2x150 bp, yielding at least 20 million reads per sample. FASTQ files were evaluated for quality via FastQC (v 0.11.9). The reads were aligned to the coding DNA reference database of the mouse genome (Ensembl Mouse database, Genome assembly: GRCm39.cdna.all, release 113) via Salmon (v1.10.3). The "DESeq2" library (v 1.48.0) was used to perform the differential expression analysis pipeline. The quantified transcript reads were mapped to genes and imported into the R environment (R version 4.5.0). Only genes with more than 10 counts in the smallest group were used in the differential analysis. PCA and uniform manifold approximation and projection (UMAP) plots were generated via the plotPCA function from DESeq2. Hierarchical clustering was performed via the pheatmap (v1.0.12) package, which focuses on the 80 most variable genes across samples. Gene set enrichment was performed via the R library "STRINGdb" 7 via the String 8 platform, which includes GO, PubMed, STRING, KEGG and Reactome, among others. Only proteins with a P value<0.05 were included. Pathway analysis was performed for each comparison. The bioconductor libraries "KEGGREST" (v 1.48) and "pathview" (v 1.48) were used. The KEGG database is accessed in this process via a RESTful web service via the R package. Pathways were analysed on the basis of gene P values via the Wilcoxon test, and graphical representations of pathways were generated, highlighting genes by expression level. In addition to the differential expression obtained, a single time series involving both the "Ctrl" and "Inj" samples at the three times (4, 10 and 30) has been modelled by designing a formula that models the type of sample and the first time point, differences over time, and any type-specific differences over time, followed by a likelihood ratio test and the removal of type-specific differences over time.

Data analysis

GraphPad Prism 9 (version 9.0.1) was used for statistical analysis. The normal distribution of the samples was confirmed with the Shapiro–Wilk test (p>0.05). The

percentages of regeneration and neuronal death were analysed via two-way ANOVA and paired t tests, respectively, followed by the Sidak's test. Histological statistical analyses were performed via two-way ANOVA followed by the Sidak's test. The total number of axons was analysed via the Kruskal–Wallis's test followed by Dunn's test. The percentage of myelinated/degenerating axons was analysed via two-way ANOVA followed by the Sidak's test. Differences were considered statistically significant if $p<0.05$. All the data are expressed as the group mean ± standard error of the mean (SEM).

Results

Response of motoneurons to nerve injury at different postnatal stages

Evaluation of neuronal death and axonal regeneration

Motoneuron death was evaluated 14 dpi by counting the total number of neuronal cell bodies present in the ipsilateral ventral horn of the lumbar portion of the spinal cord (L3-L5) and comparing them to those on the contralateral side (Figure 12a). On the contralateral side, approximately 12 motoneurons/slice were found at all the ages evaluated. When analysing the ipsilateral side, we observed a significant reduction when animals were injured at P4 (6 motoneurons/slice) and a non-significant reduction at P10 and P30 (9 and 8 motoneurons/slice respectively; Figure 12b). Whereas injuries at P10 and P30 resulted in 75% and 80% of motoneuron survival at 14 dpi, injuries at P4 resulted in only 50% survival. This reduced survival when injury is applied at P4 mice is significant compared to P10 ($p<0.05$) and P30 mice ($p<0.005$). (Figure 11c)

When we analysed the number of motor axons in intact nerves at different postnatal stages (Figure 12d, e), we observed a significantly greater number of axons in P30 mice than in P4 mice ($p<0.05$). After crush injury at different postnatal stages, we evaluated the number of motor axons growing 5 mm distal to the injury site at 4, 7 and 14 dpi. As expected, in all the experimental groups, we observed a significant reduction in the number of axons 5 mm distal to the injury at 4 dpi compared with those on the contralateral side ($p<0.05$). Interestingly, at 14 dpi, only P4 mice reached control values ($p<0.05$), indicating good axonal regeneration at this stage. However, since the basal (control) number of axons differed between postnatal stages, we normalized the number of regenerating axons distal to the lesion versus the number of intact axons in the control nerves to obtain the percentage of regenerated axons (Figure 12f). Considering this correction, when injury was applied at P4 and P10, we observed that approximately 55% of the axons regenerated at 14 dpi, a percentage that increased to 75% when injury was applied to P30 mice. However, since the death of motoneurons

directly impacts the number of axons that may regenerate after injury, we also applied a correction factor to normalize the regeneration data considering the survival of motoneurons at different ages. This correction factor was calculated as follows:

*Percentage of regenerated axons/percentage of motoneuron survival *100*.

When this correction factor was applied (Figure 12g), only P4 mice reached 100% of regeneration. Although there were no significant differences between the groups in terms of these corrected regeneration rates, motoneuron regeneration in P4 animals was considerably good, despite the high rate of neuronal loss observed.

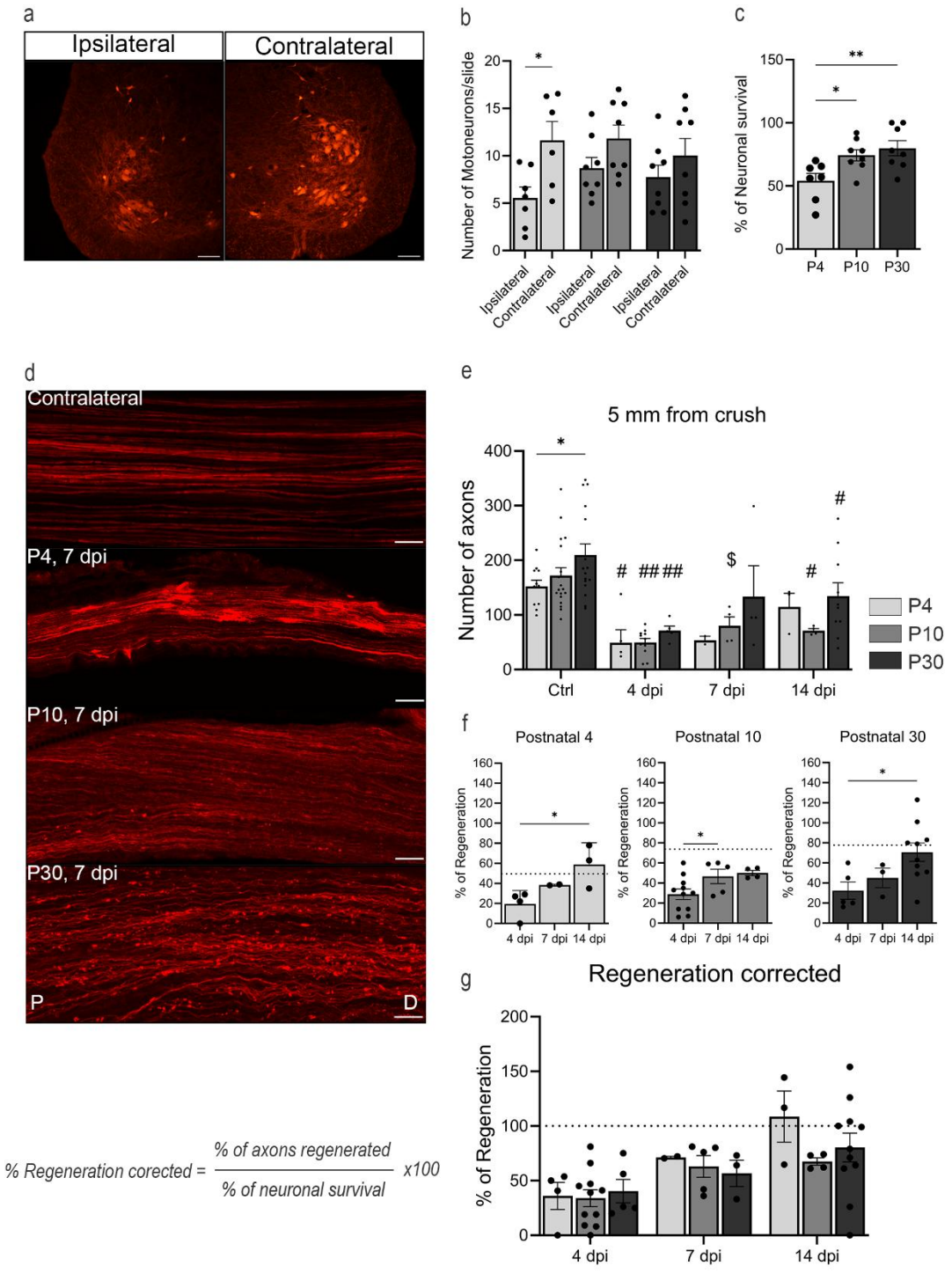

Figure 12. Histological characterization of the motor neuron response after peripheral nerve injury at different postnatal stages. (a) Representative images of the ipsilateral and contralateral ventral horns of the lumbar portion of the spinal cord of P4 mice at 14 dpi, showing the ChAT+ motoneurons in red. Scale bar=100 µm. (b) Quantification of the average number of motoneurons in the lumbar spinal cord on both the ipsilateral and contralateral sides at 14 dpi across different postnatal stages. Statistical analysis was performed via two-way ANOVA followed by Sidak's correction test. *p<0.05 (c) Percentage of surviving

motoneurons at 14 dpi in the different postnatal stages. Statistical analysis was performed via one-way ANOVA followed by Tukey's correction test. *p<0.05; **p<0.001. (d) Representative longitudinal sections of the distal portion of the sciatic nerve at 7 dpi in P4, P10, and P30 mice. Scale bar: 50 µm. P: proximal; D: distal. (e) Total number of axons 5 mm distal to the lesion site in P4, P10, and P30 mice in both control and crushed sciatic nerves at 4, 7, and 14 dpi. Statistical analysis was performed via two-way ANOVA followed by Sidak's correction test. *$p<0.5$; $ $p<0.5$ vs. control; $p<0.01$ vs. control; ##. $p<0.0001$ vs. control. (f) Percentage of regenerated axons at 4, 7, and 14 dpi in P4, P10, and P30 mice relative to the contralateral side. The dotted line represents the percentage of surviving motoneurons at 14 dpi. Statistical analysis was performed via one-way ANOVA followed by Tukey's correction test. *p<0.05 (g) Regeneration index corrected for neuronal survival at 4, 7, and 14 dpi in P4, P10, and P30 mice relative to the contralateral side. Statistical analysis was performed via two-way ANOVA followed by Sidak's correction test.

RNA isolation from ChAT-Cre/Ribotag is motoneuron specific

To further study whether the response of motoneurons to injury differed among the different postnatal stages, we used the Ribotag assay to isolate translated mRNA from motoneurons at different postnatal ages. By breeding ChAT-Cre driver mice with Ribotag mice, we could target motoneuron ribosomes, which were tagged with HA, as previously validated in our laboratory (Bolívar et al., 2024). By harvesting the ventral portion of the lumbar spinal cord, we could specifically isolate the ribosomes of the motoneurons. Following RNA isolation, RT–qPCR analysis of the IPs revealed marked enrichment of the motoneuron-specific transcript *Chat* (choline acetyltransferase), whereas the glial transcript *Fabp7* (fatty acid binding protein 7) was notably depleted across all IPs (Figure 13a). This result confirms the specificity of ribosome isolation to neuronal populations within our samples.

RNA sequencing revealed differential expression of over 15,000 genes across each group of interest. To validate the dataset, we examined the transcripts per million (TPM) of several cell type-specific markers. Motoneuron IPs were enriched for established motoneuron markers, including *ChAT*, *Mnx*, *Nefh*, *Tns1*, and *Slc18a3* (Figure 13b). In contrast, transcripts associated with glial genes, such as *Tmem119*, *Mobp*, *Olig1*, *Aqp4* and *Plp1*, were depleted in the IPs, confirming their cell type specificity (Figure 13c). RAGs, including *Gap43*, *Atf3*, *Tubb2b*, and *Ngfr*, were enriched in most of the injured samples compared with the control samples (Figure 13d). Principal

component analysis further demonstrated clear clustering of samples on the basis of their experimental group, supporting the robustness of the dataset (Figure 13e, f).

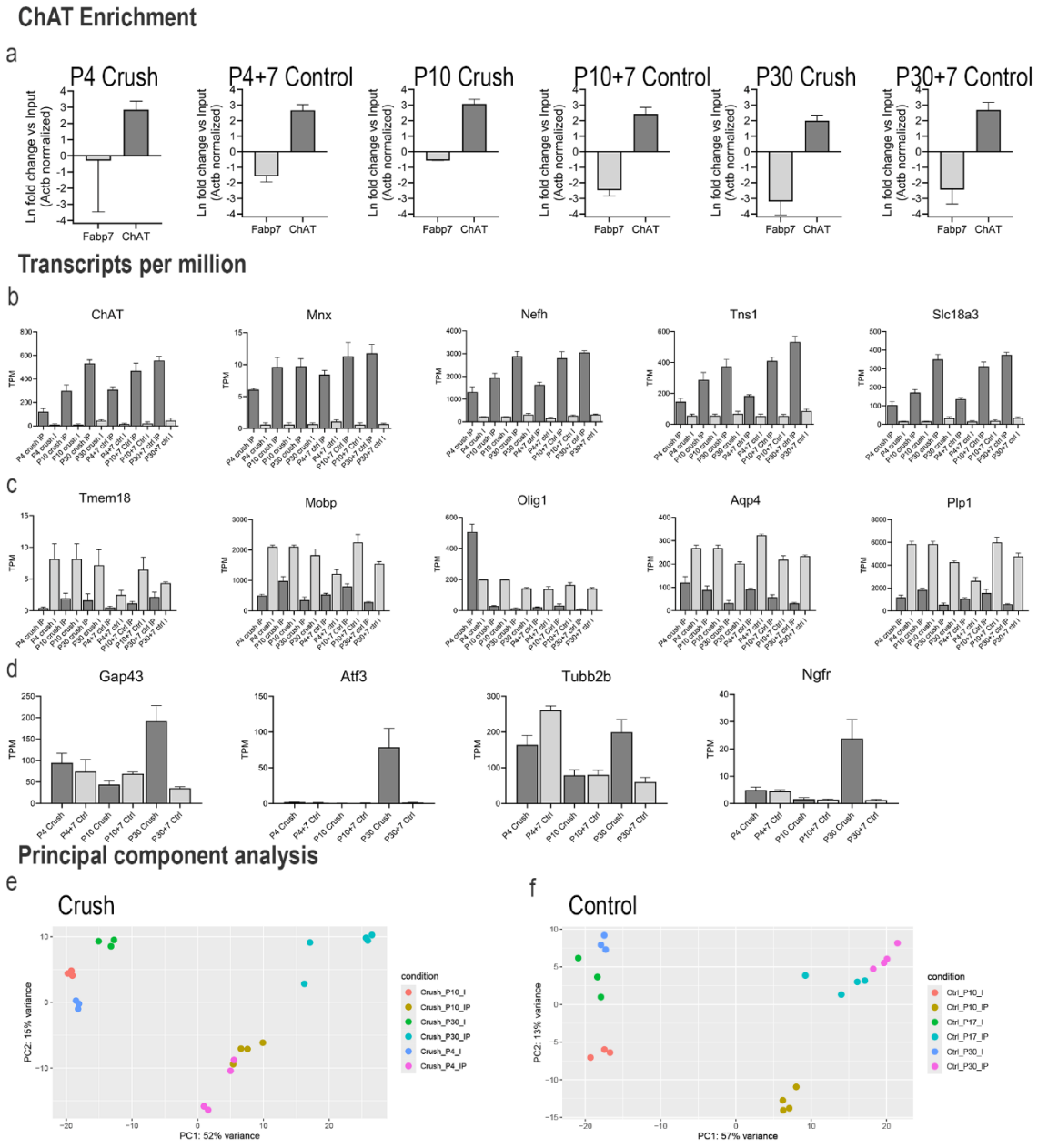

Figure 13. Validation of the specificity of the ChAT-Cre/Ribotag mice. (a) RT–qPCR revealed enrichment of cell type-specific transcripts in the IPs of ChAT and depletion of the glial transcript Fabp7. (b) TPM of motoneuron-specific genes expressed in the IP and I. (c) TPM of glial-specific genes in both the IP and I. (d) TPM of regeneration-specific genes expressed in the crush and control samples. (e, f) PCA of the crush and control samples included in the study.

Pathway enrichment analysis

To investigate the molecular response of motoneurons to sciatic nerve crush at different postnatal stages, we performed pathway enrichment analysis. The analysis revealed distinct stage-dependent profiles. In P30 mice (Figure 14a), we selected 24 enriched pathways; most of them are related to migration and cellular organization, stress response, lipidic metabolism and inflammatory response. In P4 injured mice compared to uninjured P4+7 mice (Figure 14b), the most enriched pathways are related to mitochondrial energetic metabolism and early regulatory processes. In injured P10 mice compared to uninjured Postnatal 10+7 mice (Figure 14c), most of the pathways are downregulated, including those related to neuronal homeostasis, autophagy, energetic metabolism, and cytoskeleton reorganization.

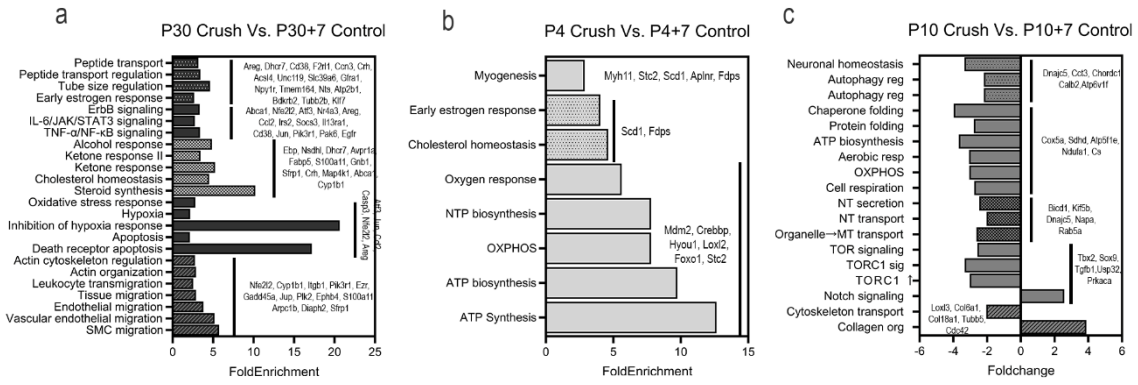

Figure 14. Pathway enrichment analysis. (a) Molecular pathways enriched in P30 crush animals compared with P30+7 control animals. (b) Molecular pathways enriched in P4 crush animals compared with P4+7 control animals. (c) Molecular pathways enriched and downregulated in P10 crush animals compared with those in P10+7 control animals.

Gene Set Enrichment Analysis (GSEA)

To investigate whether sets of genes exhibited a consistent increase or decrease in expression across different postnatal stages following injury, we performed gene set enrichment analysis (GSEA). Comparisons were made between the injured group and the corresponding age-matched control group (Injured P4 vs. Intact P4+7, Injured P10 vs. Intact P10+7, Injured P30 vs. Intact P30+7). Using our custom list of RAGs and

RStudio software (RStudio Team, 2024, version 2024.12.0+467), we conducted GSEA (Figure 15a-c). We subsequently focused on the leading-edge RAGs identified via GSEA to pinpoint the genes most significantly enriched at each postnatal stage. In P30 animals, several classical RAGs, including *Atf3*, *Ccl2*, *Ngfr*, *Gap43*, and *Adcyap1*, were upregulated compared with their noninjured counterparts. In contrast, compared with noninjured animals of the same age, injured P4 animals did not exhibit any significantly upregulated RAGs. Interestingly, injured P10 mice presented a downregulation of several classical RAGs, such as *Rac1* and *Stat3*, relative to noninjured P10+7 animals. Following the GSEA findings, we next examined the expression levels of the identified leading-edge RAGs by assessing their TPM values across the experimental groups (Figure 15d-i). Consistent with the GSEA results, injured P30 animals presented visibly greater expression of these RAGs than did their intact P30+7 counterparts. In contrast, the TPM values for these RAGs in both injured P10 and injured P4 animals showed minimal discernible changes relative to their respective age-matched intact control groups.

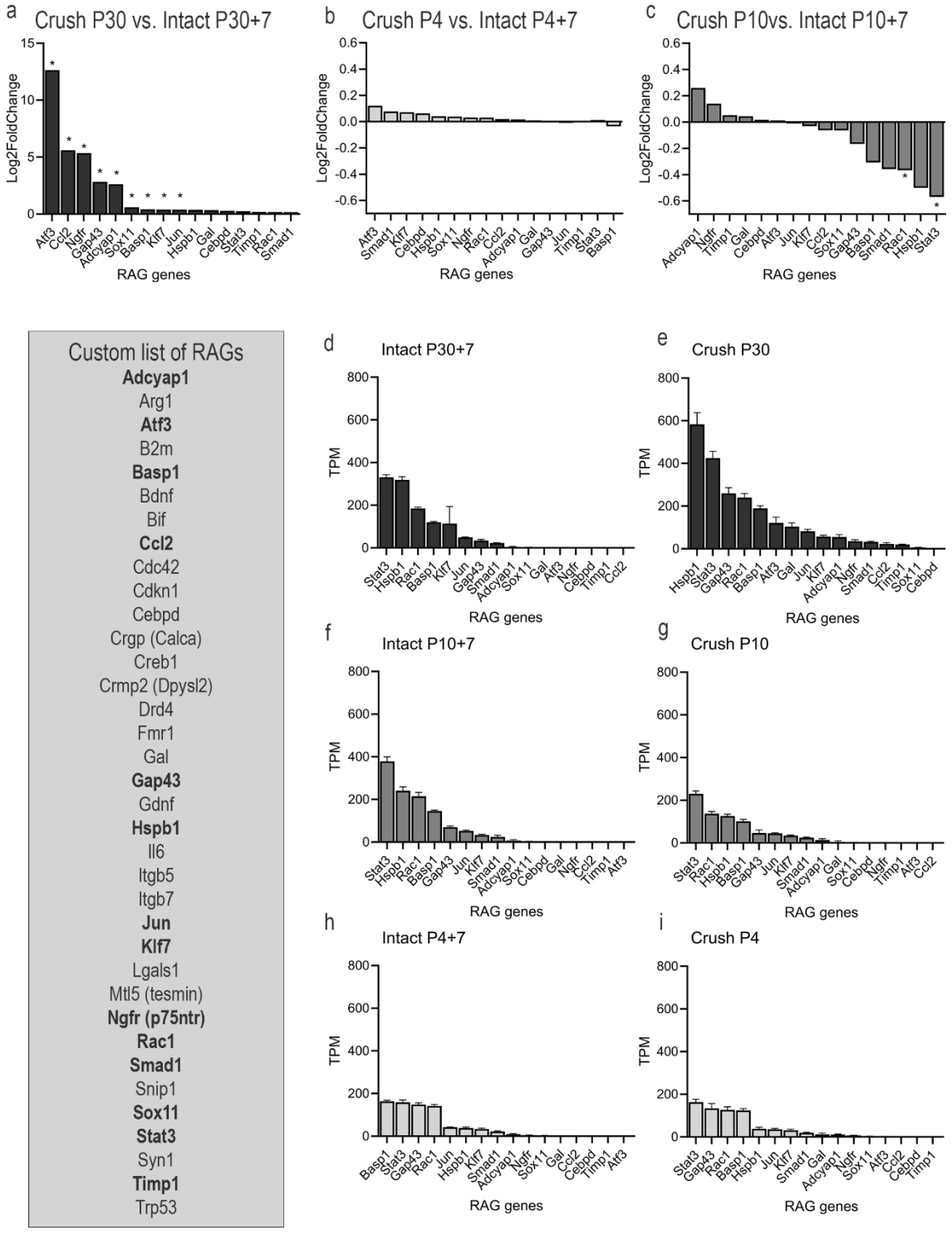

Figure 15. Expression of RAGs at different postnatal stages. (a) Log_2Fold change in the number of enriched RAGs in motor neurons from injured P30 mice compared with uninjured P30+7 controls. (b) Log_2Fold change in the number of enriched RAGs in motor neurons from injured P4 mice, analysed at P11, compared with that in age-matched uninjured P4+7 controls. (c) Log_2Fold change in the number of enriched RAG genes in motor neurons from injured P10 mice, analysed at P17, compared with those in

uninjured P10+7 controls. Differential expression and enrichment analyses in (a–c) were performed via gene set enrichment analysis (GSEA) in R. Gene sets were considered significantly enriched at false discovery rate (FDR)<0.05. (d–i) Transcripts per million (TPM) of selected RAGs in motor neurons injured at P30, P10 and P4 mice and age-matched controls. The data are presented as the means ± SEMs (*n*=4 mice per group).

Characterization of Wallerian Degeneration at Different Postnatal Stages

To evaluate Wallerian degeneration, a cut injury was applied to the sciatic nerve at different postnatal stages. This was performed to isolate the distal segment from the proximal segment, thereby preventing axonal regeneration into the distal segment.

Histological characterization of Wallerian degeneration

LFB staining (Figure 16a) was used to evaluate myelin integrity in the sciatic nerve following peripheral nerve injury (PNI) at different postnatal stages. In contralateral nerves from injured animals, LFB staining consistently revealed a homogeneous and intense blue signal, indicative of intact and well-organized myelin sheaths. In contrast, ipsilateral nerves from animals at all ages examined (P4, P10, and P30) presented altered LFB staining patterns characterized by reduced staining intensity and increased heterogeneity, suggesting progressive demyelination post injury. Quantification of the LFB-labelled area (Figure 16b) revealed robust myelin content in the contralateral nerves of P30 mice, which was significantly lower in P4 and P10 mice. Following injury, myelin clearance in P30 mice gradually occurred, with maximal loss observed at 7 dpi. In P10 mice, myelin clearance also progressed over time, reaching a peak at 4 dpi, suggesting a more rapid response than at P30. Notably, P4 mice exhibited an absence of detectable myelin as early as 2 dpi, with levels remaining consistently low through 14 dpi. These results indicate that while P10 and P30 mice follow a similar profile of progressive myelin clearance, P4 mice display an atypical response, likely reflecting developmental immaturity and distinct cellular mechanisms engaged following injury at this early postnatal stage.

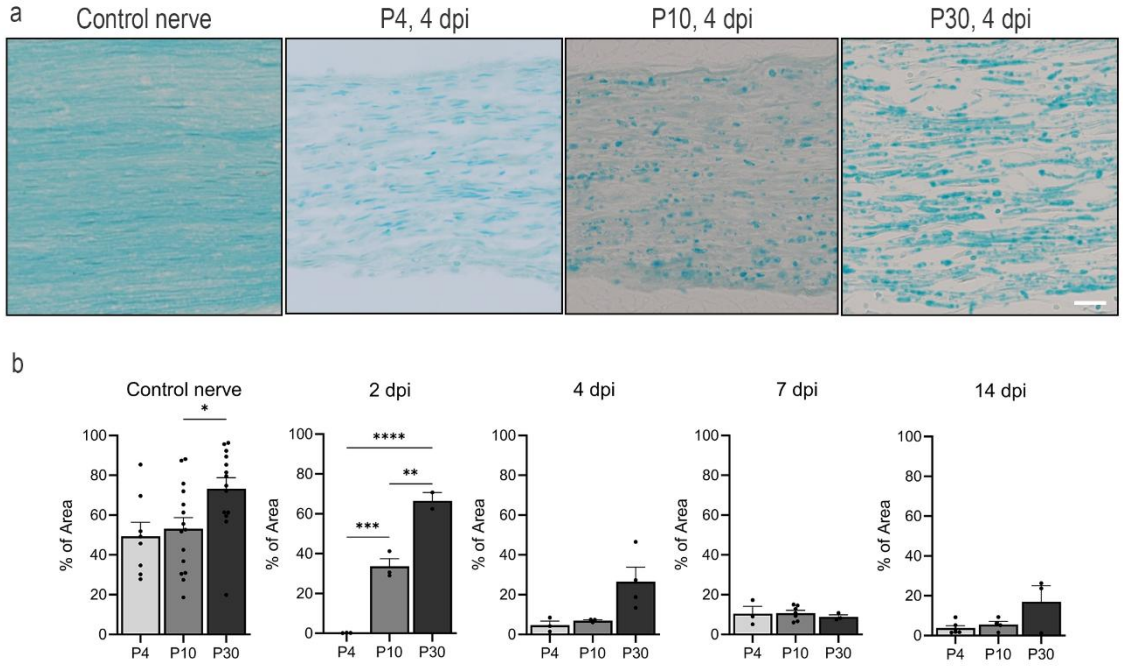

Figure 16. Histological evaluation of myelin clearance dynamics in different postnatal stages. (a) Representative images of LFB staining of the distal portion of the sciatic nerve at different postnatal stages after a cut lesion at 4 dpi and contralateral to it. (b) Percentage of the area stained with myelin in the distal portion of the different postnatal sciatic nerves (P4, P10 and P30) after a cut injury without repair at 2, 4, 7 and 14 dpi. (n= 3–7 animals per group) * p<0.05, **p<0.01, *** p<0.001, **** p<0.0001 calculated by two-way ANOVA followed by Bonferroni correction for multiple comparisons. Scale bar: 100 µm.

ORO staining (Figure 17a) was employed to assess lipid droplet accumulation resulting from myelin degradation following PNI at different postnatal stages. In sciatic nerve tissue from uninjured control animals, a uniform and faint reddish staining pattern was consistently observed. In contrast, injured nerves from all age groups exhibited a heterogeneous staining pattern characterized by the presence of discrete, intensely red lipid aggregates along the nerve fibres and within the surrounding connective tissue. Quantification of the ORO-labelled area (Figure 17b) in contralateral nerves revealed no lipid accumulation at any postnatal stage. Following injury, P30 mice presented a progressive increase in lipid accumulation, peaking at 7 dpi. In P4 mice, lipid droplets were observed at 4 dpi but rapidly decreased by 7 and 14 dpi. P10 mice displayed a gradual accumulation of lipids, reaching a peak at 4 dpi, followed by a progressive decline through 14 dpi. These findings suggest that lipid accumulation dynamics following PNI vary with developmental stage, with P10 and P30 mice

exhibiting more sustained lipid accumulation than transient accumulation, as observed in P4 mice.

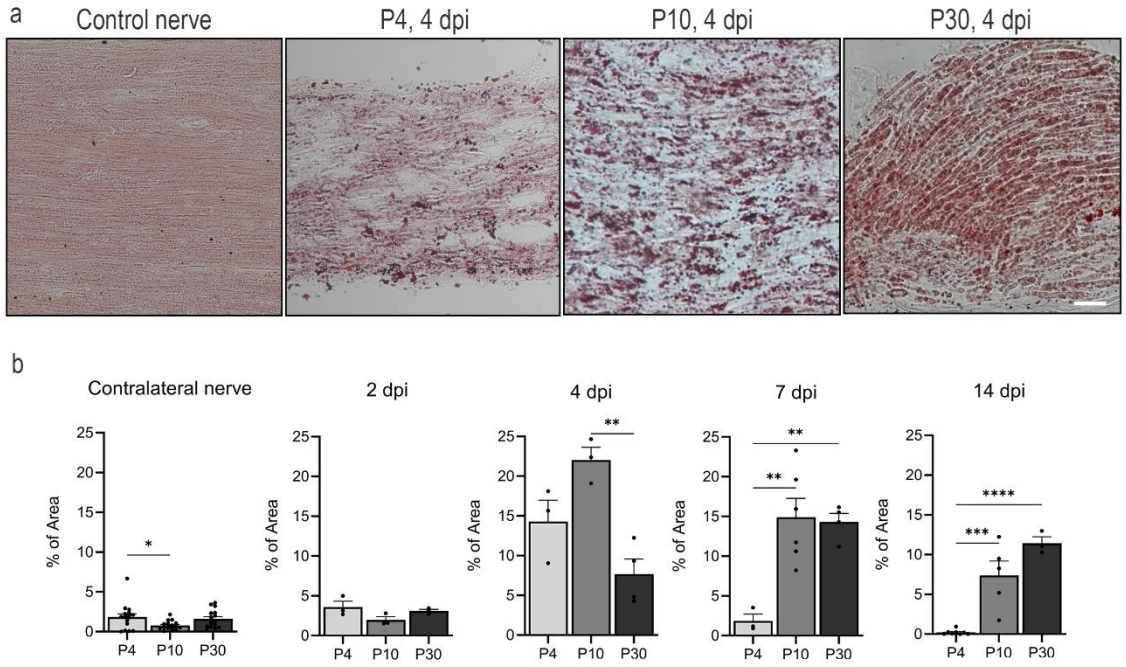

Figure 17. Histological evaluation of lipid accumulation in different postnatal stages. (a) Representative images of ORO staining of the distal portion of the sciatic nerve at different postnatal stages after a cut injury at 4 dpi and contralateral to it. (b) Percentage of the area stained with lipid droplets in the distal portion of the different postnatal sciatic nerves (P4, P10 and P30) after a cut injury without repair at 2, 4, 7 and 14 dpi. (n= 3–7 animals per group) *p<0.05, **p<0.01, *** p<0.001, **** p<0.0001 calculated by two-way ANOVA followed by Bonferroni's correction for multiple comparisons. Scale bar: 100 µm.

To quantify the degree of macrophage recruitment in the sciatic nerve following PNI across different postnatal stages, immunofluorescence staining for CD68 was performed (Figure 18a). In contralateral nerves from injured animals, only sparse, small CD68-positive cells—consistent with resident macrophages—were observed. In contrast, injured nerves from P10 and P30 mice presented a marked increase in macrophage density, with cells exhibiting a larger and rounder morphology characteristic of phagocytic activity. Quantification of the CD68-labelled area (Figure 18b) in contralateral nerves confirmed the absence of macrophage recruitment and active phagocytosis across all postnatal stages. After injury, macrophage recruitment in P30 mice increased progressively over time, peaking at 14 dpi. P10 mice displayed a similar trend, with maximal macrophage accumulation at 7 dpi followed by a reduction

at 14 dpi. Notably, P4 mice did not exhibit a significant increase in the number of macrophages at any time point. These results indicate that macrophage recruitment and activation following PNI are developmentally regulated, with P4 nerves showing an absence of macrophage recruitment, whereas P10 and P30 nerves mount more robust and temporally distinct macrophage responses.

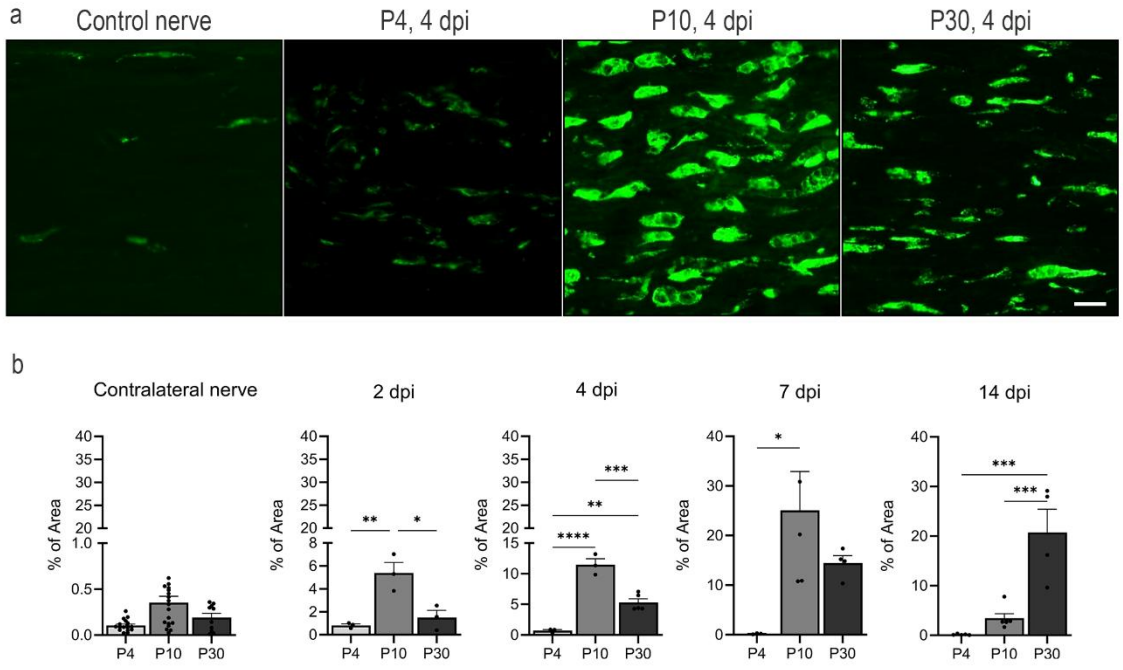

Figure 18. Histological evaluation of the activity of phagocytosing macrophages in different postnatal stages. (a) Representative images of anti-CD68 immunostaining in the distal portion of the sciatic nerve at different postnatal stages after a cut injury at 4 dpi and contralateral to it. (b) Percentage of the area stained with phagocytosing macrophages in the distal portion of the different postnatal sciatic nerves (P4, P10 and P30) after a cut injury without repair at 2, 4, 7 and 14 dpi. (n= 3–7 animals per group) *p<0.05, **p<0.01, ***p<0.001, ****p<0.0001 calculated by two-way ANOVA followed by Bonferroni's correction for multiple comparisons. Scale bar: 100 μm.

Structural analysis of transverse sciatic nerve sections (Figure 19a) revealed the presence of myelinated axons in the contralateral nerves across all postnatal stages. In uninjured nerves (Figure 19b), myelinated axons were readily identifiable by their characteristic circular to oval morphology, with dense, compact myelin sheaths surrounding lighter central axoplasmic regions. The myelin appeared uniform in both thickness and organization, which was consistent with intact and mature nerve fibres. In nerves from uninjured P4 mice, we also observed axons encased by Schwann cells

with a diameter compatible with myelinated fibres but lacking a clearly defined myelin sheath. These structures likely represent axons undergoing early stages of myelination (Supplementary figure 1). Quantification of the total number of myelinated axons (Figure 19c) revealed an increase in axon number with increasing postnatal age. The injured (ipsilateral) nerves of P10 and P30 mice (Figure 19d) revealed a gradual reduction in the number of myelinated axons over time. In contrast, injured P4 nerves exhibited a complete absence of myelinated axons from 2 to 7 dpi. Injured nerves displayed hallmark features of Wallerian degeneration (Figure 19e), including disorganized tissue architecture, myelin sheath fragmentation, and axonal swelling. The myelin rings appeared collapsed, folded, or partially degraded, and numerous vacuolated axonal profiles and myelin debris were scattered throughout the tissue (white arrows), which was consistent with ongoing myelin breakdown and axonal degeneration. The quantification of degenerating axons in the ipsilateral nerves (Figure 19f) revealed a consistent temporal pattern across all postnatal stages: the number of degenerating axons peaked at 4 dpi. This peak was less clear in P30 animals, with similar numbers of degenerating axons at 4 and 7 dpi.

The number of degenerating axons with intact nerves was normalized to calculate the percentage of degenerating axons found over time in the different postnatal stages (Figure 19g). In P10 and P30 mice, ~50% of the axons were degenerating at 2 dpi, with degeneration peaking at 7 dpi. Interestingly, in P4 mice, ~85% of the axons had already degenerated at 2 dpi, reaching a peak of degeneration at 4 dpi, suggesting a more rapid degenerative response in the most immature nerves.

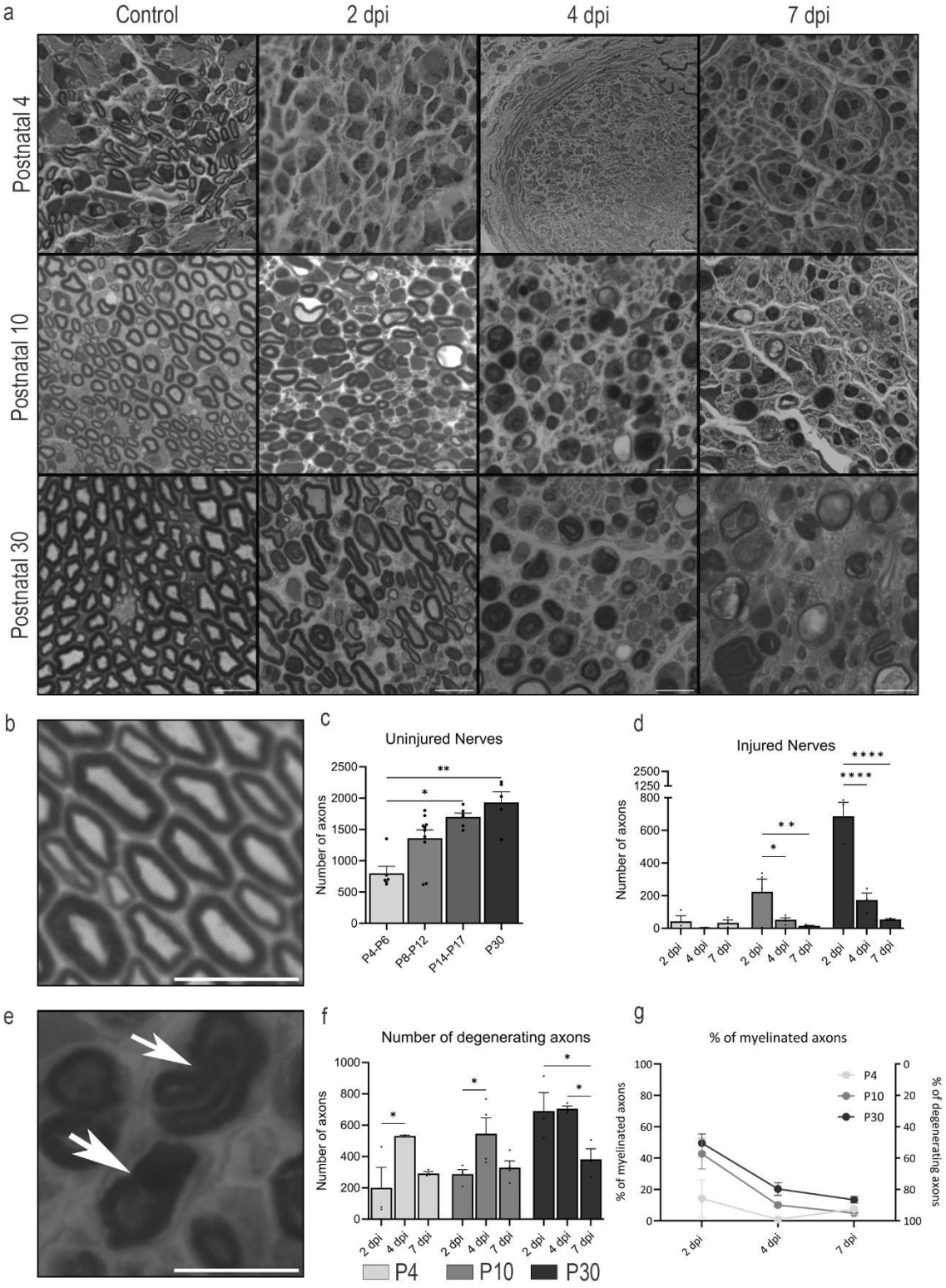

Figure 19. Ultrastructural analysis and axonal density dynamics following sciatic nerve injury across postnatal stages. (a) Representative images of transverse sciatic nerve sections from uninjured (control) and injured (2, 4, and 7 dpi) P4, P10, and P30 mice. (b) Representative image of axons surrounded by myelin sheaths. (c) Quantification of the total number of myelinated axons in control sciatic nerves at different postnatal stages. (d) Quantification of the total number of myelinated axons in injured sciatic

nerves at different postnatal stages. (e) Representative image of different degenerating axons after PNI. (e) Quantification of the total number of degenerating axons in injured sciatic nerves at different postnatal stages. (e) Percentages of myelinated and degenerating axons in the different postnatal stages over time. Statistical significance was determined by the Kruskal–Wallis's test or two-way ANOVA followed by Tukey's correction for multiple comparisons; * p<0.05, ** p<0.01 ****p<0.0001. Scale bar: 10 µm

Transcriptomic analyses from injured sciatic nerves during the postnatal stages

To investigate the transcriptomic differences underlying Wallerian degeneration at different postnatal stages, we performed RNA-seq on sciatic nerves from injured P4, P10, and P30 mice. Age-matched uninjured nerves served as controls. The dataset included 5 samples per group, with sequencing yielding an average of ~23.5 million paired end reads per sample. PCA analysis (Figure 20) shows clustering of the samples based on their gene expression profiles. The left and right panels display the control (Ctrl) and injured (Inj) samples, respectively.

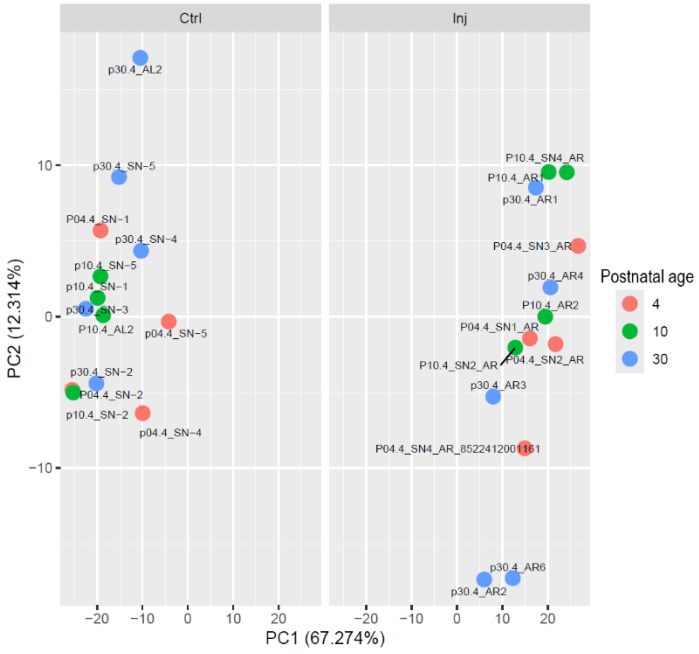

Figure 20. PCA of the sciatic nerve samples included in this study, control (Ctrl) and injured (Inj). Each dot represents an individual sample, showing spatial segregation by condition.

Pathway enrichment analysis

Transcriptomic analysis of the distal sciatic nerve in P30 injured mice (Figure 21a) revealed strong activation of several signalling pathways and biological processes. The most prominent were cell adhesion molecules, axon guidance, MAPK signalling, and cytokine–receptor interaction. Processes linked to cell cycle, apoptosis, and DNA replication were also enriched, pointing to cellular turnover and injury responses. Immune and inflammatory pathways were prominent, including TNF, NF-κB, Toll-like and NOD-like receptor signalling, chemokine signalling, and IL-17. Additional enriched pathways included sphingolipid metabolism, Hippo signalling, and lysosomal genes. Overall, these findings indicate that the distal nerve responds to injury by activating genes involved in adhesion, axonal remodelling, inflammation, stress responses, and regulation of cell cycle and cell death. In P4 injured mice (Figure 21b), transcriptomic profiling of the distal nerve showed marked enrichment of inflammatory and immune-related pathways. The most significant were chemokine signalling, sphingolipid metabolism, cell adhesion molecules, and NF-κB signalling. Other enriched pathways included cytokine–receptor interaction, IL-17 signalling, and NOD-like receptor signalling, together with endocytosis and phagosome formation, reflecting immune activation and clearance processes. Further pathways, such as TNF signalling, axon guidance, Toll-like receptors, leukocyte migration, MAPK, Hippo, apoptosis, gap junctions, and RIG-I-like receptor signalling, were also evident. This pattern suggests that at P4, the distal nerve mounts a strong inflammatory, immune, and cellular remodelling response. In P10 injured mice (Figure 21c), a different enrichment profile was observed. The most significant pathways were cell adhesion molecules and focal adhesion, with strong enrichment in axon guidance and actin cytoskeleton regulation. Signalling routes linked to cellular communication and growth, such as Rap1, MAPK, PI3K–Akt, and ErbB, were also prominent. Other enriched processes included leukocyte migration, ECM–receptor interaction, NK cell-mediated cytotoxicity, and fatty acid biosynthesis and elongation. These findings indicate that at P10, the distal nerve activates pathways related to adhesion, axonal and cytoskeletal remodelling, immune cell migration, and metabolism, reflecting both tissue reorganisation and immune responses.

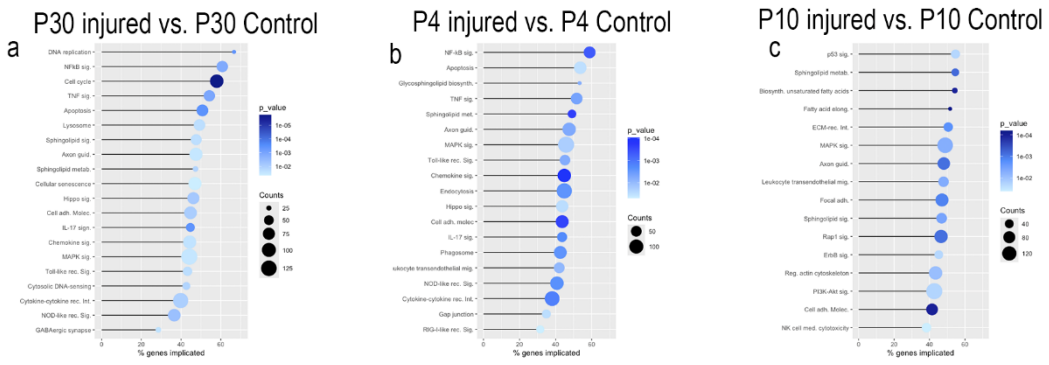

Figure 21. Differential enrichment of KEGG signalling pathways across postnatal stages. Lolliplots display the main enriched signalling pathways identified by gene over-representation analysis ordered by the percentage of genes implicated for that pathway, with p value represented by a colour scale, and number of genes (counts) by a size scale, in sciatic nerve after injury, compared to controls. (a) P30 injured vs. P30 control (b) P4 injured vs. P4 control (c) P10 injured vs. P10 control.

Gene Set Enrichment Analysis (GSEA)

We performed a customized list of canonical myelin-associated genes (J. Li et al. 2013; Yi et al. 2015; Zhao et al. 2022) , including *Mag* (myelin-associated glycoprotein), *Mal* (myelin and lymphocyte protein), *Mbp* (myelin basic protein), *Plp* (proteolipid protein), *Pmp22* (peripheral myelin protein 22), and *Prx* (periaxin) to evaluate their expression after injury. For all the selected genes, we observed a negative Log2fold change values following injury. GSEA of these myelination markers revealed significant downregulation across all examined age groups (Figure 12a, Table 1), with negative normalized enrichment scores (NES) across all time points: P4 (NES=-1,928, p.adj=1,86x10^{-6}), P10 (NES=-1,978, p.adj=3,75x10^{-7}), and P30 (NES=-1,911, p.adj=1,73x10^{-5}), indicating consistent and significant downregulation of this gene set following nerve injury.

We also assessed classical pro-regenerative genes upregulated by SC and macrophages in the distal degenerating stump (Terenghi 1999; Yi et al. 2015; Lee and Cho 2021; Contreras et al. 2022), such as *Gap43* (Growth associated protein 43), *Gdnf* (Glial cell line-derived neurotrophic factor), *Igf1* (Insulin-like Growth factor 1), *Il1a* (Interleukin 1 alpha), *Il1b* (Interleukin 1 beta), *Il6* (Interleukin 6), *Lif* (Leukemia inhibitory factor), *Ncam1* (Neural cell adhesion molecule 1), *Ngf* (Nerve growth factor),

Ngfr (Nerve growth factor receptor) and *Tnf* (Tumor necrosis factor). These genes displayed similar expression profiles across age groups (Figure 22b, Table 1). GSEA analysis revealed significant enrichment of these markers with positive NES values: P4 (NES=1,775, p.adj=0,005), P10 (NES=1,585, p.adj=0,041), and P30 (NES=1,772, p.adj=0.003).

The enrichment analysis demonstrated statistically significant patterns for both mature myelinating Schwann cell markers and pro-regenerative markers across all age groups, with all adjusted p-values<0.05. The enrichment scores indicated consistent downregulation of myelination programs and upregulation of regenerative programs following sciatic nerve transection across the examined developmental stages.

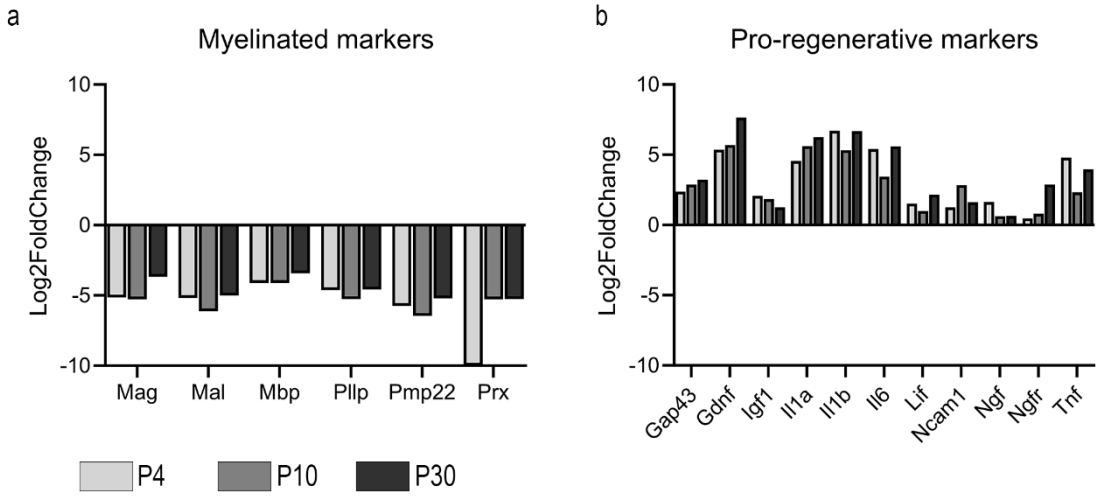

Figure 22. Gene Set Enrichment Analysis (GSEA) showing Log2FoldChange of (a) myelinated markers (Mag, Mal, Mbp, Plp, Pmp22, Prx) and (b) pro-regenerative markers (Gap43, Gdnf, Igf1, Il1a, Il1b, Il6, Lif, Ncam1, Ngf, Ngfr, Tnf) across P4, P10 and P30 injured nerves compared to control ones.

	Mature Myelinated SC markers			**Pro-regenerative markers**		
	P4	**P10**	**P30**	**P4**	**P10**	**P30**
Enrichment score	-0,977	-0,976	-0,972	0,757	0,675	0,774
NES	-1,928	-1,978	-1,911	1,775	1,585	1,772
P. adjusted	1,86E-06	3,75E-07	1,73E-05	0,005	0,041	0,003

Table 1. Results of the Gene Set Enrichment Analysis for mature myelinating Schwann cell markers and pro-regenerative markers in P4, P10, and P30 injured sciatic nerves from mice. Reported values include the enrichment score, NES (normalized enrichment score), and significance values (adjusted P value). A negative NES indicates that the corresponding gene set is downregulated compared with control nerves,

whereas a positive NES indicates that the corresponding gene set is upregulated compared to control nerves.

Analysis of canonical marker gene enrichment revealed dynamic regulation of immune and glial cell populations in the distal sciatic nerve across postnatal development (Figure 23). Macrophage markers showed consistent upregulation at all ages after injury. Genes such as Arg1, Mac-2/Lgals3, Ms4a4c, Trem2, and Marco displayed robust fold enrichment and strong statistical significance (high – log10(padj)), especially at P30 and P4, indicating pronounced macrophage activation in the injured nerve. Notably, Arg1 exhibited the highest enrichment and significance throughout, suggesting strong polarization/activation of macrophages. By contrast, markers like Mertk displayed minimal or negative fold enrichment, indicating selective involvement of subpopulations. Schwann cell markers demonstrated heterogeneous enrichment patterns. Major developmental regulators such as JunB and Ccl2 showed highly significant enrichment after injury at all ages, particularly at P30 and P4. Other markers, including Shh and Artn, were consistently upregulated, while markers like Sox2 and Ncam1 showed modest or variable enrichment, especially at P4 and P10. These data reflect dynamic activation alongside diversity in Schwann cell responses after nerve injury, dependent on age and marker specificity.

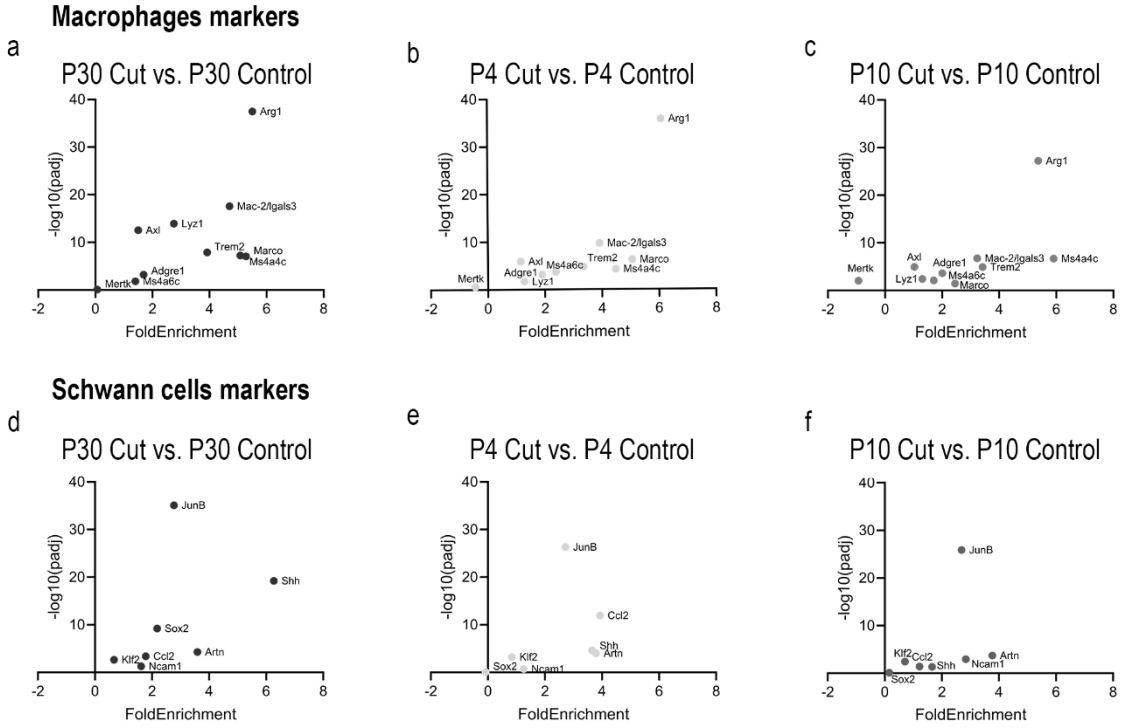

Figure 23. Enrichment of macrophage and Schwann cell marker genes in distal sciatic nerve after transection at different developmental stages. Scatterplots show the fold enrichment and statistical significance (-log10 adjusted p value) for canonical marker genes of macrophages (a-c) and Schwann cells (d-f). Comparisons are shown between injured and control at three ages: (a, d) P30 injured vs. P30 control. (b, e) P4 injured vs. P4 control. (c, f) P10 injured vs. P10 control.

Discussion

It is generally assumed that younger neurons display a greater regenerative capacity following peripheral nerve injury. This notion is mainly based on studies reporting faster regeneration and functional recovery in younger animals (Belin et al., 1996; Brenner et al., 2006). However, part of this apparent advantage might be biased by the massive motoneuron death observed in the earliest postnatal stages (Navarrete and Vrbová 1984; Lowrie and Vrbová 1984). This high mortality rate has also limited the number of studies performed in early postnatal stages. Therefore, it is critical to simultaneously assess both neuronal survival and regenerative capacity during these periods.

In this study, we quantified motoneuron survival and regenerative capacity after peripheral nerve injury using histological and molecular approaches, taking advantage of *Chat-Cre/Ai9* and *Chat-Cre/Ribotag* mice models. In addition, we complemented these data with a descriptive and molecular analysis of Wallerian degeneration. All experiments were performed in animals injured at postnatal days 4, 10 and 30 (P4, P10 and P30).

Death and axonal regeneration of motoneurons when injured at different postnatal stages

Our results first show that nerve injury at P4 induces a substantial loss of motoneurons (~50%), whereas no significant neuronal death was observed at P10 or P30. These findings are consistent with previous studies in postnatal rats and mice, that describes a well-defined period of motoneuron loss (P0–P5 in rodents) after nerve lesions (Navarrete & Vrbová, 1984; Schmalbruch, 1984; Lowrie et al., 1987; Kemp et al., 2015b). We also explored the regenerative capability of motoneurons when injured at these different postnatal stages. For a fair comparison between postnatal ages, it was important to characterize intact nerves. The number of Chat+ axons observed in the nerve increased with age, fact that can be related to a progressive myelination of axons. Thin and still not myelinated axons may be not detected in the confocal microscope and

thus, lower number of fluorescent axons are observed at early postnatal stages compared to juvenile ones. Therefore, for a fair comparison of the regenerative capability at different ages, we normalized the number of regenerating axons by the number of axons in the corresponding contralateral intact nerve. Moreover, the amount of motoneuron death would also impact on the total number of regenerating axons through the distal stump. Therefore, the percentage of regenerating axons after injury was corrected for neuronal death. This correction can have some limitations, since regenerating axons usually extends some sprout when regenerating (Witzel et al., 2005) and therefore, age differences in extending collaterals could affect this ratio, but still contributes to a better understanding of the regenerative capacity of neurons at different postnatal stage. By doing so, we observed that animals injured at P4 exhibited the highest proportion of regenerating axons, whereas regeneration in P10 and P30 animals did not reach control levels at 14 days post injury. These results support the hypothesis that immature animals possess a strong regenerative potential, which may be masked by the high motoneuron death.

Transcriptional programs activated in axotomized motoneurons at different ages

To determine whether these differences depend on the intrinsic growth potential of motoneurons, we analysed the translatome of injured motoneurons at P4, P10 and P30 using the Ribotag assay (Sanz et al., 2019). In juvenile (P30) injured motoneurons, we detected the activation of a regenerative programme, extensively described in the literature (reviewed in Allodi et al., 2012; He & Jin, 2016), with overexpression of several regeneration-associated genes (RAGs), including *Atf3, Gap43, Ngfr* and *Ccl2*. In contrast, upregulation of classical RAGs was absent in P4 and P10. Despite the lack of upregulation of RAGs, these motoneurons were able to regenerate, fact that suggests that these neurons retain a strong outgrowth potential and, therefore, do not need to switch to a pro-regenerative transcriptional program. However, we cannot rule out that the absence of changes in our dataset may be influenced by the timing of analysis (7 dpi), and earlier timepoints (2–4 dpi) might reveal a more pronounced transcriptional response.

The analysis of specific pathways enriched after injuring juvenile motoneuron supports a mature regenerative programme capable of integrating cell survival mechanisms, metabolic adaptations and tissue remodelling. Pathways related with axonal regeneration and cell survival, such as Hypoxia-related responses (Cho et al., 2015; Smaila et al., 2020) and enrichment in steroid biosynthesis and cholesterol homeostasis (Porcu et al., 2016; Lin et al., 2020; Tang 2022), were upregulated. Inflammatory pathways, including TNF-α/NF-kB, were also strongly upregulated; NF-kB in particular plays a central role in both inflammation and neuronal survival, regulating genes downstream of TNF-α and IL-1β (Anilkumar & Wright-Jin, 2024). Other relevant pathways included IL6/Stat3, essential for axonal regrowth (Cafferty et al., 2004), glial activation, proliferation and anti-apoptotic responses (Shimizu, Kiyooka, and Ohshima 2021; Leibinger et al., 2021), and the Neuregulin-1/ErbB system, which supports both axonal regeneration and motoneuron protection under excitotoxic stress (Chang et al., 2013; Mòdol-Caballero et al., 2018; Romero-Ortega et al., 2023). Finally, enrichment of cytoskeletal remodelling and cell migration pathways was observed, consistent with their essential roles in growth cone formation and axonal regrowth (Blanquie and Bradke 2018; Leite et al., 2021). Despite the limited death of injured motoneurons observed at these stages, we found enrichment of apoptosis- and death receptor-related pathways, including the activation of genes such as *caspase-3* and oxidative stress responses (Martin et al., 2005).

In terms of signalling, surviving motoneurons at P4 displayed enrichment in pathways linked to elevated ATP production, notably oxidative phosphorylation, key element in the aerobic metabolism, that predominates in mature neurons and confers them protection against stressors (Jimenez-Blasco et al., 2024). *Foxo1*, a key regulator of cell survival under adverse conditions (Du & Zheng, 2021) was also upregulated. However, this upregulation seems insufficient to rescue axotomized neurons from death at these stages. Additional enriched pathways included cholesterol homeostasis, relevant for axonal growth (Tang, 2022), and estrogenic responses, consistent with reported neuroprotective effects (Fargo et al., 2009). Classical pathways related with death were not upregulated despite the marked motoneuron death detected at this stage.

In P10 animals, no significant motoneuron loss was observed compared to uninjured controls, but regenerative capacity was not as good as in P4 and P30 animals. Previous studies have reported that regeneration is limited at this developmental window (P10–P15), likely due to progressive loss of plasticity, increased neurotrophic dependence and a more pro-inflammatory environment (Fitzgerald & McKelvey, 2016). A down-regulation of some RAGs after the injury could contribute to this impaired regenerative capability. Moreover, the increase of T3 hormone levels during this period have been related with a reduced axonal regenerative potential (Avci et al., 2012). The combination of an unfavourable environment and reduced growth factor signalling could explain the poor RAG upregulation (Schwab and Bartholdi 1996; Oishi et al., 2004). The signalling profile at P10 was markedly different from P4 and P30. Specifically, we found widespread downregulation of mTORC1/TOR, a central pathway for axonal growth and regeneration (Switon et al., 2017). Inhibition of cytoskeletal remodelling and axonal transport pathways, processes essential for growth cone dynamics, were also observed (Bisby and Tetzlaff 1992; Blanquie and Bradke 2018). Downregulation of cellular respiration pathways could lead to an insufficient energy production to support regeneration. Finally, autophagy response was downregulated, which is critical for organelle clearance and cellular renewal (Huang et al., 2016; Chen et al., 2025), further contributing to reduced regenerative competence.

Wallerian degeneration of the distal injured nerve at different postnatal stages

Since we evaluated the regenerative capability of motoneurons in vivo, extrinsic factors must also be considered, particularly Wallerian degeneration. Axonal regeneration depends largely on the efficiency of this process, which clears myelin and axonal debris to create a permissive environment (Rotshenker, 2011). To characterise this response, we used a complete sciatic nerve transection model without repair, which prevents spontaneous regeneration and allows a precise description of degeneration dynamics during the first post-injury week.

In P30 and P10 mice, nerve injury triggers the canonical degenerative cascade, characterised by progressive myelin breakdown, lipid accumulation, macrophage

recruitment and the transition of Schwann cells towards a repair phenotype (Geuna et al., 2009; Gaudet et al., 2011) as previously described (Rotshenker, 2011). In contrast, P4 nerves degenerated rapidly, with near-complete myelin loss within 2–4 dpi, minimal increase of macrophages (CD68), low transient lipid accumulation and scarce myelin remnants (LFB).

Despite some differences at the molecular level, at all ages studied we could observe a successful downregulation of Schwann cell myelination genes, such as *Mag, Mal, Mbp, Pllp, Pmp22* and *Prx* (J. Li et al., 2013; Yi et al., 2015; Zhao et al., 2022). and an up regulation of pro-regenerative ones such as *Gap43, Gdnf, Igf1a, Il1a, Il1b, Lif, Ncam1, Ngf, Ngfr* and *Tnf* (Terenghi 1999; Yi et al., 2015; Lee and Cho 2021; Contreras et al., 2022). It is worth to note that, despite the reduced number of macrophages observed in degenerating nerves injured at P4, upregulation of genes whose products are secreted by macrophages during Wallerian degeneration are also observed at this stage. Again, it seems that the low quantity of these cells in the degenerating nerves of these animals does not impact on the pro-regenerative environment of the distal nerve. The apparent contradiction of our findings at P4 (low increase of macrophages in the injured nerve but an inflammatory profile like the one observed at P30) could be linked with the lower amount of myelin observed in immature nerves. In these circumstances, a modest increase of macrophages is sufficient to phagocyte the myelin, that in fact is rapidly cleared; but these macrophages, together with Schwann cells, orchestrate a good pro-regenerative response, that contribute to the successful growth of the axons of surviving motoneurons. In fact, at all three stages, we also detected strong expression of phagocytic and repair macrophage markers, including *Arg1* (Ydens et al., 2012; Stratton et al., 2020; Msheik et al., 2022), *Lgals3* (Stratton et al., 2020), *Trem2* (Ydens et al., 2012; Stratton et al., 2020; Peshoff et al., 2023) and *Marco* (Stratton et al., 2020). We also identified markers of repair Schwann cells, such as *JunB* (Jessen and Mirsky 2016), *Ccl2*, essential for macrophage recruitment, *Shh*, which promotes c-Jun activation, and *Artn*, that supports neuronal survival and axonal regeneration (Jessen and Mirsky 2016; Jessen and Mirsky 2019; Kalinski et al., 2020).

Besides these similarities, pathways were differentially enriched depending on the age. In P30 animals, we observed robust activation of inflammatory and immune

pathways, including NOD-like receptors (Ydens et al., 2015), IL-17 signalling, crucial for macrophage recruitment (Bombeiro et al., 2024) (Y. Huang et al., 2024), and TNF-α (Alhamdi et al., 2025). In parallel, we detected strong activation of proliferative and repair programmes, consistent with Schwann cell expansion post-injury (Hung et al., 2015; Painter et al., 2014). Signalling analysis highlighted MAPK/ERK (Lindwall Blom, Mårtensson, and Dahlin 2014; Wei et al., 2024; Liu and Zhou 2025), which promotes Schwann cell reprogramming, and the Hippo pathway (Feltri et al., 2021; Wang et al., 2023), implicated in differentiation towards the myelinating phenotype. We also identified upregulation of sphingolipid metabolism, relevant for neuronal signalling (Meyer zu Reckendorf et al., 2020; C. Li et al., 2024), and lysosomal activation, essential for myelin clearance.

In P4 animals, transcriptomic profiles showed enrichment of chemokine signalling pathways, a hallmark of the neonatal inflammatory response (F. Wang et al., 2025). NF-kB was also activated, driving the production of inflammatory mediators such as TNF-α and IL-1β (Zhang et al., 2025). Despite these differences, P4 shared with P30 the activation of IL-17, MAPK/ERK, Hippo and sphingolipid metabolism, indicating that both ages engage similar degenerative mechanisms to create a permissive environment for regeneration.

By contrast, P10 animals exhibited a transcriptional profile that could contribute to lower regenerative capacity. Notably, we detected activation of p53 pathway and pro-apoptotic genes such as *Bax* and inhibition of survival genes (Culmsee & Mattson, 2005; Li et al., 2023). Nevertheless, several pathways were shared with P30, including sphingolipid metabolism, adhesion molecule signalling and axon-related pathways. Therefore, at this stage, there is an active response attempting to promote axonal regeneration, albeit not as complete as in juvenile mice.

Taken together, our results indicate that Wallerian degeneration proceeds efficiently at all the developmental stages analysed, despite some molecular or structural differences that could influence axonal regeneration. A lower amount of macrophage infiltration at early postnatal stages only reflects a reduced demand of phagocytosis due to the low myelination ratios at these ages, that does not interfere

with the ability of the distal stump to create a permissive milieu for regeneration. In contrast, we observed robust differences in the transcriptional profile of axotomized motoneurons depending on the age when were injured. Therefore, differences in regenerative capacity seems primarily determined by the intrinsic growth state of motoneurons at the time of injury. At P4, motoneurons remain in a growth state reminiscent of the embryonic stage and therefore do not require the activation of a dedicated pro-regenerative transcriptional programme, as occurs in P30 neurons. In contrast, juvenile motoneurons undergo a marked upregulation of regeneration-associated genes (RAGs), which are essential to ensure axonal regeneration in mature peripheral neurons. P10 neurons, however, could be in a transitional stage: they have already begun to downregulate their growth-related profile but still fail to efficiently activate a pro-regenerative programme after injury. This may underlie a slightly lower regenerative capacity compared with both younger postnatal and more mature neurons. However, it is important to remark that motoneurons at all ages retained a good regenerative ability, and the major limiting factor in early postnatal stages is the massive neuronal death.

Conclusion

Despite the massive loss observed in motoneurons when axotomized at P4, surviving ones shown a robust regenerative capacity, that surprisingly is not dependent on the activation of RAGs. These neurons probably do not need to switch to a pro-regenerative program since still retaining an embryonic growth like state. On the other hand, although early studies proposed that the immaturity of Schwann cells might contribute to neuronal loss at these early stages, our results indicate that Wallerian degeneration is already efficient in both clearing myelin debris and creating a permissive pro-regenerative environment at neonatal stages. Instead, it is the transcriptomic profile of injured motoneurons that differs substantially with age, highlighting intrinsic neuronal factors as the key determinants of regenerative success. Further investigation into the pathways that are differentially regulated between P4, P10 and P30 motoneurons could therefore provide critical insights into the mechanisms driving motoneuron vulnerability and death at early postnatal stages

Funding

This work was funded by the project PID2021-127626OB-I00 from Ministerio de Asuntos económicos y Transformación Digital of Spain. The author's research was also supported by funds from CIBERNED and TERCEL networks, co-funded by European Union (ERDF/ESF, "Investing in your future").

Acknowledgements

The authors appreciate the technical help of Neus Hernández. Mònica Espejo and Jessica Jaramillo.

Declaration of Competing Interest

The authors declare no competing financial interests.

Author Contributions

Beatriu Molina Esteve, Natalia Lago, and Esther Udina contributed to the conception and design of the study. Material preparation, data collection, and analysis were performed by all authors (Beatriu Molina Esteve, Marina Pujol-Masip, David Ovelleiro, José Antonio Gómez-Sánchez, Natalia Lago, and Esther Udina). The first draft of the manuscript was written by Beatriu Molina Esteve, and all authors commented on previous versions of the manuscript. Supervision and critical revision for important intellectual content were provided by Natalia Lago and Esther Udina. All authors read and approved the final manuscript.

Supplementary Data

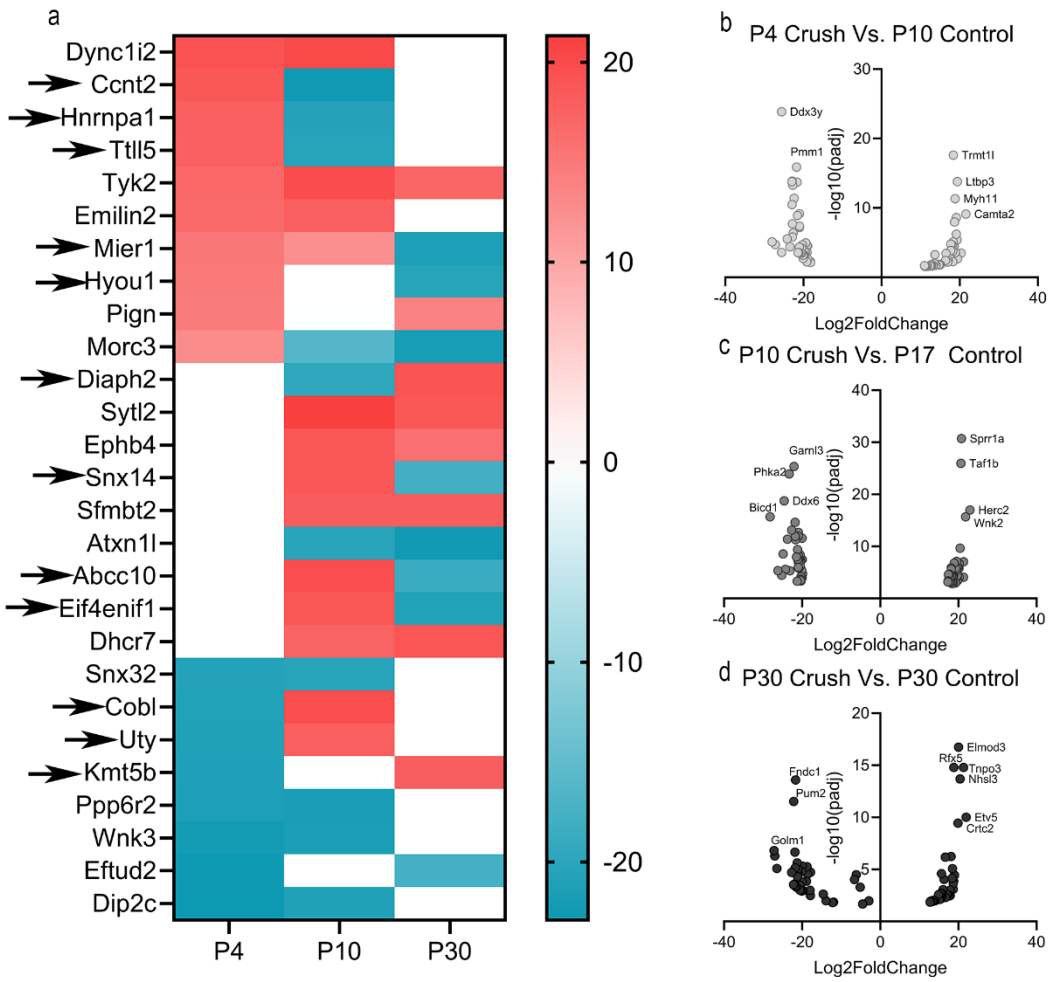

Supplementary Figure 1. Changes in gene expression 7 days after the crush injury in the motoneuron translatome in P4, P10 and P30 mice. (a) Heatmap showing the variation in expression of selected genes at P4, P10 and P30. Genes highlighted with arrows were selected for their relevance. The colour scale indicates the range of expression (Log2FoldChange), from upregulation (red) to downregulation (blue). (b-d) Volcano plots showing changes in gene expression (Log2FoldChange) and significance (-log10(padj)) between crush and control conditions for the indicated time point comparisons. (b) P4 Crush vs. P10 Control (c) P10 Crush vs. P17 Control (d) P30 Crush vs. P30 Control. Labelled gene names highlight those most significantly regulated in each contrast.

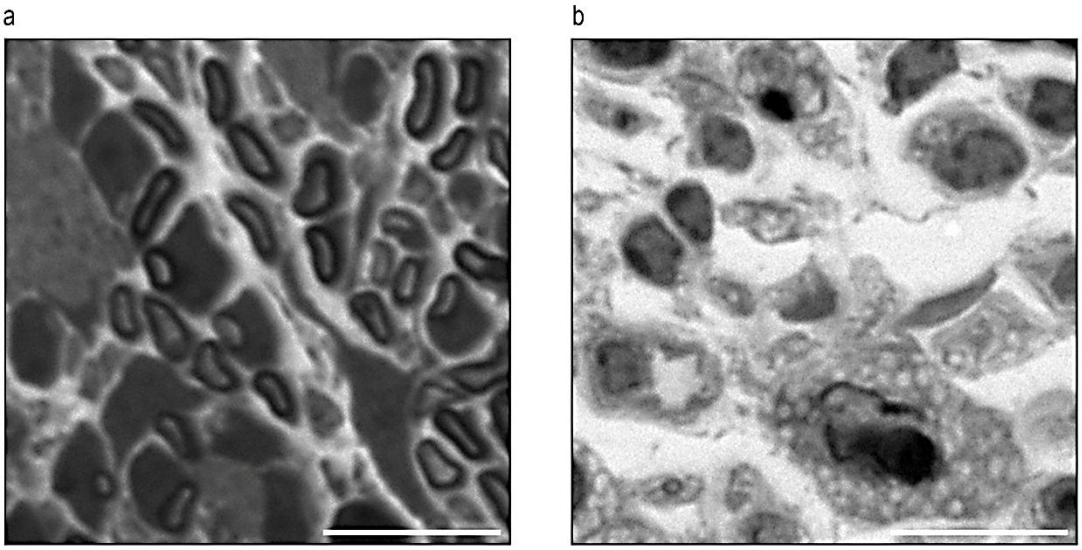

Supplementary Figure 2. (a) Representative image of uninjured nerve from P4 mice, showing the immature myelinating nerves. (b) Representative image of phagocyting bodies present after an injury in the sciatic nerve. Scale bar: 10 μm

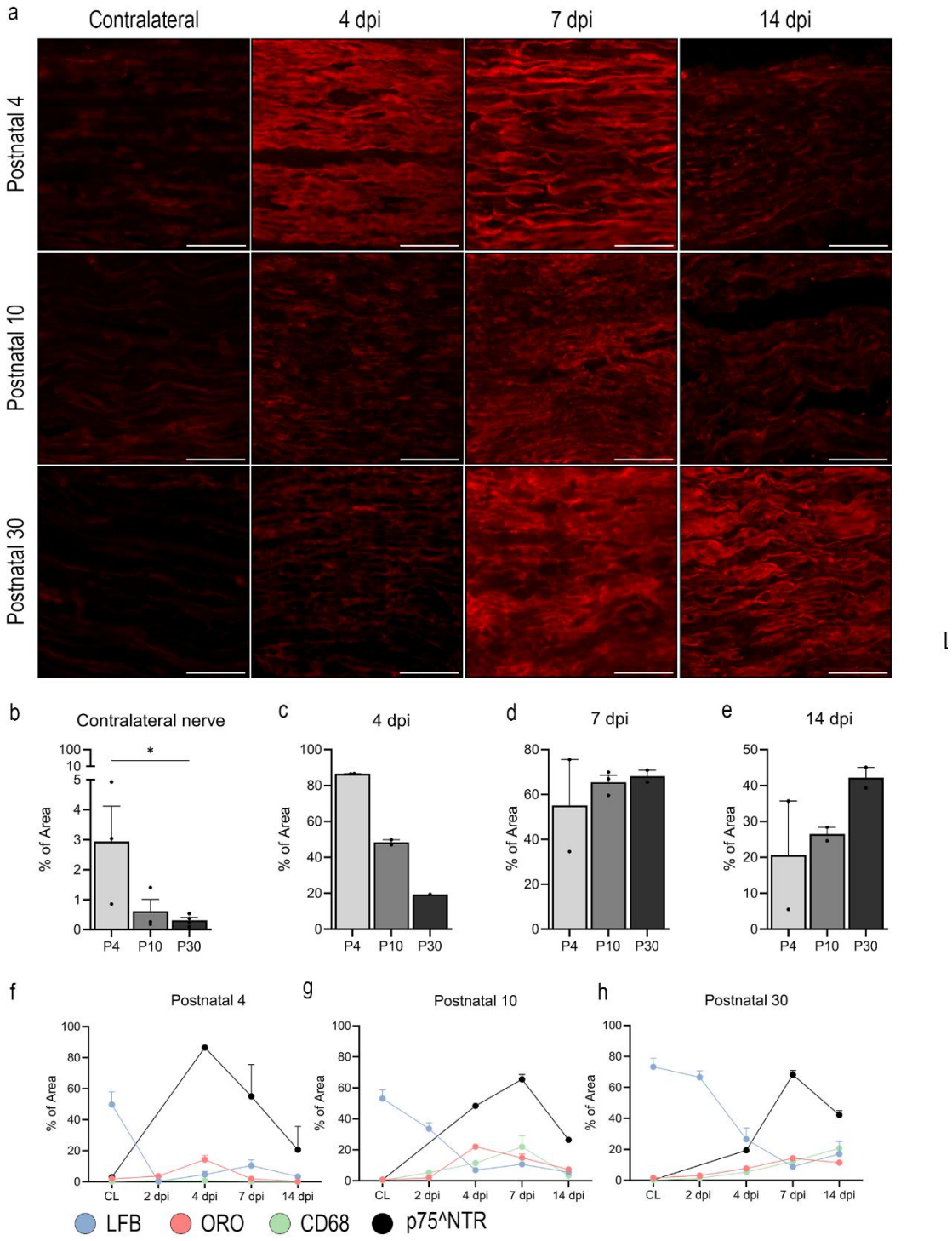

Supplementary Figure 3. (a) Representative images of p75^NTR immunostaining in injured nerves of P4, P10 and P30 mice 4,7 and 14 dpi and its contralateral. (b-e) Percentage of area stained with anti-p75^NTR in P4, P10 and P30 contralateral and injured nerves. Statistics: Kruskal-Wallis test. $p<0.05$. (f-g) Percentage of area stained with LFB, ORO, CD68 and p75^NTR of contralateral and injured nerves of P4, P10 and P30 mice 2, 4, 7 and 14 dpi.

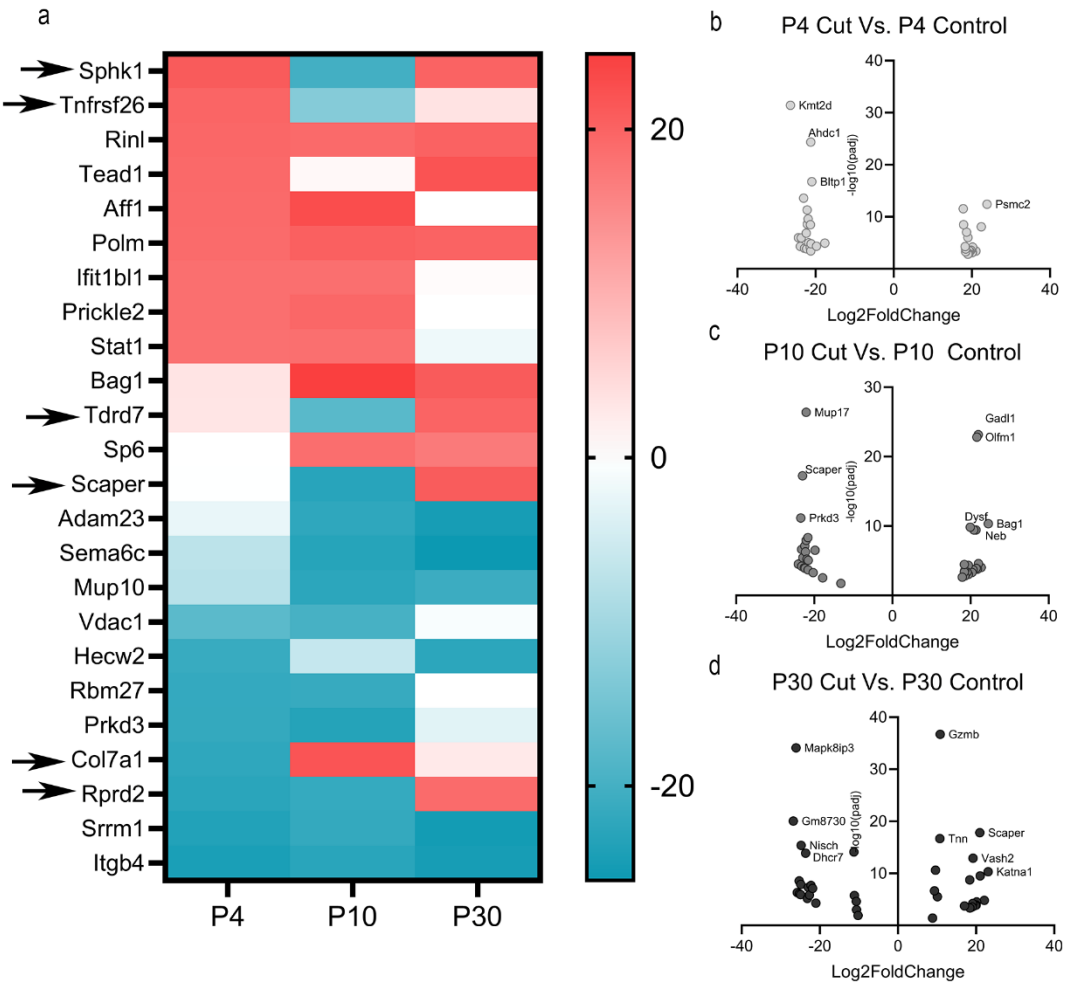

Supplementary Figure 4. Changes in gene expression 4 days after the cut injury in the Sciatic nerve transcriptome in P4, P10 and P30 mice. (a) Heatmap showing the variation in expression of selected genes at P4, P10 and P30. Genes highlighted with arrows were selected for their relevance. The colour scale indicates the range of expression (Log2FoldChange), from upregulation (red) to downregulation (blue). (b-d) Volcano plots showing changes in gene expression (Log2FoldChange) and significance (-log10(padj)) between cut and control conditions for the indicated time point comparisons. (b) P4 Cut vs. P4 Control (c) P10 Cut vs. P10 Control (d) P30 Cut vs. P30 Control. Labelled gene names highlight those most significantly regulated in each contrast.

	P30		P4		P10	
Gene ID	**Log2FC**	**padj**	**Log2FC**	**padj**	**Log2FC**	**padj**
Katna1	23,079	4,79E-11	1,502	7,65E-01	0,545	9,15E-01
Tead1	22,109	1,52E-05	19,277	1,11E-03	0,925	9,01E-01
Bag1	21,044	2,99E-10	3,407	4,31E-01	24,565	4,58E-11
Scaper	20,935	1,52E-18	-0,224	9,52E-01	-23,011	5,70E-18

Rinl	20,145	2,93E-05	19,521	4,20E-04	19,132	4,30E-04
Sphk1	20,040	1,10E-04	21,050	3,90E-04	-20,271	5,10E-04
Polm	20,036	1,10E-04	18,986	1,51E-03	20,358	4,80E-04
Sh3pxd2	19,945	3,64E-05	-14,824	1,04E-02	0,256	9,72E-01
Tdrd7	19,824	1,40E-04	3,307	6,41E-01	-17,839	2,92E-03
Vash2	19,223	1,22E-13	0,803	8,28E-01	1,053	7,68E-01
Brpf1	19,143	6,29E-05	0,234	9,77E-01	2,619	6,80E-01
Rprd2	18,984	2,70E-04	-22,826	1,10E-04	-21,585	2,00E-04
Eif2b4	18,433	4,30E-04	-5,007	4,69E-01	0,352	9,64E-01
Shf	18,362	1,74E-09	-0,617	8,94E-01	-0,879	8,37E-01
Sp6	17,042	1,70E-04	-0,165	9,82E-01	18,526	2,60E-04
Gzmb	10,827	1,92E-37	8,094	3,96E-21	6,473	1,05E-09
Tnn	10,735	2,07E-17	7,651	1,73E-07	10,393	2,86E-13
Gria1	10,126	3,03E-06	8,451	7,80E-04	2,823	2,42E-01
Cxcl3	9,612	2,47E-11	9,266	1,65E-08	7,048	2,00E-05
Myh3	9,336	2,30E-07	6,456	1,80E-03	6,239	2,09E-03
Ankrd1	7,843	4,00E-04	21,384	1,54E-16	7,898	1,73E-03
Atp1b4	6,703	1,02E-03	3,122	1,47E-01	10,997	7,11E-07
Igfn1	5,433	7,00E-04	2,085	3,14E-01	11,143	2,39E-09
Tnfrsf26	3,597	5,33E-01	19,798	2,50E-04	-13,156	1,84E-02
Col7a1	2,713	6,79E-01	-22,292	1,40E-04	21,751	1,60E-04
Ahdc1	2,655	1,41E-01	-21,227	4,53E-25	1,657	4,24E-01
Tro	2,094	7,44E-01	0,519	9,47E-01	20,639	1,80E-04
Nfia	2,017	5,41E-01	-0,816	8,36E-01	-22,784	1,06E-13
Adcy7	2,014	5,90E-01	0,462	9,21E-01	21,396	3,58E-10
Fndc3b	1,807	7,56E-01	20,197	6,62E-05	-0,301	9,64E-01
Slc6a2	1,522	7,91E-01	-21,122	1,52E-05	0,235	9,72E-01
C5ar2	1,518	6,95E-01	18,625	8,74E-08	0,871	8,40E-01
Aftph	1,440	6,62E-01	17,880	3,41E-09	1,124	7,52E-01
Dysf	1,244	7,24E-01	0,932	8,12E-01	19,939	1,47E-10
Slc25a14	1,027	8,63E-01	-1,570	8,00E-01	-21,626	7,72E-06
Olfm1	1,026	6,49E-01	2,290	3,09E-01	21,640	1,55E-23

Wdr26	0,658	9,31E-01	20,065	7,40E-04	0,082	9,92E-01
Gadl1	0,606	8,03E-01	2,272	3,22E-01	21,978	7,04E-24
Ifit1bl1	0,472	9,44E-01	18,442	5,10E-04	18,434	4,00E-04
Kmt2a	0,421	9,51E-01	-13,267	1,93E-02	22,036	2,62E-05
Phlpp2	0,150	9,84E-01	-5,356	4,44E-01	-24,075	3,16E-05
Uvssa	0,132	9,81E-01	-22,381	1,41E-07	-1,198	8,22E-01
Ankrd2	0,128	9,79E-01	21,438	2,31E-09	-0,057	9,91E-01
Ryr1	0,096	9,90E-01	17,263	4,22E-03	17,890	2,36E-03
Ilf3	0,080	9,87E-01	22,438	8,22E-09	1,945	6,71E-01
Rbm27	-0,009	9,99E-01	-21,748	9,48E-06	-21,548	8,66E-06
Aff1	-0,037	9,96E-01	19,105	1,40E-03	22,723	9,06E-05
Primpol	-0,041	9,94E-01	-0,320	9,57E-01	-22,414	7,31E-08
Zbtb43	-0,074	9,79E-01	21,594	5,24E-22	0,382	8,86E-01
Prickle2	-0,149	9,81E-01	18,409	1,50E-04	19,430	4,56E-05
Neb	-0,321	9,41E-01	-0,303	9,49E-01	20,854	3,69E-10
Tyrp1	-0,625	9,35E-01	-6,402	3,39E-01	18,551	1,56E-03
Spg7	-0,852	8,79E-01	-2,047	7,16E-01	-23,220	2,35E-07
Ttbk2	-0,856	8,21E-01	-22,172	4,79E-12	-1,519	6,85E-01
Nlgn3	-0,955	7,86E-01	-23,026	2,52E-14	-1,618	6,42E-01
Rnf213	-0,965	7,39E-01	-3,248	2,39E-01	-24,922	4,33E-22
Pcbd2	-1,097	8,74E-01	0,350	9,65E-01	21,431	1,20E-04
Scn8a	-1,109	6,84E-01	17,804	2,90E-12	-1,668	5,45E-01
Kmt2d	-1,174	6,08E-01	-26,407	3,95E-32	-0,765	7,64E-01
Bltp1	-1,390	5,87E-01	-20,970	1,77E-17	-3,685	1,34E-01
Csrnp1	-1,600	7,19E-01	0,720	8,92E-01	-22,058	1,14E-08
Psmc2	-1,613	6,59E-01	23,877	3,81E-13	-0,771	8,51E-01
Slc25a13	-1,887	6,47E-01	-22,120	2,53E-09	-2,904	4,85E-01
Stat1	-1,975	6,96E-01	18,292	5,18E-05	18,421	3,41E-05
Mup17	-2,102	2,63E-01	16,566	4,04E-15	-22,047	4,18E-27
Celf1	-2,571	6,99E-01	20,148	7,10E-04	-0,199	9,80E-01
Tmod2	-3,021	4,17E-01	-21,312	3,34E-09	-2,989	4,55E-01
Prkd3	-3,316	3,44E-01	-21,896	2,65E-10	-23,455	6,91E-12

Ppfia3	-3,619	3,39E-01	-3,558	4,01E-01	-21,601	4,69E-09
Cobl	-3,883	4,03E-01	-2,742	6,11E-01	-22,227	5,24E-07
Nlrx1	-6,673	7,59E-02	18,987	9,96E-07	1,003	8,35E-01
Ppp6r2	-7,424	2,05E-01	-21,210	3,50E-04	0,718	9,24E-01
Smtn	-10,212	1,20E-02	-6,555	1,78E-01	-4,593	3,39E-01
Ttc17	-10,614	9,00E-04	-9,494	1,04E-02	-3,992	2,85E-01
Rps3a3	-10,651	2,40E-05	17,156	1,59E-09	-0,063	9,87E-01
Rps3a2	-11,148	1,77E-06	2,373	4,34E-01	-0,128	9,70E-01
Cntn1	-11,287	7,85E-15	-5,922	5,64E-06	-7,233	2,93E-08
Mup10	-21,015	5,10E-05	-7,639	2,53E-01	-22,577	1,00E-04
Mup10	-21,015	5,10E-05	-7,639	2,53E-01	-22,577	1,00E-04
Ptk2b	-21,824	7,78E-08	-8,419	9,35E-02	1,613	7,76E-01
Hecw2	-22,640	1,44E-06	-21,337	7,87E-05	-6,297	2,86E-01
Hecw2	-22,640	1,44E-06	-21,337	7,87E-05	-6,297	2,86E-01
Epha4	-22,959	5,01E-08	-1,060	8,68E-01	0,735	9,05E-01
Ino80d	-23,182	6,71E-06	-0,363	9,65E-01	17,699	2,60E-03
Ino80d	-23,182	6,71E-06	-0,363	9,65E-01	17,699	2,65E-03
Dhcr7	-23,638	1,36E-14	-5,332	1,68E-01	-3,301	3,96E-01
Nisch	-24,799	4,12E-16	-2,898	4,68E-01	0,987	8,19E-01
Itgb4	-24,878	1,29E-08	-24,375	1,07E-06	-22,926	3,71E-06
Itgb4	-24,878	1,29E-08	-24,375	1,07E-06	-22,926	3,71E-06
Adam23	-24,892	1,18E-06	-2,406	7,43E-01	-22,339	1,20E-04
Adam23	-24,892	1,18E-06	-2,406	7,43E-01	-22,339	1,20E-04
Srp54c	-25,241	8,13E-07	-16,810	6,32E-03	-2,287	7,47E-01
Srrm1	-25,260	2,80E-09	-23,679	1,16E-06	-21,889	5,88E-06
Srrm1	-25,260	2,80E-09	-23,679	1,16E-06	-21,889	5,88E-06
Sema6c	-25,766	4,67E-07	-7,251	2,80E-01	-23,209	6,22E-05
Sema6c	-25,766	4,67E-07	-7,251	2,80E-01	-23,209	6,22E-05
Mapk8ip3	-26,047	7,42E-35	-3,177	2,01E-01	-2,589	2,95E-01
Gm8730	-26,764	8,59E-21	16,931	3,99E-07	-1,451	7,06E-01
Thsd4	-30,000	6,26E-09	2,430	7,40E-01	-0,032	9,96E-01

Supplementary table 1. 120 most up and down regulated genes expressed in the injured motoneurons at P30, P4 and P10 vs uninjured motoneurons at P30, P10 and P17 respectively.

	P30		P4		P10	
Gene ID	**Log2FC**	**padj**	**Log2FC**	**padj**	**Log2FC**	**padj**
Katna1	23,07917	4,79E-11	1,501669	0,76498	0,545466	0,91469
Tead1	22,10926	1,52E-05	19,27691	0,00111	0,924681	0,90086
Bag1	21,04386	2,99E-10	3,407312	0,43132	24,56493	4,58E-11
Scaper	20,93481	1,52E-18	-0,22382	0,95179	-23,0106	5,70E-18
Rinl	20,14543	2,93E-05	19,52082	0,00042	19,13224	0,00043
Sphk1	20,04023	0,00011	21,0495	0,00039	-20,2712	0,00051
Polm	20,03607	0,00011	18,98626	0,00151	20,35802	0,00048
Sh3pxd2	19,94495	3,64E-05	-14,824	0,01035	0,256432	0,97216
Tdrd7	19,82364	0,00014	3,307255	0,64093	-17,8393	0,00292
Vash2	19,22289	1,22E-13	0,803446	0,82777	1,052568	0,76757
Brpf1	19,14345	6,29E-05	0,233679	0,97664	2,618925	0,68036
Rprd2	18,98411	0,00027	-22,8264	0,00011	-21,5846	0,00020
Eif2b4	18,43305	0,00043	-5,00663	0,46853	0,352486	0,96391
Shf	18,36205	1,74E-09	-0,61727	0,89353	-0,87867	0,83714
Sp6	17,04172	0,00017	-0,16495	0,98236	18,52577	0,00026
Gzmb	10,82656	1,92E-37	8,093789	3,96E-21	6,473336	1,05E-09
Tnn	10,73501	2,07E-17	7,651223	1,73E-07	10,39341	2,86E-13
Gria1	10,12552	3,03E-06	8,451137	0,00078	2,823461	0,24195
Cxcl3	9,612205	2,47E-11	9,265997	1,65E-08	7,048408	2,00E-05
Myh3	9,336363	2,30E-07	6,456478	0,00180	6,238639	0,00209
Ankrd1	7,842653	0,00040	21,38376	1,54E-16	7,898072	0,00173
Atp1b4	6,702862	0,00102	3,122306	0,14744	10,9968	7,11E-07
Igfn1	5,432694	0,00070	2,084802	0,31391	11,14282	2,39E-09
Tnfrsf26	3,596619	0,5332	19,79766	0,00025	-13,1559	0,01838
Col7a1	2,712504	0,67912	-22,292	0,00014	21,75071	0,00016
Ahdc1	2,655241	0,14100	-21,2267	4,53E-25	1,657074	0,42398
Tro	2,094214	0,74429	0,519323	0,94684	20,63874	0,00018
Nfia	2,016632	0,54116	-0,81551	0,83628	-22,7835	1,06E-13

Adcy7	2,014264	0,58960	0,462076	0,9207	21,39553	3,58E-10
Fndc3b	1,807116	0,75550	20,19653	6,62E-05	-0,30123	0,96391
Slc6a2	1,521895	0,79112	-21,1218	1,52E-05	0,234517	0,97160
C5ar2	1,518206	0,6954	18,62507	8,74E-08	0,870767	0,83996
Aftph	1,440322	0,66156	17,88008	3,41E-09	1,123961	0,75209
Dysf	1,243534	0,7244	0,932058	0,81235	19,939	1,47E-10
Slc25a14	1,027367	0,86286	-1,5699	0,80000	-21,6259	7,72E-06
Olfm1	1,026024	0,64894	2,290001	0,3094	21,64016	1,55E-23
Wdr26	0,65847	0,93053	20,0654	0,00074	0,081922	0,99199
Gadl1	0,606065	0,80312	2,271605	0,32153	21,97817	7,04E-24
Ifit1bl1	0,472155	0,94436	18,44224	0,00051	18,43353	0,00040
Kmt2a	0,420976	0,9508	-13,2673	0,01930	22,03587	2,62E-05
Phlpp2	0,14996	0,98412	-5,35602	0,44377	-24,075	3,16E-05
Uvssa	0,131878	0,98143	-22,3807	1,41E-07	-1,19752	0,82160
Ankrd2	0,128102	0,97892	21,43772	2,31E-09	-0,05719	0,99084
Ryr1	0,095668	0,98979	17,26313	0,00422	17,89004	0,00236
Ilf3	0,079708	0,98726	22,43789	8,22E-09	1,944516	0,67076
Rbm27	-0,0092	0,9986	-21,7482	9,48E-06	-21,5478	8,66E-06
Aff1	-0,03689	0,99589	19,10513	0,00140	22,72264	9,06E-05
Primpol	-0,04058	0,99394	-0,32045	0,95738	-22,4142	7,31E-08
Zbtb43	-0,07432	0,97910	21,59444	5,24E-22	0,382009	0,88592
Prickle2	-0,14856	0,98143	18,40905	0,00015	19,4296	4,56E-05
Neb	-0,32073	0,94060	-0,30264	0,94882	20,85406	3,69E-10
Tyrp1	-0,62493	0,93518	-6,40238	0,33914	18,55115	0,00156
Spg7	-0,85249	0,87927	-2,04719	0,71621	-23,2201	2,35E-07
Ttbk2	-0,85585	0,82099	-22,1718	4,79E-12	-1,51884	0,68488
Nlgn3	-0,95534	0,78598	-23,0259	2,52E-14	-1,61789	0,64249
Rnf213	-0,96454	0,73933	-3,24808	0,23937	-24,9219	4,33E-22
Pcbd2	-1,09731	0,87388	0,350297	0,96520	21,43066	0,00012
Scn8a	-1,10858	0,68401	17,8039	2,90E-12	-1,66828	0,54515
Kmt2d	-1,1742	0,60839	-26,4071	3,95E-32	-0,76497	0,76419
Bltp1	-1,39034	0,58682	-20,9697	1,77E-17	-3,68529	0,13359

Csrnp1	-1,60013	0,71923	0,719605	0,89168	-22,0582	1,14E-08
Psmc2	-1,61345	0,65942	23,87661	3,81E-13	-0,771	0,85076
Slc25a13	-1,88655	0,64654	-22,1196	2,53E-09	-2,90383	0,48526
Stat1	-1,97476	0,69636	18,29234	5,18E-05	18,42128	3,41E-05
Mup17	-2,10152	0,26260	16,56602	4,04E-15	-22,0473	4,18E-27
Celf1	-2,57076	0,69931	20,14806	0,00071	-0,19896	0,98043
Tmod2	-3,02097	0,41674	-21,312	3,34E-09	-2,98943	0,45499
Prkd3	-3,3163	0,34408	-21,8959	2,65E-10	-23,4546	6,91E-12
Ppfia3	-3,61871	0,33904	-3,55762	0,40052	-21,6012	4,69E-09
Cobl	-3,88251	0,40287	-2,7418	0,61119	-22,2273	5,24E-07
Nlrx1	-6,67339	0,07588	18,98705	9,96E-07	1,002712	0,83475
Ppp6r2	-7,42398	0,20453	-21,2099	0,00035	0,718171	0,92403
Smtn	-10,2116	0,01195	-6,55531	0,17758	-4,59315	0,33876
Ttc17	-10,6141	0,0009	-9,4936	0,01037	-3,99158	0,28489
Rps3a3	-10,6506	2,40E-05	17,15565	1,59E-09	-0,06275	0,98687
Rps3a2	-11,1476	1,77E-06	2,372527	0,43355	-0,12813	0,96961
Cntn1	-11,2871	7,85E-15	-5,92241	5,64E-06	-7,23335	2,93E-08
Mup10	-21,0146	5,10E-05	-7,63936	0,25300	-22,5772	0,00010
Mup10	-21,0146	5,10E-05	-7,63936	0,25300	-22,5772	0,00010
Ptk2b	-21,8237	7,78E-08	-8,41912	0,09349	1,612882	0,77637
Hecw2	-22,6395	1,44E-06	-21,3366	7,87E-05	-6,29716	0,28622
Hecw2	-22,6395	1,44E-06	-21,3366	7,87E-05	-6,29716	0,28622
Epha4	-22,9594	5,01E-08	-1,05954	0,86818	0,735461	0,90499
Ino80d	-23,1817	6,71E-06	-0,36314	0,96539	17,6985	0,0026
Ino80d	-23,1817	6,71E-06	-0,36314	0,96539	17,6985	0,00265
Dhcr7	-23,6383	1,36E-14	-5,33163	0,16779	-3,30098	0,39564
Nisch	-24,7994	4,12E-16	-2,89797	0,46765	0,987142	0,81927
Itgb4	-24,8784	1,29E-08	-24,3747	1,07E-06	-22,9261	3,71E-06
Itgb4	-24,8784	1,29E-08	-24,3747	1,07E-06	-22,9261	3,71E-06
Adam23	-24,8921	1,18E-06	-2,40584	0,74277	-22,3386	0,00012
Adam23	-24,8921	1,18E-06	-2,40584	0,74277	-22,3386	0,00012
Srp54c	-25,2409	8,13E-07	-16,8098	0,00632	-2,28656	0,74731

Srrm1	-25,2604	2,80E-09	-23,6789	1,16E-06	-21,889	5,88E-06
Srrm1	-25,2604	2,80E-09	-23,6789	1,16E-06	-21,889	5,88E-06
Sema6c	-25,7662	4,67E-07	-7,25058	0,28041	-23,2086	6,22E-05
Sema6c	-25,7662	4,67E-07	-7,25058	0,28041	-23,2086	6,22E-05
Mapk8ip3	-26,0468	7,42E-35	-3,17744	0,20138	-2,58898	0,29512
Gm8730	-26,764	8,59E-21	16,93149	3,99E-07	-1,45066	0,70601
Thsd4	-30	6,26E-09	2,429732	0,74018	-0,03207	0,99637

Supplementary table 2. 100 most up and down regulated genes expressed in the injured sciatic nerve at P30, P4 and P10 vs uninjured sciatic nerve at P30, P4 and P10 respectively.

	P30		**P4**		**P10**	
Pro-inflammatory macrophages						
Gene ID	**log2FC**	**padj**	**log2FC**	**padj**	**log2FC**	**padj**
Arg1	5,501	3,3E-38	6,093	1,7E-36	5,378	6,0E-28
Lgals3	4,704	2,6E-18	3,929	2,0E-10	3,231	1,8E-07
Marco	5,288	9,1E-08	5,065	5,3E-06	2,452	3,5E-02
Ms4a4c	5,089	5,6E-08	4,485	5,2E-05	5,912	2,1E-07
Trem2	3,922	1,3E-08	3,351	1,7E-05	3,430	1,3E-05
Ccl5	3,648	7,5E-08	1,910	1,4E-02	2,584	8,6E-04
Ccr7	3,801	4,3E-06	2,686	3,4E-03	2,725	4,8E-03
Cd38	1,348	3,9E-06	1,350	5,3E-05	1,307	8,2E-05
Cd80	2,267	6,8E-05	1,711	1,7E-02	2,285	1,0E-03
Cd86	0,309	5,8E-01	0,664	2,4E-01	0,338	5,7E-01
Cxcl10	1,872	2,2E-04	1,314	2,7E-02	0,907	1,4E-01
Fpr2	4,080	7,5E-04	3,863	5,0E-03	3,388	2,5E-02
Il1b	6,672	1,3E-10	6,711	1,8E-09	5,326	6,6E-05
Il23a	-3,081	6,1E-13	-2,815	2,2E-09	-5,455	5,3E-11
Il6	5,590	1,4E-01	5,412	2,1E-01	3,441	4,4E-01
Inhba	2,556	3,6E-07	2,145	6,8E-04	2,835	8,2E-07
Nos2	1,884	1,1E-01	1,824	1,7E-01	3,448	6,0E-03
S100a8	1,682	3,4E-01	4,807	6,1E-03	4,168	2,0E-02
Socs1	2,182	2,0E-02	2,311	2,9E-02	2,223	3,6E-02

Tlr2	2,110	3,1E-07	2,279	1,0E-06	1,884	6,6E-05
Tlr4	1,258	5,6E-04	1,968	1,6E-06	1,344	1,1E-03
Tnf	3,965	1,1E-04	4,789	3,3E-05	2,325	5,7E-02
Anti-inflammatory macrophages						
Arg1	5,501	3,3E-38	6,093	1,7E-36	5,378	6,0E-28
Cd163	-1,087	1,7E-01	-0,338	7,4E-01	0,222	8,3E-01
Egr2	-2,896	3,5E-15	-3,901	3,7E-21	-4,078	2,3E-23
Fabp4	0,550	4,1E-01	1,343	4,3E-02	1,459	2,3E-02
Fn1	1,985	5,0E-04	0,230	7,8E-01	3,487	1,9E-08
Il10	3,674	5,7E-03	4,409	8,4E-04	2,868	8,6E-02
Mfge8	1,499	8,0E-08	1,151	3,7E-04	1,178	2,3E-04
Mrc1	0,355	6,4E-01	0,996	1,8E-01	1,414	4,4E-02
Pdgfa	-0,321	5,7E-01	-1,055	5,3E-02	-0,279	6,5E-01
Retnla	2,386	4,9E-01	1,515	7,0E-01	2,187	5,5E-01
Tgfb1	2,279	1,6E-21	1,570	1,1E-08	1,932	9,8E-13
Vegfa	0,481	6,1E-01	1,569	8,4E-02	1,291	1,6E-01
Repair Schwann cell						
Artn	3,596	5,1E-05	3,795	1,0E-04	3,772	2,0E-04
Ccl2	1,784	4,3E-04	3,932	1,1E-12	1,229	3,7E-02
Shh	6,279	6,2E-20	3,659	2,4E-05	1,668	4,7E-02
Atf3	3,276	1,6E-28	2,709	9,5E-16	1,891	2,9E-08
Cxcl12	-0,362	3,2E-01	-1,063	3,6E-03	-0,214	6,1E-01
Gap43	3,228	1,1E-15	2,374	2,6E-07	2,880	2,3E-10
Gdnf	7,635	3,4E-44	5,355	6,1E-17	5,698	4,0E-19
Gfap	-0,755	3,5E-01	1,381	1,2E-01	-1,018	2,4E-01
Id2	-0,152	9,0E-01	-0,494	6,7E-01	-0,148	9,1E-01
Junb	2,775	8,2E-36	2,727	4,8E-27	2,697	1,4E-26
Lif	2,155	8,2E-02	1,522	3,0E-01	0,993	5,1E-01
Ncam1	1,621	5,3E-02	1,262	1,9E-01	2,843	1,2E-03
Ngf	0,650	6,3E-01	1,637	2,2E-01	0,619	6,7E-01
Ngfr	2,878	2,7E-14	0,471	3,5E-01	0,804	8,2E-02
Olig1	7,943	3,5E-14	6,113	1,2E-27	7,280	2,4E-13

Osm	2,072	3,3E-03	3,592	2,9E-06	2,031	2,0E-02
S100b	-2,402	2,9E-08	-3,788	3,5E-15	-4,340	6,7E-20
Sox2	2,181	6,3E-10	-0,083	8,8E-01	0,164	7,5E-01

Supplementary table 3. Representative Pro-inflammatory anti-inflammatory macrophage and repair Schwann cell genes expressed in the injured sciatic nerve at P30, P4 and P10 vs uninjured sciatic nerve at P30, P4 and P10 respectively.

Chapter 2

Outgrowth of Mouse Sensory Neurons is not Mediated by Regeneration Associated Genes in Early Postnatal Stages

Outgrowth of Mouse Sensory Neurons is not Mediated by Regeneration Associated Genes in Early Postnatal Stages

Beatriu Molina-Esteve[1,2] Jose Crugeiras[1,2], María Rodríguez-Brañas[1,2], Ana Sanchez-Maldonado[1,2], David Ovelleiro[3], Natalia Lago[1,2*], Esther Udina[1,2*]

[1] Universitat Autònoma de Barcelona, Cell Biology, Physiology and Immunology, Bellaterra, Spain

[2] Centro de Investigación Biomédica en Red sobre Enfermedades Neurodegenerativas (CIBERNED), Bellaterra, Spain

[3] Peripheral Nervous System, Vall d'Hebron Institut de Recerca (VHIR), Vall d'Hebron Hospital Universitari, Vall d'Hebron Barcelona Hospital Campus, Barcelona, Spain

** These authors share senior coauthorship*

Abstract

Peripheral neurons exhibit robust regeneration after nerve injury in adulthood; a process linked to the activation of regeneration-associated genes (RAGs). However, the mechanisms underlying nerve regeneration during early postnatal development remain poorly understood. In a previous work, we observed that motoneurons axotomized at early postnatal stages regenerate without overexpressing RAGs, contrasting with the expected RAG activation observed in postnatal day 30 (P30) mice. To determine whether this phenomenon extends to sensory neurones, we investigated two paradigmatic dorsal root ganglia populations: proprioceptive (PV^+) and nociceptive ($TrpV1^+$) neurones, which exhibit distinct regenerative capacities in adult mice.

Following sciatic nerve crush injury at P4, P10, and P30, both neuronal subtypes demonstrated robust axonal regeneration across all postnatal stages, with nociceptors exhibiting significantly superior regeneration compared to proprioceptors. Remarkably, no substantial neuronal death was observed at any developmental timepoint. However, RNA sequencing revealed that P4 and P10 sensory neurones failed to upregulate RAGs following injury, whereas P30 neurones exhibited the expected pro-regenerative transcriptional programme. Pathway enrichment analysis confirmed that classical regeneration-associated signalling pathways were activated exclusively in young adults, whilst developmental and inflammatory pathways predominated in early postnatal stages.

Using the conditioning lesion paradigm in primary dorsal root ganglia cultures, we demonstrated that only P30 neurones exhibited enhanced neurite outgrowth following conditioning lesion, whilst P4 and P10 neurones showed no conditioning effect or reduced outgrowth, respectively. These findings indicate that early postnatal sensory neurones possess intrinsic growth capacity independent of RAG activation, suggesting fundamentally distinct regenerative mechanisms across developmental stages.

Graphical abstract

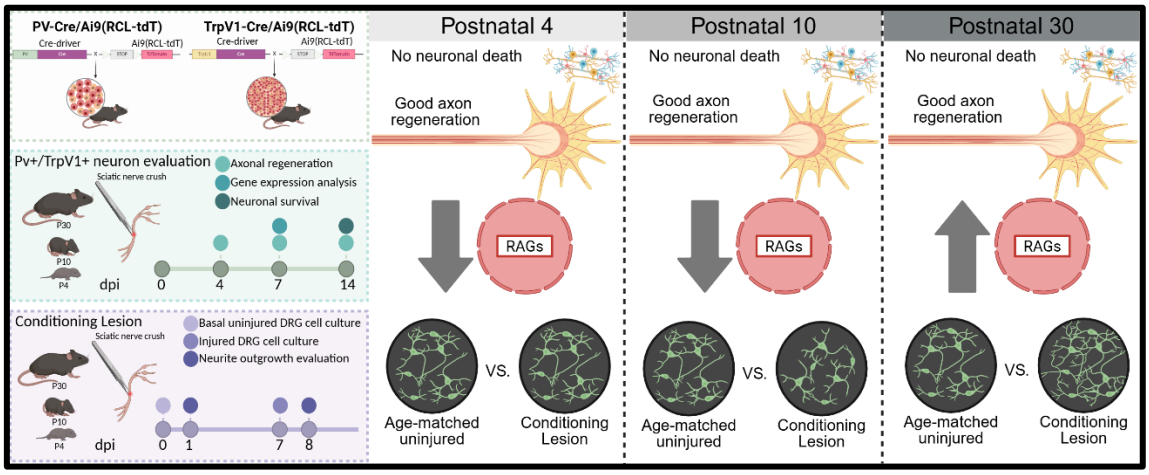

Keywords: Neonatal nerve injury, Nerve regeneration, Regeneration Associated Genes, Transcriptomic analysis, Conditioning lesion

Introduction

It is well known that peripheral neurons can regenerate after nerve injuries. This regenerative ability has been linked to a successful Wallerian degeneration in the distal nerve stump to create a permissive environment for growth, and to the capacity of injured neurons to switch from a neurotransmitter state to a pro-regenerative state, that includes the overexpression of regeneration associated genes (RAGs), key elements for a successful regeneration. However, this phenomenon does not occur in a uniform way across all neuronal subpopulations (Navarro et al., 1994; Janko 1976; Brushart et al., 2020; Bolívar et al., 2024) nor during all developmental stages (Kemp et al., 2015a; Kemp et al., 2015b).

During the postnatal stage, the peripheral nervous system undergoes profound transformations that influence neuronal plasticity and the response to injury. In contrast to adulthood, young neurons display a greater susceptibility to neuronal death following axotomy (Lowrie and Vrbová 1984; Lowrie et al., 1987; Pollin et al., 1991) yet they also possess a molecular environment that can promote axonal regrowth and functional recovery, provided they survive the injury (Donnerer 2003; Christie and Zochodne 2013; Renthal et al., 2020). Despite that classical works focus mainly on the massive death of motoneurons after postnatal nerve injuries, sensory neurons can also be affected (Kemp et al., 2015a).

In a previous work (Molina-Esteve et al., 2025) we analysed the regenerative capacity of motoneurons after injuries at different postnatal stages, and we observed that despite a good regenerative response, motoneurons axotomized at postnatal day 4 (P4) or postnatal day 10 (P10) did not overexpress RAGS, whereas postnatal day 30 (P30) mice showed the expected activation of these pro-regenerative genes. To further elucidate the growth programs activated by postnatal neurons after axotomy, we have explored the regenerative capability of two paradigmatic sensory subtypes (proprioceptors and nociceptors) at different postnatal stages. Within the dorsal root ganglia (DRG), proprioceptive neurons (PV+) constitute a large-diameter neuronal population characterized by myelinated axons that innervate muscle spindles and Golgi tendon organs. They play a crucial role in proprioception and the

regulation of motor coordination (Madden et al., 2020; Wu et al., 2021). Nociceptive sensory neurons (TrpV1^{+}) are distinguishable by their small soma diameters and unmyelinated (C fibres) or lightly myelinated axons (Madden et al., 2020) and are responsible for the chemical, thermic and mechanic nociception (Dubin & Patapoutian, 2010).

These two populations show different regenerative capability in adult mice (Bolívar et al., 2024). The genetic program that these populations or motoneurons activated after axotomy is also different, but share common pathways, that include the overexpression of RAGs (Bolívar et al., 2024). Therefore, in this work we want to investigate the regenerative response of proprioceptive and nociceptive sensory neurons, whether postnatal sensory neurons neither express RAGs when injured at early postnatal stages and whether a prior lesion to the sciatic nerve is conditioning the neuron to promote regeneration.

As expected, both proprioceptive and nociceptive neurons showed good regenerative potential when injured at different postnatal stages, being nociceptors significatively better than proprioceptors. However, an RNAseq of the whole DRG showed that P4 and P10 sensory neurons did not overexpress RAGs after injury, as we had previously observed in injured motoneurons of the same age. To further elucidate whether these postnatal neurons do not overexpress RAGs because they still retain a growth state or they activate a different pro-regenerative program, we performed primary sensory cultures and used the conditioning lesion paradigm (Smith & Skene, 1997). Since neurons need to switch to a pro-regenerative program to be able to extend neurites, a previous axotomy would positively condition the neurons. This conditioning lesion effect would not be present in postnatal neurons if their growth ability is due to their basal state and not to the activation of a strong pro-regenerative program as the one observed in adults.

Material and Methods

Mice

P4 to P30-day-old mice were used for all studies. Males and females were used in approximately equal numbers for all groups in all experiments. The mice were housed in a controlled environment (12-h light-dark cycle, 22 ± 2°C) in open cages with water and food *ad libitum*. P4 and P10 mice were housed with their mothers. The strains used in this study were acquired from Jackson Laboratory (Bar Harbor, ME, USA) and maintained in our animal facility. C57BL/6J mice were used as wild type (WT) animals. Mice expressing the fluorescent protein TdTomato in the proprioceptive neurons Pv-Cre/Ai9 and nociceptive neurons TrpV1-cre/Ai9 were generated by breeding homozygous Ai9 (RCL-tdT) mice (JAX stock #007909) (Madisen et al., 2010) with B6 PV-Cre (Parvalbumin, JAX stock #017320) or TRPV1^{cre} (transient receptor potential cation channel, subfamily V, member 1, JAX stock #017769).

Experimental design

For the evaluation of axonal regeneration and neuronal death, a sciatic nerve crush injury was applied to PV-Cre/Ai9(RCL-tdT) and TrpV1-Cre/Ai9(RCL-tdT) mice at P4, P10 and P30, followed by histological analyses (Figure 24a). To characterize the transcriptomics of the sensory neurons after a crush injury at the same postnatal stages, RNA from L3-L5 DRGs WT mice was isolated and RNAseq was performed (Figure 24b). To assess if a conditioning lesion promotes neurite outgrowth in vitro, a sciatic nerve crush was applied to WT mice at the same postnatal stages, and neurons from L3-L5 DRGs were cultivated for 24 hours (Figure 24c).

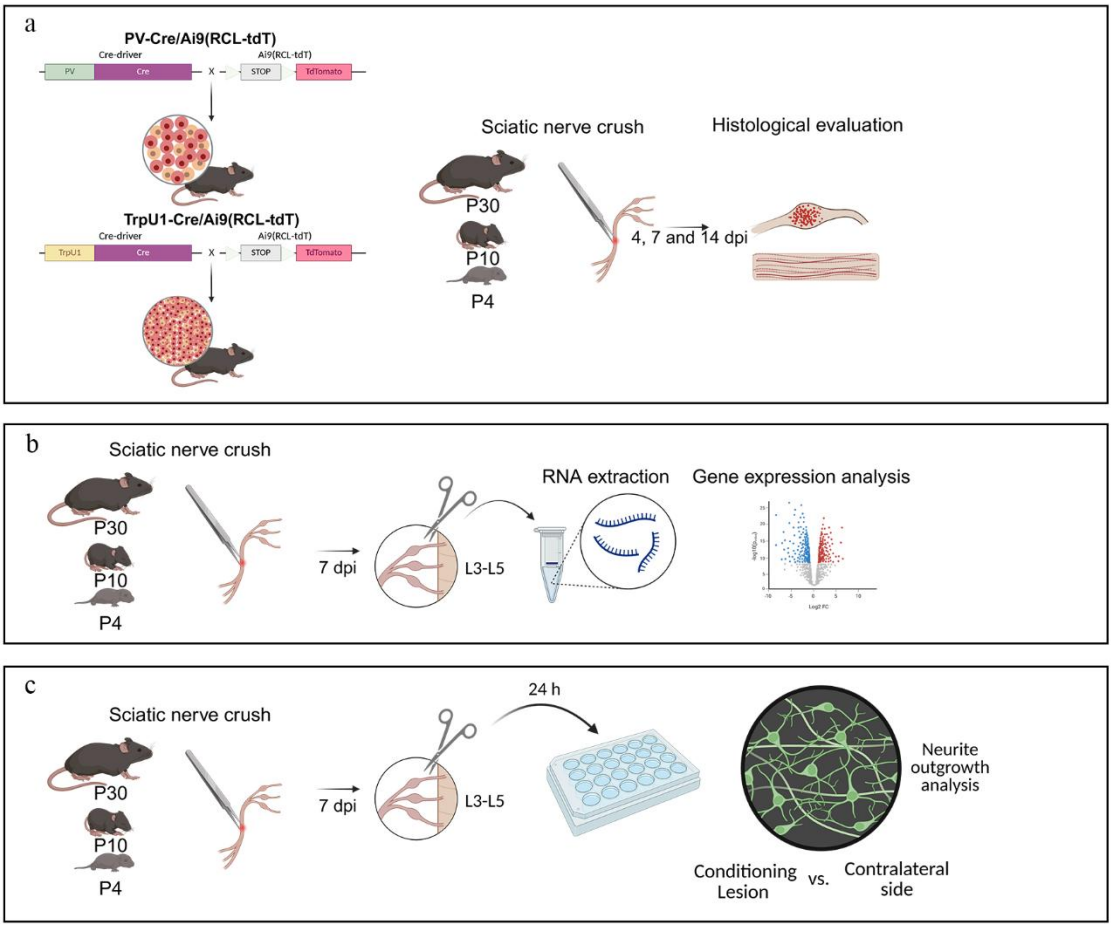

Figure 24. Experimental design (a) Schematic representation of the transgenic mice and experimental design used for the evaluation of proprioceptive and nociceptive sensory neurons survival and axonal regeneration. (b) Schematic representation of the experimental design used for sensory neurons transcriptomics analysis. (c) Schematic representation of the experimental design used for evaluation of neurite outgrowth after a conditioning lesion. Intact animals were also used to evaluate basal growth.

Surgeries

All experimental procedures were approved by the Animal Experimentation Ethical Committee of the Universitat Autònoma de Barcelona and followed the European Communities Council Directive 2010/63/EU and Spanish National law (RD 53/2013). All surgical procedures were carried out aseptically under an operating microscope. Ketamine (90 mg/kg or 18mg/kg) and xylazine (10 mg/kg or 2 mg/kg) was administered intraperitoneally to anaesthetize P30 and P10 mice respectively. In P4 animals, short-term hypothermia was used to anaesthetize the pups, taking advantage of the short period needed to perform the surgery (Flecknell

et al., 2015) . A mid-thigh incision was made, and the right sciatic nerve was exposed and crushed. Standard N°. Five Jeweller forceps were used for 30 seconds, resulting in axonotmesis or Sunderland grade 2 injury (Bridge et al., 1994). The incision was sutured with a 6–0 silk suture and disinfected with povidone iodine. All mice were kept in a warm environment until recovery. During the follow-up, assessment of general health and mobility was performed daily for the first week. All the animals were sacrificed at the time of study termination under deep anaesthesia with Dolethal (0.03 ml/30 g) administered intraperitoneally. Death was confirmed by decapitation.

Axon regeneration and neuronal death

To evaluate the number of proprioceptive and nociceptive axons per nerve and the number of neuron cell bodies 4, 7 and 14 days after sciatic nerve crush injury, the ipsilateral and contralateral sciatic nerves and the ipsilateral and contralateral L3-L5 DRGs were harvested and stored in PBS with 30% sucrose at 4ºC, being post-fixed before storage. The sciatic nerves were placed on a glass slide and mounted with Fluoromount-G medium (Southern Biotech). Pressure was applied to the coverslips to flatten the nerves, and images 5 and 10 mm distal from the lesion point were taken via a confocal microscope (Leica SP5, 20x, z-step size of 1 µm). Axons were counted in stacks of 5 µm every 10 µm to avoid double counting and compared to the contralateral side. The L3-L5 DRGs were placed on a glass slide and mounted with Fluoromount-G medium (Southern Biotech). Images every 1 µm were taken via a confocal microscope (Leica SP5, 20x, z-step size of 1 µm). Proprioceptive and nociceptive neurons were counted in stacks of 1 µm every 20 µm to avoid double counting and compared to its contralateral side to assess neuronal death. All neuron counts were corrected with the Abercrombie formula (Abercrombie & Johnson, 1946) $(N=nt/(t+d))$ where N is the corrected number of counted neurons, n is the number of cells that have been counted, t is the thickness of the section, and d is the average diameter of the cells. The diameter of neurons was measured in 100 randomly chosen neurons (per group), using Image Tool software and the mean value was calculated. To calculate the percentage of neuronal death or neuronal

survival, the total number of neurons on the ipsilateral side was compared with the total number of neurons on the contralateral side.

Transcriptomic analyses

Seven days after the sciatic nerve crush, all mice were euthanized with intraperitoneal Dolethal (0.03 ml/30 g) and the L3-L5 DRGs were dissected and placed on cold's Gey's solution enriched with glucose (6 mg/mL) until used. DRG's were homogenized in 1 mL of buffer. Both female and male were used in this experiment, at least four animals were used for age and group. After centrifugation of the homogenate, 50 µL of the supernatant was used for RNA isolation using the RNAeasy Micro Kit (QIAGEN, #74004) and quantified wit Quant-it RiboGreen RNA assay kit (Thermo Fisher, #R11490).

Library preparation and RNA sequencing

BGI Genomics Co., Ltd. (Shenzhen, China) performed the RNA quality control and RNA sequencing. Library preparation and RNA sequencing for this report were carried out as follows: The library type was "DNBSEQ Eukaryotic Strand-specific mRNA library," and all samples were sequenced on the DNBSEQ platform (DNBSEQ Technology) with a read length of 2x150 bp (PE150), ensuring a minimum of 20 million clean reads per sample, always reaching Q20 and Q30 quality scores above 95% and 89%, respectively. Library quality control included mRNA enrichment from total RNA using oligo dT, mRNA fragmentation, and double-stranded cDNA synthesis using random primers, with dUTP incorporation in the second strand to ensure strand specificity. Next, end-repair and 3' adenylation, adapter ligation, PCR, library quality control, circularization, and amplification in DNA nanoballs were performed before sequencing. FASTQ file quality was assessed using SOAPnuke software (developed by BGI), and the results confirm that the data meets quality and filtering standards, using Phred+33 encoding. Reads were quantified using the coding DNA reference database (Ensembl Mouse database, genome assembly: GRCm39.cdna.all, release 113) via Salmon (v1.10.3). A total of 27 samples were analysed. The "DESeq2" library (v 1.48.0) was utilised to perform the differential expression

analysis pipeline. Only genes with more than 10 counts in the smallest group were included in the differential analysis. Principal Component Analysis (PCA) was performed to visualise the overall effect of experimental covariates and batch effects. Uniform Manifold Approximation and Projection (UMAP) was implemented with n_neighbors parameter set to 15. Hierarchical clustering was performed using the R "pheatmap" function (v 1.0.12), focusing on the 80 most variable genes determined using the MatrixGenerics::rowVars function. Gene set enrichment was performed using the R library "STRINGdb" (v 2.20) via the STRING platform. Only genes with P-values<0.05 were included in the analysis. Multiple databases were utilised, including Gene Ontology (Biological Process, Molecular Function, Cellular Component), PubMed reference publications, KEGG pathways and Reactome pathways among others. Pathway analysis was conducted using Bioconductor libraries "KEGGREST" (v 1.48) and "pathview" (v 1.48). The KEGG database was accessed via RESTful web services through the R package.

In vitro cultures of DRG sensory neurons

Cell cultures of the L3-L5 DRGs were performed in intact P4, P10 and P30 mice or mice at these postnatal stages one week after receiving a sciatic nerve crush (conditioning lesion). Mice were euthanized administering intraperitoneally an overdose of Dolethal (0.03 ml/30 g), and the L3-L5 DRGs were dissected and placed in colds Gey's solution (Sigma, Cat #G9779) enriched with glucose (6 mg/mL) (Sigma, Cat #G7021-1KG) until used. Bilateral DRG were used in intact animals. In animals previously injured, homolateral lumbar DRG were used to evaluate the conditioning lesion effect, being the contralateral used as a control. DRGs were enzymatically dissociated in Hank's Balanced Salt Solution (Sigma, Cat #14170-088) supplemented with 10% trypsin (2.5 mg/mL; Sigma, Cat #T-4674), 10% collagenase A (12.5 collagen digestion units/ml; Sigma, Cat #C2674) and 10% DNAse (1 mg/mL; Roche, Cat #11284932001) for 45 minutes at 37°C, followed by mechanical dissociation. After the enzymes were blocked with 10% high Foetal Bovine Serum (hiFBS) in Dulbecco's Modified Eagle Medium (DMEM) (Sigma, Cat #41966052) and centrifuged at 900 rpm for 7 min, the cells were centrifuged again in 15% Bovine Serum Albumin (BSA) (Sigma, Cat #A6003) in Neurobasal A (Gibco, Cat

#10088022). The supernatant was withdrawn, and 1 mL of culture medium was added. The medium consisted of Neurobasal A supplemented with 2% B27 (Gibco, Cat #17504044), 0.033 M glucose, 1 mM glutamine (Gibco, Cat #35050-038), 1× penicillin/streptomycin (Sigma, Cat #P0781), and 20 mM HEPES (Sigma, Cat #H0887). To culture the cells, 24-well plates were used. The plates were previously coated with 100 µg/mL poly-D-lysine (PDL; Sigma, Cat #P6407) for 2 h at 37°C, washed, dried and further coated with 1 µL/mL laminin for a minimum of 2 hours (Sigma, Cat #L-2020). Then, neurons were plated at a density of 3×10^3 neurons/mL and incubated for 24h.

Cell cultures were fixed with 4% paraformaldehyde (PFA) in phosphate buffer saline (PBS) buffer for 20 minutes, then washed three times with PBS and incubated for 30 minutes in blocking solution (5% normal donkey serum (NDS) in PBS-Triton 0,3% (PBST)). After removal of the blocking solution, cultures were incubated for 1 hour at room temperature in a humidified chamber with the primary antibody mouse anti-β-III-tubulin (1:500, Biolegend, #MMS435P) diluted in blocking solution. Following three washes in PBS, cultures were incubated for 2 hours at room temperature with the appropriate secondary antibody (Alexa Fluor 488 Donkey x Mouse, Invitrogen, A21202) diluted in blocking solution and protected from light. Three additional PBS washes were performed. Finally, coverslips were mounted onto glass slides using Fluoromount G mounting medium (Southern Biotech, #0100-20) and allowed to dry before imaging.

Neurite outgrowth quantification

The samples were examined using a fluorescence microscope (Nikon Eclipse Ni, Japan) equipped with a DS-RI2 digital camera and operated via the dedicated NIS Elements software. Image acquisition was performed for each well using a 10x objective, with a resolution of 1600×1200 pixels. For the morphometric quantification of neurite growth, the obtained images were processed and analysed with Fiji/ImageJ software. The analysis included the delineation and measurement of the longest neurite per neuron, using a manual tool within the software.

Data analysis

All statistical analyses were performed using GraphPad Prism 9 (version 9.0.1). The normality of data distributions was assessed with the Shapiro-Wilk test ($p>0.05$ was considered normally distributed). Data are presented as mean ± standard error of the mean (SEM). Statistical significance was set at $p<0.05$. For comparisons of multiple groups and variables, two-way ANOVA was used, where appropriate, post hoc Sidak's correction was applied for pairwise multiple comparisons. For paired measurements, paired t-tests were applied and one-way ANOVA with Tukey's post hoc test was employed for single-factor group comparisons. When the data did not meet criteria for normal distribution, non-parametric analysis was performed using the Kruskal-Wallis's test followed by Dunn's test. For transcriptomic data, differential gene expression was analysed using DESeq2 after filtering for minimum read counts. Principal Component Analysis (PCA), Uniform Manifold Approximation and Projection (UMAP), and hierarchical clustering were used for exploratory and batch effect analyses. Gene set enrichment and pathway analyses were conducted using STRINGdb and Bioconductor libraries.

Results

Response of proprioceptive and nociceptive neuros to nerve injury at different postnatal stages

Evaluation of neuronal somas

Neuronal survival was assessed 14 dpi by quantifying the total number of neuronal cell bodies in the ipsilateral (L3–L5) DRGs. Pv-Cre/Ai9(RCL-tdT) mice were used to identify proprioceptive neurons (Figure 25a), and TrpV1-Cre/Ai9(RCL-tdT) mice to identify nociceptive neurons (Figure 25c), across P4, P10, and P30 animals. Due to high variability between animals and the differences in the size of ganglia between ages, all comparisons were performed within the same animal (using the contralateral lumbar DRG).

The large diameter and low number of proprioceptive neurones facilitate the counting and about 300 neurons in total were counted (Supplementary Figure 5). We estimated a survival rate of ~80% at P4 and >90% at P10 and P30 (Figure 25b) reduction that was not significant at any age ($p>0.05$). The smaller diameter and large number of nociceptive neurons difficult the counting and lead to high variability between ages, but percentage of survival was similar to the one reported in proprioceptors, of about ~80% at P4 and reached ~100% at P10 and P30 (Figure 25d). No significant neuronal loss was detected at any age ($p>0.05$).

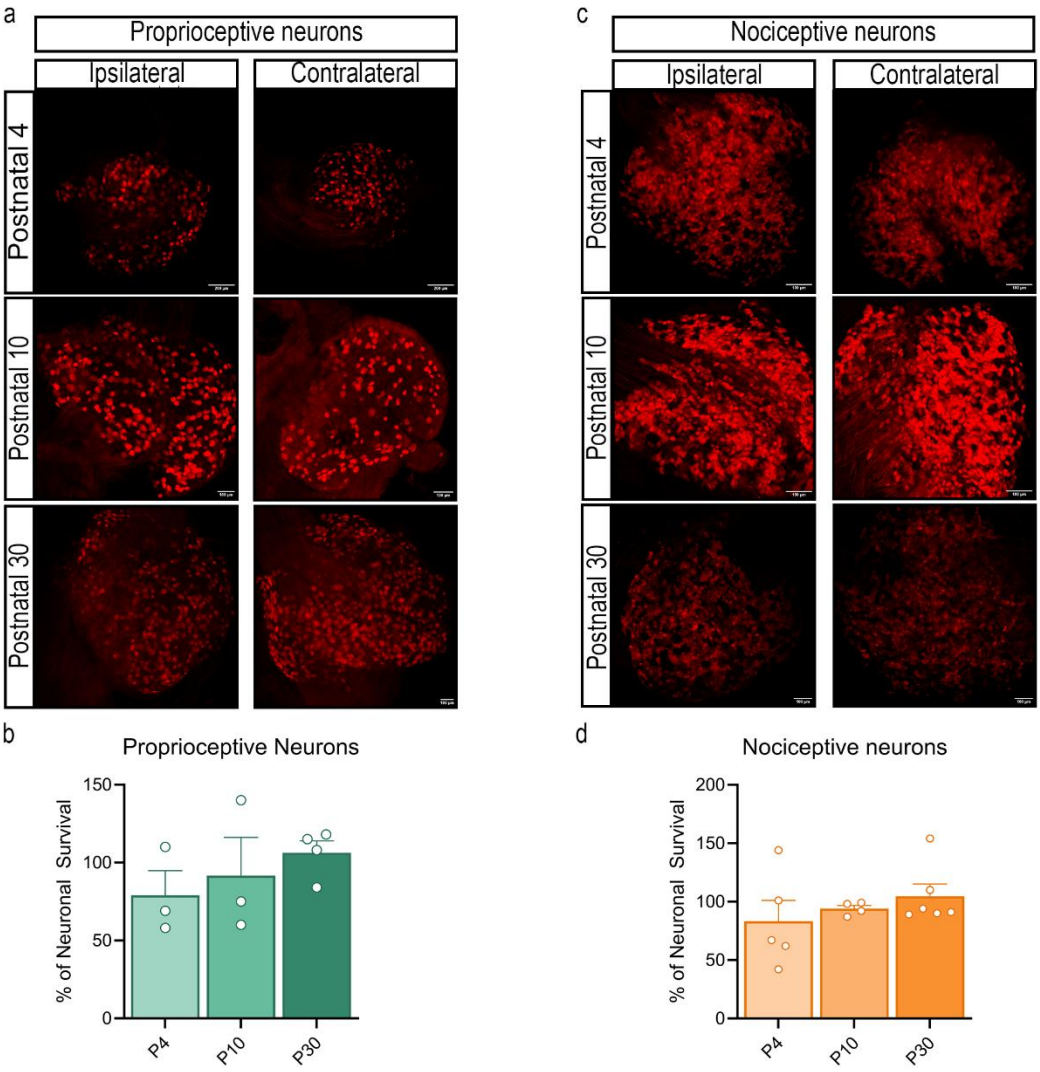

Figure 25. Survival of proprioceptive and nociceptive neurons after a nerve injury at different postnatal stages. (a) Representative images of the ipsilateral and contralateral L3-L5 DRGs of P4 mice at 14 dpi, showing the PV^+ neurons in red. Scale bar= 200 µm. (b) Percentage of surviving PV^+ neurons at 14 dpi in the different postnatal stages. Statistical analysis was performed via one-way ANOVA followed by Tukey's correction test. (c) Representative images of the ipsilateral and contralateral L3-L5 DRGs of P4 mice at 14 dpi, showing the $TrpV1^+$ neurons in red. Scale bar= 200 µm. (d) Percentage of surviving $TrpV1^+$ neurons at 14 dpi in the different postnatal stages. Statistical analysis was performed via one-way ANOVA followed by Tukey's correction test.

Evaluation of axonal regeneration

When analysing the number of proprioceptive and nociceptive axons in intact nerves at different postnatal stages (Figures 26, 4), we found a significantly higher number of PV^+ axons in P10 and P30 mice compared with P4 mice ($p<0.05$; Figure

27a). Since PV⁺ axons are highly myelinated, incomplete myelination at early postnatal stage could difficult the visualization of these axons in P4 animals in the confocal microscope. For TrpV1⁺ axons, P10 mice showed a greater number of axons than P4 mice ($p<0.05$), although this difference was not observed when compared with P30 mice ($p>0.05$; Figure 27e). Again, the lower amount of myelin in P4 nerves could reduce the number of axons detected by the confocal microscopy at this age compared to more mature animals.

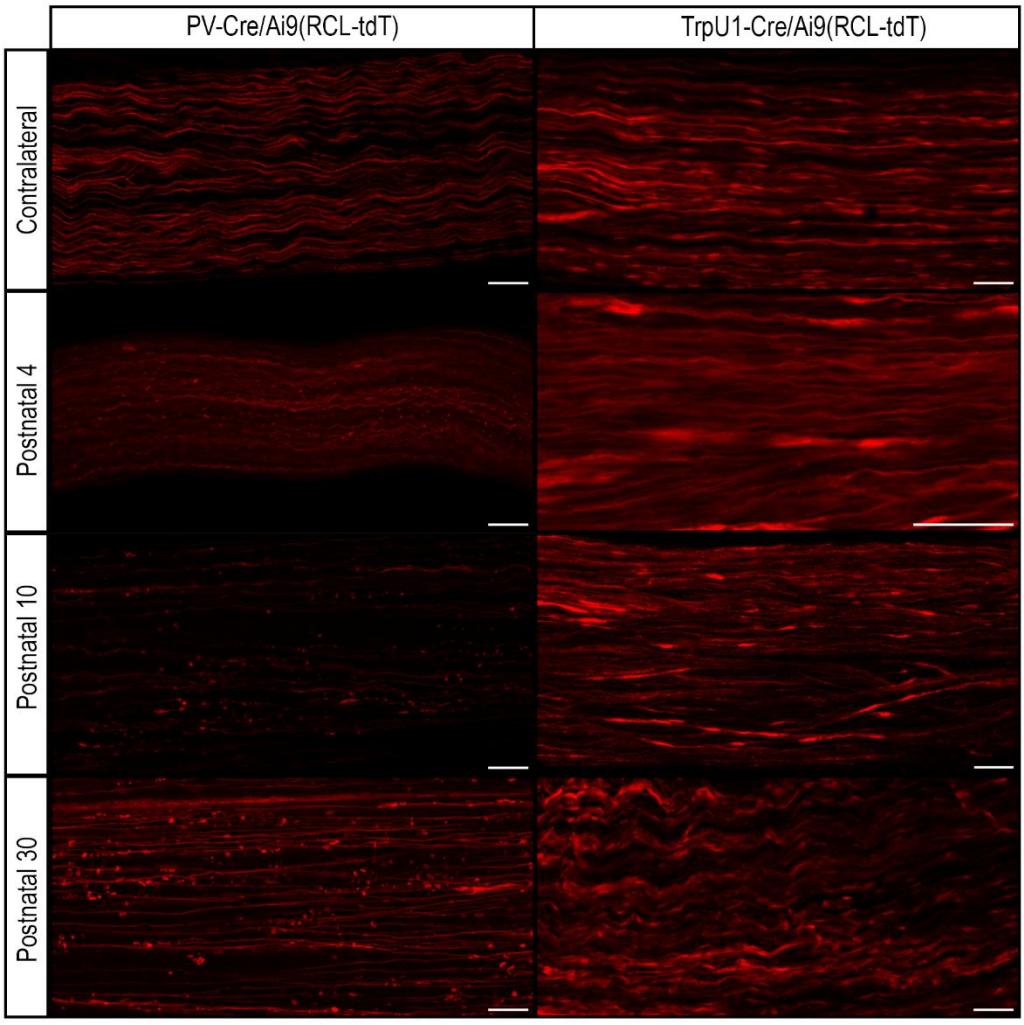

Figure 26. Representative images of longitudinal sections of contralateral and ipsilateral sciatic nerves taken 5 mm distal to the lesion site. Nerves from P4, P10 and P30 PV-Cre/Ai9(RCL-tdT) and TrpV1-Cre/Ai9(RCL-tdT) mice at 7 dpi are shown. tdTomato fluorescence highlights proprioceptive (PV⁺) and nociceptive (TrpV1⁺) axons, allowing visualisation of axonal distribution and continuity across postnatal stages following sciatic nerve crush. Scale bar: 50 μm.

Following a crush injury at different postnatal stages, we quantified the number of proprioceptive and nociceptive axons 5 and 10 mm distal to the lesion site at 4 (Figures 27b, f), 7 (Figures 27c, g) and 14 dpi (Figures 27d, h). As expected, all experimental groups displayed a reduction in axon number 5 and 10 mm distal to the injury at 4 dpi, compared to intact nerves, followed by a progressive increase at 7 and 14 dpi.

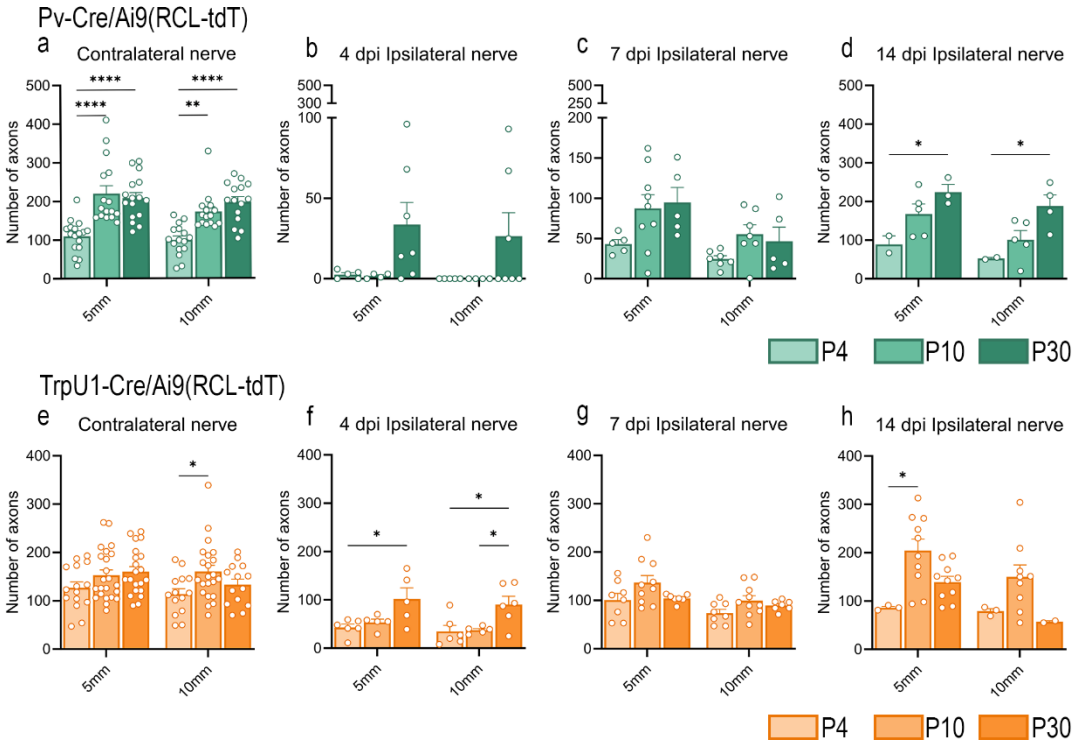

Figure 27. Total number of intact axons counted in contralateral (a, e) and ipsilateral sciatic nerves of P4, P10 and P30 PV-Cre/Ai9(RCL-tdT) and TrpV1-Cre/Ai9(RCL-tdT) mice at 4 (b, f), 7 (c, g) and 14 dpi (d, h). Statistical comparisons were performed using two-way ANOVA followed by Sidak's post hoc correction. Significance levels: *p<0.05; **p<0.01; ****p<0.0001.

To assess the proportion of axons that have regenerated over time across the different postnatal stages, we compared the total number of axons at 4, 7 and 14 dpi with the corresponding contralateral nerve. In proprioceptive neurons (Figures 28a–c), all postnatal stages showed a low percentage of regenerated axons at 4 dpi, which increased at 7 and 14 dpi. Only P30 mice achieved complete regeneration, reaching 100% of contralateral axon numbers at 14 dpi. In nociceptive neurons (Figures 28d–f), all ages showed an approximately 50% reduction in regenerated

axons at 4 dpi, followed by an increase at 7 dpi. By 14 dpi, all groups reached 100% 5 mm from the crush site regeneration relative to the contralateral nerve.

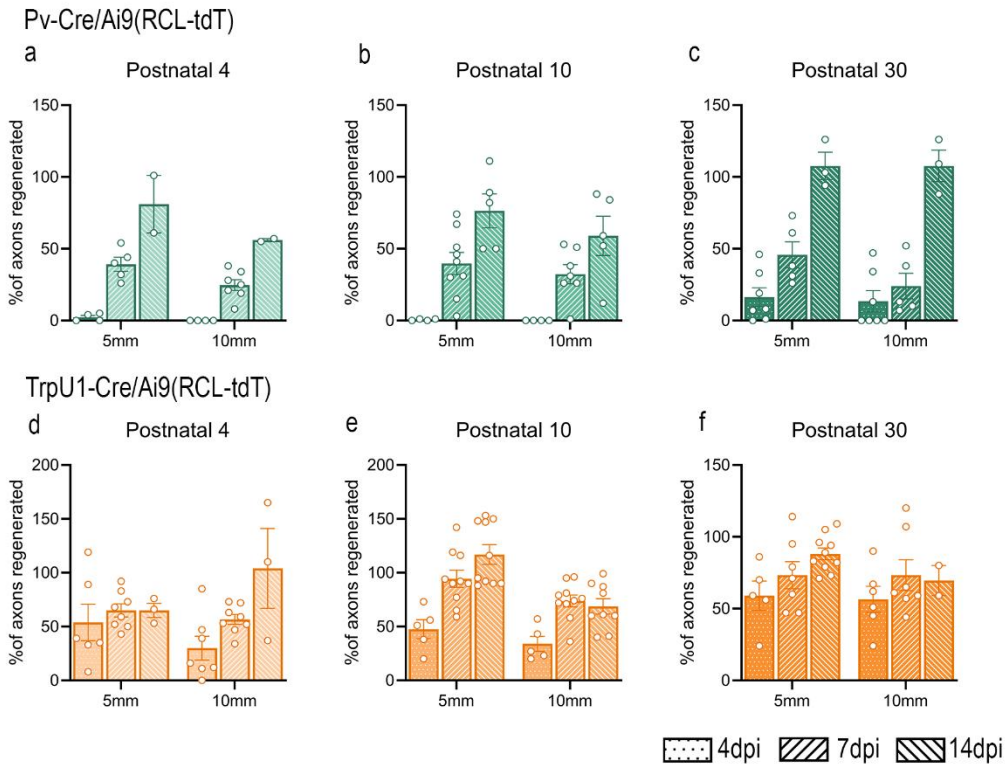

Figure 28. Percentage of regenerated proprioceptive (PV^+) and nociceptive ($TrpV1^+$) axons at 4, 7 and 14 dpi in P4 (a, d), P10 (b, e) and P30 (c, f) PV-Cre/Ai9(RCL-tdT) and TrpV1-Cre/Ai9(RCL-tdT) mice. Percentages were calculated by comparing the number of axons 5 and 10 mm from the crush injury site with the corresponding contralateral nerve.

We next compared the percentage of regenerated axons between P4, P10 and P30 mice at 5 and 10 mm distal to the lesion site (Figure 29). For proprioceptive neurons (Figures 29a, b), P30 mice reached full regeneration (100%) at 10 mm by 14 dpi, statistically significant compared with both P4 and P10 mice. For nociceptive neurons (Figures 29c, d), at 7 dpi P10 mice displayed a higher percentage of regenerated axons than P4 mice ($p<0.05$), whereas at 14 dpi, this difference was significant compared to both P4 and P30 mice. However, when axons were quantified 10 mm from the injury site, no differences were observed between postnatal stages.

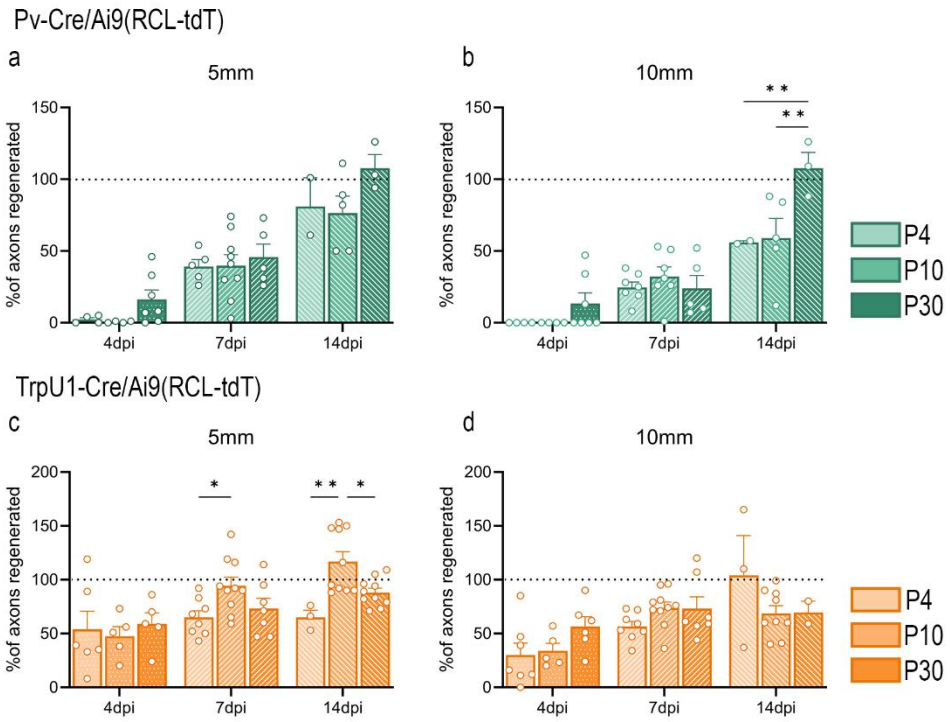

Figure 29. Comparison of the percentage of regenerated proprioceptive (PV^+) and nociceptive ($TrpV1^+$) axons at 5 mm (a, c) and 10 mm (b, d) distal to the lesion site in P4, P10 and P30 mice. Statistical analyses were performed using two-way ANOVA with Sidak's post hoc test. Significance levels: *p<0.05; **p<0.01.

Transcriptomic analyses from injured DRGs during the postnatal stages

To investigate the transcriptomic differences underlying regeneration at different postnatal stages, we performed RNAseq on L3-L4 DRGs from injured P4, P10, and P30 mice. DRGs from age-matched uninjured mice (P4+7, P10+7 and P30+7) served as controls. The dataset included 4-5 samples per group, with sequencing yielding an average of ~23.5 million paired end reads per sample (Figure 7a). PV4CR2I, PV4CR7I and PV4CT2I samples were removed from the analysis due to a number of clean reads inferior to 10.000.000 (Figure 30a, bars in red). UMAP analysis (Figure 30b) shows clustering of the samples based on their gene expression profiles.

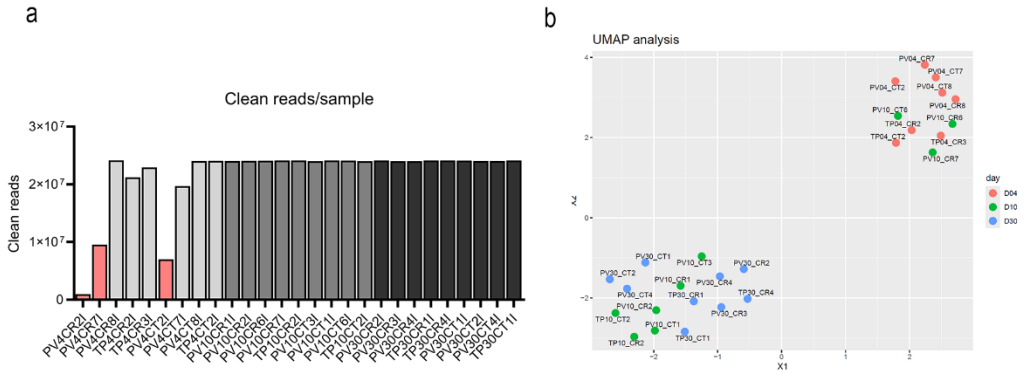

Figure 30. Quality control and exploratory analysis of the transcriptomic dataset. (a) Distribution of the clean reads per sample after a quality filter, showing an homogenous coverage among 27 samples analysed. (b) UMAP analysis of the global clustering of DRGs samples, D04, D10 and D30. Each dot represents an individual sample, showing spatial segregation by condition and time.

Gene Set Enrichment Analysis (GSEA)

To investigate whether sets of genes exhibited a consistent increase or decrease in expression across different postnatal stages following injury, we performed gene set enrichment analysis (GSEA). Comparisons were made between the injured group and the corresponding age-matched control group (Injured P4 vs. Intact P4+7, Injured P10 vs. Intact P10+7, Injured P30 vs. Intact P30+7). Using our custom list of RAGs and RStudio software (RStudio Team, 2024, version 2024.12.0+467), we conducted GSEA (Figure 31a-c). We subsequently focused on the leading-edge RAGs identified via GSEA to pinpoint the genes most significantly enriched at each postnatal stage. In P30 animals, these classical RAGs, were upregulated compared with their noninjured counterparts (Figure 31a). In contrast, compared with noninjured animals of the same age, injured P4 and P10 mice did not exhibit any significantly upregulated RAGs (Figure 31b, c). Following the GSEA findings, we next examined the expression levels of the identified leading-edge RAGs by assessing their transcripts per million (TPM) values across the experimental groups (Figure 32a-f). Consistent with the GSEA results, injured P30 animals presented visibly greater expression of these RAGs than did their intact P30+7 counterparts. In contrast, the TPM values for these RAGs in both injured P10 and

injured P4 animals showed minimal discernible changes relative to their respective age-matched intact control groups.

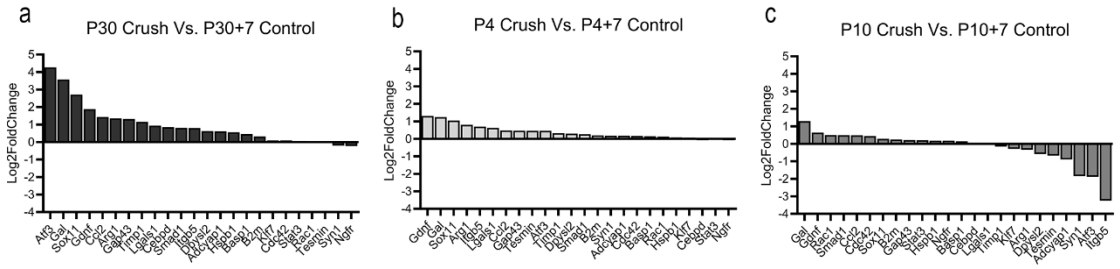

Figure 31. GSEA showing Log2FoldChange of RAGs (Atf3, Gal, Sox11, Gdnf, Ccl2, Arg1, Gap43, Timp1, Lgals1, Cebpd, Smad1, Itgb5, Dpysl2, Adycap1, Hspb1, Basp1, B2m, Klf7, Cdc42, Stat3, Rac1, Tesmin, Syn1, Ngfr) across P4, P10 and P30 injured L3-L5 DRGs compared to control ones.

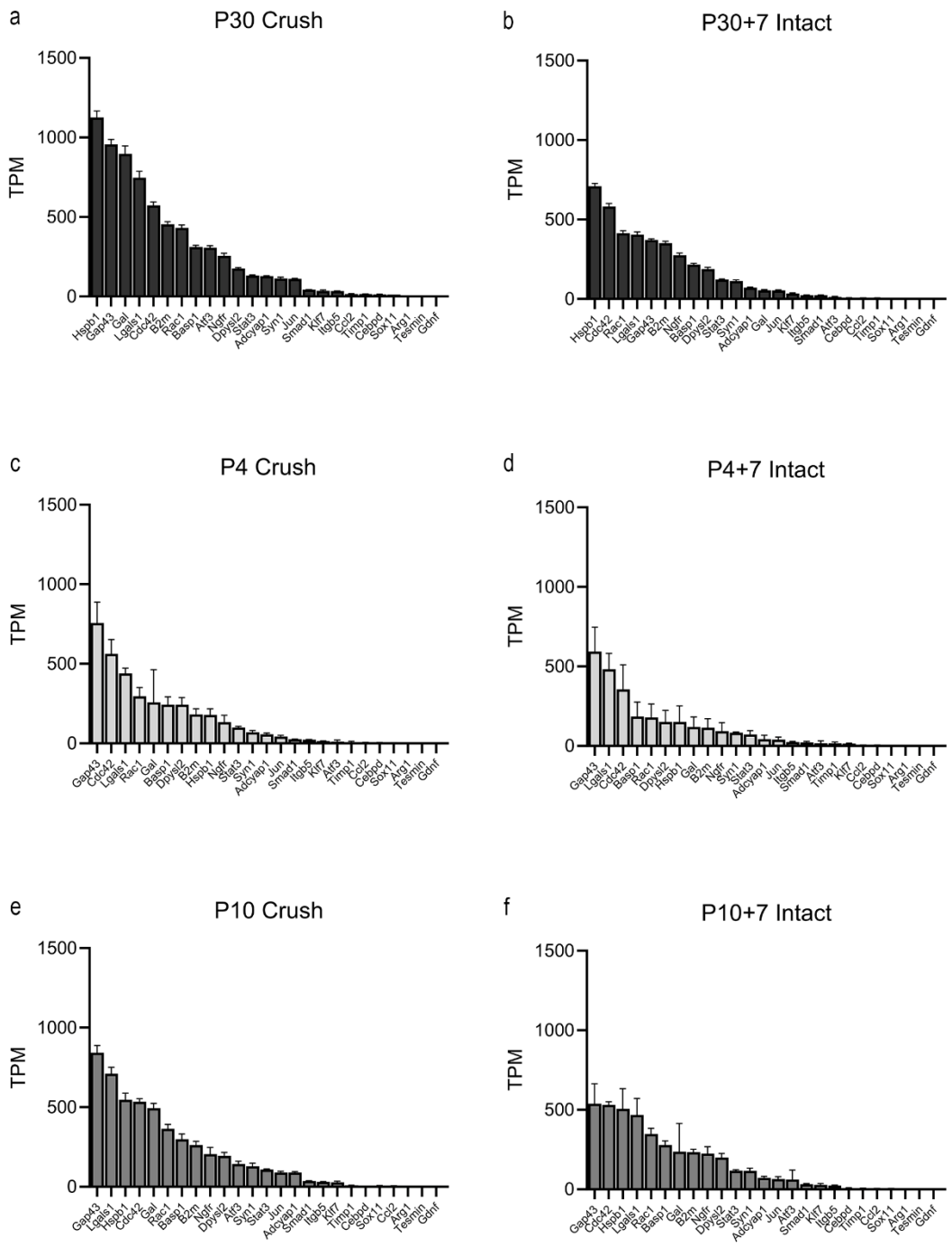

Figure 32. (a–f) Transcripts per million (TPM) of selected RAGs in intact and injured DRGs from P30, P30+4, P4, P4+7, P10 and P10+7 mice. The data are presented as the means ± SEMs (*n* = 3-5 mice per group).

Pathway enrichment analysis

To investigate the molecular response of sensory neurons to sciatic nerve crush at different postnatal stages, we performed pathway enrichment analysis

(Figure 33, Supplementary Table 4). When the analysis was performed, only the P30 mice exhibited upregulated signalling pathways with a statistical significance of *padj*<0.05, whereas the animals injured at P4 and P10 showed none. Therefore, to gain an approximate view of pathways that might be either up- or downregulated, we selected those displaying a *p*-value<0.05, even though their *padj* exceeded 0.05 (Supplementary Figure 6).

The analysis revealed distinct stage-dependent profiles. In injured P30 mice, compared to age-matched controls (Figure 33a), we observed upregulation of pathways related to dendritic cell chemotaxis, response to chemokines, and calcium homeostasis, among others. In injured P4 mice (Figure 33b), most identified pathways—including those involved in axon extension and morphogenetic development—were downregulated; however, pathways associated with the response to calcium were upregulated. In injured P10 mice compared to uninjured age-matched animals (Figure 33c), pathways related to axon extension and neuronal projection were downregulated, whilst pathways associated with the inflammatory response were upregulated.

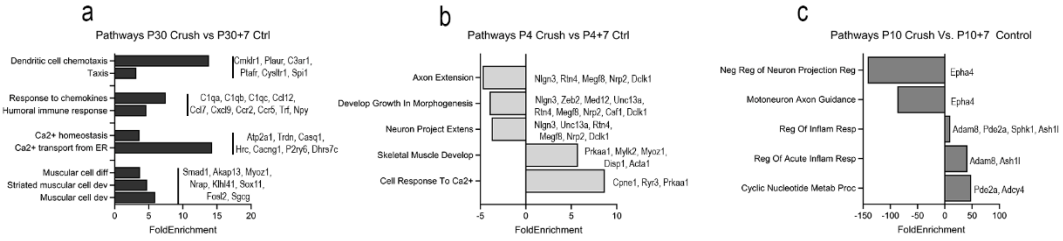

Figure 33. Pathway enrichment analysis. (a) Molecular pathways enriched in P30 crush animals compared with P30+7 control animals. (b) Molecular pathways enriched in P4 crush animals compared with P4+7 control animals. (c) Molecular pathways enriched and downregulated in P10 crush animals compared with those in P10+7 control animals.

Based on the enriched signalling pathways (upregulated or downregulated), we selected a series of genes primarily related to the immune response and the recruitment of macrophages and satellite cells (Figure 34a, Table 2), as well as others associated with nervous system development, axonal guidance, and synaptic plasticity (Figure 34b, Table 3).

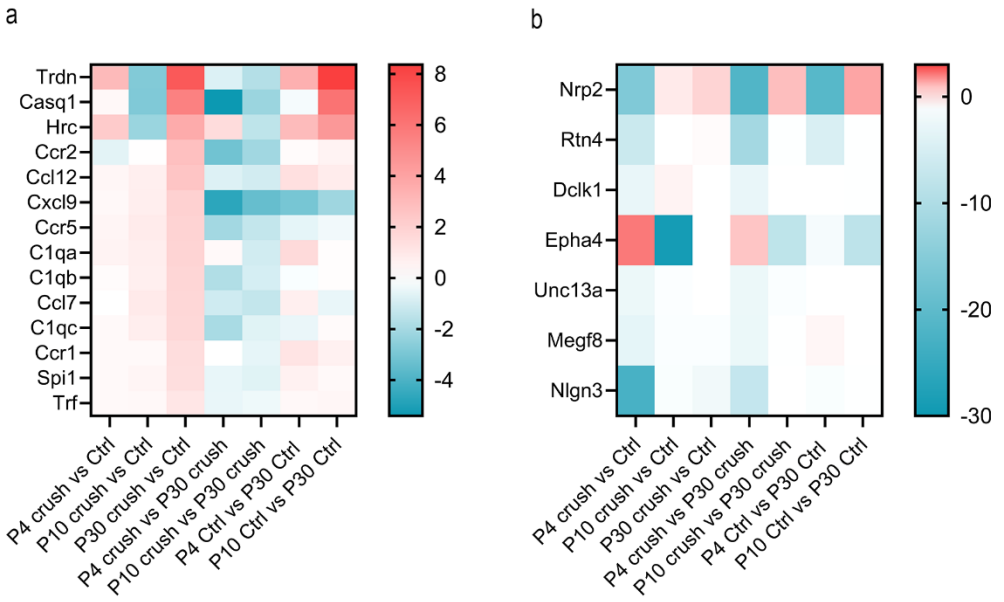

Figure 34. a) Heatmap representing the differential expression (Log2 fold change) of genes related to the inflammatory response across developmental stages (P4, P10, P30) and experimental conditions (crush, control) b) Heatmap representing the differential expression (Log2 fold change) of genes related to axonal growth across developmental stages (P4, P10, P30) and experimental conditions (crush, control). Colour scale indicates Log2 fold change, with red representing upregulation and blue representing downregulation compared to the indicated comparison groups.

When examining genes related to the immune response (Table 2) (Ccl12, Ccl7, Ccr5, Ccr2, Cxcl9, Ccr1, C1qa, C1qb, C1qc, Trf, and Spi1), we observed significant overexpression in injured animals at P30 compared with uninjured P30+7 animals (Log2FC>1, padj<0.05). This pattern was not observed in injured animals at P4 or P10 when compared with their respective age-matched controls (padj>0.05). When comparing these same genes between injured animals at P4 or P10 versus injured animals at P30, several genes were found to be downregulated at P4 (Ccl7, Ccr5, Ccr2, Cxcl9, C1qb, C1qc) and at P10 (Ccl7, Cxcl9, C1qb) (Log2FC<0, padj<0.05). However, when comparing control animals at P4 versus control animals at P30, certain genes showed higher expression levels (Ccl12, Ccr1, C1qa; Log2FC>1, padj<0.05), whilst others exhibited lower expression (Cxcl9; Log2FC<0, padj<0.05).

When examining genes related to nervous system development, axonal guidance, and synaptic function (Table 3) (Nlgn3, Unc13a, Rtn4, Megf8, Nrp2, Dclk1, Epha4), comparison of injured animals at P4 and P10 with their respective age-

matched controls revealed that all genes except Epha4 exhibited lower expression levels (Log2FC<0; padj<0.05). This pattern was not observed in injured animals at P30 (except for the Nrp2 gene). When comparing injured animals at P4 and P10 with injured animals at P30, only the Epha4 gene showed lower expression in injured animals at P4 (Log2FC<0; padj<0.05). No differences were observed between control animals at P4 and P10 versus control animals at P30 (Log2FC≈0; padj>0.05).

	P4 Crush vs Control		P10 Crush vs Control		P30 Crush vs Control		P4 vs P30 (Crush)		P10 vs P30 (Crush)		P4 vs P30 (Control)		P10 vs P30 (Control)	
Gene ID	**Log2FC**	**padj**	**Log2FC**	**padj**	**Log2FC**	**padj**	**Log2FC**	**padj**	**Log2FC**	**padj**	**Log2FC**	**padj**	**Log2FC**	**padj**
Ccl12	0,36	0,912	0,68	1,000	2,5	2,7E-06	-0,78	0,098	-1,03	0,168	1,35	0,010	0,79	0,940
Ccl7	-0,01	0,999	0,89	1,000	1,74	2,6E-03	-1,09	0,021	-1,36	0,024	0,67	0,194	-0,5	1,000
Ccr5	0,41	0,921	0,85	1,000	1,89	6,2E-03	-2,09	1,8E-03	-1,36	0,082	-0,6	0,340	-0,32	1,000
Ccr2	-0,64	0,944	0,07	1,000	2,74	3,4E-02	-3,22	0,002	-2,13	0,109	0,16	0,895	0,54	1,000
Cxcl9	0,32	0,987	0,73	1,000	2	4,1E-02	-4,75	8,3E-08	-3,45	0,000	-3,07	0,002	-2,18	0,101
Ccr1	0,27	0,946	0,23	1,000	1,46	4,3E-02	-0,02	0,971	-0,57	0,941	1,16	0,029	0,65	1,000
C1qa	0,55	0,867	0,72	1,000	1,87	2,2E-02	0,27	0,689	-1,04	0,502	1,59	0,010	0,11	1,000
C1qb	0,14	0,962	0,68	1,000	1,77	2,9E-07	-1,77	2,2E-08	-0,96	0,021	-0,14	0,704	0,13	1,000
C1qc	0,24	0,923	0,76	1,000	1,69	9,6E-06	-1,94	1e-08	-0,72	0,248	-0,49	0,189	0,21	1,000
Trf	0,25	0,885	0,34	1,000	1,08	3,3E-03	-0,51	0,092	-0,39	0,836	0,32	0,318	0,35	1,000
Spi1	0,28	0,947	0,44	1,000	1,44	5,0E-02	-0,52	0,325	-0,71	0,732	0,64	0,250	0,29	1,000

Table 2. Differential expression of genes related to the inflammatory response across developmental stages and experimental conditions. Log2 fold change (Log2FC) and adjusted p-values (padj) for each gene were calculated for the indicated experimental groups. Comparisons include P4, P10, and P30 after nerve crush versus their respective age matched controls (Ctrl), and pairwise comparisons between ages for both crush and control conditions (P4 vs P30, P10 vs P30). Genes with padj<0.05 are considered significantly differentially expressed.

	P4 Crush vs Control		P10 Crush vs Control		P30 Crush vs Control		P4 vs P30 (Crush)		P10 vs P30 (Crush)		P4 vs P30 (Control)		P10 vs P30 (Control)	
Gene	**Log2FC**	**padj**	**Log2FC**	**padj**	**Log2FC**	**padj**	**Log2FC**	**padj**	**Log2FC**	**padj**	**Log2FC**	**padj**	**Log2FC**	**padj**
Nlgn3	-22,98	4,1E-11	-7,39	0,030	-0,87	8,2E-01	-0,85	1,000	-0,14	1,000	-0,27	1,000	-1,96	1,000
Unc13a	-2,48	9,7E-04	-2,44	4,0E-05	-0,11	8,6E-01	-0,62	1,000	-0,68	0,832	-0,21	1,000	-0,16	1,000
Rtn4	-6,67	1,7E-03	-11,48	01,3E-12	-4,76	2,4E-04	-0,06	1,000	-0,4	1,000	-0,29	1,000	0,05	1,000
Megf8	-3,26	1,1E-02	-2,5	0,007	0,13	9,0E-01	-0,74	1,000	-0,32	1,000	-0,21	1,000	-0,63	1,000
Nrp2	-15,93	1,8E-02	-21,83	01,7E-06	-21,07	9,9E-06	0,32	1,000	1,01	1,000	1,4	1,000	0,66	1,000
Dclk1	-2,8	4,8E-02	-2,83	0,002	-0,05	9,6E-01	0,19	1,000	-0,15	1,000	-0,36	1,000	-0,02	1,000
Epha4	2,1	9,4E-01	0,91	0,825	-1,33	7,5E-01	-29,13	1,7E-14	-8,2	0,187	-8,29	0,368	-0,08	1,000

Table 3. Differential expression of genes related to axonal growth across developmental stages and experimental conditions. Log2 fold change (Log2FC) and adjusted p-values (padj) for each gene related to axonal growth were calculated for the indicated experimental groups. Comparisons include P4, P10, and P30 after nerve crush versus their respective controls (Ctrl), and pairwise comparisons between ages for both crush and control conditions (P4 vs P30, P10 vs P30). Genes with padj<0.05 are considered significantly differentially expressed

Neurite outgrowth after a conditioning lesion

To assess the intrinsic capacity for neurite outgrowth at different postnatal stages, and to determine whether a peripheral nerve injury is conditioning sensory neurons to enhance this outgrowth, we quantified neurite extension under basal conditions (P4, P10, and P30, Figure 35) and 7 days after a conditioning lesion (Figure 36). Immunostaining for β-III-tubulin revealed differences in neuronal morphology and neurite length between ages and experimental conditions (Figure 35, 36).

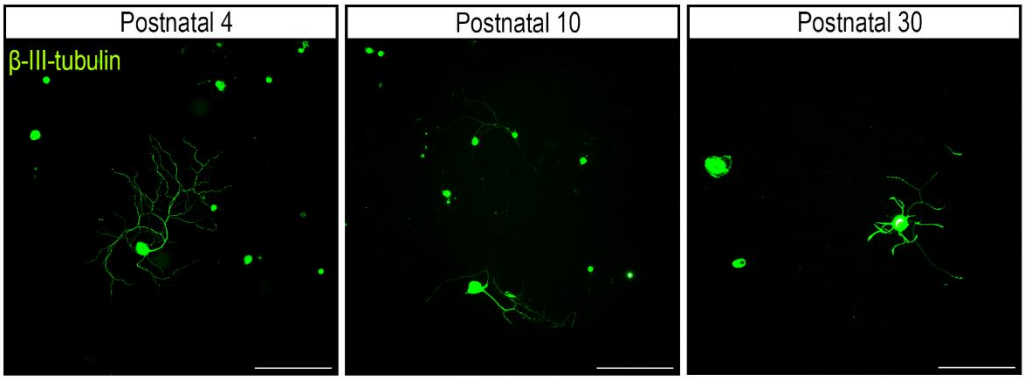

Figure 35. Representative images of β-III-tubulin immunostained primary sensory neurons from lumbar DRG of P4, P10 and P30 mice (left to right), cultured for 24h. Scale bar: 100 µm.

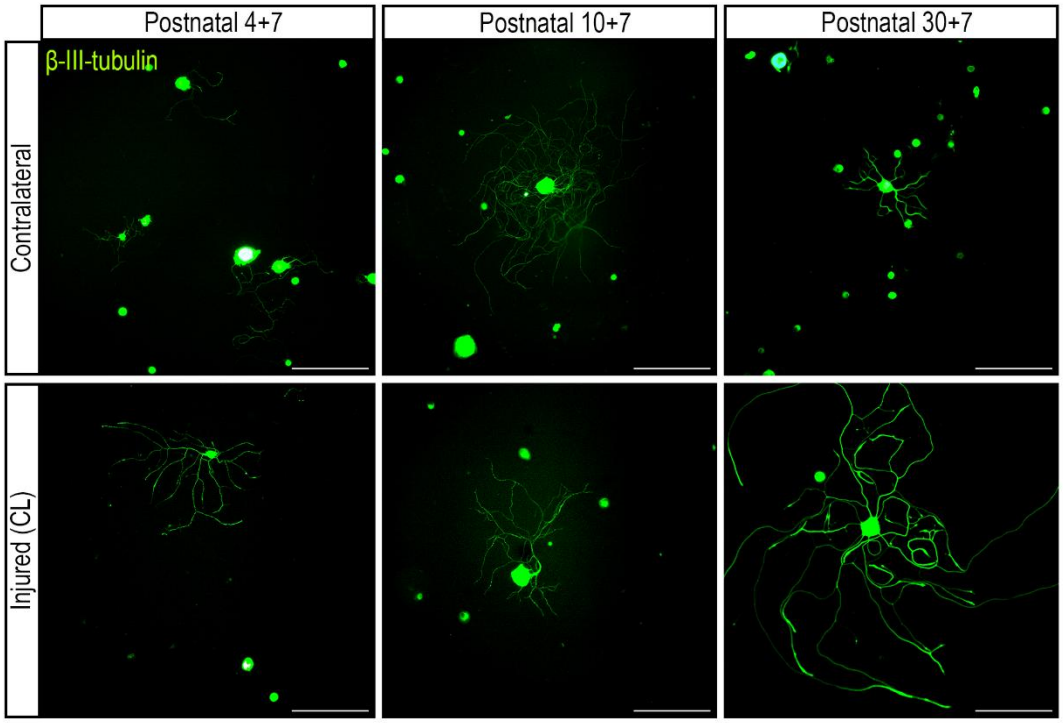

Figure 36. Representative images of cultured primary sensory neurons from lumbar DRG of P4, P10 and P30 mice (left to right) with a prior *in vivo* crush injury to the right sciatic nerve (conditioning lesion) 7 days before (P4+7, P10+7, P30+7). Contralateral (upper row), and injured -ipsilateral- (conditioning lesion, lower row) conditions are shown. Neurons were immunostained with the panmarker β-III-tubulin in. Scale bar: 100 µm

Under basal (uninjured) conditions sensory neurons from P4, P10, and P30 cultured for 24h showed a similar morphology and heterogeneity, with neurons without neurites and others extending neurites of different lengths (Figure 37). There were no statistically significant differences in the percentage of neurons bearing neurites (Figure 37a), mean neurite length (Figure 37b), or the length of the longest neurite (Figure 37c) between these ages, although all parameters had the tendency to be higher in P4 neurons.

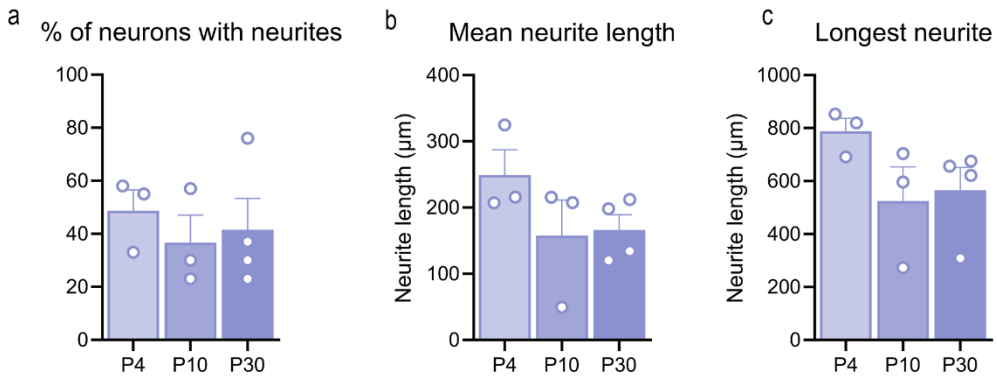

Figure 37. Neurite outgrowth of neurons at different postnatal stages. (a) Percentage of neurons with neurites at P4, P10 and P30. (b) Mean neurite length of neurons with neurites at P4, P10 and P30. (c) Longest neurite at P4, P10 and P30. Statistical analyses were performed using One-way ANOVA with Tukey post hoc test.

We also evaluated the effect of the conditioning lesion at different postnatal stages by focusing on the longest neurite for each culture. We observed a marked increase in that length following conditioning lesion at P30+7 compared to its contralateral side ($p<0.05$). In contrast, P4+7 mice displayed no difference between sides ($p>0.05$), and P10+7 mice showed a reduction in the longest neurite after injury relative to their contralateral side ($p<0.05$) (Figure 38a-c).

When comparing other parameters between ages, we observed that a conditioning lesion increases the percentage of neurons with neurites at P30+7 compared to P4+7 mice; this effect was not observed on the contralateral side (Figure 38d). Comparisons of mean neurite length revealed that P30+7 mice exhibited significantly greater neurite length than P4+7 ($p<0.01$) and P10+7 ($p<0.05$) mice on the ipsilateral side, but not on the contralateral side (Figure 38e). Interestingly, neurons from the contralateral side behave similar to basal neurons of the same age (P4+7 vs P10 and P30+7 vs P30), although with a tendency to show higher values in all the parameters evaluated (Supplementary Figure 7).

For a fair comparison of the effects of the CL among postnatal stages, we calculated the percentage of change in the length of the longest neurite in axotomized neurons compared to contralateral non injured ones. We observed a 66% increase in the length of the longest neurite following injury in P30 mice. In contrast, injury at P4

and P10 resulted in a decrease of approximately 20% and 25%, respectively. Overall, these results confirm that a conditioning lesion at P30 significantly enhances neurite outgrowth compared to P4 ($p<0.05$) and P10 ($p<0.01$) (Figure 38f)

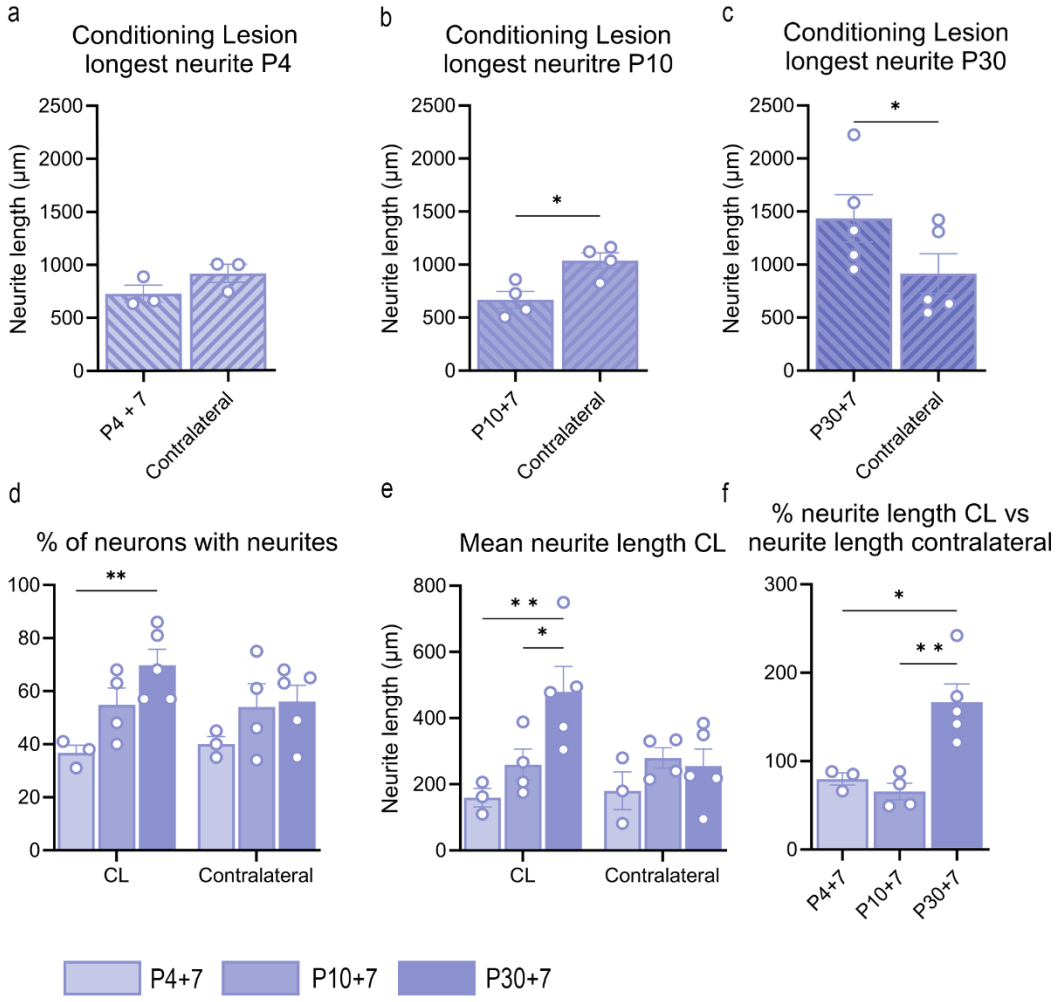

Figure 38. Quantitative analysis of neurite outgrowth following a conditioning lesion at different postnatal stages. (a-c) Longest neurite length for neurons at P4+7 (d), P10+7 (e), and P30+7 (f) in the CL and contralateral groups. Statistical analyses were performed using a paired t test *$p < 0.05$, **$p < 0.01$. (d) Percentage of neurons with neurites 7 dpi after a conditioning lesion in the ipsilateral injured side and the contralateral side at P4, P10 and P30. Statistical analyses were performed using two-way ANOVA with Sidak's post hoc test. Significance levels: **$p<0.01$ (e) Mean neurite length 7 dpi after a conditioning lesion in the ipsilateral injured side and the contralateral side at P4, P10 and P30. Statistical analyses were performed using two-way ANOVA with Sidak's post hoc test. Significance levels: *$p<0.05$ (f) Comparison of longest neurite length between CL and contralateral groups at P4+7, P10+7 and P30+7. Statistical analyses were performed using One-way ANOVA with Tukey post hoc test. Significance levels: *$p<0.05$ ** $p<0.01$.

Discussion

In this study, our main objective is to explore if genetic program activated by injury in primary sensory neurons differ at different postnatal stages. To achieve this, we integrate morphological, molecular, transcriptomic, and *in vitro* approaches, aiming to shed light on the fundamental mechanisms that drive the regenerative response in the postnatal peripheral nervous system.

To evaluate the regenerative capacity of sensory neurons, we selected two paradigmatic subtypes, proprioceptors and nociceptors. Interestingly, they present differences in the regenerative response after a peripheral nerve injury in adult stages, although share common pro-regenerative pathways, too (Bolívar et al., 2024).

We observe a notable absence of death of both types of neurons during early postnatal development (P4 and P10) following peripheral nerve injury, which contrasts with the marked reduction of motoneurons reported in our previous work (Molina-Esteve et al., 2025). In fact, massive loss of postnatal injured motoneurons have been extensively documented in the literature (Lowrie et al., 1982; Liang Low et al., 2003; Greensmith et al., 1994; Lowrie and Vrbová & 1992) and it is restricted to early postnatal stages, whereas loss of sensory neurons is more moderate (Bahadori et al., 2001) and can be extended to juvenile (Kemp et al., 2015a) and even adults (Cooper et al., 2024; Tandrup et al., 2000) where it has been described that the small non-peptidergic nociceptors are most susceptible to axotomy. If we assume that the same population of neurons would die at early postnatal stages, only populations including these small neurons should be vulnerable to injury. Therefore, no reduction in proprioceptors but in nociceptors would be expected. Unfortunately, the analysis in the whole DRG stacked in the confocal microscope could limited our capacity to detect the whole population of TrpV1^{+} neurons, in a prominent manner the smaller ones, and therefore, prevented us to detect its loss.

Both proprioceptors and nociceptors exhibited a high capacity for regeneration following sciatic nerve injury across all postnatal stages (P4, P10, P30), with nociceptive neurons showing significantly greater regeneration than proprioceptive

neurons in the early postnatal stages. These findings are consistent with established literature demonstrating that unmyelinated axons possess superior regenerative velocity compared to their myelinated counterparts (Navarro et al., 1994; Bolívar et al., 2024).

Nociceptors exhibited a distinctive regenerative dynamic, and the number of axons measured at 14 dpi reached basal values at all ages at some distances. In fact, more regenerative axons were observed at some points and ages compared to control values. It is well known that the tip of the regenerating axons can extend a bundle of sprouts at early stages of regeneration (Witzel et al., 2005) and therefore, the estimated number of axons can also reflect this phenomenon.

When focusing on proprioceptive neurons, significant differences emerged between the early postnatal groups (P4 and P10) with lower regenerative outcomes than P30 injured animals. These findings parallel our observations with motoneurons described previously (Molina-Esteve et al., 2025), demonstrating superior regenerative capacity in P30 mice attributed to the robust activation of RAGs, that was not observed in P4 and P10 mice.

Similarly, in sensory neurons no overexpression of RAGs was detected after injury during the early postnatal stages, while such overexpression occurred in injured mice at P30. Transcriptomic analyses revealed that classical pro-regenerative pathways were activated only in young adults, whereas pathways related to development and inflammatory processes were regulated in early postnatal mice. By applying a conditioning injury, we could further explore the impact of these different genetic programs in neurite growth. Despite neurons of different ages extend similar neurites in vitro, the conditioning lesion paradigm was only observed in young adult (P30) mice, where the additional injury clearly promoted enhanced growth capacity; this conditioning lesion effect has been extensively reported in the literature (Smith and Skene 1997; Lankford et al., 1998; Dubový et al., 2019; Seo et al., 2025). In contrast, when applying injuries to P4 and P10 mice, this effect was not observed, supporting the idea that these neurons are in a basal state that inherently promotes growth and therefore, no genetic switch towards a pro-regenerative state is needed for a successful

regenerative response. In fact, in P10 animals we paradoxically observed impaired regenerative responses following a conditioning lesion. Therefore, the age-dependent conditioning response observed in this study underscores the fundamental shift from an axonal growth program in neonatal neurons to a neurotransmitter state in mature ones, that need a genetic shift to reactivate their growth capacities.

Our findings provide compelling evidence that RAGs are robustly upregulated exclusively at P30, remain dormant at P4, and exhibit active downregulation at P10. Our findings are in line with our results in motoneurons (Molina-Esteve et al., 2025) and with previous works that point that P10 represents a critical developmental window characterized by compromised regenerative capacity of peripheral neurons (Fitzgerald & McKelvey, 2016).

It is well established that a dramatic reduction of axon growth rates is observed in neonatal ages, since when developing neurons reach their target, switch from an outgrowth program to a neurotransmitter mode (Goldberg et al., 2002). Peripheral neurons retain the ability to reactivate this growth state after injury, ability that is well reflected in the paradigm of the conditioning lesion. In fact, the robust regenerative response observed in juvenile neurons can be mediated, mainly, by the ability of these neurons to upregulate RAGs. In contrast, P4 and P10 neurons seem to be in a transition state, with a decline in the intrinsic growth capacity reminiscent of the embryonic stages but still not mature enough to activate a regenerative program in response to injury.

The incapacity of early postnatal neurons to activate the paradigmatic program than adult peripheral neurons upregulate can be inherent to the immaturity of neurons at these ages, but also to extrinsic factors, such the inflammatory response triggered by the injury, both at the distal stump and around neuronal somas. Despite it has been proposed that neonatal Schwann cells might fail to create a permissive environment for regeneration and participate in neuronal death (Liang Low et al., 2003), in our previous work (Molina-Esteve et al., 2025), when characterizing Wallerian degeneration at different ages, we did not find evidence that that at early stages Schwann cells in the distal nerve stump failed to create a permissive environment for regeneration. In the

other hand, macrophage infiltration at the DRG seems to contribute to the shift of injured neurons to a pro-regenerative state (Xin Lu and Richardson 1991; Xin Lu and Richardson 1993; Niemi et al., 2013; Kwon et al., 2013) and therefore, we cannot discard that differences in the inflammatory response between ages could had contribute to the final regenerative outcomes, both in vivo and in vitro. It is important to consider that, this conditioning lesion, despite being analysed *in vitro*, has been applied *in vivo* and, therefore, it partially dependent of this inflammatory response. In fact, neuronal Ccl2 by mediating neuron–macrophage interaction through monocytic Ccr2 receptor, has been proposed as a key element for conditioning sensory neurons (Niemi et al., 2013; Kwon et al., 2015). Ccl2 was significantly upregulated in DRG when injury was applied at P30 but not at early postnatal stages. Other chemokines that could compensate the lack of Ccl2 (Talsma et al., 2022) such as Ccl7 or Ccl2, also ligands of Ccr2, were neither upregulated at P4 and P10 after injury.

Ccr2, that was also markedly upregulated in P30 DRG after injury, is one of the main mediators of monocyte migration to tissues, and therefore, not typically expressed in neurons. But the fact that we analysed bulk RNA can lead to mixed responses from different populations of cells present in DRG, such as macrophages or satellite glial cells. In fact, when analysing specifically the translatome of motoneurons (Molina-Esteve et al., 2025), a larger activation of genes and pathways was observed, exposing the limitations of a non-specific tissue RNA analysis. But for technical reasons, mainly related with the low amount of specific RNA per subpopulation of sensory neurons, we chose a simpler design (whole DRG), that despite its constraints, allowed us to see a similar genetic profile between injured motoneurons and sensory neurons of the same age.

In conclusion, the age-dependent conditioning response observed in this study underscores the fundamental shift from an axonal growth program in neonatal neurons to a neurotransmitter state in mature ones (that retain the ability to shift to a pro-regenerative state if needed). The lack of upregulate RAGs in the injured neurons and the absence of conditioning lesion effect is in accordance with this appreciation.

Supplementary information

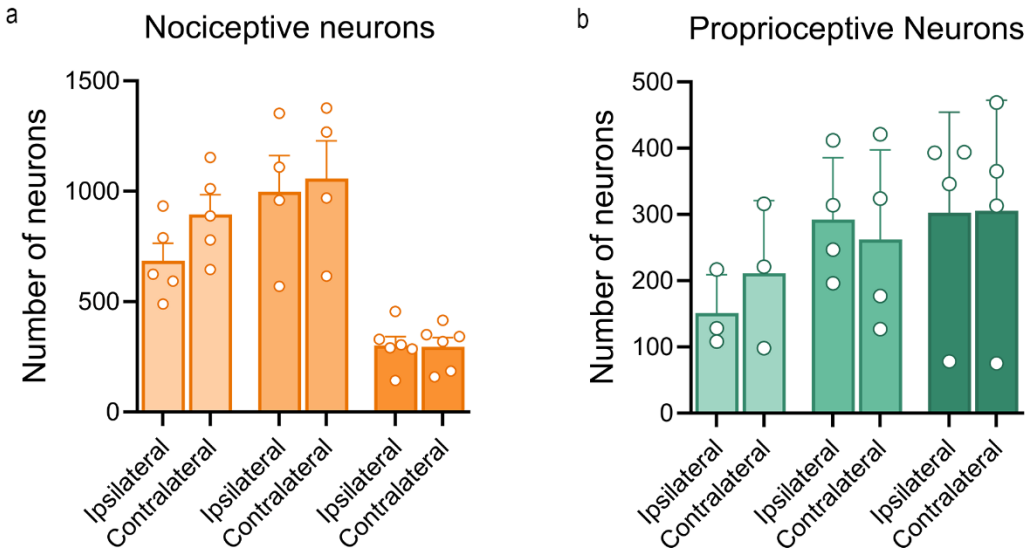

Supplementary figure 5. (a) Quantification of the average number of PV⁺ neurons in the L3-L5 DRGs on both the ipsilateral and contralateral sides at 14 dpi across different postnatal stages. Statistical analysis was performed via two-way ANOVA followed by Sidak's correction test. (b) Quantification of the average number of TrpU1⁺ neurons in the L3-L5 DRGs on both the ipsilateral and contralateral sides at 14 dpi across different postnatal stages. Statistical analysis was performed via two-way ANOVA followed by Sidak's correction test.

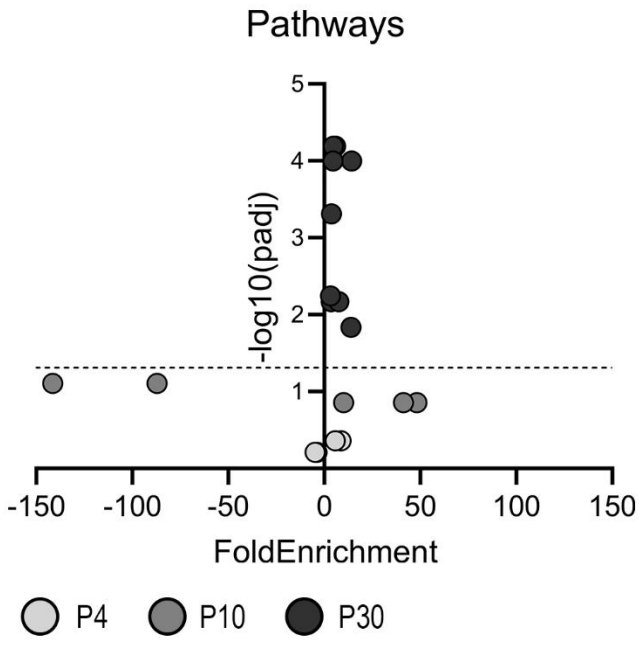

Supplementary figure 6. Selected signalling pathways from animals injured at P4 (light grey circles), P10 (grey circles) and P30 (dark grey circles) showing fold enrichment and -log10(padj). Pathways below the dotted line correspond to those with *padj*>0.05 but *p-value*<0.05.

P4 Crush vs P4+7 Control					
Pathway	**FoldEnrichment**	**pvalue**	**p.adjust**	**Gene Count**	**Key Genes**
Developmental Growth Involved in Morphogenesis	-3,98	0,000453	0,6165	9	Nlgn3, Zeb2, Med12, Unc13a, Rtn4, Megf8, Nrp2, Csf1, Dclk1
Neuron Projection Extension	-3,76	0,005410	0,6165	6	Nlgn3, Unc13a, Rtn4, Megf8, Nrp2, Dclk1
Axon Extension	-4,74	0,004160	0,6165	5	Nlgn3, Rtn4, Megf8, Nrp2, Dclk1
Cellular Response to Calcium Ion	8,69	0,004980	0,4380	3	Cpne1, Ryr3, Prkaa1
Skeletal Muscle Organ Development	5,75	0,001770	0,4380	5	Prkaa1, Mylk2, Myoz1, Disp1, Acta1
P10 Crush vs P10+7 Control					
Pathway	**FoldEnrichment**	**pvalue**	**p.adjust**	**Gene Count**	**Key Genes**
Regulation Of Inflammatory Response	10,03	0,000546	0,1389	4	Adam8, Pde2a, Sphk1, Ash1l
Negative Regulation of Neuron Projection Regeneration	-141,46	0,007050	0,0785	1	Epha4
Motor Neuron Axon Guidance	-87,05	0,011400	0,0785	1	Epha4
Cyclic Nucleotide Metabolic Process	48,3	0,000766	0,1389	2	Pde2a, Adcy4
Regulation Of Acute Inflammatory Response	41,26	0,001050	0,1389	2	Adam8, Ash1l
P30 Crush vs P30+7 Control					
Pathway	**FoldEnrichment**	**pvalue**	**p.adjust**	**Gene Count**	**Key Genes**
Muscular cell development	5,97	0,000000	0,0001	13	Acta1, Mybpc2, Myom2, Myoz1, Tcap, Casq1
Striated muscular cell development	4,77	0,000000	0,0001	16	Acta1, Ccl12, Mybpc2, Myom2, Myoz1, Tcap
Muscular cell differentiation	3,74	0,000003	0,0005	17	Atp2a1, Trdn, Casq1, Hrc
Calcium ion transport from ER	14,32	0,000001	0,0001	7	Atp2a1, Trdn, Casq1, Hrc
Calcium ion homeostasis	3,63	0,000065	0,0068	13	Atp2a1, Ccl12, Ccl7, Trdn, Casq1, Ccr5, Hrc, Ccr2, Cxcl9, Ccr1
Humoral immune response	4,66	0,000001	0,0002	15	C1qa, C1qb, C1qc, Ccl12, Ccl7, Trf
Response to chemokines	7,5	0,000041	0,0051	7	Ccr5, Ccr2, Ccr1, Spi1
Taxis	3,17	0,000049	0,0057	16	Ccl12, Ccl7, Ccr5, Ccr2, Cxcl9, Ccr1, Spi1
Dendritic cell chemotaxis	13,85	0,000182	0,0146	4	Ccr5, Ccr2, Ccr1, Spi1

Supplementary Table 4. Significantly enriched biological processes in lumbar DRG (L3-L5) injured at P4, P10, and P30 and compared to age-matched uninjured controls. Pathways are ranked by statistical significance within each timepoint. Fold enrichment values indicate pathway activation (positive values)

or suppression (negative values). Key genes represent the most relevant genes within each enriched pathway.

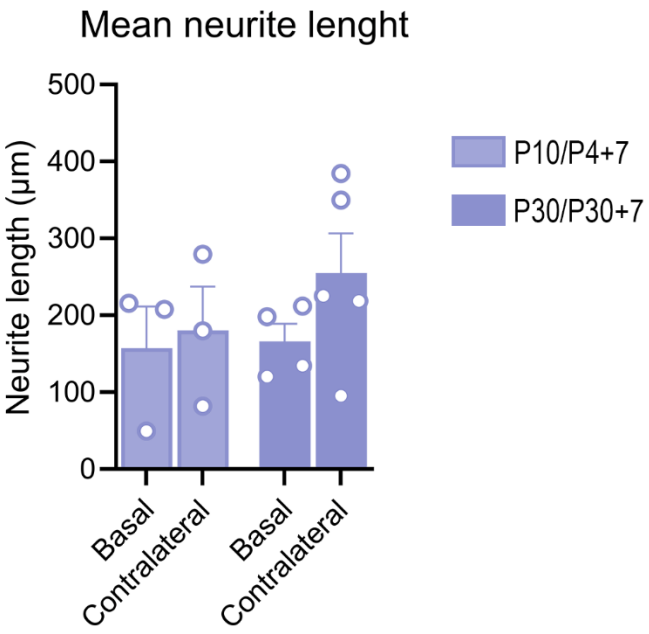

Supplementary figure 7. Mean neurite length of neurons cultured in basal conditions (P10 and P30) neurons 7dpi from the contralateral uninjured side of mice injured at P4 and P30. Statistical analyses were performed using two-way ANOVA with Sidak's post hoc test.

Chapter 3

Age matters: Neuronal Subtype-specific Regeneration After Femoral Nerve Injury

Age matters: Neuronal Subtype-specific Regeneration After Femoral Nerve Injury

Beatriu Molina-Esteve[1,2], Sara Bolívar[3], María Rodríguez-Brañas[1,2], Esther Udina[1,2]

[1] *Universitat Autònoma de Barcelona, Cell Biology, Physiology and Immunology, Bellaterra, Spain*

[2] *Centro de Investigación Biomédica en Red sobre Enfermedades Neurodegenerativas (CIBERNED), Bellaterra, Spain*

[3] *Nuffield Department of Clinical Neurosciences, The University of Oxford, Oxford, UK*

Esther.Udina@uab.cat (corresponding author)

Abstract

Peripheral neurons can regenerate their axons after injury; however, functional recovery depends not only on axonal elongation but also on accurate target reinnervation. Preferential motor reinnervation (PMR) describes the tendency of regenerating motoneurons to reinnervate motor rather than cutaneous pathways. Although PMR has been extensively characterised in adult animals, its occurrence during postnatal development remains less understood. Here, we evaluated the regenerative capacity and specificity of motoneurons, proprioceptive sensory neurons, and non-proprioceptive sensory neurons after femoral nerve transection and fibrin glue repair in postnatal day 10 (P10) PV-Cre/Ai9 mice. Eight weeks after injury, retrograde tracers were applied to the muscular and cutaneous branches, and labelled neurons were quantified in the spinal cord and dorsal root ganglia. Our results showed that motoneurons and proprioceptive neurons displayed a clear preference for reinnervating the motor branch, whereas non-proprioceptive sensory neurons regenerated without specificity. When compared with adult mice, P10 animals exhibited more precise reinnervation, with motoneurons and proprioceptive neurons maintaining significantly higher branch selectivity. Non-proprioceptive sensory neurons failed to show age-dependent differences, regenerating equally into muscular and cutaneous pathways. These findings demonstrate that specificity in regeneration is better preserved in motoneurons and proprioceptive neurons during early postnatal stages, but not in other sensory subpopulations. The results highlight the influence of developmental stage on peripheral nerve regeneration and suggest that mechanisms operating in juvenile neurons and their environment may be harnessed to enhance selective regeneration in adults. Such insights could contribute to therapeutic strategies aimed at improving functional recovery following peripheral nerve injury.

Graphical abstract

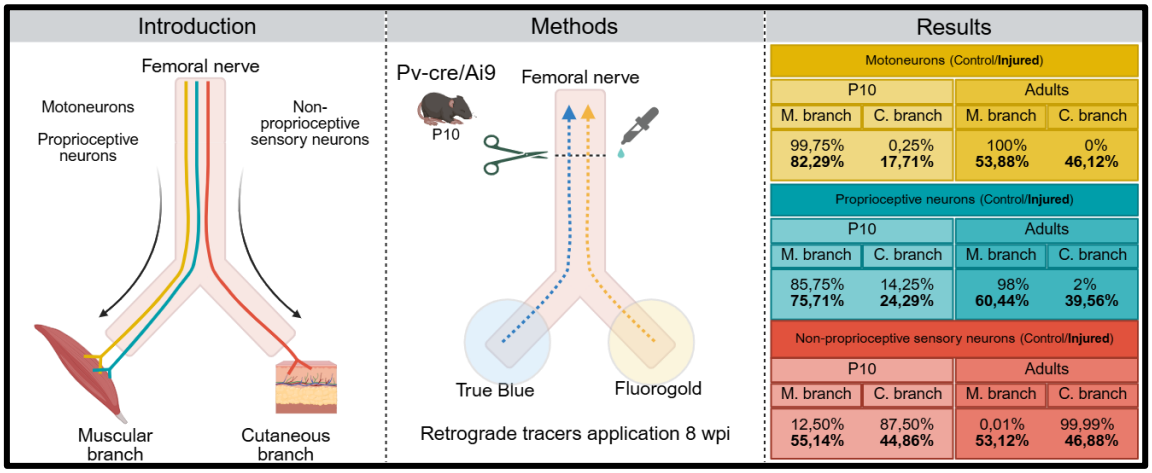

Key words: Preferential motor reinnervation, specific regeneration, postnatal mice, motoneuron, proprioceptive neuron, sensory neuron, nerve injury.

Introduction

Peripheral neurons have the ability to regenerate after a nerve injury, but functional recovery may be compromised if reinnervation lacks specificity. Following nerve transection, axons elongate in response to environmental cues provided by Schwann cells and target tissues (Robinson & Madison, 2005). Preferential motor reinnervation (PMR) refers to the tendency of regenerating motor axons to reinnervate motor pathways associated with muscle targets, rather than cutaneous pathways leading to skin targets (Brushart, 1988, Brushart, 1990).

This phenomenon has been mainly described experimentally using the femoral nerve, that provides an ideal model to investigate target-specific regeneration due to its clear anatomical segregation. Proximally, motor and sensory axons travel together; distally, the nerve separates into a muscle branch innervating the quadriceps and a cutaneous branch (the saphenous nerve) innervating the skin of the hindlimb. Upon injury, regenerating axons have equal access to Schwann cell tubes associated with both branches, allowing for unbiased assessment of reinnervation specificity (Brushart, 1993; Robinson & Madison, 2005). After nerve injury and surgical repair, motor axons initially have equal access to both appropriate (motor) and inappropriate (cutaneous) pathways. In adult mice, it has been reported that two weeks after nerve repair, similar numbers of motor axons reinnervate both branches. By ten weeks post-injury, approximately 60–70% of motor neurons project correctly to the quadriceps muscle, while 20–30% project to the skin, and only a small proportion innervate both targets (Irintchev, 2011).

However, this phenomenon remains controversial and appears to depend on multiple variables, including species, age, and repair methods. Most studies have focused on PMR in motor neurons, whereas investigations into preferential regeneration among sensory neurons are comparatively scarce. Sensory neurons of the peripheral nervous system represent a highly heterogeneous population, comprising proprioceptors, low-threshold mechanoreceptors, and nociceptors, which can be located in both muscle and cutaneous branches of uninjured nerves. Due to this heterogeneity, there is no universal “correct” path for dorsal root

ganglion (DRG) neurons, making the study of target-specific regeneration in sensory populations considerably more complex (Bolívar & Udina, 2022). Most sensory neurons innervate cutaneous targets and terminate within the superficial layers of the dorsal horn. In contrast, proprioceptive neurons project to muscle sensory organs, such as muscle spindles (group Ia and II afferents) and Golgi tendon organs (group Ib afferents). These neurons are typically characterized by large soma size, heavy myelination, and fast conduction velocity. In rodents, the calcium-binding protein parvalbumin (PV) is commonly used as a marker of proprioceptive sensory neurons due to its selective expression in large-diameter DRG cells (Madden et al., 2020).

In neonatal mammals, peripheral nerve lesions are often followed by remarkably accurate muscle reinnervation, suggesting that regenerating motor axons are guided with high precision during early postnatal stages. Studies on the facial nerve in neonatal rats have shown that transection and subsequent regeneration lead to near-complete restoration of the original pattern of muscle innervation, despite a reduced number of surviving motor neurons (Aldskogius & Thomander, 1986). This target-specific regeneration is thought to be driven by a combination of intrinsic spinal cord cues and extrinsic, possibly diffusible, signals present in immature target tissues. In contrast, regenerative accuracy appears to decline with age, with older animals exhibiting increased axonal misrouting. These findings underscore the importance of developmental stage in determining the specificity of peripheral nerve regeneration.

In this study we complemented previous results from our laboratory (Bolívar & Udina, 2022) by comparing preferential regeneration of motoneurons, proprioceptive sensory neurons, and non-proprioceptive sensory neurons when the femoral nerve is injured at postnatal day 10 (P10) mice compared to adult stages. This developmental stage represents a period of ongoing peripheral nervous system maturation and may reveal unique features of regeneration that are lost with age/in

adulthood.

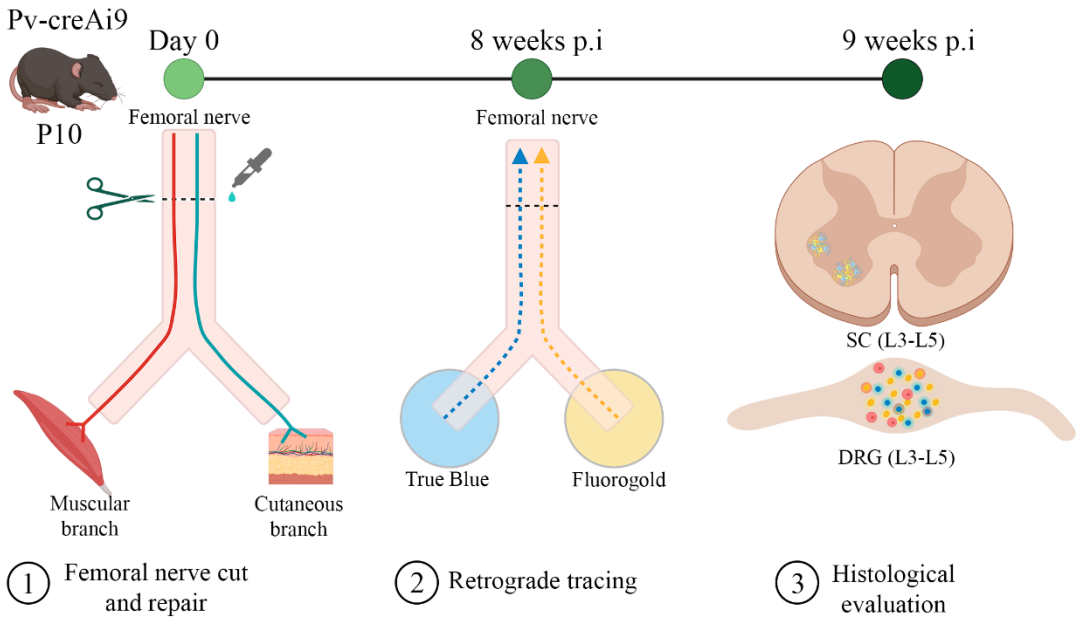

Figure 39. Experimental design of the study. Transgenic mice were obtained by breeding RCL-TdTomato mice and Pv-Cre mice. The femoral nerve was transected and repaired proximally to the bifurcation. 8 weeks after the lesion, the nerve was re-exposed and the retrograde tracers TrueBlue and Fluorogold were applied in the muscular and the cutaneous branch alternately. Histological evaluation was performed 1 week after the application of the retrograde tracers.

Methods

Animals

Double transgenic P10 mice were used (n=7, 2:5 Female:Male) to evaluate preferential regeneration. These mice were generated by breeding homozygous Ai9(RCL-tdT) mice (JAX stock #007909) with B6 PV-cre mice (Parvalbumin, #017320). Four additional non-injured P10 mice (1:1 Female:Male) served as controls. Since no sex-related differences were previously observed (Bolívar & Udina, 2022), data from males and females were pooled for analysis. For comparison with adult animals, previously published data from Pv-Cre/Ai9 adult mice were used (Bolívar & Udina, 2022). All mice were maintained under standard laboratory conditions with access to food and water ad libitum. All experimental procedures were approved by the Universitat Autònoma de Barcelona Animal Experimentation Ethical Committee and followed the European Communities Council Directive 2010/63/EU and the Spanish National law (RD 53/2013).

Surgical Procedure

Mice were anesthetized with intraperitoneal ketamine (90 mg/kg) and xylazine (10 mg/kg) diluted in a 1:5 saline solution. The left femoral nerve was exposed via an inguinal approach. Subcutaneous adipose tissue was removed to visualize the nerve and its branches. The femoral nerve was transected proximally to its bifurcation, and the separated ends were immediately apposed using 5-10 µL of fibrin glue. The fibrin glue consisted of thrombin (25 U/mL, ICN Biomedicals, #0215416305) in calcium chloride (45 mM, Sigma, #C1016), human fibrinogen (100 mg/mL, Sigma, #F3879), and bovine fibronectin (8 mg/mL, Sigma, #F4759) mixed in a 2:1:1 ratio, as previously described (Guest et al., 1997) (Akhter et al., 2019). Following polymerization of the fibrin glue, the incision was closed with a 6-0 nylon suture (Arago). Animals were allowed to recover on a heating pad and were subsequently returned to their mothers. Postoperative health was monitored daily for one week and then weekly.

Retrograde Tracing

Eight weeks post-surgery, the injured mice and non-injured controls were anesthetized, the femoral nerve was re-exposed, and the muscular (quadriceps) and cutaneous (saphenous) branches were distally transected at an equal distance from the original injury site. To retrogradely label neurons, the distal end of one branch was immersed in 4% Fluorogold (Fluorochrome, #52-9400), while the other was placed in 2.5% True Blue Chloride (Setareh Biotech, #7120) for 30 minutes. To create a well and prevent spillage, a small piece of Parafilm was covered with a Vaseline circumference, and the nerve stump was placed into this well, which was then filled with the tracer solution and protected from light. The procedure was the same used in the previous paper (Bolívar & Udina, 2022).

Tissue Processing and Histology

One week following retrograde tracer application, mice were euthanized with Dolethal (30 mg/kg) and transcardially perfused with 4% paraformaldehyde (PFA) in phosphate-buffered saline (PBS). Ipsilateral and contralateral L3 and L4 DRGs, spinal cords, and femoral nerves were dissected and cryoprotected in 30% sucrose in PBS. L3 DRGs and spinal cords were sectioned longitudinally at 15 μm using a cryostat (Leica), and sections were mounted on glass slides.

Microscopy and Cell Counting

DRGs and spinal cord sections were photographed using an epifluorescence microscope (Nikon Eclipse Ni, Tokyo, Japan). In DRG sections, cells double labelled with the td-Tomato and Fluorogold or TrueBlue were counted as proprioceptive neurons every 30 μm. Remaining sensory neurons, cells labelled with either True Blue, Fluorogold or both and tdTomato negative were counted every 30 μm. In spinal cord sections, motoneurons labelled with either True Blue or Fluorogold were counted every 30 μm. Since non-proprioceptive sensory neurons had not been quantified in adult animals in Bolívar and Udina (2022), we reanalysed the images obtained in that study. Specifically, DRGs sections were re-examined to quantify

neurons retrogradely labelled with True Blue, Fluorogold, or both. Neurons were counted in serial sections taken every 30 μm. Since the distinction between fluorogold and true blue is more evident at raw eye in the microscopy, a double checking (microscopy and image) of traced neurons was performed. Motoneurons were directly counted in the microscope. All cell counts were performed by an investigator blinded to the application site of each retrograde tracer.

Statistical analysis

GraphPad Prism 9 (version 9.0.1) was used for statistical analysis. The normality of the data distribution was assessed using the Shapiro–Wilk test ($p>0.05$). Comparisons between control and injured groups for total cell counts were performed using an unpaired *t*-test with Welch's correction. To compare the total number of cells regenerated towards muscular or cutaneous branch multiple Mann-Whitney comparison tests were applied. To compare between age groups, data were analysed using a two-way ANOVA followed by Sidak's multiple comparisons test.

Results

To assess neuronal regeneration at 8 weeks post-injury (wpi), we quantified the total number of motoneurons in the L3–L5 spinal cord (Figure 41a), the total number of Tomato-labelled proprioceptive neurons in the L3 DRG (Figure 41b), and the total number of non-Tomato sensory neurons labelled with either Fluorogold or True Blue in the L3 DRG (Figure 41c). We counted 13±5 traced proprioceptive neurons two months after injury, compared to 22±9 neurons in controls. Regarding non-proprioceptive sensory neurons 120±30 were traced after injury and 127±86 in control animals. In the lumbar spinal cord 130±34 motoneurons were traced after nerve lesion, and 179±65 in controls. With these values, we calculated the percentage of neurons that regenerated at 8 wpi (Figure 41d). At this time point, non-proprioceptive sensory neurons exhibited substantial regeneration, close to 90%, whereas, proprioceptive and motoneurons showed the lowest level of regeneration (60 and 70% respectively); however, this difference did not reach statistical significance when compared to control groups ($p>0.05$). Following femoral nerve injury in adulthood (Figure 41e), all three neuronal populations displayed markedly reduced regeneration at 8 wpi, not exceeding 60% of control values in any of the subtypes ($p<0.0001$). Finally, when comparing regeneration at 8 wpi after femoral nerve injury at P10 versus adulthood (Figure 41f), non-proprioceptive sensory neurons showed improved regeneration when the lesion occurred at P10, whereas no significant difference was observed in proprioceptive and motoneurons.

To assess the specificity of neuronal populations in reinnervating their target organs, we applied alternately two different retrotracers to the muscular and cutaneous branches of the femoral nerve eight weeks after the injury. One week later, we counted the total number of labelled cells from the different branches (Figure 42). In the spinal cord of control animals, 179±66 motoneurons were labelled from the muscular branch, and none from the cutaneous branch; in the injured group, 104±19 motoneurons were labelled from the muscular branch, and 26±17 motoneurons from the cutaneous branch. (Figure 42a) In the DRG, in the control

group 25±4 proprioceptive neurons were labelled from the muscular branch and only 1±0.5 from the cutaneous branch; in the injured group, 8±4 proprioceptive neurons were labelled from the muscular branch and 5±3 from the cutaneous branch. (Figure 42b) Regarding non-proprioceptive sensory neurons, in the control group, 12±10 neurons were labelled from the muscular branch, and 115±90 neurons from the cutaneous branch; in the injured group, 61±19 neurons were labelled from the muscular branch, and 59±38 neurons from the cutaneous branch. (Figure 42c)

Based on the total number of labelled neurons, we calculated the percentage of neurons that correctly reinnervated their corresponding branch. (Table 4, Figure 43) In P10 mice 75.71% of proprioceptive neurons regenerated through the muscular branch, while 24.29% regenerated through the cutaneous branch, indicating a preference of proprioceptive neurons to regenerate towards the right branch. In contrast, only 44.86% of non-proprioceptive sensory neurons regenerated through the cutaneous branch, whereas 55.14% regenerated through the muscular branch, suggesting a lack of specificity of regeneration from these sensory neurons. On the other hand, 82.29% of motor neurons regenerated through the muscular branch, and only 17.71% through the cutaneous branch, and therefore, like proprioceptive neurons, motoneurons showed a marked preference for the muscular branch in postnatal stages.

Bolívar and Udina (2022) performed the same type of injury in adult transgenic mice (Table 4, Figure 43) and found that, after two months, 60.44% of proprioceptive neurons regenerated their axons through the muscular branch, while 39.56% regenerated through the cutaneous branch. Only 53.88% of motor neurons regenerated through the muscular branch, while 46.12% regenerated through the cutaneous branch. For a direct comparison with our results, we have also analysed the number of non-proprioceptive sensory neurons traced with either retrotracer in the adult DRG of these animals, and we found that 46,88% regenerated through the cutaneous branch and 53,12% through the muscular branch.

	Postnatal 10 mice				Adult mice			
Neuronal population	**Muscular branch**		**Cutaneous branch**		**Muscular branch**		**Cutaneous branch**	
% of regenrated neurons	Control	Injured	Control	Injured	Control	Injured	Control	Injured
Motoneurons	99,75%	82,29%	0,25%	17,71%	100%	53,88%	0%	46,12%
Poprioceptive neurons	85,75%	75,71%	14,25%	24,29%	98%	60,44%	2%	39,56%
Non-proprioceptive sensory neurons	12,5%	55,14%	87,50%	44,86%	0,01%	53,12%	99,9%	46,88%

Table 4. Percentage of motoneurons, proprioceptive neurons and non-proprioceptive sensory neurons regenerating through the muscular or cutaneous branches of the femoral nerve in control and injured P10 and adult mice. Values represent the proportion of retrogradely traced neurons in each branch relative to the total number of labelled neurons within each neuronal population.

When comparing these percentages across ages (Figure 44), mice injured at P10 showed a significantly higher specificity of regeneration of motor neurons and proprioceptive neurons ($p<0.05$) after a femoral nerve cut injury compared to adults, whereas this preference was not observed for the non-proprioceptive sensory neurons ($p>0.05$).

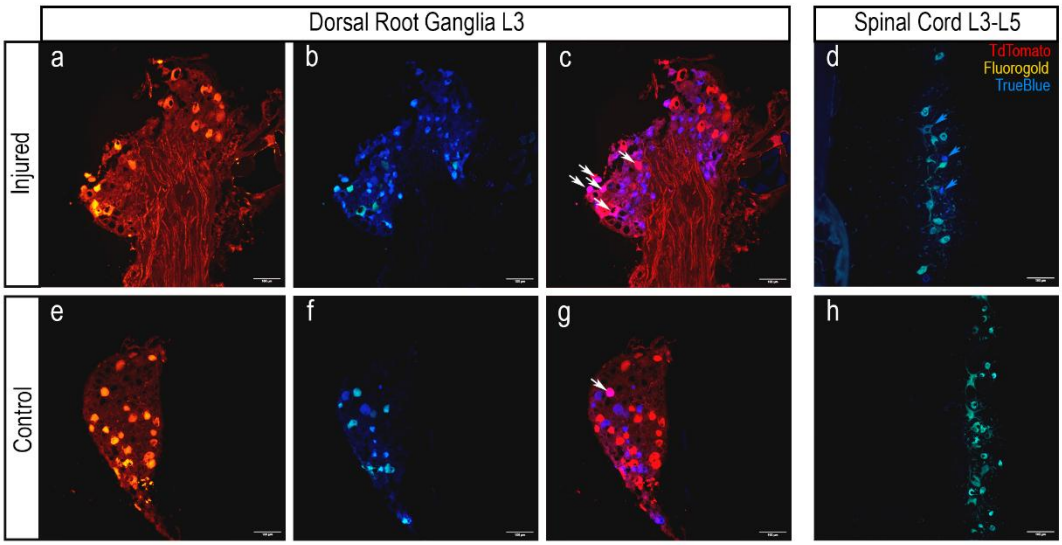

Figure 40. Serial sections of the L3 Dorsal Root Ganglia and Spinal Cord. (a, e) Injured and control samples of L3 DRGs showing PV neurons expressing the fluorescent protein TdTomato. (b, f) Injured and control samples of L3 DRGs labelled with the retrotracers True Blue (intense blue) and Fluorogold (yellowish blue in the images). (c, g) Merged images of TdTomato fluorescence and retrotracers. Arrows indicate neurons co-expressing TdTomato and the retrotracers. (d, h) Spinal cord sections showing motor neurons labelled with the retrotracers. Fluorogold was applied to the muscular branch in **h**, and to the cutaneous branch in **d**, so all motoneurons are fluorogold + in **h**, and

almost all in **h**. Blue arrows on the injured side indicate motoneurons labelled from the cutaneous branch. Scale bar: 100 µ

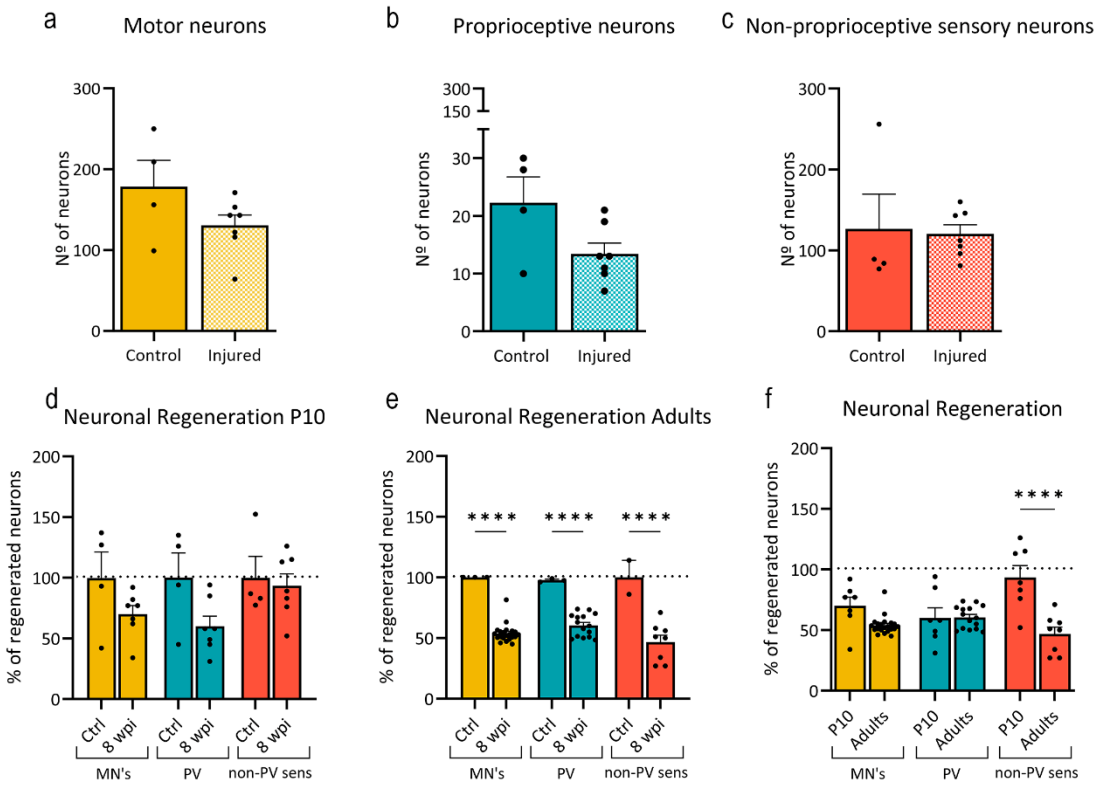

Figure 41. Number of neurons and regeneration 8 wpi after a femoral nerve cut and repair (a) Total number of Motoneurons after a femoral nerve injury at P10 8 wpi. (b) Total number of Proprioceptive neurons after a femoral nerve injury at P10 8 wpi. (c) Total number of non-proprioceptive sensory neurons after a femoral nerve injury at P10 8 wpi. (d) Percentage of Motoneurons, Proprioceptive neurons and non-proprioceptive sensory neurons regenerated 8 wpi after a femoral nerve cut injury in P10 mice. (e) Percentage of Motoneurons, Proprioceptive neurons and non-proprioceptive sensory neurons regenerated 8 wpi after a femoral nerve cut injury in adult mice. (f) Comparison of the % of regenerated Motoneurons, Proprioceptive neurons and non-proprioceptive neurons between P10 and adult mice. Statistics**:** Unpaired t-test with Welch's correction; Two-way ANOVA with Šídák's multiple comparisons test. ****p≤0.0001

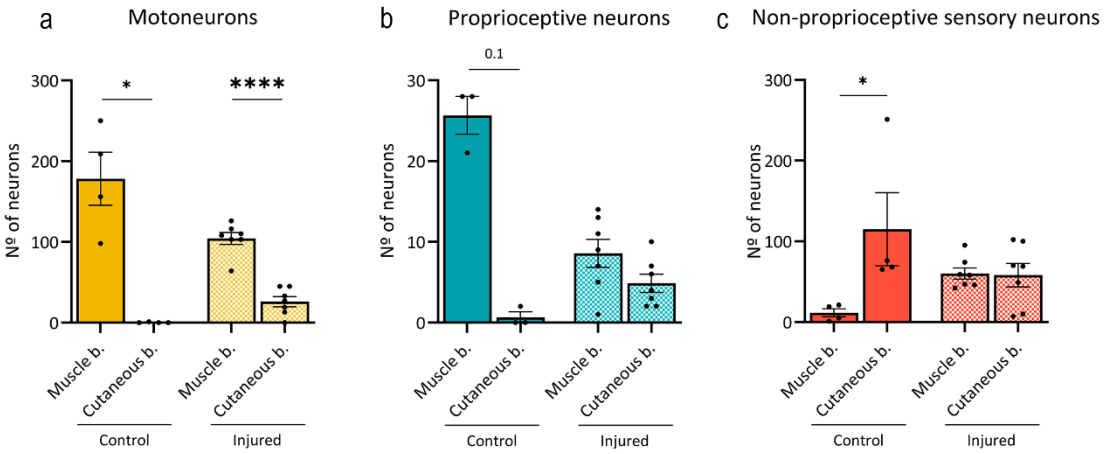

Figure 42. Total number of retrotraced neurons differentiated between the muscular and cutaneous branches. (a) Motoneurons (b) Proprioceptive neurons (c) Non-proprioceptive sensory neurons. Statistics: Two-way ANOVA with Šídák's multiple comparisons test. **p≤0.01, **p≤0.0001.

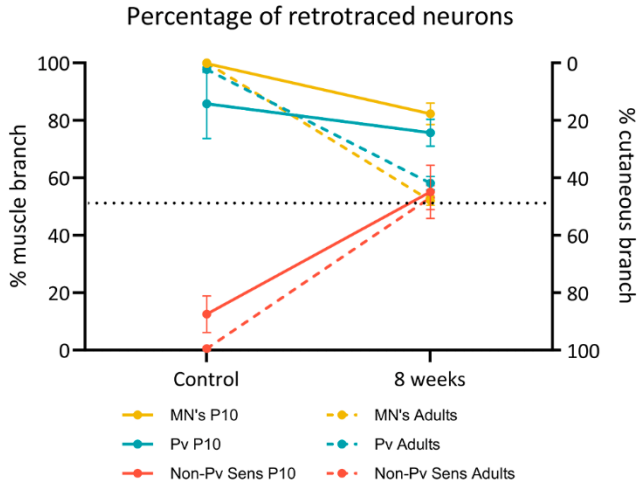

Figure 43 Percentage of retrotraced neurons by neuronal population. Percentage of proprioceptive, motor, and non-proprioceptive sensory retrotraced neurons in postnatal 10 and adult mice.

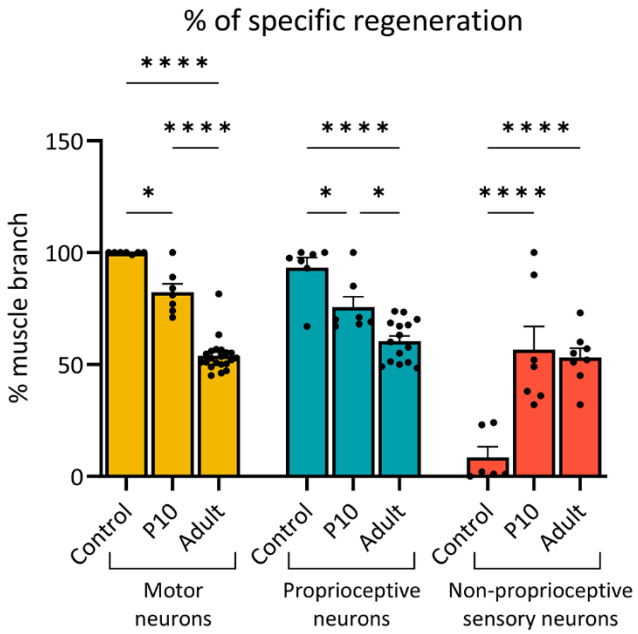

Figure 44. Percentage of proprioceptive, motor neurons and non-proprioceptive sensory neurons regenerated through the muscular branch 8 weeks after injury in P10 and adult mice. Control groups include P10 and adult non-injured mice. Statistics: Two-way ANOVA followed by Sidak's multiple comparisons test. *$p \leq 0.05$, ****$p \leq 0.0001$.

Discussion

In this study, we evaluated the specific regenerative capacity of axons originating from motoneurons, proprioceptive neurons, and non-proprioceptive sensory neurons after a transection injury with repair of the femoral nerve in Pv-cre/Ai9 mice at P10. Our results show that, compared to adult animals (Bolívar & Udina, 2022), the neuronal regeneration capacity is higher when the injury is applied at P10 mice compared with adult mice in non-proprioceptive sensory neurons. Also, motoneurons and proprioceptive neurons in P10 animals exhibit significantly higher regeneration toward the motor branch, whereas non-proprioceptive sensory neurons do not display clear age-related differences. These findings suggest that the ability for regeneration and specific reinnervation is influenced by the developmental stage of the peripheral nervous system and appears to be better preserved in neurons projecting to skeletal muscle during early postnatal stages.

The higher regenerative capacity observed in P10 animals compared with adults is consistent with previous studies showing that age is a critical determinant of axonal regrowth efficiency (Blackandraymond & Lasek', 1979; Kang & Lichtman, 2013).

However, the greater regenerative efficiency in immature neurons is insufficient to guarantee a proper functional recovery, since axons must also reinnervate the correct targets. This requirement for specificity is captured by the concept of preferential motor reinnervation (PMR), which classical studies have described as a distinctive feature of juvenile motoneurons. Brushart (1988, 1990, 1993) demonstrated that juvenile rats exhibit higher motor specificity than adults, highlighting the importance of both age and the contact with the target organ and regenerative pathway to achieve precise reinnervation. Similarly, Aldskogius & Thomander, (1986) observed that in the facial nerve of newborn rats, regenerative specificity was high despite substantial motoneuron loss, whereas in adults the neuronal survival was high, but specificity was low. Similarly, we observed a higher preference for the motor branch from motor and proprioceptive neurons when

injuries are applied at postnatal mice compared to adult ones. Altogether, these findings emphasize that age is a key determinant of specificity preservation.

Le et al., (2001) further addressed this issue using cross-grafting experiments between young (P28) and adult (10 months) rats. They showed that motor preference was robust in young animals regardless of graft origin, but in adults, it was only partially preserved when the graft came from young donors. These results suggest that not only the age of the neuron, but also the environment through which axons regenerate, plays a critical role. Additional evidence supports the notion that regeneration becomes slower and less specific with age; for instance, Kang & Lichtman, (2013) demonstrated that in aged animals, myelin debris clearance is less efficient, thereby delaying regeneration and reducing accuracy.

Species and methodological differences must also be considered. Whereas most studies in young animals have been conducted in rats, divergent results have been reported in mice. Robinson & Madison, (2003) showed that in adult mice, PMR depended on the repair method: following femoral nerve transection, PMR was absent with suture repair but present when fibrin glue was used. Subsequently, Robinson & Madison, (2005) demonstrated that target contact is essential for PMR in adult mice, since when this contact was prevented, motoneurons predominantly regenerated into the cutaneous branch. Later, Robinson & Madison, (2006) confirmed that motoneuron specificity is more pronounced in juvenile mice than in adults, even when target contact is blocked.

In line with Le et al., (2001), our study found no regenerative specificity in non-proprioceptive sensory neurons, either in postnatal or adult mice. This suggests that, unlike motoneurons and proprioceptive neurons, postnatal development does not influence the regenerative specificity of this population. Our results are also consistent with Bolívar & Udina, (2022), who reported in adult mice a preferential regeneration of 54% in motor axons and of 60% in proprioceptive axons. When focusing on a subpopulation of sensory neurons mainly projecting to the cutaneous branch (Npy2r neurons), preference for the correct branch was also observed, but if we just evaluated the population of non-proprioceptive sensory neurons as a whole,

these also exhibited a random preference (of the 47% for the cutaneous branch), similar to what we found in postnatal mice.

The higher specificity of regeneration observed in motoneuron and proprioceptive neurons when injured at P10 compared to adult could be related with the rate of axonal elongation, that decreases with age due to reduced axonal transport of essential growth proteins (Blackandraymond & Lasek', 1979). In fact, a dramatic reduction of axon growth rates is observed at the neonatal ages (Goldberg et al., 2002). All neurons in the development stages establish axonal growth programs (Konishi et al., 2004), but when the axon reaches its target, neuronal cell bodies switch from an outgrowth mode to a neurotransmitter mode. Peripheral neurons also suffer this decline, although retaining the ability to reactivate this growth state after injury (He & Jin, 2016). However, the reactivation of the pro-regenerative program is transcription-dependent and requires some days to be achieved (Smith & Skene, 1997). In fact, the application of a conditioning lesions — a previous injury prior to the tested one — can increase regeneration speed of peripheral neurons by up to 61% in adult rats (Sjöberg & Kanje, 1990), since these injured neurons are already in a pro-regenerative state. Similarly, postnatal neurons, by retaining a growing mode, would show greater regenerative capacity after injury.

Nevertheless, we did not detect a higher regenerative capacity of motoneurons and proprioceptive neurons when injured at postnatal ages compared to adult, regardless of showing a superior specificity. In contrast, non-proprioceptive sensory neurons showed a higher regenerative capacity at postnatal stages, despite the specificity of this subtype of neurons was similar to the one observed in adults. The fact that we are analysing a very heterogeneous population of neurons could influence our findings but rather suggest that the amount of regeneration is not directly related to the degree of specificity of that regeneration.

Another factor that could account for the higher specificity observed in postnatal animals can be related with Wallerian degeneration. In postnatal stages, Schwann cells switch more rapidly from myelinating to repair phenotypes, creating a more permissive environment that supports efficient regeneration. Reier & Hughes

(1972) reported that rats and mice aged 7–14 days exhibit spontaneous axonal degeneration in peripheral nerves, which could accelerate the regenerative response. On the other hand, studies using pre-degenerated grafts have demonstrated enhanced preferential regeneration (Lago et al., 2007; Abdullah et al., 2013). In this context, the immature environment of postnatal animals could promote higher specificity.

Another relevant mechanism that influences specificity is collateral sprouting. Brushart (1990, 1998) described a five- to eight-fold increase in the number of collaterals emitted by regenerating motoneurons after injury, which may initially project into both motor and cutaneous branches. Over time, selective pruning eliminates misdirected axons, mainly those projecting into the cutaneous branch. Interestingly, in P10 animals we did not detect neurons projecting simultaneously into both branches eight weeks after injury, unlike in adults, suggesting that pruning is more efficient at immature stages. This greater precision may be driven by trophic factors secreted by the developing muscle that guide elimination of incorrect sprouts while reinforcing appropriate connections (Brushart, 1990; Redett et al., 2005; Bolívar & Udina, 2022).

Molecular and biochemical differences between motor and sensory nerves also play a critical role in determining regenerative specificity. Martini et al., (1992) identified the carbohydrate epitope L2/HNK-1 on Schwann cells myelinating motor axons, which was abundant in motor nerves but virtually absent in sensory nerves, and essential for motor neurite growth (Martini et al., 1992; Martini et al., 1994) (Mears et al., 2003; Brenner et al., 2006). Similarly, high PSA expressions have been detected in regenerating motor nerves but not in sensory nerves, where it reduces axonal adhesiveness, thereby facilitating outgrowth and correct path selection (Franz et al., 2005). The enriched microenvironment provided by motor Schwann cells further supports regeneration by stimulating axonal elongation, promoting myelination, and secreting trophic factors such as NGF and BDNF that enhance survival and growth of motor and proprioceptive axons. In contrast, sensory nerves lack Schwann cells with motor-like phenotypes and thus produce fewer key factors (Nichols et al., 2004). Höke et al., (2006) demonstrated distinct growth factor

profiles between motor and sensory nerves: PTN and GDNF are enriched in motor nerves, whereas NGF, BDNF, IGF-1, HGF, and VEGF predominate in sensory nerves, supporting the heterogeneous survival and regeneration of sensory subpopulations. Finally, Santos et al., (2017) showed both *in vivo* and *in vitro* that nerve regeneration improves when a permissive environment tailored to neuronal subtype is provided; specifically, laminin and NGF/NT3 supported sensory neurite growth, whereas fibronectin and BDNF enhanced motor outgrowth.

Like any experimental approach, this study presents limitations that must be acknowledged. First, most studies on early postnatal ages have been conducted in rats, so our results in mice were compared mainly with rat data. However, the use of mice provided the advantage of employing transgenic lines, allowing the identification of specific neuronal subpopulations and thus increasing precision despite interspecies differences. Second, we only analysed one immature age (P10) compared with adults. Including intermediate developmental stages (e.g., P20, P28) and earlier ages (P4), which were excluded here due to surgical limitations, would provide a more complete developmental profile. Likewise, assessing earlier time points such as two weeks post-injury, as done in previous studies, could have determined whether motoneurons and proprioceptive neurons already exhibit specificity at earlier regenerative stages. However, it is important to consider the difficulty to apply tracers in the femoral nerve of young mice. In fact, the size of the animal itself is another issue to consider. Clearly, the distance that axons must regenerate in postnatal P10 mice (6-7g of weight) is shorter than in adult animals (25g of weight). However, in our study we observed a selective preference depending on the subpopulation of neuron analysed. In fact, motoneurons showed the highest preference, followed by proprioceptive neurons. In contrast, non-proprioceptive neurons had no clear preference, even when the distance to their target organ was equally close. This fact suggests that preference is inherent to neurons and not determined by the distance to target organ, despite the potential contribution of proximity. Finally, although sample size was modest, results were consistent across animals, and the observed differences were robust and statistically significant.

In conclusion, our findings demonstrate that specific regenerative capacity toward the motor branch is better preserved in motoneurons and proprioceptive neurons during early postnatal stages, whereas sensory neurons do not display this advantage. These results reinforce the notion that both neuronal age and the peripheral microenvironment are critical determinants of regenerative specificity. Furthermore, they suggest that the postnatal window may represent a critical period for understanding the mechanisms underlying preferential regeneration. Future studies exploring intermediate developmental stages and characterizing molecular profiles of neuronal subpopulations will be essential. Ultimately, identifying the mechanisms that enable young neurons to maintain higher regenerative specificity could contribute to the design of therapeutic strategies aimed at recreating a juvenile-like environment in the adult nervous system, thereby improving functional recovery after peripheral nerve injury.

Funding

Funding: This work was funded by the project PID2021-127626OB-I00 from Ministerio de Asuntos económicos y Transformación Digital of Spain. BM holds a PIF contract from the UAB. The author's research was also supported by funds from CIBERNED and TERCEL networks, co-funded by European Union (ERDF/ESF, "Investing in your future").

Acknowledgements

The authors appreciate the technical help of Neus Hernández. Mònica Espejo and Jessica Jaramillo.

Declaration of Competing Interest

The authors declare no competing financial interests.

VII. General Discussion

Differential responses to nerve injury depending on the postnatal stage

In this thesis we have characterized the regenerative response of three different subtypes of neurons after nerve injuries at different postnatal stages. We have used a complementary histological and genetic approach to describe and compare these responses at the neuronal soma but also in the distal nerve. We have observed a massive loss of motoneurons when injured at P4. However, the surviving neurons showed a good regenerative capacity. This capacity was in general higher at P4 compared to 10 mice and was also good in juvenile stages (P30). Interestingly, only injured P30 neurons showed the classical upregulation of RAGs. Wallerian degeneration had also a distinct profile depending on the postnatal stage. Therefore, these findings indicate that each postnatal stage exhibits a distinct and characteristic pattern of response to peripheral nerve injury.

Postnatal 4: High vulnerability yet exceptional growth potential

When a sciatic nerve injury is applied at very early postnatal stages (P4), we observe a drastic reduction—approximately 50%—in the total number of lumbar motoneurons, a mortality rate that far exceeds that described in adult models (Xu et al., 2010; Kemp et al., 2015). This vulnerability is not universal: both proprioceptive and nociceptive sensory neurons show high survival rates (>80–90%). This divergence does not appear to stem from differential lesion toxicity, but rather from intrinsic differences in neuronal susceptibility. In immature motoneurons, this vulnerability may be related to critical dependence on muscle-derived trophic factors (Oppenheim, 1989; Oppenheim et al., 2001; Taylor et al., 2007) and possible glutamate-mediated overexcitation associated with overexpression of immature NMDA receptors (Mentis et al., 1993; Virgo et al., 2000; Greensmith, Hasan, and Vrbová 1994; Petsanis et al., 2012). Additionally, peripheral Schwann cells are still immature and cannot provide adequate trophic support (Jessen et al., 2015; Monk et al., 2015; Endo et al. 2022).

This phenomenon is not novel: classic studies by Romanes (1946) and Schmalbruch (1984) previously described this massive postnatal death. However, our transgenic approach (ChAT-Cre/Ai9 and ChAT-Cre/RiboTag) allows histological and genetic correlations that point that surviving motoneurons retain an intact regenerative potential. This is relevant because the high mortality in neonates was traditionally attributed to an intrinsic inability to regenerate (Liang Low et al., 2003); in contrast, this elevated mortality could mask an exceptional growth capacity in the neurons that persist.

Regarding sensory neurons, technical limitations must be considered: the high density of nociceptive neurons and their heterogeneous distribution could obscure subtle losses (Cooper et al., 2024). Nevertheless, studies using specific markers (PV-Cre, TrpV1-Cre) do not show significant death (Medici & Shortland, 2015), suggesting these neurons are intrinsically more resistant to axotomy than motoneurons at these stages.

To fairy evaluate the regenerative capacity of surviving motoneurons, we take into account neuronal loss. By assuming that each neuron extends one regenerating axon, we corrected basal values according to neuronal survival. Although this approach has some limitations, since regenerating axons usually extend a burst of sprouts, allows to estimate the regenerative capability of surviving motoneurons. With this corrected, we have found that axonal regeneration is complete in motoneurons, moderate in proprioceptive neurons (up to ~80%), and robust in nociceptive neurons (practically complete by 14 dpi). These results indicate that at such early stages, neurons remain in an intrinsically pro-growth state that does not require activation of the classic regeneration program (Chong et al., 1992). This is corroborated by transcriptomics: we do not observe the characteristic increase of RAG levels, a finding supported by the conditioning lesion study, where we observed no differences in neurite growth and elongation between injured and uninjured cells.

Motoneuron-specific translatomics (Ribotag) show that post-injury enriched pathways are mainly associated with mitochondrial energetic metabolism

(respiratory chain, lipid β-oxidation) and early regulatory processes. In contrast, we do not detect typical induction of survival transcriptional programs. This suggests that immature motoneurons opt to maximize ATP production to maintain ionic homeostasis and axonal integrity under high energetic demand (Kiryu-Seo et al. 2016; Sheng 2017), rather than activating more complex transcriptional responses.

In DRGs, RNA-seq analysis reveals downregulation of axon extension pathways (axon guidance, cytoskeleton reorganization) and slight activation of inflammatory pathways. This apparent contradiction with histological data—showing good regeneration—may reflect temporal desynchronization: by 7 dpi, axons have already resumed growth via local mechanisms (e.g., axonal translation), while the DRG nucleus begins deactivating developmental programs to advance toward maturation. Therefore, analysing basal transcriptomics at P4 without injury and denser temporal sampling (2–4 dpi) would be relevant to capture the onset of changes.

Regarding inflammatory genes, no clear pattern is observed in P4. However, we do detect downregulation of axon growth-related genes, consistent with minimal inflammatory response, likely mediated only by satellite glial cells without hematogenous monocyte recruitment. This observation aligns with the absence of CD68+ macrophages in the distal nerve.

The injured nerve environment is essential for efficient regeneration. In immature animals, the initially low myelination state of the sciatic nerve (Eccleston et al., 1987; Jessen et al., 2015) may represent an advantage: there is less myelin to eliminate, thus requiring less intense activation of clearance mechanisms (Yuan et al., 2022) . At the ultrastructural level, we observe that a large proportion of axons at P4 are still in the myelination phase, which facilitates Schwann cell transition to a repair phenotype without prolonged dedifferentiation (Jessen & Mirsky, 2016). This cellular plasticity is characteristic of the early postnatal period and decreases progressively with expression of maturation factors such as Egr2/Krox20 (Gabet et al., 2010).

Transcriptomics of the injured sciatic nerve show downregulation of myelin genes (Mbp, Pllp, Mag, Mal) (Li et al. 2012; Hung et al. 2015; Yi et al. 2015; Yuan et al. 2022) and upregulation of pro-regenerative genes (Gdnf, Bdnf, Igf1) (Terenghi 1999; Yi et al., 2015; Lee and Cho 2021; Contreras et al., 2022). This profile defines a highly permissive environment for axonal regeneration. The lack of macrophage recruitment does not indicate an insufficient response, but rather a physiological adaptation to low myelin debris volume: Schwann cells and resident macrophages would be sufficient for phagocytosis, avoiding the excessive reactive oxygen species production typical of adult models.

The P4 stage thus constitutes a paradoxical therapeutic window: on one hand, neuronal vulnerability is maximal and would require neuroprotective strategies; on the other, regenerative potential is optimal and does not need complex transcriptional program induction. The challenge—and opportunity—lies in protecting the most immature motoneurons while preserving the non-inflammatory, highly permissive peripheral environment that characterizes this early postnatal period.

Postnatal 10: Critical transition window

The P10 stage represents a biologically critical inflection point where postnatal plasticity begins to decline but adult robustness is not yet established. Motoneuron death is significantly reduced to 20-25% (survival ~75%) (Hart et al., 2008), while proprioceptive and nociceptive sensory neurons maintain survival near 100%. These data are supported by previous studies showing that neuronal vulnerability to peripheral lesions is essentially limited to P0-P5 animals (Kemp, Chiang, et al., 2015), and that from P7-P10 onward neurons acquire greater resistance to trophic deprivation (Lowrie and Vrbová & 1992). However, this improved survival does not translate into efficient regeneration; instead, we observe a paradoxical phenotype where regenerative capacity becomes heterogeneous and suboptimal.

When analysing the regenerative capacity of these animals, we observe clearly differentiated results according to neuronal subtype. While non-myelinic

nociceptive neurons show robust and complete regeneration (100% axons regenerated at 14 dpi), myelinic proprioceptive neurons and motoneurons display a suboptimal regeneration profile, with levels around 70% in both neuronal types. This functional difference between myelinic vs. non-myelinic subtypes coincides with previous studies stating that the regenerative capacity of myelinic and non-myelinic neurons differs significantly, with non-myelinic (nociceptive) neurons having the highest capacities and fastest axonal growth speeds (Navarro et al., 1994, Bolivar et al., 2024). Additionally, the smaller body size of P10 animals implies shorter regeneration distances, which could theoretically benefit all subtypes, but results demonstrate that this mechanical advantage does not compensate for intrinsic molecular limitations.

The fact that we observe this suboptimal regenerative capacity in these neuronal subtypes coincides with results from the motoneuron translatome (Ribotag) and bulk DRG transcriptomics. In both cases, when examining expression levels of classical RAGs (Atf3, Gap43, Ngfr, Ccl2)(Allodi et al., 2012; He and Jin 2016), these were unchanged after the injury or even downregulated. This unexpected transcriptional profile suggests that the adult pro-regenerative program is not yet molecularly established at these stages, as we corroborated by using the conditioning lesion paradigm. A previous lesion to the test lesion, by accelerating the activation of RAGs, neurite growth in adult neurons. In contrast, the same injury by does not enhance neurite outgrowth of DRG cultures when applied at P10; in fact, it reduces their growth. This indicates that P10 neurons are in transition where embryonic growth mechanisms are already being dismantled, but adult regeneration mechanisms are not yet operational.

Transcriptomic analysis substantiates this "transition" hypothesis through downregulation of multiple pro-regenerative signalling cascades. The mTORC1/TOR pathway, a central regulator of neuronal growth and regeneration, shows markedly reduced activity (Switon et al., 2017) whilst parallel inhibition of cytoskeletal remodelling and axonal transport pathways—processes indispensable for growth cone dynamics—further constrains regenerative capacity (Bisby and Tetzlaff 1992; Blanquie and Bradke 2018). Collectively, these molecular deficits create a transient

developmental state where embryonic growth programmes are dismantled before adult repair mechanisms become fully operational.

The distal nerve exhibits a Wallerian degeneration profile at P10 that is intermediate between the immature P4 and the more mature P30 stages, consistent with a transitional Schwann cell phenotype. Myelin content in intact P10 nerves is lower than in P30, and after transection we observe a progressive loss of Luxol Fast Blue staining with a clear reduction by 4 dpi but not a complete absence of myelin, indicating an active yet not fully matured demyelination process. In parallel, Oil Red O staining shows a transient increase in lipid droplets that peaks around 4 dpi and then gradually declines, suggesting efficient myelin breakdown and subsequent clearance rather than persistent debris accumulation. $CD68^+$ macrophage density increases over time and reaches its maximum at 7 dpi, earlier than in P30 but later and more robust than in P4, which aligns with a scenario in which Schwann cells at P10 are already capable of triggering a substantial inflammatory response but still retain a higher intrinsic plasticity than their P30 counterparts.

Together with transcriptomics of the distal sciatic nerve, where we observe increased pro-regenerative genes (Gdnf, Bdnf, Igf1) (Terenghi 1999; Yi et al., 2015; Lee and Cho 2021; Contreras et al., 2022) and decreased myelin-associated genes (Mbp, Plp1, Mag) (J. Li et al., 2013; Yi et al., 2015; Zhao et al., 2022), these results would indicate that Schwann cells still retain faster dedifferentiation capacity, which could contribute to higher specificity of reinnervation.

Postnatal 30: Consolidation of the adult-juvenile program and maximum regenerative efficiency

At P30, sciatic nerve injury triggers a response characterised by minimal neuronal death across all three neuronal subtypes examined. Motoneuron survival exceeds 80% (comparable to adults), whilst proprioceptive and nociceptive sensory neurons maintain survival rates approaching 100%. This high resistance reflects the complete maturation of intrinsic neuroprotective mechanisms, including expression of growth factor receptors and consolidation of mitochondrial homeostatic networks that protect against excitotoxicity.

Unlike earlier stages, P30 represents the point at which the critical window of vulnerability has closed. Classic studies by Romanes (1946) and (Kemp et al., 2015) described that this susceptibility window is restricted to the first postnatal days, and our data confirm that by P30 neurons have acquired metabolic and survival autonomy that makes them resilient to muscle deprivation. However, this robustness does not imply loss of plasticity; rather, the capacity to re-activate growth programmes becomes more efficient and coordinated.

Axonal regeneration at P30 reaches maximum levels in all neuronal subtypes, but with differentiated patterns reflecting their mature specialization. Nociceptive neurons, which already showed high regeneration at earlier stages, maintain these capacities and show faster growth velocities than at P10. Proprioceptive neurons show dramatic improvement compared to P10, finally achieving 100% regeneration by 14 dpi, suggesting that maturation of axonal transport machinery and expression of neurotrophin receptors are critical for long-distance regeneration.

The most marked difference between P30 and earlier stages is the robust and coordinated activation of the complete RAG programme. In motoneurons, the analysis of the translatome shows overexpression of classical markers (Atf3, Gap43, Ngfr, Ccl2) (Allodi et al., 2012; He and Jin 2016) and transcription factors (Stat3, Smad1, Klf6) that regulate axonal reprogramming. In DRGs, we observe a similar profile: upregulation of RAGs (Ccl2, Arg1, Timp1, Lgals1) and activation of inflammatory signalling pathways (NF-κB, IL-17, TNF-α) that prepare the distal environment for regeneration.

Moreover, the conditioning lesion is effective at P30, potentiating neurite outgrowth in vitro by 40-60%, demonstrating that neurons have acquired the capacity to "remember" a prior injury and activate growth programs more rapidly.

Wallerian degeneration at P30 follows canonical adult kinetics described in the literature (Gaudet et al., 2011; Rotshenker 2011): progressive myelin loss peaking at 7 dpi, sustained lipid accumulation up to 14 dpi, and massive CD68+ macrophage recruitment also peaking at 14 dpi. This reflects a mature pro-inflammatory microenvironment where Schwann cells have completed transition to

a repair phenotype and emit robust hematogenous recruitment signals (Ccl2, Ccl7, Cxcl9)(Rotshenker, 2011).

At the ultrastructural level, P30 nerves show complete myelination basally, and post-lesion disintegration follows a classic fragmentation and phagocytosis program. Transcriptomics reveals expression of canonical myelin degradation markers alongside increased pro-regenerative markers. At this stage, a homogeneous and permissive distal environment is created, but also a more demanding one: myelin debris clearance requires a more potent inflammatory response, and remyelination is slower and more complex than at earlier stages.

Age as a key determinant of preferential regenerative capability

Besides differences in the regenerative capability of neurons depending on the postnatal stage, we also wanted to explore if these differences impact on the preferentiality of regenerating axons. It is well known that after nerve transections, despite surgical repair, regenerating axons can easily misroute, leading to inespecificity of regeneration and reinnervation failure. A well-established model to study preferential regeneration is the femoral nerve, with a muscular and cutaneous branches of similar diameter where preference of axons for any of the branches can we monitored by using retrograde tracers.

However, the reduced size of the femoral nerve raises technical concerns if a nerve lesion is intended to be applied at P4 mice. Moreover, the lesion needs a prolonged microsurgical precision exceeding 15 minutes, a duration incompatible with the hypothermia-based anaesthesia (5-minute window) required for P4 survival. Consequently, we restricted our comparative analysis to P10 versus adult phenotypes, building upon our laboratory's prior characterization (Bolívar & Udina, 2022).

At P10, we observed exceptionally high reinnervation specificity in motor-related neuronal subtypes. Motoneurons demonstrated an 82% preference for the muscular branch, whilst proprioceptive neurons achieved 75%—both significantly exceeding adult values (54% and 60%, respectively). This enhanced specificity does

not correlate with global regeneration quantity but rather reflects an intrinsic target-selection capacity that emerges selectively in neuronal populations with restricted peripheral targets. The developmental window between P10-P15 thus represents a critical period for connectional fidelity, where molecular guidance cues remain optimally expressed before age-dependent epigenetic silencing.

Conversely, the non-proprioceptive sensory population exhibited no discriminative preference at any age, with random reinnervation (~55% muscular) in both P10 and adult animals. However, it is important to take into account that most of the sensory neurons grouped under the "non-proprioceptive" term, are nociceptors and, therefore, this functional indifference likely reflects their physiological role as polymodal innervators of both cutaneous and muscular tissues, lacking evolutionary pressure for pathway selectivity. This subtype-specific divergence underscores that preferential regeneration is not a universal peripheral nerve property, but an emergent feature of neuronal subpopulations with spatially restricted targets. In fact, when specifically analysing subpopulations of sensory neurons with a main cutaneous component, we have also observed some preferentiality in adult stages (Bolívar & Udina, 2022)

Conclusion

In summary, this doctoral thesis demonstrates that postnatal peripheral nerve regeneration is a stage-specific orchestrated process where neuronal vulnerability, intrinsic growth capacity, and environmental permissiveness must align for optimal functional recovery. By mapping the molecular and cellular landscapes of P4, P10, and P30, we provide a developmental blueprint that redefines therapeutic strategies: protecting immature neurons in P4, enhancing transcriptional plasticity in P10, and rejuvenating the adult microenvironment to recapitulate the juvenile pro-regenerative state. This integrated framework moves beyond the traditional view of regeneration as a binary adult/immature distinction, offering a nuanced, stage-tailored approach to peripheral nerve repair that prioritizes not just axonal growth, but precise, functional reinnervation.

	Postnatal 4			Postnatal 10			Postnatal 30		
Neuronal subtype	Motoneurons	Proprioceptive	Nociceptive	Motoneurons	Proprioceptive	Nociceptive	Motoneurons	Proprioceptive	Nociceptive
Neuronal death	High	Low	Low	Moderate	Low	Low	Low	Low	Low
Axonal regeneration	High	Moderate	High	Low	High	High	Low	High	High
Intrinsic transcriptomic changes	No RAGs	No RAGs	No RAGs	RAGs ↓	RAGs ↓	RAGs ↓	RAGs ↑	RAGs ↑	RAGs ↑
Wallerian Degeneration	Low myelination, fast demyelination, absence of phagocytic macrophages			Faster than classical dynamics of Wallerian Degeneration			Classical dynamics of Wallerian Degeneration		
Peripheral transcriptomic changes	↓ of myelination associated genes, ↑ of pro-regenerative markers			associated genes, ↑ of pro-regenerative markers			↓ of myelination associated genes, ↑ of pro-regenerative markers		
Preferential regeneration	–	–	–	Preferential muscular branch	Preferential muscular branch	No preferential reinnervation	Lower preferential muscular branch	Lower preferential muscular branch	No preferential reinnervation

Table 5. Summary of the main findings of the thesis: neuronal subtype–specific responses in axonal regeneration, neuronal death, Wallerian degeneration dynamics and preferential reinnervation after peripheral nerve injury in P4, P10 and P30 mice.

VIII. Conclusions

Chapter 1.

1. Early postnatal nerve injury leads to marked motoneuron loss at P4 but not at P10 or P30, confirming a short critical window of extreme vulnerability to axotomy.
2. When corrected for motoneuron survival, P4 motoneurons show the highest regenerative capacity, indicating that neonatal neurons retain a strong intrinsic growth potential that is masked by high neuronal death.
3. Juvenile (P30) motoneurons activate a robust classical regeneration-associated gene program after injury, whereas P4 and especially P10 motoneurons show little or even reduced RAG induction despite their ability to regenerate.
4. Wallerian degeneration proceeds efficiently at all postnatal stages, with consistent downregulation of myelination genes and upregulation of pro-regenerative and inflammatory pathways in the distal nerve stump.

Chapter 2.

1. Proprioceptive and nociceptive neurons show robust axonal regeneration at all postnatal stages studied, with nociceptors consistently regenerating better than proprioceptors and without significant neuronal loss.
2. Early postnatal sensory neurons (P4, P10) regenerate effectively despite failing to upregulate classical regeneration-associated genes, whereas P30 neurons activate a strong RAG and pro-regenerative pathway programme after injury.
3. A conditioning lesion enhances neurite outgrowth only in P30 DRG cultured neurons, while P4 neurons show no effect and P10 neurons even display reduced outgrowth.

Chapter 3.

1. After femoral nerve transection and repair at P10 mice, motoneurons and proprioceptive DRG neurons regenerate with strong preference for the

muscular branch, whereas non-proprioceptive sensory neurons regenerate with little or no branch specificity.

2. Overall regeneration at 8 weeks post-injury is higher when the lesion occurs at P10 than in adulthood, particularly for non-proprioceptive sensory neurons.

3. The specificity of reinnervation (preferential motor and proprioceptive regeneration into the muscle branch) is better preserved at P10 than in adult mice, while non-proprioceptive sensory neurons lack this age-dependent improvement in specificity.

IX. Scientific contributions

Repository

Molina-Esteve B, Pujol-Masip M, Ovelleiro D, Gomez-Sanchez JA, Lago N*, Udina E*. 2025. Assessment of Motoneuronal Regeneration and Wallerian Degeneration Following Axotomy in Postnatal Mice. bioRxiv: https://doi.org/10.64898/2025.12.03.691768

Submitted

Molina-Esteve B, Bolívar S, Rodríguez-Brañas M, Udina E. Age matters: Neuronal Subtype-specific Regeneration After Femoral Nerve Injury.

In preparation

Molina-Esteve B, Crugeiras J, Rodríguez-Brañas M, Sanchez-Maldonado A, Ovelleiro D, Lago N*, Udina E*. Outgrowth of Mouse Sensory Neurons is not Mediated by Regeneration Associated Genes in Early Postnatal Stages.

X. References

Abdullah, M., O'Daly, A., Vyas, A., Rohde, C., & Brushart, T. M. (2013). Adult motor axons preferentially reinnervate predegenerated muscle nerve. *Experimental Neurology*, *249*, 1–7. https://doi.org/10.1016/j.expneurol.2013.07.019

Abe, N., & Cavalli, V. (2008). Nerve injury signaling. *Current Opinion in Neurobiology*, *18*(3), 276–283. https://doi.org/10.1016/j.conb.2008.06.005

Abercrombie, M., & Johnson, M. L. (1946). Quantitative Histology of Wallerian Degeneration. *Journal of Anatomy*, *80*, 37–50.

Akhter, E. T., Rotterman, T. M., English, A. W., & Alvarez, F. J. (2019). Sciatic Nerve Cut and Repair Using Fibrin Glue in Adult Mice. *Bio-Protocol*, *9*(18). https://doi.org/10.21769/BioProtoc.3363

Aldskogius, H., & Thomander, L. (1986). Selective Reinnervation of Somatotopically Appropriate Muscles After Facial Nerve Transection and Regeneration in the Neonatal Rat. *Brain Research*, *375*, 126–134. https://doi.org/https://doi.org/10.1016/0006-8993(86)90965-0

Alhamdi, A. A., Mackie, S., Trueman, R. P., & Rayner, M. L. D. (2025). Pharmacologically targeting Schwann cells to improve regeneration following nerve damage. *Frontiers in Cell and Developmental Biology*, *13*. https://doi.org/10.3389/fcell.2025.1603752

Allodi, I., Udina, E., & Navarro, X. (2012). Specificity of peripheral nerve regeneration: Interactions at the axon level. In *Progress in Neurobiology* (Vol. 98, Issue 1, pp. 16–37). https://doi.org/10.1016/j.pneurobio.2012.05.005

Anilkumar, S., & Wright-Jin, E. (2024). NF-κB as an Inducible Regulator of Inflammation in the Central Nervous System. *Cells*, *13*(6). https://doi.org/10.3390/cells13060485

Arthur-Farraj, P. J., Latouche, M., Wilton, D. K., Quintes, S., Chabrol, E., Banerjee, A., Woodhoo, A., Jenkins, B., Rahman, M., Turmaine, M., Wicher, G. K., Mitter, R., Greensmith, L., Behrens, A., Raivich, G., Mirsky, R., & Jessen, K. R. (2012). c-Jun Reprograms Schwann Cells of Injured Nerves to Generate a Repair Cell Essential for Regeneration. *Neuron*, *75*(4), 633–647. https://doi.org/10.1016/j.neuron.2012.06.021

Avci, H. X., Lebrun, C., Wehrlé, R., Doulazmi, M., Chatonnet, F., Morel, M. P., Ema, M., Vodjdani, G., Sotelo, C., Flamant, F., & Dusart, I. (2012). Thyroid hormone triggers the developmental loss of axonal regenerative capacity via thyroid hormone receptor α1 and krüppel-like factor 9 in Purkinje cells. *Proceedings of the National Academy of Sciences of the United States of America*, *109*(35), 14206–14211. https://doi.org/10.1073/pnas.1119853109

Bahadori, M. H., Al-Tiraihi, T., & Valojerdi; Mutjaba Rezazadeh. (2001). Sciatic nerve transection in neonatal rats induces apoptotic neuronal death in L5 dorsal root ganglion. *Journal of Neurocytology*, *30*, 125–130. https://doi.org/10.1023/A:1011935122963

Belin, B. M., Ball, D. J., Langer, J. C., Bridge, P. M., Hagberg, P. K., & Mackinnon, S. E. (1996). The effect of age on peripheral motor nerve function after crush injury in the rat. *The Journal of Trauma*, *40*(5), 775–777. https://doi.org/10.1097/00005373-199605000-00016

Ben-Yaakov, K., Dagan, S. Y., Segal-Ruder, Y., Shalem, O., Vuppalanchi, D., Willis, D. E., Yudin, D., Rishal, I., Rother, F., Bader, M., Blesch, A., Pilpel, Y., Twiss, J. L., & Fainzilber, M. (2012). Axonal transcription factors signal retrogradely in lesioned peripheral nerve. *EMBO Journal*, *31*(6), 1350–1363. https://doi.org/10.1038/emboj.2011.494

Birch, R., & Achan, P. (2000). Peripheral Nerve Repairs and their Results in Children. *Hand Clinics*, *16*(4), 579–595. https://doi.org/https://doi.org/10.1016/S0749-0712(21)00219-5

Bisby, M. A., & Tetzlaff, W. (1992). Changes in Cytoskeletal Protein Synthesis Following Axon Injury and During Axon Regeneration. *Molecular Neurobiology*, *6*, 107–123. https://doi.org/10.1007/BF02780547

Blackandraymond, M. M., & Lasek', J. (1979). Slowing of the Rate of Axonal Regeneration during Growth and Maturation. *Experimental Neurology*, *63*, 108–119. https://doi.org/https://doi.org/10.1016/0014-4886(79)90188-2

Blanquie, O., & Bradke, F. (2018). Cytoskeleton dynamics in axon regeneration. *Current Opinion in Neurobiology*, *51*, 60–69. https://doi.org/10.1016/j.conb.2018.02.024

Boivin, A., Pineau, I., Barrette, B., Filali, M., Vallières, N., Rivest, S., & Lacroix, S. (2007). Toll-like receptor signaling is critical for Wallerian degeneration and functional recovery after peripheral nerve injury. *Journal of Neuroscience*, *27*(46), 12565–12576. https://doi.org/10.1523/JNEUROSCI.3027-07.2007

Bolívar Martín, S. (2023). *Deciphering the Regenerative Response of Peripheral Neuron Subtypes after Nerve Injury*. Universitat Autònoma de Barcelona.

Bolívar, S., Sanz, E., Ovelleiro, D., Zochodne, D. W., & Udina, E. (2024). Neuron-specific RNA-sequencing reveals different responses in peripheral neurons after nerve injury. *ELife*, *12*. https://doi.org/10.7554/elife.91316

Bolívar, S., & Udina, E. (2022). Preferential regeneration and collateral dynamics of motor and sensory neurons after nerve injury in mice. *Experimental Neurology*, *358*. https://doi.org/10.1016/j.expneurol.2022.114227

Bombeiro, A. L., Fernandes, R. G. Q., & Ribot, J. C. (2024). New immune regulators of sciatic nerve regeneration Lessons from the neighborhood. *Neural Regeneration Research*, *19*(4), 705–706. https://doi.org/10.4103/1673-5374.382241

Bradke, F., Fawcett, J. W., & Spira, M. E. (2012). Assembly of a new growth cone after axotomy: The precursor to axon regeneration. *Nature Reviews Neuroscience*, *13*(3), 183–193. https://doi.org/10.1038/nrn3176

Brenner, M. J., Hess, J. R., Myckatyn, T. M., Hayashi, A., Hunter, D. A., & Mackinnon, S. E. (2006). Repair of motor nerve gaps with sensory nerve inhibits regeneration in rats. *Laryngoscope*, *116*(9), 1685–1692. https://doi.org/10.1097/01.mlg.0000229469.31749.91

Bridge, Peter. M., Ball, Douglas. J., Mackinnon, Susan. E., Nakao, Y., Brandt, K., Hunter, Daniel. A., & Hertl, C. (1994). Nerve Crush Injuries-A model for Axonotmesis. *Experimental Neurology*, *127*, 284–290.

Brushart, T., Kebaish, F., Wolinsky, R., Skolasky, R., Li, Z., & Barker, N. (2020). Sensory axons inhibit motor axon regeneration in vitro. *Experimental Neurology*, *323*, 113073. https://doi.org/10.1016/J.EXPNEUROL.2019.113073

Brushart, T. M. E. (1988). Preferential Reinnervation of Motor Nerves by Regenerating Motor Axons. *The Journal of Neuroscience*, *8*(3), 1026–1031. https://doi.org/https://doi.org/10.1523/JNEUROSCI.08-03-01026.1988

Brushart, T. M. E. (1990). Preferential motor reinnervation: a sequential double-labeling study. *Restorative Neurology and Neuroscience*, *1*. https://doi.org/https://doi.org/10.3233/RNN-1990-13416

Brushart, T. M. E. (1993). Motor Axons Preferentially Reinnervate Motor Pathways. *The Journal of Neuroadeooa*, *13*(6), 2730–2738. https://doi.org/https://doi.org/10.1523/JNEUROSCI.13-06-02730.1993

Brushart, T. M., Gerber, J., Kessens, P., Chen, Y.-G., & Royall, R. M. (1998). Contributions of Pathway and Neuron to Preferential Motor Reinnervation. *The Journal of Neuroscience*, *18*(21), 8674–8681. https://doi.org/https://doi.org/10.1523/JNEUROSCI.18-21-08674.1998

Cabaj, A. M., & Slawinska, U. (2012). Riluzole treatment reduces motoneuron death induced by axotomy in newborn rats. *Journal of Neurotrauma*, *29*(7), 1506–1517. https://doi.org/10.1089/neu.2011.2090

Cafferty, W. B. J., Gardiner, N. J., Das, P., Qiu, J., McMahon, S. B., & Thompson, S. W. N. (2004). Conditioning injury-induced spinal axon regeneration fails in interleukin-6 knock-out mice. *The Journal of Neuroscience : The Official Journal of the Society for Neuroscience*, *24*(18), 4432–4443. https://doi.org/10.1523/JNEUROSCI.2245-02.2004

Cammarata, G. M., Bearce, E. A., & Lowery, L. A. (2016). Cytoskeletal social networking in the growth cone: How +TIPs mediate microtubule-actin cross-linking to drive axon outgrowth and guidance. *Cytoskeleton*, *73*(9), 461–476. https://doi.org/10.1002/cm.21272

Catapano, J., Zhang, J., Scholl, D., Chiang, C., Gordon, T., & Borschel, G. H. (2017). N - acetylcysteine prevents retrograde motor neuron death after neonatal peripheral nerve injury. *Plastic and Reconstructive Surgery*, *139*(5), 1105e–1115e. https://doi.org/10.1097/PRS.0000000000003257

Chang, H. M., Shyu, M. K., Tseng, G. F., Liu, C. H., Chang, H. S., Lan, C. T., Hsu, W. M., & Liao, W. C. (2013). Neuregulin Facilitates Nerve Regeneration by Speeding Schwann Cell Migration via ErbB2/3-Dependent FAK Pathway. *PLoS ONE*, *8*(1). https://doi.org/10.1371/journal.pone.0053444

Chen, G., Luo, X., Wang, W., Wang, Y., Zhu, F., & Wang, W. (2019). Interleukin-1β promotes schwann cells de-differentiation in wallerian degeneration via the c-JUN/AP-1 pathway. *Frontiers in Cellular Neuroscience*, *13*. https://doi.org/10.3389/fncel.2019.00304

Chen, P., Piao, X., & Bonaldo, P. (2015). Role of macrophages in Wallerian degeneration and axonal regeneration after peripheral nerve injury. *Acta Neuropathologica*, *130*(5), 605–618. https://doi.org/10.1007/s00401-015-1482-4

Chen, Y., Deng, H., & Zhang, N. (2025). Autophagy-targeting modulation to promote peripheral nerve regeneration. *Neural Regeneration Research*, *20*(7), 1864–1882. https://doi.org/10.4103/NRR.NRR-D-23-01948

Chiarotto, G. B., Drummond, L., Cavarretto, G., Bombeiro, A. L., & De Oliveira, A. L. R. (2014). Neuroprotective effect of tempol (4 hydroxy-tempo) on neuronal death induced by sciatic nerve transection in neonatal rats. *Brain Research Bulletin*, *106*, 1–8. https://doi.org/10.1016/j.brainresbull.2014.04.010

Cho, Y., Shin, J. E., Ewan, E. E., Oh, Y. M., Pita-Thomas, W., & Cavalli, V. (2015). Activating Injury-Responsive Genes with Hypoxia Enhances Axon Regeneration through Neuronal HIF-1α. *Neuron*, *88*(4), 720–734. https://doi.org/10.1016/j.neuron.2015.09.050

Chong, M. S., Fitzgerald, M., Winte, J., Hu-Tsai, M., Emson, P. C., Wiese, U., & Woolf, C. J. (1992). GAP-43 mRNA in Rat Spinal Cord and Dorsal Root Ganglia Neurons: Developmental Changes and Re-expression Following Peripheral Nerve Injury. *European Journal of Neuroscience*, *4*(10), 883–895. https://doi.org/10.1111/j.1460-9568.1992.tb00115.x

Christie, K. J., & Zochodne, D. (2013). Peripheral axon regrowth: New molecular approaches. In *Neuroscience* (Vol. 240, pp. 310–324). https://doi.org/10.1016/j.neuroscience.2013.02.059

Chung, D., Shum, A., & Caraveo, G. (2020). GAP-43 and BASP1 in Axon Regeneration: Implications for the Treatment of Neurodegenerative Diseases. *Frontiers in Cell and Developmental Biology*, *8*. https://doi.org/10.3389/fcell.2020.567537

Contreras, E., Bolívar, S., Navarro, X., & Udina, E. (2022). New insights into peripheral nerve regeneration: The role of secretomes. *Experimental Neurology*, *354*. https://doi.org/10.1016/j.expneurol.2022.114069

Cooper, A. H., Barry, A. M., Chrysostomidou, P., Lolignier, R., Wang, J., Canales, M. R., Titterton, H. F., Bennett, D. L., & Weir, G. A. (2024). Peripheral nerve injury results in a biased loss of sensory neuron subpopulations. *Pain*, *165*(12), 2863–2876. https://doi.org/10.1097/j.pain.0000000000003321

Costales, J. R., Socolovsky, M., Sánchez Lázaro, J. A., & Álvarez García, R. (2019). Peripheral nerve injuries in the pediatric population: a review of the literature. Part I: traumatic nerve injuries. *Child's Nervous System*, *35*(1), 29–35. https://doi.org/10.1007/s00381-018-3974-8

Culmsee, C., & Mattson, M. P. (2005). p53 in neuronal apoptosis. *Biochemical and Biophysical Research Communications*, *331*(3), 761–777. https://doi.org/10.1016/j.bbrc.2005.03.149

Dent, E. W., & Gertler, F. B. (2003). Cytoskeletal Dynamics and Transport in Growth Cone Motility and Axon Guidance. *Neuron*, *40*(2), 209–227. https://doi.org/10.1016/s0896-6273(03)00633-0

Dent, E. W., Gupton, S. L., & Gertler, F. B. (2011). The growth cone cytoskeleton in Axon outgrowth and guidance. *Cold Spring Harbor Perspectives in Biology*, *3*(3), 1–39. https://doi.org/10.1101/cshperspect.a001800

Devi, B. I., Konar, S. K., Bhat, D. I., Shukla, D. P., Bharath, R., & Gopalakrishnan, M. S. (2018). Predictors of Surgical Outcomes of Traumatic Peripheral Nerve Injuries in Children: An Institutional Experience. *Pediatric Neurosurgery*, *53*(2), 94–99. https://doi.org/10.1159/000484174

Donnerer, J. (2003). Regeneration of primary sensory neurons. *Pharmacology*, *67*(4), 169–181. https://doi.org/10.1159/000068405

Du, S., & Zheng, H. (2021). Role of FoxO transcription factors in aging and age-related metabolic and neurodegenerative diseases. *Cell and Bioscience*, *11*(1). https://doi.org/10.1186/s13578-021-00700-7

Dubin, A. E., & Patapoutian, A. (2010). Nociceptors: The sensors of the pain pathway. In *Journal of Clinical Investigation* (Vol. 120, Issue 11, pp. 3760–3772). https://doi.org/10.1172/JCI42843

Dubový, P., Klusáková, I., Hradilová-Svíženská, I., Brázda, V., Kohoutková, M., & Joukal, M. (2019). A conditioning sciatic nerve lesion triggers a pro-regenerative state in

primary sensory neurons also of dorsal root ganglia non-associated with the damaged nerve. *Frontiers in Cellular Neuroscience*, *13*. https://doi.org/10.3389/fncel.2019.00011

Eccleston, P. A., Mirsky, R., Jessen, K. R., Sommer, I., & Schachner, M. (1987). Postnatal development of rat peripheral nerves: an immunohistochemical study of membrane lipids common to non-myelin forming Schwann cells, myelin forming Schwann cells and oligodendrocytes. *Developmental Brain Research*, *2*(432), 249–256. https://doi.org/0.1016/0165-3806(87)90049-6

Endo, T., Kadoya, K., Suzuki, T., Suzuki, Y., Terkawi, M. A., Kawamura, D., & Iwasaki, N. (2022). Mature but not developing Schwann cells promote axon regeneration after peripheral nerve injury. *Npj Regenerative Medicine*, *7*(1). https://doi.org/10.1038/s41536-022-00205-y

Fan, J., Mansfield, S. G., Redmond, T., Gordon-Weeks, P. R., & Raper, J. A. (1993). The Organization of F-Actin and Microtubules in Growth Cones Exposed to a Brain-derived Collapsing Factor. *Cell Biology*, *121*(4), 867–878. https://doi.org/10.1083/jcb.121.4.867

Fargo, K. N., Foecking, E. M., Jones, K. J., & Sengelaub, D. R. (2009). Neuroprotective actions of androgens on motoneurons. *Frontiers in Neuroendocrinology*, *30*(2), 130–141. https://doi.org/10.1016/j.yfrne.2009.04.005

Feltri, M. L., Weaver, M. R., Belin, S., & Poitelon, Y. (2021). The Hippo pathway: Horizons for innovative treatments of peripheral nerve diseases. *Journal of the Peripheral Nervous System*, *26*(1), 4–16. https://doi.org/10.1111/jns.12431

Fitzgerald, M., & McKelvey, R. (2016). Nerve injury and neuropathic pain - A question of age. *Experimental Neurology*, *275*, 296–302. https://doi.org/10.1016/j.expneurol.2015.07.013

Flecknell, P., Lofgren, J. L. S., Dyson, M. C., Marini, R. R., Michael Swindle, M., & Wilson, R. P. (2015). Chapter 24 - Preanesthesia, Anesthesia, Analgesia, and Euthanasia. In *Laboratory Animal Medicine: Third Edition* (pp. 1135–1200). Elsevier Inc. https://doi.org/10.1016/B978-0-12-409527-4.00024-9

Fontana, X., Hristova, M., Da Costa, C., Patodia, S., Thei, L., Makwana, M., Spencer-Dene, B., Latouche, M., Mirsky, R., Jessen, K. R., Klein, R., Raivich, G., & Behrens, A. (2012). C-Jun in Schwann cells promotes axonal regeneration and motoneuron survival via paracrine signaling. *Journal of Cell Biology*, *198*(1), 127–141. https://doi.org/10.1083/jcb.201205025

Franz, C. K., Rutishauser, U., & Rafuse, V. F. (2005). Polysialylated neural cell adhesion molecule is necessary for selective targeting of regenerating motor neurons. *Journal of Neuroscience*, *25*(8), 2081–2091. https://doi.org/10.1523/JNEUROSCI.4880-04.2005

G Culotti, J., & C Merz, D. (1998). DCC and netrins. *Current Opinion in Cell Biology*, *10*(10), 609–613. https://doi.org/10.1016/s0955-0674(98)80036-7

Gabet, Y., Baniwal, S. K., Leclerc, N., Shi, Y., Kohn-Gabet, A. E., Cogan, J., Dixon, A., Bachar, M., Guo, L., Turman, J. E., & Frenkel, B. (2010). Krox20/EGR2 deficiency accelerates cell growth and differentiation in the monocytic lineage and decreases bone mass. *Blood*, *116*(19), 3964–3971. https://doi.org/10.1182/blood-2010-01-263830

Gaudet, A. D., Popovich, P. G., & Ramer, M. S. (2011). Wallerian degeneration: Gaining perspective on inflammatory events after peripheral nerve injury. *Journal of Neuroinflammation*, *8*. https://doi.org/10.1186/1742-2094-8-110

Geddis, M. S., & Rehder, V. (2003). The Phosphorylation State of Neuronal Processes Determines Growth Cone Formation After Neuronal Injury. *Journal of Neuroscience Research*, *74*(2), 210–220. https://doi.org/10.1002/jnr.10741

Geuna, S., Raimondo, S., Ronchi, G., Di Scipio, F., Tos, P., Czaja, K., & Fornaro, M. (2009). Chapter 3 Histology of the Peripheral Nerve and Changes Occurring During Nerve Regeneration. In *International Review of Neurobiology* (Vol. 87, Issue C, pp. 27–46). https://doi.org/10.1016/S0074-7742(09)87003-7

Gitler, D., & Spira, M. E. (1998). Real Time Imaging of Calcium-Induced Localized Proteolytic Activity after Axotomy and Its Relation to Growth Cone Formation. *Neuron*, *20*(6), 1123–1135. https://doi.org/10.1016/s0896-6273(00)80494-8

Goldberg, J. L., Klassen, M. P., & Hua, Y. (2002). Amacrine-Signaled Loss of Intrinsic Axon Growth Ability by Retinal Ganglion Cells. *Science*, *1860*(9296), 432. https://doi.org/10.1126/science.1068428

Gomez, T. M., & Letourneau, P. C. (2014). Actin dynamics in growth cone motility and navigation. *Journal of Neurochemistry*, *129*(2), 221–234. https://doi.org/10.1111/jnc.12506

Gomez-Sanchez, J. A., Carty, L., Iruarrizaga-Lejarreta, M., Palomo-Irigoyen, M., Varela-Rey, M., Griffith, M., Hantke, J., Macias-Camara, N., Azkargorta, M., Aurrekoetxea, I., De Juan, V. G., Jefferies, H. B. J., Aspichueta, P., Elortza, F., Aransay, A. M., Martínez-Chantar, M. L., Baas, F., Mato, J. M., Mirsky, R., … Jessen, K. R. (2015). Schwann cell autophagy, myelinophagy, initiates myelin clearance from injured nerves. *Journal of Cell Biology*, *210*(1), 153–168. https://doi.org/10.1083/jcb.201503019

Greensmith, L., Hasan, H. I., & Vrbova, G. (1994). Nerve injury increases the susceptibility of motoneurons to N-methyl-d-aspartate-induced neurotoxicity in the developing rat. *Neuroscience*, *58*(4), 721–733. https://doi.org/10.1016/0306-4522(94)90450-2

Guest, J. D., Hesse, D., Schnell, L., Schwab, M. E., Bunge, M. B., & Bunge, R. P. (1997). Influence of IN-1 Antibody and Acidic FGF-Fibrin Glue on the Response of Injured Corticospinal Tract Axons to Human Schwann Cell Grafts. *J. Neurosci. Res*, *50*, 888–905. https://doi.org/https://doi.org/10.1002/(SICI)1097-4547(19971201)50:5<888::AID-JNR24>3.0.CO;2-W

Hanz, S., & Fainzilber, M. (2006). Retrograde signaling in injured nerve - The axon reaction revisited. *Journal of Neurochemistry*, *99*(1), 13–19. https://doi.org/10.1111/j.1471-4159.2006.04089.x

Hart, A. M., Terenghi, G., & Wiberg, M. (2008). Neuronal death after peripheral nerve injury and experimental strategies for neuroprotection. *Neurological Research*, *30*(10), 999–1011. https://doi.org/10.1179/174313208X362479

He, B., Su, S., Zhang, Z., Lin, Z., Qiu, Q., Yang, Y., Wen, X., & Zhu, Z. (2025). Runx2 drives Schwann cells repair phenotype switch through chromatin remodeling and Sox2 activation after nerve injury. *Molecular Medicine*, *31*(1). https://doi.org/10.1186/s10020-025-01142-4

He, Z., & Jin, Y. (2016). Intrinsic Control of Axon Regeneration. In *Neuron* (Vol. 90, Issue 3, pp. 437–451). Cell Press. https://doi.org/10.1016/j.neuron.2016.04.022

Höke, A., Redett, R., Hameed, H., Jari, R., Zhou, C., Li, Z. B., Griffin, J. W., & Brushart, T. M. (2006). Schwann cells express motor and sensory phenotypes that regulate axon regeneration. *Journal of Neuroscience*, *26*(38), 9646–9655. https://doi.org/10.1523/JNEUROSCI.1620-06.2006

Huang, H. cheng, Chen, L., Zhang, H. xing, Li, S. fa, Liu, P., Zhao, T. yun, & Li, C. xiang. (2016). Autophagy Promotes Peripheral Nerve Regeneration and Motor Recovery Following Sciatic Nerve Crush Injury in Rats. *Journal of Molecular Neuroscience*, *58*(4), 416–423. https://doi.org/10.1007/s12031-015-0672-9

Huang, Y., Wu, L., Zhao, Y., Guo, J., Li, R., Ma, S., & Ying, Z. (2024). Schwann cell promotes macrophage recruitment through IL-17B/IL-17RB pathway in injured peripheral nerves. *Cell Reports*, *43*(2). https://doi.org/10.1016/j.celrep.2024.113753

Hung, H. A., Sun, G., Keles, S., & Svaren, J. (2015). Dynamic regulation of Schwann cell enhancers after peripheral nerve injury. *Journal of Biological Chemistry*, *290*(11), 6937–6950. https://doi.org/10.1074/jbc.M114.622878

Irintchev, A. (2011). Potentials and limitations of peripheral nerve injury models in rodents with particular reference to the femoral nerve. *Annals of Anatomy*, *193*(4), 276–285. https://doi.org/10.1016/j.aanat.2011.02.019

Itoh, T., Horiuchi, M., Ikeda, R. H., Xu, J., Bannerman, P., Pleasure, D., Penninger, J. M., Tournier, C., & Itoh, A. (2014). ZPK/DLK and MKK4 form the critical gateway to

axotomy-induced motoneuron death in neonates. *Journal of Neuroscience*, *34*(32), 10729–10742. https://doi.org/10.1523/JNEUROSCI.0539-14.2014

Iwasaki, Y., Ikeda, K., Shiojima, T., & Kinoshita, M. (1995). CNQX prevents spinal motor neuron death following sciatic nerve transection in newborn rats. *Journal of the Neurological Sciences*, *134*(1–2), 21–25. https://doi.org/10.1016/0022-510x(95)00217-6

Iwasaki, Y., Shiojima, T., Tagaya, N., Kobayashi, T., & Kinoshita, M. (1997). Basic fibroblast growth factor and platelet-derived growth factor prevent the death of spinal motor neurons after sciatic nerve transection in the neonatal rats. *Neurological Research*, *19*(5), 555–557. https://doi.org/10.1080/01616412.1997.11740857

J Dickson, B. (2001). Rho GTPases in growth cone guidance. *Current Opinion in Neurobiology*, *11*(1), 103–110. https://doi.org/10.1016/s0959-4388(00)00180-x

Janko, M. (1976). Nerve Regeneration Following Primary Repair. *Aeta Neurochirurgiea*, *34*, 223–234. https://doi.org/https://doi.org/10.1007/BF01405877

Jessen, K. R., & Mirsky, R. (2016). The repair Schwann cell and its function in regenerating nerves. In *Journal of Physiology* (Vol. 594, Issue 13, pp. 3521–3531). Blackwell Publishing Ltd. https://doi.org/10.1113/JP270874

Jessen, K. R., & Mirsky, R. (2019). The success and failure of the schwann cell response to nerve injury. *Frontiers in Cellular Neuroscience*, *13*, 1–14. https://doi.org/10.3389/fncel.2019.00033

Jessen, K. R., & Mirsky, R. (2022). The Role of c-Jun and Autocrine Signaling Loops in the Control of Repair Schwann Cells and Regeneration. *Frontiers in Cellular Neuroscience*, *15*. https://doi.org/10.3389/fncel.2021.820216

Jessen, K. R., Mirsky, R., & Lloyd, A. C. (2015). Schwann cells: Development and role in nerve repair. *Cold Spring Harbor Perspectives in Biology*, *7*(7), 1–15. https://doi.org/10.1101/cshperspect.a020487

Jimenez-Blasco, D., Agulla, J., Lapresa, R., Garcia-Macia, M., Bobo-Jimenez, V., Garcia-Rodriguez, D., Manjarres-Raza, I., Fernandez, E., Jeanson, Y., Khoury, S., Portais, J.-C., Padro, D., Ramos-Cabrer, P., Carmeliet, P., Almeida, A., & Bolaños, J. P. (2024). Weak neuronal glycolysis sustains cognition and organismal fitness. *Nature Metabolism*, *6*(7), 1253–1267. https://doi.org/10.1038/s42255-024-01049-0

Jung, J., Cai, W., Lee, H. K., Pellegatta, M., Shin, Y. K., Jang, S. Y., Suh, D. J., Wrabetz, L., Feltri, M. L., & Park, H. T. (2011). Actin polymerization is essential for myelin

sheath fragmentation during Wallerian degeneration. *Journal of Neuroscience*, *31*(6), 2009–2015. https://doi.org/10.1523/JNEUROSCI.4537-10.2011

Kalinski, A. L., Yoon, C., Huffman, L. D., Duncker, P. C., Kohen, R., Passino, R., Hafner, H., Johnson, C., Kawaguchi, R., Carbajal, K. S., Jara, J. S., Hollis, E., Geschwind, D. H., Segal, B. M., & Giger, R. J. (2020). Analysis of the immune response to sciatic nerve injury identifies efferocytosis as a key mechanism of nerve debridement. *ELife*, *9*, 1–41. https://doi.org/10.7554/ELIFE.60223

Kang, H., & Lichtman, J. W. (2013). Motor axon regeneration and muscle reinnervation in young adult and aged animals. *Journal of Neuroscience*, *33*(50), 19480–19491. https://doi.org/10.1523/JNEUROSCI.4067-13.2013

Kawasaki, A., Okada, M., Tamada, A., Okuda, S., Nozumi, M., Ito, Y., Kobayashi, D., Yamasaki, T., Yokoyama, R., Shibata, T., Nishina, H., Yoshida, Y., Fujii, Y., Takeuchi, K., & Igarashi, M. (2018). Growth Cone Phosphoproteomics Reveals that GAP-43 Phosphorylated by JNK Is a Marker of Axon Growth and Regeneration. *IScience*, *4*, 190–203. https://doi.org/10.1016/j.isci.2018.05.019

Kemp, S. W. P., Chiang, C. D., Liu, E. H., Wood, M. D., Willand, M. P., Gordon, T., & Borschel, G. H. (2015a). Characterization of neuronal death and functional deficits following nerve injury during the early postnatal developmental period in rats. *Developmental Neuroscience*, *37*(1), 66–77. https://doi.org/10.1159/000368769

Kemp, S. W. P., Szynkaruk, M., Stanoulis, K. N., Wood, M. D., Liu, E. H., Willand, M. P., Morlock, L., Naidoo, J., Williams, N. S., Ready, J. M., Mangano, T. J., Beggs, S., Salter, M. W., Gordon, T., Pieper, A. A., & Borschel, G. H. (2015). Pharmacologic rescue of motor and sensory function by the neuroprotective compound P7C3 following neonatal nerve injury. *Neuroscience*, *284*, 202–216. https://doi.org/10.1016/j.neuroscience.2014.10.005

Khan, S., Carrasco, D. I., Isaacson, R., & English, A. W. (2023). Proportions of four distinct classes of sensory neurons are retained even when axon regeneration is enhanced following peripheral nerve injury. *Frontiers in Neuroanatomy*, *17*. https://doi.org/10.3389/fnana.2023.1303888

Kiryu-Seo, S., Tamada, H., Kato, Y., Yasuda, K., Ishihara, N., Nomura, M., Mihara, K., & Kiyama, H. (2016). Mitochondrial fission is an acute and adaptive response in injured motor neurons. *Scientific Reports*, *6*. https://doi.org/10.1038/srep28331

Kolodkin, A. L., & Tessier-Lavigne, M. (2011). Mechanisms and molecules of neuronal wiring: A primer. *Cold Spring Harbor Perspectives in Biology*, *3*(6), 1–14. https://doi.org/10.1101/cshperspect.a001727

Komiyama, A., & Suzuki, K. (1992). Age-related differences in proliferative responses of Schwann cells during Wallerian degeneration. *Brain Research*, *573*, 267–275. https://doi.org/10.1016/0006-8993(92)90772-2

Konishi, Y., Stegmüller, J., Matsuda, T., Bonni, S., & Bonni, A. (2004). Cdh1-APC Controls Axonal Growth and Patterning in the Mammalian Brain. *Science*, *303*. https://doi.org/10.1126/science.1093712.Epub2004Jan8.PMID:14716021

Kwon, M. J., Kim, J., Shin, H., Jeong, S. R., Kang, Y. M., Choi, J. Y., Hwang, D. H., & Kim, B. G. (2013). Contribution of macrophages to enhanced regenerative capacity of dorsal root ganglia sensory neurons by conditioning injury. *Journal of Neuroscience*, *33*(38), 15095–15108. https://doi.org/10.1523/JNEUROSCI.0278-13.2013

Kwon, M. J., Shin, H. Y., Cui, Y., Kim, H., Le Thi, A. H., Choi, J. Y., Kim, E. Y., Hwang, D. H., & Kim, B. G. (2015). CCL2 mediates neuron-macrophage interactions to drive proregenerative macrophage activation following preconditioning injury. *Journal of Neuroscience*, *35*(48), 15934–15947. https://doi.org/10.1523/JNEUROSCI.1924-15.2015

Lago, N., Rodríguez, F. J., Guzmán, M. S., Jaramillo, J., & Navarro, X. (2007). Effects of motor and sensory nerve transplants on amount and specificity of sciatic nerve regeneration. *Journal of Neuroscience Research*, *85*(12), 2800–2812. https://doi.org/10.1002/jnr.21286

Lankford, K. L., Waxman, S. G., & Kocsis, J. D. (1998). Mechanisms of enhancement of neurite regeneration in vitro following a conditioning sciatic nerve lesion. *Journal of Comparative Neurology*, *391*(1), 11–29. https://doi.org/10.1002/(SICI)1096-9861(19980202)391:1<11::AID-CNE2>3.0.CO;2-U

Lawson, S. J., & Lowrie, M. B. (1998). The role of apoptosis and excitotoxicity in the death of spinal motoneurons and interneurons after neonatal nerve injury. *Neuroscience*, *87*(2), 337–348. https://doi.org/10.1016/S0306-4522(98)00120-1

Le, T. B., Aszmann, O., Chen, Y. G., Royall, R. M., & Brushart, T. M. (2001). Effects of pathway and neuronal aging on the specificity of motor axon regeneration. *Experimental Neurology*, *167*(1), 126–132. https://doi.org/10.1006/exnr.2000.7538

Lee, J., & Cho, Y. (2021). Comparative gene expression profiling reveals the mechanisms of axon regeneration. *FEBS Journal*, *288*(16), 4786–4797. https://doi.org/10.1111/febs.15646

Leibinger, M., Zeitler, C., Gobrecht, P., Andreadaki, A., Gisselmann, G., & Fischer, D. (2021). Transneuronal delivery of hyper-interleukin-6 enables functional recovery after severe spinal cord injury in mice. *Nature Communications*, *12*(1). https://doi.org/10.1038/s41467-020-20112-4

Leite, S. C., Pinto-Costa, R., & Sousa, M. M. (2021). Actin dynamics in the growth cone: a key player in axon regeneration. *Current Opinion in Neurobiology*, *69*, 11–18. https://doi.org/10.1016/j.conb.2020.11.015

Lewis, S. E., Mannion, R. J., White, F. A., Coggeshall, R. E., Beggs, S., Costigan, M., Martin, J. L., Dillmann, W. H., & Woolf, C. J. (1999). A role for HSP27 in sensory neuron survival. *The Journal of Neuroscience : The Official Journal of the Society for Neuroscience*, *19*(20), 8945–8953. https://doi.org/10.1523/JNEUROSCI.19-20-08945.1999

Li, C., Yamamoto, T., Kanemaru, H., Kishimoto, N., & Seo, K. (2024). Effects of Sphingosine-1-Phosphate on the Facilitation of Peripheral Nerve Regeneration. *Cureus*, *16*(11). https://doi.org/10.7759/cureus.73784

Li, H., Zhang, Z., Li, H., Pan, X., & Wang, Y. (2023). New Insights into the Roles of p53 in Central Nervous System Diseases. *International Journal of Neuropsychopharmacology*, *26*(7), 465–473. https://doi.org/10.1093/ijnp/pyad030

Li, J., Parker, B., Martyn, C., Natarajan, C., & Guo, J. (2013). The PMP22 gene and its related diseases. *Molecular Neurobiology*, *47*(2), 673–698. https://doi.org/10.1007/s12035-012-8370-x

Li, L., Houenou, L. J., Wu, W., Lei, M., Prevette, D. M., & Oppenheim, R. W. (1998). Characterization of Spinal Motoneuron Degeneration Following Different Types of Peripheral Nerve Injury in Neonatal and Adult Mice. In *J. Comp. Neurol* (Vol. 396). https://doi.org/10.1002/(SICI)1096-9861(19980629)396:2<158::AID-CNE2>3.0.CO;2

Liang Low, H. U., Nogradi, A., Vrbová, G., & Greensmith, L. (2003). Axotomized Motoneurons Can Be Rescued from Cell Death by Peripheral Nerve Grafts: The Effect of Donor Age. *Journal of Neuropathology and Experimental Neurology*, *62*(1). https://doi.org/10.1093/jnen/62.1.75

Lin, J., Huang, Z., Liu, J., Huang, Z., Liu, Y., Liu, Q., Yang, Z., Li, R., Wu, X., Shi, Z., Zhu, Q., & Wu, X. (2020). Neuroprotective Effect of Ketone Metabolism on Inhibiting Inflammatory Response by Regulating Macrophage Polarization After Acute Cervical Spinal Cord Injury in Rats. *Frontiers in Neuroscience*, *14*. https://doi.org/10.3389/fnins.2020.583611

Lindwall Blom, C., Mårtensson, L. B., & Dahlin, L. B. (2014). Nerve injury-induced c-jun activation in schwann cells is JNK independent. *BioMed Research International*, *2014*. https://doi.org/10.1155/2014/392971

Liu, D., & Zhou, J. (2025). Roles of ERK signaling pathway in regulating myelination of the peripheral nervous system. *Frontiers in Molecular Neuroscience*, *18*. https://doi.org/10.3389/fnmol.2025.1617976

Lopes, B., Sousa, P., Alvites, R., Branquinho, M., Sousa, A. C., Mendonça, C., Atayde, L. M., Luís, A. L., Varejão, A. S. P., & Maurício, A. C. (2022). Peripheral Nerve Injury Treatments and Advances: One Health Perspective. *International Journal of Molecular Sciences*, *23*(2). https://doi.org/10.3390/ijms23020918

Lowery, L. A., & Vactor, D. Van. (2009). The trip of the tip: Understanding the growth cone machinery. *Nature Reviews Molecular Cell Biology*, *10*(5), 332–343. https://doi.org/10.1038/nrm2679

Lowrie, M. B., Krishnan, S., & Vrbová, G. (1987). Permanent changes in muscle and motoneurones induced by nerve injury during a critical period of development of the rat*. In *Developmental Brain Research* (Vol. 31).

Lowrie, M. B., Krishnan, S., & Vrbova, G. (1982). Recovery of slow and fast muscles following nerve injury during early post-natal development in the rat. *J. Physiol*, *331*, 51–66. https://doi.org/10.1113/jphysiol.1982.sp014364

Lowrie, M. B., Krishnan, S., & Vrbová, G. (1987). Permanent changes in muscle and motoneurones induced by nerve injury during a critical period of development of the rat. *Developmental Brain Research*, *31*, 91–101. https://doi.org/10.1016/0165-3806(87)90086-1

Lowrie, M. B., & Vrbova, G. (1984). Different Pattern of Recovery of Fast and Slow Muscles Following Nerve Injury in the Rat. *The Journal of Physiology*, *349*(1), 397–410. https://doi.org/10.1113/jphysiol.1984.sp015163

Lowrie, M. B., & Vrbová, G. (1992). Dependence of postnatal motoneurones on their targets: review and hypothesis. *Trends in Neuroscience*, *13*(3), 80–84. https://doi.org/10.1016/0166-2236(92)90014-y

Lu, X., & Richardson, P. M. (1991). Inflammation near the Nerve Cell Body Enhances Axonal Regeneration. *The Journal of Neuroscience*, *1*(4), 972–979. https://doi.org/10.1523/JNEUROSCI.11-04-00972.1991

Lu, X., & Richardson, P. M. (1993). Responses of macrophages in rat dorsal root ganglia following peripheral nerve injury. *Journal of Neurocytology*, *22*, 334–341. https://doi.org/https://doi.org/10.1007/BF01195557

Madden, J. F., Davis, O. C., Boyle, K. A., Iredale, J. A., Browne, T. J., Callister, R. J., Smith, D. W., Jobling, P., Hughes, D. I., & Graham, B. A. (2020). Functional and Molecular Analysis of Proprioceptive Sensory Neuron Excitability in Mice. *Frontiers in Molecular Neuroscience*, *13*. https://doi.org/10.3389/fnmol.2020.00036

Madisen, L., Zwingman, T. A., Sunkin, S. M., Oh, S. W., Zariwala, H. A., Gu, H., Ng, L. L., Palmiter, R. D., Hawrylycz, M. J., Jones, A. R., Lein, E. S., & Zeng, H. (2010). A robust and high-throughput Cre reporting and characterization system for the whole

mouse brain. *Nature Neuroscience*, *13*(1), 133–140. https://doi.org/10.1038/nn.2467

Madison, R. D., Archibald, S. J., & Brushart, T. M. (1996). Reinnervation Accuracy of the Rat Femoral Nerve by Motor and Sensory Neurons. *Journal of Neuroscience*, *18*(16), 5698–5703. https://doi.org/10.1523/JNEUROSCI.16-18-05698.1996

Mahar, M., & Cavalli, V. (2018). Intrinsic mechanisms of neuronal axon regeneration. *Nature Reviews Neuroscience*, *19*(6), 323–337. https://doi.org/10.1038/s41583-018-0001-8

Martin, L. J., Chen, K., & Liu, Z. (2005). Adult motor neuron apoptosis is mediated by nitric oxide and Fas death receptor linked by DNA damage and p53 activation. *Journal of Neuroscience*, *25*(27), 6449–6459. https://doi.org/10.1523/JNEUROSCI.0911-05.2005

Martini, R., Schachner, M, & Brushart, T. M. (1994). The L2/HNK-1 Carbohydrate Is Preferentially Expressed by Previously Motor Axon-associated Schwann Cells in Reinnervated Peripheral Nerves. *The Journal of Neuroscience*, *14*(11), 7180–7191. https://doi.org/https://doi.org/10.1523/JNEUROSCI.14-11-07180.1994

Martini, R., Xin, Y., Schmitz, B., & Schachner, M. (1992). The L2/HNK-1 Carbohydrate Epitope is Involved in the Preferential Outgrowth of Motor Neurons on Ventral Roots and Motor Nerves. *European Journal of Neuroscience*, *4*(7), 628–639. https://doi.org/10.1111/j.1460-9568.1992.tb00171.x

Mears, S., Schachner, M., & Brushart, T. M. (2003). Antibodies to myelin-associated glycoprotein accelerate preferential motor reinnervation. *Journal of the Peripheral Nervous System*, *8*, 91–99. https://doi.org/https://doi.org/10.1046/j.1529-8027.2003.03012.x

Medici, T., & Shortland, P. J. (2015). Effects of peripheral nerve injury on parvalbumin expression in adult rat dorsal root ganglion neurons. *BMC Neuroscience*, *16*(1). https://doi.org/10.1186/s12868-015-0232-9

Mentis, G. Z., Greensmith, L., & Vrbová, G. (1993). Motoneurons destined to die are rescued by blocking N-methyl-D-aspartate receptors by MK-801. *Neuroscience*, *54*(2), 283–285. https://doi.org/10.1016/0306-4522(93)90253-c

Meyer zu Reckendorf, S., Brand, C., Pedro, M. T., Hegler, J., Schilling, C. S., Lerner, R., Bindila, L., Antoniadis, G., & Knöll, B. (2020). Lipid metabolism adaptations are reduced in human compared to murine Schwann cells following injury. *Nature Communications*, *11*(1). https://doi.org/10.1038/s41467-020-15915-4

Mòdol-Caballero, G., Santos, D., Navarro, X., & Herrando-Grabulosa, M. (2018). Neuregulin 1 reduces motoneuron cell death and promotes neurite growth in an

in vitro model of motoneuron degeneration. *Frontiers in Cellular Neuroscience*, *11*. https://doi.org/10.3389/fncel.2017.00431

Mokarram, N., Merchant, A., Mukhatyar, V., Patel, G., & Bellamkonda, R. V. (2012). Effect of modulating macrophage phenotype on peripheral nerve repair. *Biomaterials*, *33*(34), 8793–8801. https://doi.org/10.1016/j.biomaterials.2012.08.050

Molina-Esteve, B., Pujol-Masip, M., Ovelleiro, D., Gomez-Sanchez, J. A., Lago, N., & Udina, E. (2025). *Assessment of Motoneuronal Regeneration and Wallerian Degeneration Following Axotomy in Postnatal Mice*. bioRxiv [Preprint]. https://doi.org/10.64898/2025.12.03.691768

Monk, K. R., Feltri, M. L., & Taveggia, C. (2015). New insights on schwann cell development. *GLIA*, *63*(8), 1376–1393. https://doi.org/10.1002/glia.22852

Msheik, Z., El Massry, M., Rovini, A., Billet, F., & Desmoulière, A. (2022). The macrophage: a key player in the pathophysiology of peripheral neuropathies. In *Journal of Neuroinflammation* (Vol. 19, Issue 1). BioMed Central Ltd. https://doi.org/10.1186/s12974-022-02454-6

Murtazina, A., & Adameyko, I. (2023). The peripheral nervous system. *Development (Cambridge)*, *150*(9). https://doi.org/10.1242/dev.201164

Navarrete, R., & Vrbova, G. (1984). Differential Effect of Nerve Injury at Birth on the Activity Pattern of Reinnervated Slow and Fast Muscles of the Rat. *Journal of Physiology*, *351*, 675–685. https://doi.org/10.1113/jphysiol.1984.sp015270

Navarro, X., Verdú, E., & Butí, M. (1994). Comparison of Regenerative and Reinnervating Capabilities of Different Types of Nerve Fibers. *Experimental Neurology*, *129*, 217–224. https://doi.org/https://doi.org/10.1006/exnr.1994.1163

Nichols, C. M., Brenner, M. J., Fox, I. K., Tung, T. H., Hunter, D. A., Rickman, S. R., & Mackinnon, S. E. (2004). Effects of motor versus sensory nerve grafts on peripheral nerve regeneration. *Experimental Neurology*, *190*(2), 347–355. https://doi.org/10.1016/j.expneurol.2004.08.003

Niemi, J. P., Defrancesco-Lisowitz, A., Roldan-Hernandez, L., Lindborg, J. A., Mandell, D., & Zigmond, R. E. (2013). A critical role for macrophages near axotomized neuronal cell bodies in stimulating nerve regeneration. *Journal of Neuroscience*, *33*(41), 16236–16248. https://doi.org/10.1523/JNEUROSCI.3319-12.2013

Oishi, Y., Baratta, J., Robertson, R. T., & Steward, O. (2004). Assessment of Factors Regulating Axon Growth between the Cortex and Spinal Cord in Organotypic Co-Cultures: Effects of Age and Neurotrophic Factors. *Journal of Neurotrauma*, *21*(3). https://doi.org/10.1089/089771504322972121

Oppenheim, R. W., Wiese, S., Prevette, D., Armanini, M., Wang, S., Houenou, L. J., Holtmann, B., Gö, R., Pennica, D., & Sendtner, M. (2001). Cardiotrophin-1, a Muscle-Derived Cytokine, Is Required for the Survival of Subpopulations of Developing Motoneurons. *The Journal of Neuroscience*, *4*(21), 1283–1291. https://doi.org/10.1523/JNEUROSCI.21-04-01283.2001

Oppenheim Ronald W, R. W. (1989). *The neurotrophic theory and naturally occurring motoneuron death*.

Painter, M. W., Brosius Lutz, A., Cheng, Y. C., Latremoliere, A., Duong, K., Miller, C. M., Posada, S., Cobos, E. J., Zhang, A. X., Wagers, A. J., Havton, L. A., Barres, B., Omura, T., & Woolf, C. J. (2014). Diminished Schwann cell repair responses underlie age-associated impaired axonal regeneration. *Neuron*, *83*(2), 331–343. https://doi.org/10.1016/j.neuron.2014.06.016

Patodia, S., & Raivich, G. (2012). Role of transcription factors in peripheral nerve regeneration. *Frontiers in Molecular Neuroscience*, *5*. https://doi.org/10.3389/fnmol.2012.00008

Peshoff, M. M., Gupta, P., Trivedi, R., Oberai, S., Chakrapani, P., Dang, M., Milam, N., Maynard, M. E., Vaillant, B. D., Huse, J. T., Wang, L., Clise-Dwyer, K., & Bhat, K. P. (2023). Triggering receptor expressed on myeloid cells 2 (TREM2) regulates phagocytosis in glioblastoma. *Neuro-Oncology*, *25*(5). https://doi.org/10.1101/2023.04.05.535792

Petsanis, K., Chatzisotiriou, A., Kapoukranidou, D., Simeonidou, C., Kouvelas, D., & Albani, M. (2012). Contractile properties and movement behaviour in neonatal rats with axotomy, treated with the NMDA antagonist DAP5. *BMC Physiology*, *12*(5). https://doi.org/10.1186/1472-6793-12-5

Pollin, M. M., Mchanwell, S., & Slater, C. R. (1991). The effect of age on motor neurone death following axotomy in the mouse. *Development*, *112*, 83–89. https://doi.org/10.1242/dev.112.1.83

Porcu, P., Barron, A. M., Frye, C. A., Walf, A. A., Yang, S. Y., He, X. Y., Morrow, A. L., Panzica, G. C., & Melcangi, R. C. (2016). Neurosteroidogenesis Today: Novel Targets for Neuroactive Steroid Synthesis and Action and Their Relevance for Translational Research. In *Journal of Neuroendocrinology* (Vol. 28, Issue 2, pp. 1–19). Blackwell Publishing Ltd. https://doi.org/10.1111/jne.12351

Ramesh, R., Manurung, Y., Ma, K. H., Blakely, T., Won, S., Moreno-Ramos, O. A., Wyatt, E., Awatramani, R., & Svaren, J. (2022). JUN Regulation of Injury-Induced Enhancers in Schwann Cells. *Journal of Neuroscience*, *42*(34), 6506–6517. https://doi.org/10.1523/JNEUROSCI.2533-21.2022

Redett, R., Jari, R., Crawford, T., Chen, Y. G., Rohde, C., & Brushart, T. M. (2005). Peripheral pathways regulate motoneuron collateral dynamics. *Journal of*

Neuroscience, *25*(41), 9406–9412. https://doi.org/10.1523/JNEUROSCI.3105-05.2005

Reichert, F., & Rotshenker, S. (2019). Galectin-3 (MAC-2) controls microglia phenotype whether amoeboid and phagocytic or branched and non-phagocytic by regulating the cytoskeleton. *Frontiers in Cellular Neuroscience*, *13*. https://doi.org/10.3389/fncel.2019.00090

Reier, P. J., & Hughes, A. (1972). EVIDENCE FOR SPONTANEOUS AXON DEGENERATION DURING PERIPHERAL NERVE MATURATION (1). *American Journal of ANatomy*, *135*(1), 147–152. https://doi.org/https://doi.org/10.1002/aja.1001350113

Renthal, W., Tochitsky, I., Yang, L., Cheng, Y.-C., Li, E., Kawaguchi, R., Geschwind, D. H., & Woolf, C. J. (2020). Transcriptional reprogramming of distinct peripheral sensory neuron subtypes after axonal injury. *Neuron*, *108*(1), 128–144. https://doi.org/10.1101/838854

Robinson, G. A., & Madison, R. D. (2003). Preferential motor reinnervation in the mouse: comparison of femoral nerve repair using a fibrin sealant or suture. *Muscle Nerve*, *28*, 227–231. https://doi.org/https://doi.org/10.1002/mus.10422

Robinson, G. A., & Madison, R. D. (2005). Manipulations of the mouse femoral nerve influence the accuracy of pathway reinnervation by motor neurons. *Experimental Neurology*, *192*(1), 39–45. https://doi.org/10.1016/j.expneurol.2004.10.013

Robinson, G. A., & Madison, R. D. (2006). Developmentally regulated changes in femoral nerve regeneration in the mouse and rat. *Experimental Neurology*, *197*(2), 341–346. https://doi.org/10.1016/j.expneurol.2005.10.007

Robinson, L. R. (2004). Traumatic injury to peripheral nerves. *Supplements to Clinical Neurophysiology*, *57*(C), 173–186. https://doi.org/10.1016/S1567-424X(09)70355-1

Romanes, G. J. (1946). Motor localization and the effects of nerve injury on the ventral horn cells of the spinal cord. *Journal of Anatomy*, *80*(3), 117–131.

Romero Ortega, M., Gu, X., Rahman, F., Tran, B., Miyata, J., Reynoso, A. H., Anand, S., & Bendale, G. (2023). *Pleiotrophin-Neuregulin1 promote axon regeneration and sorting in conduit repair of critical nerve gap injuries*. https://doi.org/10.21203/rs.3.rs-3429258/v1

Rossi, J., Balthasar, N., Olson, D., Scott, M., Berglund, E., Lee, C. E., Choi, M. J., Lauzon, D., Lowell, B. B., & Elmquist, J. K. (2011). Melanocortin-4 receptors expressed by cholinergic neurons regulate energy balance and glucose homeostasis. *Cell Metabolism*, *13*(2), 195–204. https://doi.org/10.1016/j.cmet.2011.01.010

Rotshenker, S. (2011). Wallerian degeneration: The innate-immune response to traumatic nerve injury. *Journal of Neuroinflammation*, *8*. https://doi.org/10.1186/1742-2094-8-109

Rotshenker, S., Reichert, F., Gitik, M., Haklai, R., Elad-Sfadia, G., & Kloog, Y. (2008). Galectin-3/MAC-2, ras and PI3K activate complement receptor-3 and scavenger receptor-AI/II mediated myelin phagocytosis in microglia. *GLIA*, *56*(15), 1607–1613. https://doi.org/10.1002/glia.20713

Santos, D., González-Pérez, F., Giudetti, G., Micera, S., Udina, E., Del Valle, J., & Navarro, X. (2017). Preferential enhancement of sensory and motor axon regeneration by combining extracellular matrix components with neurotrophic factors. *International Journal of Molecular Sciences*, *18*(1). https://doi.org/10.3390/ijms18010065

Sanz, E., Bean, J. C., Carey, D. P., Quintana, A., & McKnight, G. S. (2019). RiboTag: Ribosomal Tagging Strategy to Analyze Cell-Type-Specific mRNA Expression In Vivo. *Current Protocols in Neuroscience*, *88*(1). https://doi.org/10.1002/cpns.77

Schaefer, A. W., Schoonderwoert, V. T. G., Ji, L., Mederios, N., Danuser, G., & Forscher, P. (2008). Coordination of Actin Filament and Microtubule Dynamics during Neurite Outgrowth. *Developmental Cell*, *15*(1), 146–162. https://doi.org/10.1016/j.devcel.2008.05.003

Schmalbruch, H. (1984). Motoneuron death after sciatic nerve section in newborn rats. *Journal of Comparative Neurology*, *224*(2), 252–258. https://doi.org/10.1002/cne.902240206

Schwab, M. E., & Bartholdi, D. (1996). Degeneration and Regeneration of Axons in the Lesioned Spinal Cord. *Physiological Reviews*, *76*(2). https://doi.org/10.1152/physrev.1996.76.2.319

Seddon, H. J. (1942). *A Classification of Nerve Injuries*. *2*, 237–239. https://doi.org/10.1136/bmj.2.4260.237

Seo, J. W., Balog, B. M., Pinkevitch, M., Niemi, J. P., Patru, M., Paranjape, S., & Zigmond, R. E. (2025). Somatosensory neurons respond heterogeneously to a conditioning lesion. *Experimental Neurology*, *392*. https://doi.org/10.1016/j.expneurol.2025.115342

Sheng, Z. H. (2017). The Interplay of Axonal Energy Homeostasis and Mitochondrial Trafficking and Anchoring. In *Trends in Cell Biology* (Vol. 27, Issue 6, pp. 403–416). Elsevier Ltd. https://doi.org/10.1016/j.tcb.2017.01.005

Shimizu, Y., Kiyooka, M., & Ohshima, T. (2021). Transcriptome Analyses Reveal IL6/Stat3 Signaling Involvement in Radial Glia Proliferation After Stab Wound

Injury in the Adult Zebrafish Optic Tectum. *Frontiers in Cell and Developmental Biology*, *9*. https://doi.org/10.3389/fcell.2021.668408

Sjöberg, J., & Kanje, M. (1990). The initial period of peripheral nerve regeneration and the importance of the local environment for the conditioning lesion effect. *Brain Research*, *529*, 79–84. https://doi.org/https://doi.org/10.1016/0006-8993(90)90812-P

Skene, J. H. P., Jacobson, R. D., Snipes, G. J., Brlan Mcguireu, C., Norden, J. J., & Freeman, J. A. (1986). A Protein Induced During Nerve Growth (GAP-43) Is a Major Component of Growth-Cone Membranes. *Science*, *233*(4765), 783–786. https://doi.org/10.1126/science.3738509

Smaila, B. D., Holland, S. D., Babaeijandaghi, F., Henderson, H. G., Rossi, F. M. V., & Ramer, M. S. (2020). Systemic hypoxia mimicry enhances axonal regeneration and functional recovery following peripheral nerve injury. *Experimental Neurology*, *334*. https://doi.org/10.1016/j.expneurol.2020.113436

Smith, D. S., & Skene, J. H. P. (1997). A Transcription-Dependent Switch Controls Competence of Adult Neurons for Distinct Modes of Axon Growth. *The Journal of Neuroscience*, *17*(2), 646–658. https://doi.org/10.1523/JNEUROSCI.17-02-00646.1997

Stoll, G., & Müller, W. (1999). Nerve Injury, Axonal Degeneration and Neural Regeneration: Basic Insights. *Brain Pathology*, *9*, 313325. https://doi.org/10.1111/j.1750-3639.1999.tb00229.x

Stratton, J. A., Eaton, S., Rosin, N. L., Jawad, S., Holmes, A., Yoon, G., Midha, R., & Biernaskie, J. (2020). Macrophages and Associated Ligands in the Aged Injured Nerve: A Defective Dynamic That Contributes to Reduced Axonal Regrowth. *Frontiers in Aging Neuroscience*, *12*. https://doi.org/10.3389/fnagi.2020.00174

Sulaiman, W., & Gordon, T. (2013). Neurobiology of Peripheral Nerve Injury, Regeneration, and Functional Recovery: From Bench Top Research to Bedside Application. *The Ochsner Journal*, *13*(1), 100–108.

Suter, D. M., & Forscher, P. (2000). Substrate-Cytoskeletal Coupling as a Mechanism for the Regulation of Growth Cone Motility and Guidance. *Neurobiology*, *44*(2), 97–113.

Switon, K., Kotulska, K., Janusz-Kaminska, A., Zmorzynska, J., & Jaworski, J. (2017). Molecular neurobiology of mTOR. *Neuroscience*, *341*, 112–153. https://doi.org/10.1016/j.neuroscience.2016.11.017

Sydney Sunderland, B. (1951). A Classification of Peripheral Nerve Injuries Producing Loss of Functions. *Brain*, *74*(4), 491–516. https://doi.org/10.1093/brain/74.4.491

Talsma, A. D., Niemi, J. P., Pachter, J. S., & Zigmond, R. E. (2022). The primary macrophage chemokine, CCL2, is not necessary after a peripheral nerve injury for macrophage recruitment and activation or for conditioning lesion enhanced peripheral regeneration. *Journal of Neuroinflammation*, *19*(1). https://doi.org/10.1186/s12974-022-02497-9

Tandrup, T., Woolf, C. J., & Coggeshall, R. E. (2000). Delayed Loss of Small Dorsal Root Ganglion Cells After Transection of the Rat Sciatic Nerve. *J. Comp. Neurol*, *422*(2), 172–180. https://doi.org/10.1002/(SICI)1096-9861(20000626)422:2<172::AID-CNE2>3.0.CO;2-H

Tang, B. (2022). Cholesterol synthesis inhibition or depletion in axon regeneration. In *Neural Regeneration Research* (Vol. 17, Issue 2, pp. 271–276). Wolters Kluwer Medknow Publications. https://doi.org/10.4103/1673-5374.317956

Taylor, A. R., Gifondorwa, D. J., Newbern, J. M., Robinson, M. B., Strupe, J. L., Prevette, D., Oppenheim, R. W., & Milligan, C. E. (2007). Astrocyte and muscle-derived secreted factors differentially regulate motoneuron survival. *Journal of Neuroscience*, *27*(3), 634–644. https://doi.org/10.1523/JNEUROSCI.4947-06.2007

Terenghi, G. (1999). Peripheral nerve regeneration and neurotrophic factors. *Journal of Anatomy*, *194*, 1–14. https://doi.org/10.1046/j.1469-7580.1999.19410001.x

Tessier-Lavigne, M., & S. Goodman, C. (1996). The Molecular Biology of Axon Guidance. *Science*, *274*(5293), 1123–1133. https://doi.org/10.1126/science.274.5290.1123

Topp, K. S., & Boyd, B. S. (2012). Peripheral nerve: From the microscopic functional unit of the axon to the biomechanically loaded macroscopic structure. *Journal of Hand Therapy*, *25*(2), 142–152. https://doi.org/10.1016/j.jht.2011.09.002

Usoskin, D., Furlan, A., Islam, S., Abdo, H., Lönnerberg, P., Lou, D., Hjerling-Leffler, J., Haeggström, J., Kharchenko, O., Kharchenko, P. V., Linnarsson, S., & Ernfors, P. (2015). Unbiased classification of sensory neuron types by large-scale single-cell RNA sequencing. *Nature Neuroscience*, *18*(1), 145–153. https://doi.org/10.1038/nn.3881

Virgo, L., Dekkers, J., Mentis, R., Navarrete, R., & de Belleroche, J. (2000). Changes in expression of NMDA receptor subunits in the rat lumbar spinal cord following neonatal nerve injury. *Neuropathology and Applied Neurobiology*, *26*(3), 258–272. https://doi.org/10.1046/j.1365-2990.2000.00244.x

Vitriol, E. A., & Zheng, J. Q. (2012). Growth Cone Travel in Space and Time: The Cellular Ensemble of Cytoskeleton, Adhesion, and Membrane. *Neuron*, *73*(6), 1068–1081. https://doi.org/10.1016/j.neuron.2012.03.005

Waller, A. (1851). Experiments on the Section of the Glosso-Pharyngeal and Hypoglossal Nerves of the Frog, and Observations of the Alterations Produced Thereby in the Structure of Their Primitive Fibres. *Edinburgh Medical and Surgical Journal*, *76*(189), 369–376.

Wang, F., Zhao, C., Jing, Z., Wang, Q., Li, M., Lu, B., Huo, A., Liang, W., Hu, W., & Fu, X. (2025). The dual roles of chemokines in peripheral nerve injury and repair. In *Inflammation and Regeneration* (Vol. 45, Issue 1). BioMed Central Ltd. https://doi.org/10.1186/s41232-025-00375-4

Wang, J., Chen, H., Hou, W., Han, Q., & Wang, Z. (2023). Hippo Pathway in Schwann Cells and Regeneration of Peripheral Nervous System. *Developmental Neuroscience*, *45*(5), 276–289. https://doi.org/10.1159/000530621

Wei, C., Guo, Y., Ci, Z., Li, M., Zhang, Y., & Zhou, Y. (2024). Advances of Schwann cells in peripheral nerve regeneration: From mechanism to cell therapy. *Biomedicine and Pharmacotherapy*, *175*. https://doi.org/10.1016/j.biopha.2024.116645

Witzel, C., Rohde, C., & Brushart, T. M. (2005). Pathway sampling by regenerating peripheral axons. *Journal of Comparative Neurology*, *485*(3), 183–190. https://doi.org/10.1002/cne.20436

Wu, H., Petitpré, C., Fontanet, P., Sharma, A., Bellardita, C., Quadros, R. M., Jannig, P. R., Wang, Y., Heimel, J. A., Cheung, K. K. Y., Wanderoy, S., Xuan, Y., Meletis, K., Ruas, J., Gurumurthy, C. B., Kiehn, O., Hadjab, S., & Lallemend, F. (2021). Distinct subtypes of proprioceptive dorsal root ganglion neurons regulate adaptive proprioception in mice. *Nature Communications*, *12*(1). https://doi.org/10.1038/s41467-021-21173-9

Xu, Q. G., ForDen, J., Walsh, S. K., Gordon, T., & Midha, R. (2010). Motoneuron survival after chronic and sequential peripheral nerve injuries in the rat. *Journal of Neurosurgery*, *112*(4), 890–899. https://doi.org/10.3171/2009.8.JNS09812

Ydens, E., Cauwels, A., Asselbergh, B., Goethals, S., Peeraer, L., Lornet, G., Almeida-Souza, L., Van Ginderachter, J. A., Timmerman, V., & Janssens, S. (2012). Acute injury in the peripheral nervous system triggers an alternative macrophage response. *Journal of Neuroinflammation*, *9*. https://doi.org/10.1186/1742-2094-9-176

Ydens, E., Demon, D., Lornet, G., De Winter, V., Timmerman, V., Lamkanfi, M., & Janssens, S. (2015). Nlrp6 promotes recovery after peripheral nerve injury independently of inflammasomes. *Journal of Neuroinflammation*, *12*(1). https://doi.org/10.1186/s12974-015-0367-8

Yi, S., Zhang, H., Gong, L., Wu, J., Zha, G., Zhou, S., Gu, X., & Yu, B. (2015). Deep sequencing and bioinformatic analysis of lesioned sciatic nerves after crush injury. *PLoS ONE*, *10*(12). https://doi.org/10.1371/journal.pone.0143491

Yuan, Q., Su, H., Guo, J., Wu, W., & Lin, Z. X. (2014). Induction of phosphorylated c-Jun in neonatal spinal motoneurons after axonal injury is coincident with both motoneuron death and regeneration. *Journal of Anatomy*, *224*(5), 575–582. https://doi.org/10.1111/joa.12165

Yuan, Y., Wang, Y., Wu, S., & Yue Zhao, M. (2022). Review: Myelin clearance is critical for regeneration after peripheral nerve injury. *Frontiers in Neurology*. https://doi.org/10.3389/fneur.2022.908148

Zhang, X., Zhang, Y., Chen, Y., Ji, Y., Lyu, Y., Miao, Z., Duan, X., & Liu, X. (2025). Unraveling the immune system's role in peripheral nerve regeneration: a pathway to enhanced healing. *Frontiers in Immunology*, *16*. https://doi.org/10.3389/fimmu.2025.1540199

Zhao, X. F., Huffman, L. D., Hafner, H., Athaiya, M., Finneran, M. C., Kalinski, A. L., Kohen, R., Flynn, C., Passino, R., Johnson, C. N., Kohrman, D., Kawaguchi, R., Yang, L. J. S., Twiss, J. L., Geschwind, D. H., Corfas, G., & Giger, R. J. (2022). The injured sciatic nerve atlas (iSNAT), insights into the cellular and molecular basis of neural tissue degeneration and regeneration. *ELife*, *11*. https://doi.org/10.7554/ELIFE.80881

Agraïments